Functions of mutant and wildtype Piezo1 channels

Elizabeth Louise Evans

Submitted in accordance with the requirements for the degree of
Doctor of Philosophy

The University of Leeds

Faculty of Medicine and Health
Leeds Institute of Cardiovascular and Metabolic Medicine

November, 2019

Funded by the British Heart Foundation

The candidate confirms that the work submitted is her own and that appropriate credit has been given where reference has been made to the work of others.

Acknowledgements

Firstly, I would like to thank my primary supervisor Professor David Beech. I have been given so many opportunities as your PhD student and you have always been so supportive. I really value how you have always provided such quick feedback and that every suggestion is taken seriously. By trusting in me and giving me the freedom to develop my project, you have given me confidence in myself as a scientist. I would also like to thank my co-supervisors; Dr Sarah Calaghan, for joining my supervisory team during a more difficult time of my PhD and always being supportive even from another faculty, Dr Neil Turner for being a great mentor and Dr Mark Drinkhill for help with echocardiography training. I would like to thank all of your for all of your helpful comments on my thesis. Also thank you to Dr Jing Li for supervising me during the early part of my PhD.

One of the aspects of science that I like the most is the collaboration with others. My PhD would not have been possible without the expertise of other members of the laboratory and University. I would like to thank Kevin Cuthbertson (Compound Kev) for designing and synthesising the Yoda1 analogues and Dr Naima Endesh for her technically challenging wire myography experiments which have provided some fantastic results; I am really proud of the paper we have all published together. I would also like to thank Dr Oleksandr Postyvan (Sasha) for your impressive patch-clamp experiments on RBCs.

I owe a special thank you to Dr Melanie Ludlow who designed the Piezo1 M-R mouse model and made this PhD project possible. I am extremely appreciative of the opportunity to work on such an exciting project and I have learnt so much from you about the world of CRISPR/Cas9 and molecular biology. Dr Laeticia Lichtenstein has been an incredible support with the Piezo1 M-R mice and has been so generous with her time and expertise. I also owe a big thank you to Dr Simon Futers, who has always been so happy to help and for Melanie Raey who has been a big support in CBS.

I will not just be leaving Leeds with a PhD, but with some amazing friends who have celebrated the ups and supported me through the occasional tough times. You have made this experience unforgettable and I have so many fond memories that will stay with me far more than any results I have generated. Kat, you have been a HUGE support especially during these last few months of writing up. I really appreciate you always being willing to take time out of your day to go for a well needed break, a motivating pep talk (remember a ship is safe in the harbour, but that’s not what ships are built for), a gym session, pints or eating an impressive amount of snacks. You have taught me the importance of taking time for myself and I think after 3 years I am finally getting there! Nikki, thank you for

putting up with me at the desk, making me laugh, trying to organise me and tidying my lab bench. Katie, thank you for always being on hand for a hug (even if it's 5 times in one day), being so thoughtful and sharing my love of food. Han, I have missed you so much this year, thank you for the memories of your red face at the gym, providing us with so much fun as our social secretary (minus the jagerbombs) and for being an amazing support.

Marj and Fiona, thank you for encouraging my French alto ego Liz Sauvage to come out of her shell (she says thanks for the chips). You have made such a difference to the lab since you have arrived and I am so glad that I have been able to spend 2 years with you. You are such generous friends and you have provided so much fun with your GIFs (thanks Fiona), games, Fluor and Irish. Remember, if in doubt- stay casual (I can teach you). Lucia, thank you for providing some much needed class and sophistication to our friendship group. It always brightens up my day speaking to you and seeing you with your espresso cup. We made it! Pete and Adam, thank you for all the fun (minus having to down a pint during your wedding Pete), Lara, thank you for the support with the qPCR life and Nele, thank you for being with me from the start of the PhD (and cute little Leni). Also a special thanks to Katie Simmons for always being on hand for advice over the 4 years.

Aside from a certain 3 weeks (if you know, you know) I have been incredibly lucky to live with some lovely housemates who have made a house, a home and given me somewhere to relax, laugh and remind me there is more to life than Piezo1 (who knew). I must thank Jay and Kate for taking me under their wing when I first moved to Leeds and being big sisters for 2 years in Broomfield Road. You made the move to a new city feel so easy. Then a huge shout out to Charlotte, Matt, Will and Hope, then Rachel, Daniela and Ash for 2 years in Cardigan Road, filled with M&S prosecco, chocolate oranges, weeknight dances round the living room and of course, Darude Sandstorm.

A huge thank you to my friends back in Essex who have been a constant support, even during times I haven't been able to go home and visit much. Ally, thank you for always being there and organising my calendar to make sure I have fun things planned back home. My godson, Harrison for keeping me smiling and making the drives back home seem much quicker. It was well worth driving to and from Essex the night before my transfer viva to meet you an hour after you were born. Sarah for always checking in for a phone call and Tania for keeping me laughing at myself. Also a big thank you to Rosie for your constant encouragement.

I must thank my family for giving me the confidence for doing a PhD in the first place. Thank you Mum for reminding me about life admin and Dad, for telling

Mum off for reminding me about life admin too much. I really appreciate all of your trips to come and see me in Leeds, for your continual support and for being proud of me regardless. Thank you to my brother Michael for regular check-ins and for always being on the end of the phone. I am lucky to be able to call my brother a friend.

Finally, thank you to the British Heart Foundation as their funding has allowed me to undertake this PhD. I am extremely grateful to have had this opportunity and will strive to put it to good use for the rest of my career.

Abstract

Background

Piezo1 is a mechanically-activated ion channel with a widespread role in mechanotransduction in mammalian physiology. Mutations of the channel which confer gain of function (GOF) are causative of dehydrated hereditary stomatocytosis (DHS), a form of anaemia. Heterologous expression studies suggest that that GOF arises from a delaying of channel inactivation, however this mechanism has not been confirmed in endogenous channels in affected red blood cells (RBCs). Pharmacological tools with which to modulate Piezo1 activity are very limited and additional compounds are required if therapeutic targeting is to be possible.

Methods and Results

A CRISPR-Cas9 mouse model (Piezo1 M-R) was generated harbouring the murine equivalent of DHS-causing Piezo1 mutation, M2225R. Like humans with the mutation, Piezo1 M-R mice demonstrated signs of DHS, providing important validation of the model. Electrophysiological studies of affected RBCs revealed a dramatic delaying of channel deactivation following mechanical stimulus. Non-RBC phenotypic effects of Piezo1 GOF were identified for the first time, most strikingly a disposition towards lipogenesis and insulin resistance. Piezo1 M-R mice following high fat diet intervention did not exhibit the same increased lipogenesis, but instead had reduced physical activity.

Analogues of Piezo1 agonist Yoda1 were synthesised by the School of Chemistry and were tested for their ability to activate the channel or inhibit the Yoda1 response. Important structural requirements for Piezo1 interaction were identified, in addition to a new pharmacological tool, Dooku1, which can inhibit Yoda1-induced Piezo1 activation in endogenously expressed channels.

Conclusion

The data reveal that the true mechanisms for Piezo1-causing disease are distinct from those identified by overexpression studies. This is important for targeting therapies to treat these diseases. Additionally, the study has revealed that in addition to DHS, people with Piezo1 GOF mutations may have other disease risk. This is relevant due to high incidence of Piezo1 mutations in people of African origin, owing to a protection against malaria. Understanding the mechanism for Piezo1 GOF and phenotypic effects of such a defect is important for uncovering additional physiological roles of the channel and for relation to DHS patients with Piezo1 mutations.

Table of Contents

List of Tables

List of Figures

Abbreviations

ANP	Atrial Natriuretic Peptide
ASIC	Acid Sensing Ion Channel
ATP	Adenosine Triphosphate
BAT	Brown Adipose Tissue
BNP	Brain Natriuretic Peptide
BSA	Bovine Serum Albumin
CED	C-terminal Extracellular Domain
CD	C-terminal Domain
ChREBP	Carbohydrate Response Element Binding Protein
CICR	Calcium Induced Calcium Release
CHOP	C/EBP Homologous Protein
CLAMs	Comprehensive Laboratory Animal Monitoring System
CRISPR	Clustered Regularly Interspaced Short Palindromic Repeats
DHS	Dehydrated Hereditary Stomatocytosis
DPBS	Dulbecco’s Phosphate Buffered Saline
DGAT2	Diacylglycerol O-Acyltransferase
DMEM	Dulbecco’s Modified Eagle’s Medium
DMSO	Dimethylsulfoxide
ECM	Extracellular Matrix
EDHF	Endothelial Derived Hyperpolarising Factor
EDTA	Ethylenediaminetetraacetic Acid
ELOVL6	Fatty Acid Elongase 6
ENaC	Epithelial Sodium Channel
EM	Electron Microscopy
eNOS	Endothelial Nitric Oxide Synthase
eWAT	Epididymal White Adipose Tissue
ER	Endoplasmic Reticulum
FA	Focal Adhesions

FAS	Fatty Acid Synthase
FS	Fractional Shortening
GAPDH	Glyceraldehyde 3-Phosphate Dehydrogenase
GFP	Green Fluorescent Protein
GOF	Gain Of Function
GLD	Generalised Lymphatic Dysplasia
gRNA	Guide RNA
GTT	Glucose Tolerance Test
H&E	Hematoxylin & Eosin
HEK	Human Embryonic Kidney
HDL	High Density Lipoprotein
HDR	Homology Directed Repair
HDW	Haemoglobin Distribution Width
HFD	High Fat Diet
HMGCoAR	Hydroxyl Methylglutaryl CoA Reductase
HSL	Hormone Sensitive Lipase
HUVEC	Human Umbilical Vein Endothelial Cells
HX	Hereditary Xerocytosis
IP_3R	IP_3 Receptor
ITT	Insulin Tolerance Test
K2P	Two Pore Domain Potassium Channel
KCNN4	Potassium Activated Calcium Channel
kDA	Kilodaltons
KO	Knockout
LPL	Low Density Lipoprotein
LVID	Left Ventricular Internal Diameter
MA	Mechanically Activated
MCH	Mean Corpuscular Haemoglobin
MCV	Mean Corpuscular Volume
MCP1	Monocyte Chemoattractant Protein 1

mLSEC	Mouse Liver Sinusoidal Endothelial Cells
MMP9	Matrix Metalloproteinase 9
mRNA	Messenger RNA
MTTP	Microsomal Triglyceride Transfer Protein
N2A	Mouse Neuroblastoma Cell Line
NAADP	Nicotinic Acid Adenine Dinucleotide Phosphate
NCX	Na^{+}-Ca^{2+} Exchanger
NMR	Nuclear Magnetic Resonance
NO	Nitric Oxide
P2X	ATP-Gated Purinoreceptor
PE	Phenylephrine
PFA	Paraformaldehyde
PGC1a	PPARγ Coactivator 1 Alpha
PMCA	Plasma Membrane Ca^{2+} ATPase
PPAR	Peroxisome Proliferator Activated Receptor
PVDF	Polyvinylidene Fluoride
RBC	Red Blood Cell
RDW	Red Cell Distribution Width
RER	Respiratory Exchange Ratio
RT	Room Temperature
RT-PCR	Real Time- Quantitative Polymerase Chain Reaction
RyR	Ryanodine Receptor
SBS	Standard Bath Solution
SCD1	Stearoyl-CoA Desaturase 1
scWAT	Subcutaneous White Adipose Tissue
SERCA	Sarcoplasmic Reticulum Ca^{2+} ATPase
SDS	Sodium Dodecyl Sulphate
siRNA	Short Interfering RNA
SOCE	Store Operated Calcium Entry
SREBP	Sterol Regulatory Element Binding Protein

STIM1	Stromal Interaction Molecule 1
TNFα	Tumour Necrosis Factor α
TPC	Two Pore Channel
TRP	Transient Receptor Potential
TRPA	Transient Receptor Potential Ankyrin
TRPC	Transient Receptor Potential Canonical
TRPM	Transient Receptor Potential Melastatin
TRPML	Transient Receptor Potential Mucolipin
TRPV	Transient Receptor Potential Vanilloid
VGCC	Voltage Gated Calcium Channel
VLDL	Very Low Density Lipoprotein
WT	Wildtype

Publications and Communications

First author

Evans, E.L*., Cuthbertson, K*., Endesh, N*., Rode, B., Blythe, N.M., Hyman, A.J., Hall, S.J., Gaunt, H.J., Ludlow, M.J., Foster, R and Beech, D.J. (2018). Yoda1 analogue (Dooku1) which antagonizes Yoda1-evoked Piezo1 and aortic relaxation. *British Journal of Pharmacology* 175: 1744-1759. (*) Equal contributors.

Evans, E.L*., Postyvan, O.V*., De Vecchis, D., Macrae, F., Lichtenstein, L., Futers, TS., Parsonage, G., Humphreys, N., Adamson, A., Kalli, A.C., Ludlow, M.J and Beech. D.J. Slow kinetics of native RBC Piezo1 and the disruption of deactivation by Dehydrated Hereditary Stomatocytosis mutation. **Submitted.** (*) Equal contributors.

Evans, E.L., Endesh, N., Ludlow, M., Blythe, N.M., Musialowski, K.E., Bartoli, F., Futers, TS., Myers, D., Parsonage, G., Humphreys, N., Adamson, A., Li, J., Calaghan, S.C., Drinkhill, M.J., Turner, N.A., Lichtenstein, L and Beech, D.J. Diverse RBC-independent effects of Piezo1 gain-of-function. **In preparation.**

Co-author

Blythe, N.M., Muraki, K., Ludlow, M.J., Stylianidis. V., Gilbert, H.T.J., **Evans, E.L.,** Cuthbertson, K., Foster, R., Swift, J., Li, J., Drinkhill, M.J., van Nieuwenhoven, F.A., Porter, K.E., Beech, D.J and Turner, N.A. (2019). Mechanically activated Piezo1 channels of cardiac fibroblasts stimulate p38 mitogen-activated protein kinase activity and interleukin-6 secretion. *Journal of Biological Chemistry.*

Bartoli, F., Debant, M., **Evans, E.L.,** Lichtenstein, L., Futers, T.S., Roberts, L.D and Beech, DJ. Endothelial Piezo1 determines muscle microvascular density and physical capability. **In preparation.**

Lichtenstein, L., Bartoli, F., **Evans, E.L.,** Debant, M., Futers, T.S., Raey, M., Parsonage, G., Roberts, L.D, Sukumar, P and Beech, D.J. Piezo1 force sensor in endothelium regulates hepatic lipid metabolism and insulin sensitivity. **In preparation.**

Communications

Haematological characterisation of mice with Piezo1 gain-of-function mutation. **E L Evans**, J Shi, M J Ludlow, L Lichtenstein and D J Beech. BPS19. 63rd Annual Meeting of the Biophysical Society, Baltimore, Maryland (2019).

Dooku1- an inhibitor of Yoda1-induced Piezo1 channel activity. **EL Evans**, K Cuthbertson, N Endesh, B Rode, NM Blythe, MJ Ludlow and DJ Beech. International Union of Physiological Societies (IUPS) 38th World Congress, Rhythms of Life, Rio de Janeiro (2017).

Chapter 1 Introduction

Piezo1 is a mechanosensitive cation channel, first identified in 2010. The era of mechanobiology post Piezo1 discovery has been dynamic and exciting with many previous mysteries of mechanotransduction now being answered. The channel has vast physiological functions in important bodily systems such as the vasculature. Additionally, human conditions associated with Piezo1 mutations exist; namely an anaemia termed dehydrated hereditary stomatocytosis (DHS) and generalised lymphatic dysplasia (GLD). Gain of function mutations in the Piezo1 channel which generally cause DHS are conserved, particularly within the African population where they exist in 1/3 of people, owing to a protection against malaria (Albuisson et al., 2013, Andolfo et al., 2013, Zarychanski et al., 2012, Ma et al., 2018). Therefore, understanding the nature of Piezo1 mutations, both how they affect channel function and also the body as a whole, is important for detecting unrecognised disease predisposition in these patients and uncovering additional roles of Piezo1. Developing new pharmacological tools with which to possibly target these diseases or other functions of the channel is important for Piezo1 therapies to be realised.

This chapter will provide a background to the Piezo1 ion channel, detailing its electrophysiological properties and roles in physiology, both within and outside the cardiovascular system. It will also present the role of Piezo1 in pathophysiology, discussing mutations in the channel associated with disease. Some of the complexities of Piezo1 channel kinetics will be presented which are often affected by disease-causing mutations, in addition to the current pharmacological tools with which to study the channel.

1.1 Mechanotransduction

Cells are both subjected to and exert their own mechanical forces which provide information about the nature of their environment and allow for interaction of cells with the outside world and with each other. In order to understand and react to these mechanical cues, organisms have developed mechanotransduction; the ability to produce specific biological responses to mechanical forces. Mechanosensitivity is a common property of all cells conserved across animal,

plant and prokaryotic species. Within mammals, the heart and vasculature are influenced by pressure and shear stress from circulating blood, bone shape is determined by compression forces and muscle contraction, pulmonary physiology is regulated by inflation and deflation of the lungs and sensory systems such as hearing and touch are founded on responses to pressure. Even the growth of cells and tissues is dependent on mechanical forces.

Due to the vast array of mechano-dependent events in physiology, the mechanisms of mechanotransduction are varied to grant sensitivity and selectivity to distinct mechanical cues. In general, conformational changes conferred on proteins directly from the mechanical force result in functional modifications facilitating signal transduction (Orr et al., 2006). A large number of mechanosensors or transducers have been identified, namely integrins, G protein coupled receptors, growth factor receptors and mechanically-activated (MA) ion channels. However, only integrins and MA ion channels are inherently mechanosensitive.

1.1.1 Mechanosensation

1.1.1.1 Integrins

Integrins are present at focal adhesions (FA) which are sites at which the cell interacts with the extracellular matrix (ECM). Here, mechanical cues such as extracellular changes in stiffness or tension can be detected and communicated to the cell cytoskeleton. Integrins are heterodimers composed of α and β subunits of which there are many different types, the combination of which can grant selectivity for different ECM proteins, including fibronectin, laminins and collagen. Integrins span the membrane so that their extracellular domain is in contact with the ECM, whereas their cytoplasmic domain interacts with the cytoskeleton. When exposed to their ECM ligand, integrins undergo a conformational change and become activated, recruiting numerous proteins and coupling to different signalling cascades within the cell to mediate mechanotransduction (Martino et al., 2018).

Important functions of integrins are found throughout physiology, including the vasculature, immune system and central nervous system. Mice deficient in integrin subtype β8 are not viable or die shortly after birth with leaky, disorganised blood vessels (Zhu et al., 2002). Within the immune system integrins play a role

in T cell differentiation and migration to specific target organs (Bertoni et al., 2018). They are also important mediators of axonal regeneration following nerve injury (Nieuwenhuis et al., 2018). Integrin-mediated mechanotransduction is affected in diseases such as cancer which can cause dysregulation of the ECM and tissue stiffening (Sun et al., 2016).

1.1.1.2 Mechanically-activated ion channels

The existence of MA ion channels has been known for several decades (Guharay and Sachs, 1984), but their molecular identity has remained elusive. In order for a candidate MA channel to be classified as inherently mechanosensitive, certain criteria have been suggested (Ernstrom and Chalfie, 2002). Firstly, the ion channel should be expressed in a mechanosensitive cell and ablation of the gene should result in a loss of mechanosensitivity. Introduction of the gene to an otherwise insensitive cell should confer mechanical sensitivity and evidence that the candidate forms the pore-forming subunit of the ion channel is needed. Additionally, the candidate should still retain mechanosensitivity without the presence of auxiliary proteins when purified and reconstituted into lipid bilayers. Many channels contribute to mechanosensitivity in mammals, but only a few putative mechanosensitive channels have been identified which meet all of these requirements and will be detailed below (Ranade et al., 2015).

1.1.1.2.1 Two- pore potassium channels

Potassium channels are unique in that their activation causes membrane hyperpolarisation rather than depolarisation, therefore opposing cellular excitation. These channels have an important role in setting the resting membrane potential in excitable cells. Mechanically-gated potassium channels belong to the family of two-pore (2P) domain K^+ channels and mechanically sensitive members include TREK-1, TREK-2 and TRAAK (Brohawn et al., 2014). All these channels activate in response to negative pressure and TREK-1 and TRAAK are also sensitive to cellular volume and close in response to hyperosmolarity. It is likely that mechanical forces are transmitted to the channels indirectly via the lipid bilayer. The channels are polymodal, activated by a number of stimuli including polyunsaturated fatty acids (Patel and Honoré, 2001). Mice deficient in either of the channels are more sensitive to mechanical stimuli,

consistent with the hypothesis that K2P channels act to dampen the activity of neurons (Heurteaux et al., 2004, Noël et al., 2009, Pereira et al., 2014).

1.1.1.2.2 TRP channels

Transient receptor potential (TRP) channels are tetrameric non-selective cation channels made up of a large family of 28 members in mammals, comprising of six subgroups; TRPC (canonical), TRPV (vanilloid), TRPM (melastatin), TRPA (ankyrin), and TRPML (mucolipin). They are polymodal sensors able to participate in chemosensation, thermosensation and photosensation in addition to mechanosensation (Venkatachalam and Montell, 2007).

Members of many of the subgroups have been identified as mechanosensitive (Startek et al., 2019). Members of the TRPV (TRPV1/TRPV2/TRPV4) and TRPM (TRPM3/7) families can respond to osmotic swelling (Naeini et al., 2006, Muraki et al., 2003, Liedtke et al., 2000, Grimm et al., 2003, Numata et al., 2007). Physiological roles of TRP mechanosensation have been elucidated. TRPV4 is present in chondrocytes, the cellular components of cartilage, where the channels can mediate current in response to deflection stimuli and have an important role in transduction of mechanical forces to support joint health (Rocio Servin-Vences et al., 2017, O'Conor et al., 2014). TRPM4 is able to sense pressure in smooth muscle cells and contribute to myogenic vasoconstriction (Earley et al., 2004). Additional roles of mechanosensitive TRP channels in the vasculature are found with TRPC6 which can be activated by mechanical stimuli and appears to sense vascular pressure and control vascular tone. TRPM7 is also able to respond to fluid flow (Oancea et al., 2006). TRPP1 and 2 have been implicated in fluid sensation in the renal epithelium (Nauli et al., 2003) and mutations in these proteins are linked to polycystic kidney disease (Mochizuki et al., 1996, The European Polycystic Kidney Disease, 1994). However, the intrinsic mechanosensitivity of these channels is debated (DeCaen et al., 2013).

1.1.1.2.3 Piezo channels

More recently the Piezo family of ion channels have been discovered, comprised of Piezo1 and Piezo2 (Coste et al., 2010). These channels are inherently mechanosensitive, responding to a range of mechanical stimuli. The following section of this chapter will focus on Piezo1 and detail the discovery of the channel

and its role in physiology and pathophysiology. A short section on Piezo2 will follow.

1.2 Piezo1

1.2.1 Discovery

Despite a few known MA channels which have been described, the proteins involved in many mammalian mechanotransduction events remained elusive. In 2010 a dramatic breakthrough in the field of mechanobiology emerged with the discovery of two new MA cation channels (Coste et al., 2010). The group responsible for this finding observed robust MA currents in a mouse neuroblastoma cell line (N2A) which responded to both positive pressure in the form of cell poking and negative pressure via suction of the cell-membrane. To identify the responsible MA ion channels, the group used microarrays to identify transcripts enriched in N2A cells. They focused their search by scanning for proteins predicted to span the membrane at least twice (a common feature of all ion channels). Using an siRNA targeted approach, these candidates were knocked down in turn and the MA currents of the cells were measured. After a thorough screen, it was found knockdown of *Fam38A* caused a dramatic decrease in these currents; the gene was named Piezo1 from the Greek word for pressure.

Investigating the phylogenetic tree of Piezo revealed that many plant, animal and eukaryotic species contain Piezo1 and vertebrates have two members; Piezo1 and Piezo2. Piezo1 was well expressed in the mouse with presence in bladder, colon, lung, kidney and skin. Piezo2 was also observed in the bladder, colon and lung but had strong expression in dorsal root ganglion (DRG) sensory neurons, suggesting a role of the protein in somatosensation.

Cloning full-length versions of Piezo1 and Piezo2 and transfecting these into mechanically insensitive HEK293 cells, resulted in MA currents proving that the Piezo proteins are themselves mechanically sensitive and are likely MA ion channels, if not non-conducting subunits of MA ion channels. Evidence that the Piezos were in fact ion channels in their own right was later shown by reconstituting mouse Piezo1 into lipid bilayers with no other cellular compartments and observing cationic ion channel activity which was sensitive to non-selective cation channel inhibitor, ruthenium red (Coste et al., 2012).

1.2.2 Piezo1 structure

Piezo1 has a unique structure which shares little homology with other ion channels (Figure 1-1). Despite distinct genetic backgrounds, it is most similar in structure to the purinergic receptor, P2X and acid-sensing ion channels (ASIC) (Kawate et al., 2009, Gonzales et al., 2009). All three channels are trimeric, the pores have a large extracellular domain and each has a lateral fenestration below this extracellular domain which opens to the pore. It has been hypothesised that these features are necessary for a trimeric ion channel of this type, whereas the other features of Piezo1 (beam and flexible blades) may be necessary to confer mechanosensitivity (Guo and MacKinnon, 2017). Originally, photobleaching with GFP-tagged mPiezo1 and crosslinking studies, predicted that Piezo1 existed as a homotetramer (Coste et al., 2012). However, the cryo-EM structure of full-length (2,547 amino acids) mouse Piezo1 was resolved in 2015 to 4.8 Å and revealed it exists as a trimer with a distinctive propeller-like structure of 900 kDA (Ge et al., 2015). The N-terminal regions form flexible blades which surround the central conducting pore and it was proposed that these peripheral regions could represent the force sensors of the ion channel.

More recently, higher resolution cryo-EM structures have emerged which each complement each other (Zhao et al., 2018, Saotome et al., 2017, Guo and MacKinnon, 2017). Nine-repetitive units (termed Piezo repeats) with four transmembrane helices each (38 total) have been identified which comprise the highly-curved blade region (Zhao et al., 2018). The central C-terminal domain is linked to these transmembrane helices by long rods, termed beams, which are considered an ideal structure for mechanical transduction from the distal blades to the central ion-conducting pore. It was noted that the Piezo1 repeats cause local membrane deformation in the form of a dome which was hypothesised to change upon channel opening (Guo and MacKinnon, 2017, Saotome et al., 2017). This characteristic has since been studied in more detail via atomic force microscopy and it has been shown that upon force, Piezo1 flattens in plane with the membrane (Lin et al., 2019).

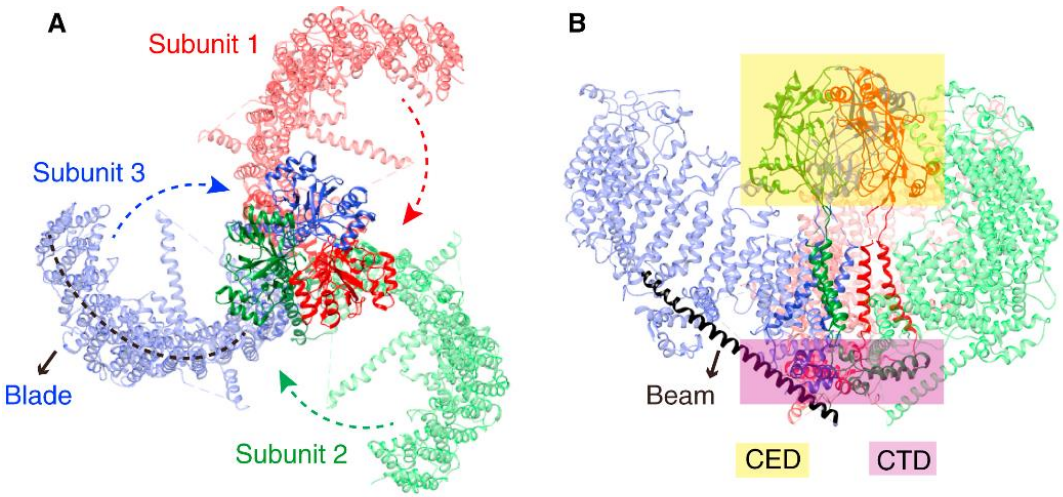

Figure 1-1 Cryo-EM structure of Piezo1. (A) Top view of Piezo1 showing the organisation of the 3 subunits, each shown in a different colour. The dashed black line indicates one of the 3 'blades'. (B) Side view of Piezo1 with CED (C-terminal extracellular domain) highlighted in yellow and CTD (C-terminal domain) highlighted in pink. One of the 3 'beams' is indicated in black (Liang and Howard, 2018).

1.2.3 Piezo1 properties

Piezo1 has electrophysiological properties which are typical for non-selective cation channels, notably that the current-voltage (IV) plot for the channel is linear, with the reversal potential at 0mV. Single-channel conductance is 22.9 pS (Coste et al., 2010). The channel is permeable to monovalent and some divalent cations, such as Mg^{2+} and Ca^{2+} (Gnanasambandam et al., 2015, Gottlieb et al., 2012), but of particular interest is its permeability to Ca^{2+} as calcium entry through MA channels has been linked to downstream physiological effects (Hoyer et al., 1994, Wang et al., 2016). The importance of Ca^{2+} homeostasis will be described in a later section in this chapter.

The channel can be activated by a whole host of mechanical stimuli, notably cell poking, suction, laminar flow, cellular compression and membrane tension and does not require other cellular components or second messengers for mechanical activation (Coste et al., 2010, Li et al., 2014, Lee et al., 2014, Lewis and Grandl, 2015, Syeda et al., 2016). Piezo1 is sensitive to the amount of force applied and conducts more current and permits more Ca^{2+} entry with increased mechanical load, rather than an all or nothing approach when a necessary

mechanical threshold is reached (Coste et al., 2012, Li et al., 2014). This suggests the channels are able to fine-tune their responses to mechanical forces and provide specialised responses dependent on the stimulus.

Piezo1 channels are sensitive to pH and voltage. Low pH which is caused in the body by tissue injury such as myocardial infarction reduces Piezo1 mediated current (Bae et al., 2015). Piezo1 is modulated by voltage and inactivation is much slower or completely absent at positive voltages compared to negative voltages. Additionally, desensitisation of the channels which can occur with repetitive mechanical stimuli can be removed following outward permeation through Piezo1, driven by positive electrochemical gradients (Moroni et al., 2018).

1.2.4 Piezo1 in physiology

Due to the multitude of mechanical stimuli which can activate Piezo1, in addition to its widespread expression, it is perhaps not surprising that the channel has an extensive role in mammalian physiology. One of the first noted functions of Piezo1 and of particular interest to our laboratory is the role of the protein in the vasculature, specifically within the endothelial cells which line the blood vessels. Research demonstrating the importance of Piezo1 function in this area is convincing and will be presented in detail, before brief coverage of additional channel functions throughout the body.

1.2.4.1 Cardiovascular biology

1.2.4.1.1 Vascular development

Piezo1 is essential in sensing the mechanical environment in blood vessels, by being able to detect laminar blood flow, termed shear stress. Our laboratory has been particularly interested in decoding Piezo1's role in endothelial cells, the specialised cells that line the inside of blood vessels. Global deletion of Piezo1 proved embryonically lethal, most pups only surviving until embryonic day E9.5-11.5 which is a critical time for vascular development. Staining of the vasculature from embryos and yolk sacs revealed that the vessels in these pups were not well developed with leaky, disorganised vasculature compared to Piezo1 WT littermates. Deletion of Piezo1 specifically from endothelial cells produced the

same phenotype, suggesting a requirement of the ion channel in these specialised cells (Li et al., 2014).

Mechanical force in the form of fluid flow was able to cause Ca^{2+} entry in HUVECs (Human Umbilical Vein Endothelial Cells) which was Piezo1 dependent, revealing Piezo1's role as a shear stress sensor. Alignment of endothelial cells in the direction of fluid flow is a process that occurs naturally in blood vessels, but this was suppressed in HUVECs by Piezo1 depletion or pharmacological inhibition and a similar phenomenon was observed in endothelial cells isolated from Piezo1 knockout (KO) embryos. It was hypothesised that shear stress induced Ca^{2+} entry via Piezo1 was coupled to the activity of calpain-2, a Ca^{2+}-activated proteolytic enzyme with a role in endothelial cell alignment to shear stress (Li et al., 2014). The role of Piezo1 in vascular development and shear stress sensing has been confirmed by another group who showed similar findings (Ranade et al., 2014a). More recently endothelial Piezo1 has been implicated in angiogenesis in adult mice, whereby endothelial Piezo1 KO mice have impaired wound healing and delayed re-vascularisation following vessel ligation (Kang et al., 2018).

1.2.4.1.2 Hypertension-dependent arterial remodelling

In addition to expression in vascular endothelium, Piezo1 is also expressed in arterial smooth muscle cells. The opening of mechanosensitive ion channels in these smooth muscle cells has previously been suggested to contribute to the myogenic response (Folgering et al., 2008). This describes the vasoconstriction of small diameter blood vessels following an increase in vascular pressure, a mechanism present to facilitate blood flow and produce basal tone which can be acted on by vasorelaxing agents (Davis and Hill, 1999). However, it appears Piezo1 is not involved as normal myogenic tone was observed in multiple vascular beds from mice lacking the channel from smooth muscle cells (Retailleau et al., 2015).

Instead, smooth muscle Piezo1 is involved in arterial remodelling following hypertension. Wild-type (WT) mice experienced an increase in caudal artery diameter and cross-sectional area after hypertensive conditions, but this remodelling was absent in smooth muscle Piezo1 KO mice, indicating that the channel facilitates adaptive responses to mechanical stress (Retailleau et al.,

2015). Arterial remodelling occurring in hypertensive patients is associated with increased risk of cardiovascular events, indicating Piezo1 may be a useful therapeutic target (Mathiassen et al., 2007).

1.2.4.1.3 Blood pressure control

The role of Piezo1 in blood pressure control is less clear than its role in vascular development. Shear stress and pharmacologically induced Ca^{2+} entry via Piezo1 has been shown to be coupled to phosphorylation of endothelial nitric oxide synthase (eNOS), which produces nitric oxide (NO), the primary vasorelaxing factor produced by endothelial cells. Application of fluid flow to mesenteric arteries resulted in a strong vasodilation which was absent from mice lacking endothelial Piezo1. Conditional knockout of endothelial Piezo1 from adult mice by tamoxifen injection, resulted in an increase in systolic blood pressure (10-15 mmHg), which correlated with a decrease in plasma nitrate levels and phosphorylation of eNOS, suggesting Piezo1-mediated signalling in endothelial cells is a key regulatory mechanism controlling vascular tone (Wang et al., 2016).

However, conditional knockout of endothelial Piezo1 in our laboratory had no impact on blood pressure of inactive mice, and in fact lowered blood pressure in active mice, which correlated with a decreased physical performance (Rode et al., 2017). Wire myography experiments with mesenteric artery from endothelial Piezo1 KO mice showed that the presence of Piezo1 has an anti-EDHF (endothelial dependent hyperpolarising factor) effect. That is to say the channel naturally mediates constriction in these vessels, by contributing to depolarisation of endothelial cell membranes and therefore activating voltage-gated Ca^{2+} channels in neighbouring vascular smooth muscle cells. This anti-EDHF effect was vascular bed specific and not present in saphenous artery (supplying blood to the skeletal muscle of the leg) or carotid artery (supplying blood to the brain). It was suggested that Piezo1 can act as an exercise sensor in the vasculature, resulting in the constriction of resistance mesenteric arteries, allowing useful diversion of blood to the active muscles, improving physical performance (Rode et al., 2017).

More recently, the role of Piezo1 in combination with Piezo2 has been shown in neural control of blood pressure, suggesting Piezos may act as baroreceptors; stretch-sensitive neurons within the ganglia in the walls of the aorta and carotid

sinus (Zeng et al., 2018). Activation of baroreceptors via an increase in blood pressure is transmitted to the central nervous system via afferent signals, resulting in the 'baroreceptor response'; a decrease in heart rate, cardiac output and vascular resistance, all acting to oppose the original increase in blood pressure (Wehrwein and Joyner, 2013). Other ion channels have been proposed to contribute to baroreception (ENaC, ASIC2, TRPC5) however, the baroreceptor response still remains even when channel activity is abolished (Drummond et al., 1998, Lu et al., 2009, Lau et al., 2018, Thakore et al., 2018).

Expression of Piezo1 and Piezo2 mRNA was detected in baroreceptors and the effect of knocking out the expression of either channel, or both in combination, from ganglia involved in the baroreceptor reflex, was tested against a baroreceptor response resulting from phenylephrine (PE) injection. PE induces vasoconstriction, therefore increasing blood pressure and initiating the baroreceptor response resulting in a decrease in heart rate and blood pressure. The baroreceptor reflex measured by the change in heart rate and blood pressure after PE injection was dramatically reduced in the double KO, but interestingly not in either of the single KOs (Zeng et al., 2018). There was also increased variability in blood pressure of awake double KO mice measured over 72 hours. The study suggests that both Piezo1 and Piezo2 are required for baroreceptor function.

To date the precise role of Piezo1 in blood pressure regulation is unclear, but it is evident the channel can participate in both peripheral and central control. In part this uncertainty can be due to the multi-factorial control of blood pressure, but also that cation entry through peripheral Piezo1 can conceivably cause both vessel relaxation via coupling to nitric oxide and contraction via depolarisation and activation of voltage-gated Ca^{2+} channels in smooth muscle cells (Rode et al., 2017). A clear picture of Piezo1's involvement in blood pressure is essential if it is ever to be harnessed as a therapeutic target.

1.2.4.1.4 Heart function

The rhythmic pumping of the heart results in constant mechanical stimulation of cardiac cells. Therefore it is conceivable that Piezo1 may have a role in cardiac physiology or pathophysiology, however, studies of the ion channel in this important organ are still limited. Heart failure induced by myocardial infarction in

rats caused an increase in Piezo1 mRNA and protein expression in whole heart. To determine why Piezo1 expression was upregulated in heart failure, neonatal rat ventricular cardiomyocytes (NVRMs) were treated with various stimulating factors secreted during cardiac remodelling and only angiotensin II (AngII) increased Piezo1 mRNA and protein levels. The AngII type 1 receptor (AT1) blocker losartan was able to inhibit AngII-mediated increases in Piezo1 mRNA expression in NVRMs and MI-mediated increases in Piezo1 expression in rats (Liang et al., 2017). On the other hand, cyclic stretch of an adult human ventricular cardiomyocyte cell line (AC16) showed reduced Piezo1 expression as early as 24h after stretching (Wong et al., 2018).

Piezo1 has been implicated in cardiac aortic valve development. Disrupting Piezo1 signalling in zebrafish, resulted in impaired, misshapen development of aortic valves which are essential for regulating blood flow ejected from the ventricle. Exome sequencing of ~50 patients with valvulopathies identified 3 variants in Piezo1 in varying regions of the protein which were all predicted to be pathogenic (Faucherre et al., 2019).

Functional Piezo1 protein has also been detected in cardiac fibroblasts in our laboratory. Yoda1 treatment of murine or human cardiac fibroblasts increased the expression of interleukin-6 (IL-6), a cytokine promoting cardiac hypertrophy and fibrosis following cardiac injury. This was Piezo1 dependent and occurred via p38 MAP kinases, downstream of Ca^{2+} entry (Blythe et al., 2019b). The data suggest that activation of Piezo1 in cardiac fibroblasts may play a role in cardiac remodelling, a process which originally acts to preserve cardiac output, but can become maladaptive leading to fibrosis and reduced cardiac function (Fan et al., 2012).

1.2.4.1.5 Red blood cells

Red blood cells (RBCs) encounter constant mechanical forces as they manoeuvre through the circulatory system, being squeezed through narrow capillaries repeatedly in their lifetime. Mechanical forces exerted on RBCs are able to cause increased Ca^{2+} entry which activate downstream anionic and cationic channels, notably the Ca^{2+}-activated K^+ channel (termed Gardos channel) which can affect RBC hydration and therefore volume (Dyrda et al., 2010). Piezo1 was identified as the protein responsible for this mechanically-

induced Ca^{2+} transient in RBCs as mice lacking the channel in their RBCs showed no Ca^{2+} influx following mechanical stimulation (Cahalan et al., 2015). This correlated with alterations in RBC volume regulation as RBCs from these mice appeared overhydrated with increased osmotic fragility; overhydrated RBCs have also been observed in zebrafish lacking Piezo1, although this is disputed (Faucherre et al., 2014, Shmukler et al., 2015).

Chemical activation of Piezo1 channels resulted in opposing changes in RBC volume causing dehydration, which was missing in the Piezo1 RBC KO mutants. Chemical activation also reduced osmotic fragility which could be rescued by Gardos channel antagonist, TRAM-34, linking Ca^{2+} entry through Piezo1 to downstream channel activation as previously mentioned and depicted in Figure 1-2. Mutations of Piezo1 have been identified in humans with disorders resulting from abnormal red blood cell hydration, confirming the importance of the channel in red blood cell volume regulation. These are discussed in more detail in a later section.

Mechanical stimulation has also been shown to induce release of ATP from RBCs (Wan et al., 2008). This released ATP can contribute to vascular tone by binding to and activating P2Y receptors on endothelial cells of blood vessels, stimulating the release of vasorelaxing agent, nitric oxide (Janigro et al., 1996). Treatment of human RBCs with Piezo1 inhibitors reduced shear stress induced Ca^{2+} influx and ATP-release demonstrating a further role of the channel in RBCs (Cinar et al., 2015).

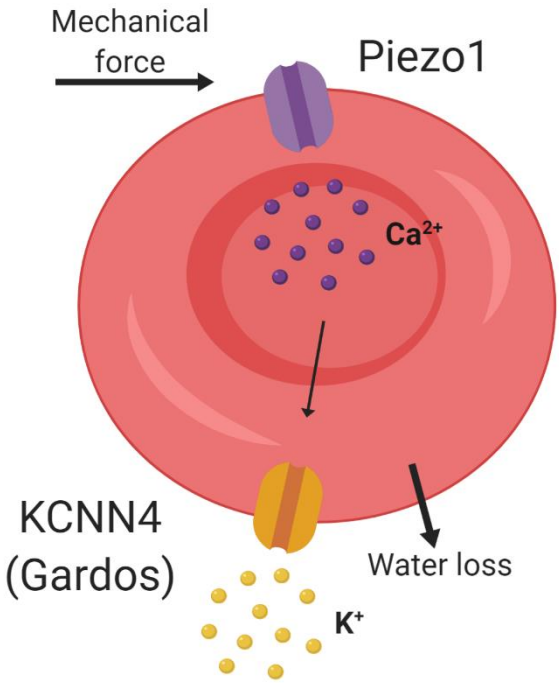

Figure 1-2 Mechanism of RBC dehydration via Piezo1 activation. Mechanical force activates Piezo1 leading to Ca^{2+} entry. This then activates the Ca^{2+} - activated K^+ channel (KCNN4/Gardos), leading to K^+ loss and then water loss via osmosis.

1.2.4.2 Piezo1 functions beyond the cardiovascular system

Piezo1 has extensive roles in physiology, outside of the cardiovascular system; as summarised in Figure 1-3. The channel appears to be the body's global mechanotransducer and additional roles of the protein are emerging at an impressive rate. As Piezo1 can be activated by and respond to many different types of force it is adept at sensing varying mechanical stimuli within the body.

Piezo1 is important for neural development as the channel is able to sense the mechanical environment and direct the lineage choice of neural stem cells (Pathak et al., 2014). There are also reports that the channel can contribute to axon growth in *Xenopus* retinal ganglion cells (Koser et al., 2016), however Piezo1 appears to have an inhibitory effect on axon regeneration following injury in *Drosophila* and murine sensory neurons (Song et al., 2019), suggesting species or cell specific contributions to the channels role in the nervous system.

Within the musculoskeletal system, Piezo1 is present in chondrocytes of cartilage and mediates Ca^{2+} influx at hyper-physiological levels of compression, suggesting a role in joint injury (Lee et al., 2014). Interestingly, Piezo1 does this is synergy with Piezo2 presenting the possibility that the proteins can form a heteromeric channel. Additionally, Piezo1 is present in the bone forming osteoblasts and is required for healthy bone tissue growth in mice. Interestingly, in human patients with osteoporosis, a decrease in levels of the protein correlate with increased bone loss (Sun et al., 2019). Piezo1 is also a regulator of skeletal muscle formation, being modulated by changes in distribution of membrane lipids during myotube elongation (Tsuchiya et al., 2018).

More recently, a role of Piezo1 in metabolism has been presented with the observation that mice lacking the channel from adipocytes exhibit an altered metabolic phenotype including a reduction in white adipose tissue mass and insulin resistance (Zhao et al., 2019). The signalling events contributing to this altered metabolic phenotype remain undiscovered as yet.

Piezo1 is expressed in the epithelial cells in the proximal convoluted tubule (Peyronnet et al., 2013) and collecting duct of the kidney where it plays a role in regulating urinary osmolarity, after dehydration (Martins et al., 2016). The channel is also present in bladder urothelium where it mediates stretch-induced Ca^{2+} influx and ATP release *in vitro* and therefore likely contributes to detecting bladder distention (Miyamoto et al., 2014). More recently, analysis of Piezo1 expression has shown the channel is present throughout the whole urinary tract including the kidneys, ureters, bladder and urethra and in many cell types including epithelial, endothelial, parietal and smooth muscle cells (Dalghi et al., 2019).

The lungs are repeatedly exposed to mechanical stretch due to the cyclic nature of respiration and pulmonary injury tends to increase mechanical load. Although it has been known Piezo1 is expressed in the lung since its discovery (Coste et al., 2010), the function of the channel in the pulmonary system has remained unknown until recently. High pulmonary vascular pressures caused by high altitude, trauma and left heart failure can disrupt and breakdown the endothelial barrier, leading to leakage and pulmonary oedema. Piezo1 is present in the endothelial cells in the lung and when activated by increased microvascular pressure, promotes degradation of adherens junction (AJ) proteins via activation

of calpain, a calcium-dependent protease. Conditional deletion of Piezo1 from endothelial cells from mice, protects against oedema in mice subjected to increased microvascular pressure (Friedrich et al., 2019). Further roles of Piezo1 in pulmonary injury have been reported in acute respiratory distress syndrome and pulmonary hypertension where Piezo1 appears to contribute to apoptosis (Liang et al., 2019, Wang et al., 2019b). Additionally, Piezo1 signalling in myeloid cells of the lung aggravates a murine model of pulmonary fibrosis by potentiating autoinflammation (Solis et al., 2019).

Furthermore, Piezo1 is involved in mechanosensation in the immune system where it contributes to T cell activation (Liu et al., 2018). Mechanical force is also able to fine-tune the innate inflammatory response by communicating the nature of the microenvironment to recruited immune cells. Myeloid cells subjected to cyclical hydrostatic pressure similar to that experienced by cells in the lung, caused expression of proinflammatory molecules which was absent in cells from mice with conditional knockout of Piezo1 from myeloid cells. These gene-edited mice responded poorly to bacterial infection with increased bacterial loads and reduced immune-cell recruitment compared to WT littermates (Solis et al., 2019).

Piezo1 can sense both cellular crowding and stretch and can control epithelial cell density by triggering apoptosis or cell division (Gudipaty et al., 2017). Disruption of Piezo1 can result in the accumulation of epithelial cell masses (Eisenhoffer et al., 2012) and a functional channel has been detected in breast cancer (Li et al., 2015, Weng et al., 2018), gastric cancer (Yang et al., 2014) and prostate cancer cell lines (Han et al., 2019) where it is upregulated and contributes to cell migration and tumour growth. Additionally, in breast cancer patients, increased Piezo1 mRNA in the primary tumour is correlated with reduced survival (Li et al., 2015). However, the seemingly detrimental effect of Piezo1 in cancer development is not ubiquitous as loss-of-function mutations in the channel have been found in patients with colorectal adenomatous polyposis (Spier et al., 2016) and there is reduced Piezo1 expression in lung cancer cell lines, which resulted in increased cell migration via integrins (McHugh et al., 2012). Reduced Piezo1 expression is also found in cancerous tissue from lung cancer patients and higher Piezo1 expression in these patients correlated with improved survival (Huang et al., 2019).

Contribution of Piezo1 to pathological conditions is also evident in the pancreas, whereby infusion of Piezo1 agonist, Yoda1 into the pancreatic duct was sufficient to induce acute pancreatitis in mice. Pharmacological inhibition of Piezo1 or genetic deletion was sufficient to protect against a model of pressure-activated pancreatitis highlighting therapeutic potential of blocking Piezo1 activity (Romac et al., 2018).

Overall, it is evident that the physiological roles of Piezo1 are vast and the channel is an “all-rounder” of mechanosensation, adept at sensing varied mechanical cues and mediating specialised responses via calcium and collaboration with different signalling partners. Functional Piezo1 is necessary for many bodily functions, but balance of channel activation seems important as increased Piezo1 activity can be detrimental in disease progression (e.g. during pulmonary injury or pancreatitis). It is also noteworthy that the activity of Piezo1 can be both beneficial and seemingly damaging in cancer progression, depending on the tissue affected.

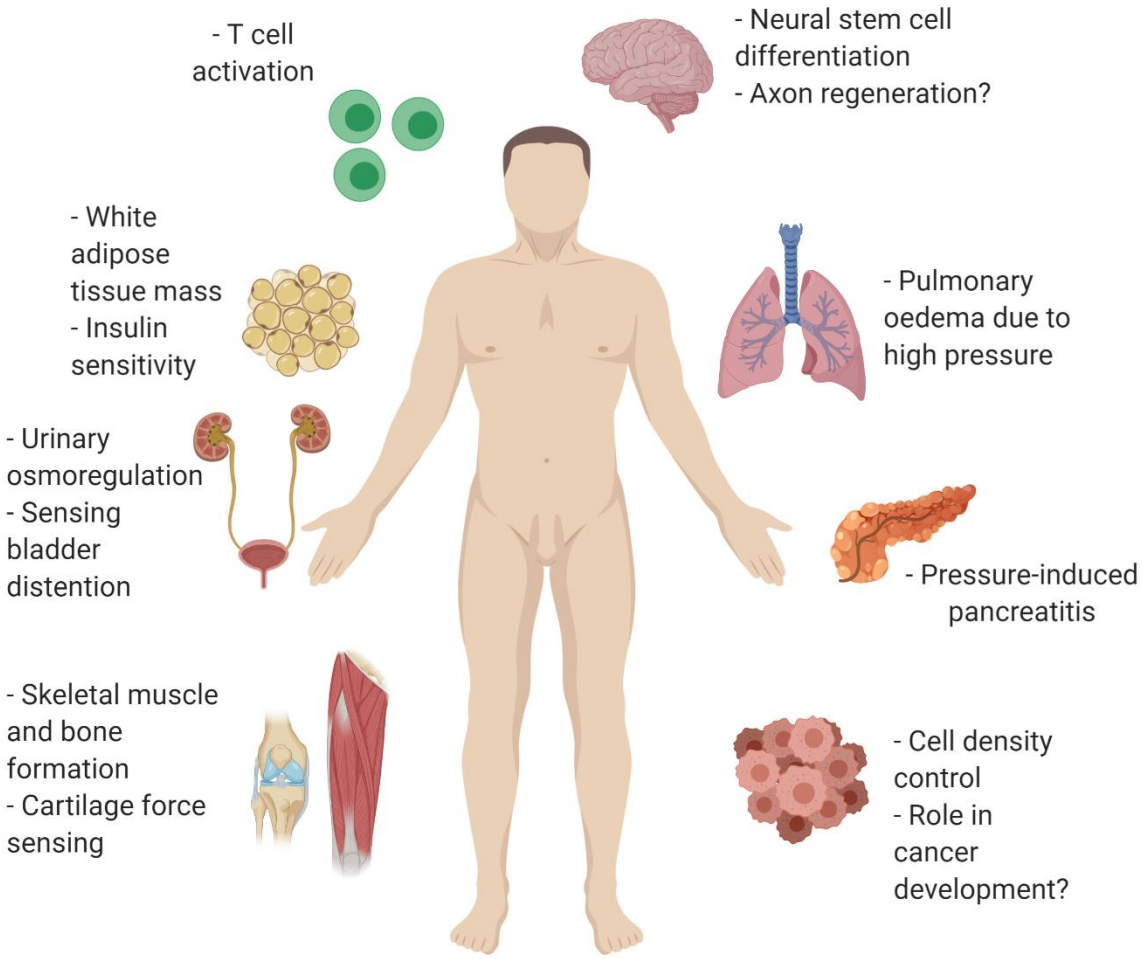

Figure 1-3 Non-vascular functions of Piezo1. Summary diagram showing the wide array of Piezo1 functions outside of the vasculature. A question mark is present when there are contradicting results for Piezo1 involvement.

1.2.5 Piezo1 in pathophysiology

The Piezo1 research presented so far has described the physiological effects of a functional Piezo1 channel. However, mutations in Piezo1 affecting the channel have been identified which correlate with two diseases; dehydrated hereditary stomatocytosis and generalised lymphatic dysplasia. The location of the residues mutated, in addition to the functional effects of the mutations and a description of the diseases themselves will be detailed.

1.2.5.1 Dehydrated hereditary stomatocytosis

Dehydrated hereditary stomatocytosis (DHS), also known as hereditary xerocytosis (HX) is a form of haemolytic anaemia, characterised by abnormal cation leak in RBCs resulting in RBC dehydration (Miller et al., 1971). It leads to cell fragility and loss of RBCs, the presence of “coffee-bean” shaped stomatocytes in blood smears, splenomegaly and occasionally perinatal oedema (Basu et al., 2003, Andolfo et al., 2016, Glogowska and Gallagher, 2015). The clinical phenotype of patients is variable with some patients exhibiting very few symptoms, whilst others experience potentially fatal hydrops fetalis, therefore it is a condition which can be difficult to diagnose (Andolfo et al., 2016). True diagnosis of DHS can only be confirmed with osmotic-gradient ektacytometry which reveals a leftward shift in the curve from cell dehydration, but the need for specialised equipment means this test can only be carried out in a limited number of laboratories (Delaunay, 2004).

In a genome-wide search for the DHS locus, the genetic cause of the disease was previously mapped to chromosome 16 (Grootenboer et al., 2000, Carella et al., 1998, Houston et al., 2011), prior to the discovery of Piezo1 which is located on this chromosome. Piezo1 was first associated with DHS in 2012 where whole-exome sequencing detected two mutations (M2225R and R2456H) in the C-terminal region of the channel in two unrelated kindreds with DHS. The mutations were dominantly inherited with most patients being heterozygous and the three homozygous patients exhibiting a more severe phenotype (Zarychanski et al., 2012). Additional, reports of Piezo1’s involvement in DHS quickly followed with the identification of novel channel mutations, mostly located in the 2nd half of the protein (Albuisson et al., 2013, Andolfo et al., 2013). This C-terminal domain has previously been shown to be important in determining the pore-related properties

of the channel (Coste et al., 2015). Following these early reports, multiple DHS-associated Piezo1 mutations have been identified and these are depicted in Figure 1-4. Many of these are from clinical case reports of patients with DHS (Beneteau et al., 2014, Risinger et al., 2014, Sandberg et al., 2014, Shmukler et al., 2014, Paessler and Hartung, 2015, Glogowska et al., 2017, Imashuku et al., 2016, Fermo et al., 2017, Andolfo et al., 2018a, Rotordam et al., 2018, Knight et al., 2019). Genotype-phenotype correlation analysis determined that those patients with Piezo1 mutations in the pore domain were more severely affected than those in the non-pore domain (Andolfo et al., 2018b).

DHS-associated Piezo1 mutations cloned and transfected into HEK293 cells mostly cause channel gain-of-function (GOF) by delaying channel inactivation after mechanical stimulation (Albuisson et al., 2013, Bae et al., 2013a). The mutants also display a latency of activation suggesting the mutations slow both channel opening and closing via an inactivation mechanism. However, it is important to note that both fast and delayed activation are observed in the same mutant in this study (Bae et al., 2013a). Some mutations caused an increased sensitivity to pressure (R2456H), but this was not evident with all mutations (M2225R) (Bae et al., 2013a, Glogowska et al., 2017). Several Piezo1 DHS mutations have been identified which do not delay channel inactivation, but instead cause increased mechanical sensitivity (Glogowska et al., 2017). Interestingly, the mutations which do not delay inactivation have been shown to have partial intracellular retention, whereas the mutations which delay inactivation exhibit normal membrane trafficking (Andolfo et al., 2013, Glogowska et al., 2017, Andolfo et al., 2018a).

Calcium entry through Piezo1 in RBCs in mouse has been linked to activity of the Ca^{2+}-activated K^{+} channel, KCNN4 (also known as the Gardos channel), mutations of which are also associated with DHS and are reviewed elsewhere (Iolascon et al., 2019). Treating RBCs from DHS patients with Piezo1 mutations with KCNN4 blockers, TRAM-34 or Senicapoc was able to prevent leftward shift in osmotic fragility (Rapetti-Mauss et al., 2017) showing the coupling of these channels in DHS development. In fact the nomenclature of the disease has changed to represent these two linked causes of the disease; DHS1 represents DHS caused by Piezo1 mutations, whereas DHS2 encompasses disease caused

by KCNN4 mutations (Andolfo et al., 2018a). The prevalence of DHS1 is more common (Andolfo et al., 2018b).

Recapulation of a DHS-causing Piezo1 mutation in mouse erythrocytes (R2456H), resulted in an anaemia-like phenotype presenting many of the clinical symptoms observed in humans. Notably, crossing these Piezo1 GOF mice with KCNN4 KO mice resulted in a reversal of reduced RBC osmotic fragility, confirming the interaction of these channels in DHS. Interestingly, like with other anaemias, such as sickle-cell, the presence of DHS was able to reduce severity of infection with rodent malaria parasite, *Plasmodium berghei,* resulting in increased survival time after infection. Comparative genetics analysis strikingly revealed a novel Piezo1 GOF mutation, E756del, which is present in 1/3rd of the African population where malaria is endemic (Ma et al., 2018). Therefore, the presence of Piezo1 GOF mutations are likely more prevalent than diagnosis of DHS.

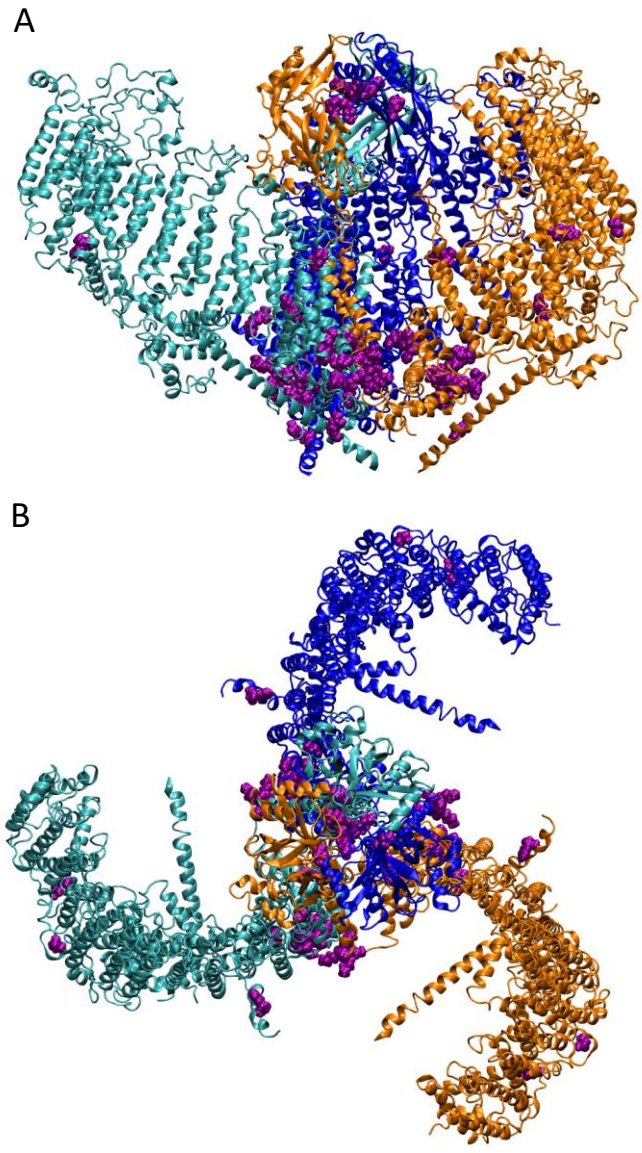

Figure 1-4 Model of human Piezo1 showing DHS-associated residues. The 3 subunits of Piezo1 are each shown in a different colour, with DHS-associated residues highlighed in purple. (A) Side view of Piezo1. (B) Top view of Piezo1. Figure made in collaboration with Dr Antreas Kalli (University of Leeds).

1.2.5.2 Generalised lymphatic dysplasia

Generalised lymphatic dysplasia (GLD) is a form of primary lymphoedema; a chronic swelling due to ineffective drainage by the lymphatic system. GLD is characterised by a widespread lymphoedema affecting most parts of the body and is often detectable in utero by hydrops fetalis, the abnormal accumulation of fluid in the developing foetus (Connell et al., 2013).

Piezo1 was identified as the candidate gene responsible for a mild form of GLD in six families, who had no mutations in the other genes associated with GLD (Fotiou et al., 2015). As with DHS-causing mutations, a large number of disease-associated variants were detected and the majority of these occurred in the C-terminal domain of the protein. An additional sibling pair with GLD were found to harbour biallelic mutations in Piezo1 (a splice variant causing early truncation and a missense mutation) (Lukacs et al., 2015).

Functional analysis of these mutations demonstrated the mutations affected cell surface expression of Piezo1 (Fotiou et al., 2015, Lukacs et al., 2015) and in patients with two affected Piezo1 alleles, mechanical and pharmacologically-induced Ca^{2+} entry in RBCs was abolished. Cloning of the missense mutation G2029R into HEK293 cells showed that the mutation severely reduces Piezo1 current amplitudes in response to mechanical stimulus (Lukacs et al., 2015). Therefore, it appears GLD is caused by a loss of Piezo1 channel function (LOF). It is interesting to note that loss of Piezo1 in the mouse is embryonically lethal (Li et al., 2014, Ranade et al., 2014a), however humans (as described above) and zebrafish with Piezo1 LOF are still viable (Faucherre et al., 2014, Shmukler et al., 2015).

1.2.5.3 Phenotypic overlap of Piezo1 mutations

Although it appears that Piezo1 GOF mutations cause DHS and Piezo1 LOF mutations cause GLD, there are in fact overlapping phenotypes observed as discussed by Martin-Almedina 2018 (Martin-Almedina et al., 2018) and the true picture of Piezo1 pathophysiology is slightly blurred. Abnormal RBCs in the form of spherocytes have been observed in blood films from patients with GLD (Fotiou et al., 2015). Additionally, patients with DHS occasionally present with hydrops fetalis, which is not caused by their anaemia (Entezami et al., 1996). A cystic hygroma, a fluid filled sac caused by a blockage in the lymphatic system, has

also been observed in a patient with DHS, suggesting additional lymphatic alterations (Ami et al., 2009).

One patient with DHS has been observed who harbours a LOF mutation in Piezo1 (K1877del), where inactivation of the channel is quicker (Glogowska et al., 2017). Additional Piezo1 mutations have been found in patients with blood conditions other than DHS, including overhydrated stomatocytosis, although the effect of these mutations on channel function has not been investigated. Both spherocytes and stomatocytes were present on the blood smears of the three patients investigated (Knight et al., 2019).

Recently, the haematological properties of a patient with GLD caused by a LOF Piezo1 mutation has been investigated. The patient has a rightward shift in the ektacytometry curve indicating the presence of overhydrated RBCs and peripheral blood smear revealed spherocytes and stomatocytes (Andolfo et al., 2019). Further identification of channel function in patients with Piezo1 mutations, in addition to cross-checking for blood defects in GLD patients and vice versa is essential to determine the true effect of Piezo1 mutations and to establish whether the two phenotypes are in fact linked.

1.2.6 Piezo1 pharmacology

Piezo1 pharmacology is limited, but is an area which is slowly developing. As yet, compounds with activity against the channel are chemical tools, rather than drug-like molecules which can be used *in vivo*, but these are nonetheless helpful in uncovering the vast physiological roles of the channel. It is not yet known whether activation or blockade of Piezo1 would be therapeutically beneficial, particularly due to seemingly global activity, but understanding how chemical modulation of Piezo1 is possible is essential if therapeutic potential of the channel is to be harnessed in the future.

1.2.6.1 Activators

Applying mechanical force to activate Piezo1 channels is beneficial as it perhaps more closely mimics physiology, however can be technically challenging and also does not allow for sole activation of Piezo1. The first chemical activator of the channel was identified via a high-throughput screen of 3.25 million low molecular weight compounds. It was named Yoda1 after the iconic Star Wars character (Syeda et al., 2015). Yoda1 can effectively activate both human and mouse

Piezo1 channels without any mechanical stimulation (Evans et al., 2018, Syeda et al., 2015), but it can also act as a gating modifier with mechanical force, reducing the amount of force needed to open the channels and keeping the channels open for longer (Syeda et al., 2015).

Yoda1 does not activate Piezo2 suggesting a specific pharmacological binding site on Piezo1. Chimeras of mouse Piezo1 and Piezo2 were engineered to locate the necessary residues for Yoda1 sensitivity and identified the region between amino acid residues 1961-2063, located between the blade and pore, as Yoda1-sensitive (Lacroix et al., 2018). Structure-activity relationships of Yoda1 activity have highlighted important chemical requirements for Piezo1 activation, strengthening the existence of a possible pharmacological binding site (Evans et al., 2018), but this still remains unknown.

The discovery of Yoda1 has facilitated Piezo1 studies including demonstrating the role of the channel in RBC volume regulation, which would have proved difficult without this chemical tool (Cahalan et al., 2015). However, Yoda1 has its limitations including poor water solubility (insoluble >20 μM) and a short half-life (Cuthbertson, 2018) restricting its use *in vitro* and preventing *in vivo* applications.

Additional Piezo1 activators have been identified more recently from a screen of 3000 compounds, named Jedi1 and Jedi2 (Wang et al., 2018b). These compounds are structurally distinct from Yoda1 and activate the channel via a different mechanism, acting on the extracellular loops on the blade, suggesting long-range gating. Similar to Yoda1, Jedi1/2 causes a leftward shift in the pressure-current curve and therefore potentiate the mechanosensitivity of the channel. They also exhibit selectivity for Piezo1 rather than Piezo2. The compounds have increased water solubility compared to Yoda1 (up to 2mM), however the EC_{50} of Jedi1/2 is 200 μM and 158 μM respectively, limiting their use. The compounds have not yet been utilised in Piezo1 studies.

1.2.6.2 Inhibitors

Inhibitors of Piezo1 are fairly limited to generic inhibitors of non-selective cation channels; gadolinium chloride and ruthenium red which both act as pore-blockers ((Drew et al., 2002, Suchyna et al., 2004, Bowman et al., 2007). GsMTx4, a spider toxin offers inhibition restricted to mechanosensitive ion channels, likely acting indirectly on the lipid bilayer, but is still not specific for Piezo1 (Bae et al., 2011).

Another amphipathic inhibitor of Piezo1, amyloid peptide (Aβ), has been identified which reduces Piezo1-mediated shear-stress induced Ca^{2+} influx (Maneshi et al., 2018). The specificity of Aβ has not been investigated, but it is likely it also effects the activity of other mechanosensitive ion channels, due to its indirect mechanism of action.

Structure-activity relationship studies of Yoda1 resulted in the discovery of Dooku1; a Yoda1 analogue with no Piezo1 activity, thereby acting effectively as an antagonist of Yoda1-induced Piezo1 activity (Evans et al., 2018). The compound is useful in blocking chemical activation of the channel, but is ineffective at reducing constitutive channel activity. Therefore an effective, specific inhibitor of mechanically induced Piezo1 activation is still needed.

1.2.7 Piezo1 gating

Due to the vast role of Piezo1 in physiology, modulation of channel gating, rather than a blanket activation or inhibition may be more effective therapeutically. It is likely that channel gating varies depending on the cell type which may explain why pathophysiology that affect Piezo1 activity appear phenotypically restricted, despite global expression and function of the channel. Therefore, studies investigating the gating properties of Piezo1 are important in elucidating the subtleties of the channel and providing possible avenues for modulation.

1.2.7.1 Piezo1 inactivation

Channel inactivation refers to the decaying of current, whilst still in the presence of the stimulus, indicating an intrinsic mechanism of ion pore closure. The kinetics of Piezo1 inactivation vary greatly in published material, depending on endogenous vs overexpression systems and the method of electrophysiological recording. The first studies of the channel reported a very fast inactivation (~ 50ms) following channel activation via mechanical indentation, recorded in whole-cell configuration (Coste et al., 2010). These observations of fast channel inactivation are common in Piezo1 publications, particularly in overexpression studies (Gottlieb et al., 2012, Lewis et al., 2017).

However, it has been demonstrated that the electrophysiological technique applied can vastly change these channel kinetics, with very little inactivation observed in outside-out configuration and much faster inactivation observed in cell-attached (Lewis and Grandl, 2015). Much slower, incomplete inactivation is

observed in the original Piezo1 discovery, recorded in cell-attached configuration, compared to whole-cell (Coste et al., 2010). It is possible that preparation of the patch membrane could affect the kinetics of the channel as repetitive stimulation of the Piezo1 has been shown to lead to an irreversible loss of inactivation (Gottlieb et al., 2012).

In fact in studies of endogenous channel activity in a variety of cell types including endothelial, smooth muscle, epithelial and stem cells, Piezo1 inactivation is not complete, or even observed at all and does not show the extremely fast kinetics originally reported (Rode et al., 2017, Retailleau et al., 2015, Martins et al., 2016, Del Mármol et al., 2018). It is conceivable, that for some cells, such as endothelial cells or RBCs which constantly experience shear stress, that fast switching off of the channel would not be physiologically advantageous. Therefore it is important to record endogenous Piezo1 activity from physiologically relevant cells to compare to heterologous expression systems.

Multiple studies have attempted to elucidate the molecular basis of Piezo1 inactivation and identify contributing structural features. Hydrophobic residues (L2475 and V2476) within the pore-lining have been determined as important mediators of Piezo1 inactivation, as mutations in these residues to hydrophilic amino acids, resulted in prolonging of inactivation in the murine channel in whole-cell and cell-attached current recordings. Combination of these mutations, in addition to M2493/F2494 (which form a constriction in the C-terminal domain of the pore) to glutamates, resulted in complete abolishment of Piezo1 inactivation suggesting at least two inactivation gates are required (Zheng et al., 2019). Piezo1 deactivation following mechanical stimulus was also absent in this mutant.

Many of the DHS causing mutations which delay channel inactivation occur in the C-terminal domain of Piezo1 indicating this portion of the protein is essential for channel gating. Removal of the C-terminus on human Piezo1 with insertion of a stop codon at residue 2218 resulted in a channel with no inactivation and slow deactivation (Bae et al., 2013a). Residues 2225 and 2456 which are both associated with DHS, seem particularly important as double mutation of these residues (M2225R and R2456K) also result in a non-inactivating form of the channel (Bae et al., 2013b). Additionally, chimeras of Piezo1 with the C-terminal extracellular domain (CED) of Piezo2 conferred the faster inactivation properties of Piezo2. The same was true with the opposite channel configuration suggesting

the intrinsic mechanism for Piezo inactivation resides within the CED (Wu et al., 2017).

However, inactivation kinetics of Piezo1 can be modified by factors other than the DNA sequence of the channel. Mouse embryonic stem cells (mES) exhibit slow inactivation (incomplete inactivation after 100ms) which becomes faster as the cells differentiate into neurons. This was not due to the amino acid sequence of the channel as cloned Piezo1 cDNA from these cells exhibited fast inactivation kinetics in a heterologous expression system (Del Mármol et al., 2018). Dietary fatty acids are able to modulate channel inactivation indicating that the distinct lipid profile of cells can confer different Piezo1 gating. In fact supplementation of polyunsaturated fatty acid, eicosapentaenoic acid (EPA) to N2A cells transfected with Piezo1 DHS mutants, ablated the delayed inactivation usually observed with these mutations (Romero et al., 2019). Additionally, other proteins are able to modulate Piezo1 inactivation. TMEM150C/Tetonin 3 is able to prolong Piezo1 channel inactivation measured via whole-cell and cell-attached when co-expressed in HEK293 cells (Anderson et al., 2018).

Overall, the mechanism of Piezo1 inactivation is complicated and multi-factorial and as yet the field does not have a complete picture of its role in endogenous Piezo1 channels. Many disease-causing mutations of the channel affect kinetics of inactivation specifically, so understanding its role in physiology and how it may be modulated could provide important for therapeutic targets.

1.2.8 Piezo2

Piezo2 has a very similar structure to Piezo1 with three subunits, each with 38 transmembrane helices (Wang et al., 2019a). The electrophysiological properties of the channel are also similar, but Piezo2 mediates faster inactivation (Coste et al., 2010). Despite the apparent similarities, there are differences between the channels. Whereas Piezo1 appears to have a global role in mechanotransduction, the functional roles of Piezo2 are more specialised to the sensory system. Additionally, Piezo2 is insensitive to the chemical activator Yoda1, suggesting gating differences between the channels (Syeda et al., 2015).

Piezo2 is involved in somatosensation, with a particular role in sensing light touch rather than nociception (Woo et al., 2014, Ranade et al., 2014b). However, its activity can be increased by inflammatory molecules (Dubin et al., 2012) and

Piezo2 has been implicated in the development of mechanical allodynia, an altered sensation in which light touch can be perceived as pain, highlighting possible therapeutic potential of the ion channel (Murthy et al., 2018, Szczot et al., 2018). To date, no pharmacological modulators of Piezo2 have been identified. As with Piezo1, deletion of Piezo2 is embryonically lethal, indicating a perhaps unknown function of the channel with more severity than altered touch sensation (Dubin et al., 2012).

Mutations in Piezo2 are associated with several arthrogryposis conditions; distal arthrogryposis 3 (DA3) (Gordon syndrome), DA5 and Marden-Walker syndrome, which share similar phenotypes, primarily consisting of congenital contractures of the joints in addition to pulmonary hypertension (Ma et al., 2019, McMillin et al., 2014). Interestingly, both GOF (Coste et al., 2013) and LOF (Haliloglu et al., 2016, Delle Vedove et al., 2016) mutations are associated with these overlapping conditions, suggesting that like Piezo1, abrogated Piezo2 signalling in either direction can produce similar phenotypes.

As has been discussed in the above sections, there are some examples of physiological functions which require both Piezo1 and Piezo2, within cartilage force sensing and the baroreceptor response (Lee et al., 2014, Zeng et al., 2018). To date the relevance and mechanism of cross-Piezo interaction is unknown but will be an interesting and important investigation.

1.3 Ca^{2+}

Many of the effects of Piezo1 activation result from Ca^{2+} influx through the channel. Ca^{2+} is arguably the most important signalling molecule in physiology, acting as a versatile second messenger, facilitating varied and specialised responses (Berridge et al., 2000, Clapham, 2007). Ca^{2+} signalling is fundamental for cell health, promoting a number of cellular activities including proliferation, migration, survival, exocytosis and gene expression, transcription and muscle contraction. However, when Ca^{2+} levels within the cell become too high, this can act as a trigger for cell destruction via apoptosis or necrosis. Therefore, the control of intracellular Ca^{2+} needs to be tightly regulated to balance the advantageous and detrimental effects of the ion. Altered Ca^{2+} signalling has been linked to a multitude of disease states including cancer and cardiovascular disease (Monteith et al., 2012, Hammoudi and Lebeche, 2015). In order to

produce these precise responses, cells have intricate mechanisms for Ca^{2+} handling.

1.3.1 Control of intracellular Ca^{2+}

Cells need to be sensitive to Ca^{2+} fluxes, to allow for an efficient response following a given stimulus. As such, the intracellular Ca^{2+} concentration is maintained at extremely low levels (~100nM), approximately 20,000 times less than extracellular levels (~2mM), generating the steepest concentration gradient of any physiological ion. In order to maintain this concentration gradient and quickly return intracellular Ca^{2+} to baseline, following a Ca^{2+} entry event, cells have specialised pumps and transporters to maintain Ca^{2+} homeostasis (Berridge et al., 2003). Cells also have internal Ca^{2+} stores primarily within the endoplasmic reticulum (ER), but also mitochondria, Golgi and lysosomes which can release Ca^{2+} to orchestrate an amplification of a Ca^{2+} signal, but can also sequester the ion to dampen cytoplasmic levels. These stores also have specialised membrane transport proteins, highly adapted for efficient Ca^{2+} homeostasis. The proteins involved in Ca^{2+} handling are depicted in Figure 1-5.

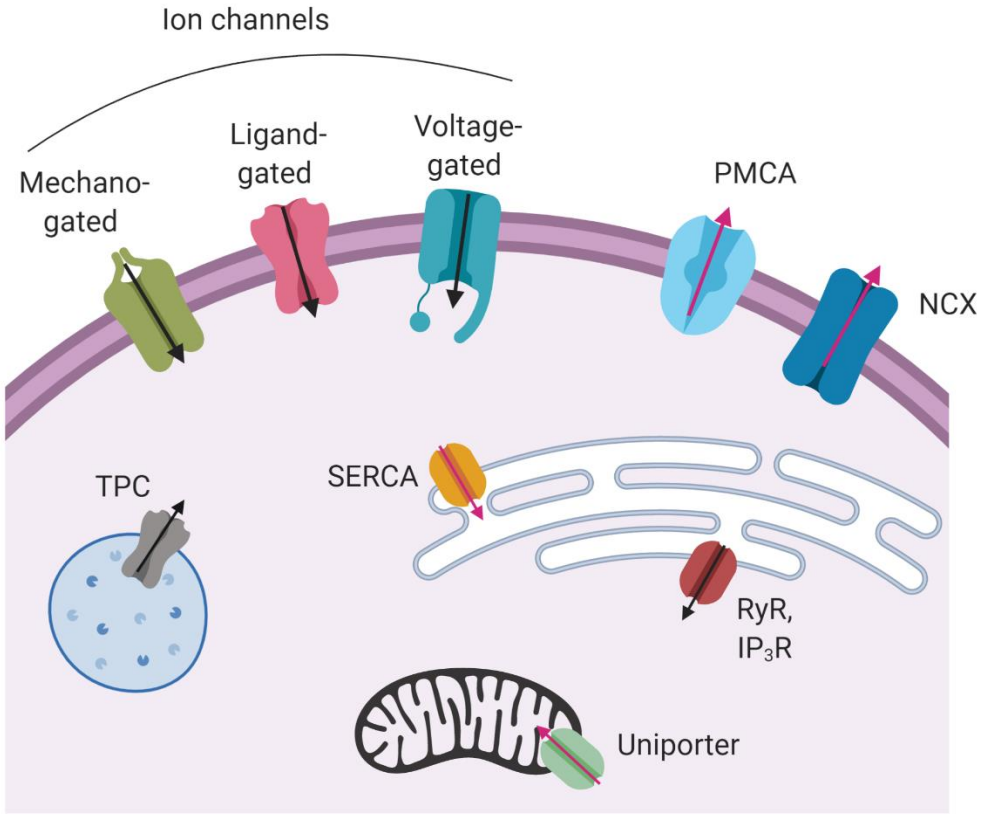

Figure 1-5 Proteins involved in Ca^{2+} homeostasis. Intracellular Ca^{2+} is raised via Ca^{2+} entry through ion channels on the plasma membrane which are gated by different stimuli. It can also be raised through Ca^{2+} release from intracellular Ca^{2+} stores, located in the endoplasmic reticulum and lysosomes. Intracellular Ca^{2+} is reduced via cell surface pumps and transporters or via uptake into stores (SERCA, mitochondrial uniporter). Proteins that act to increase intracellular Ca^{2+} are depicted with a black arrow to show the direction of Ca^{2+} movement, whereas proteins that reduce intracellular Ca^{2+} are depicted with a pink arrow. PMCA (plasma membrane Ca^{2+} ATPase), NCX (Na^{+}/Ca^{2+} exchanger), SERCA (sarcoplasmic reticulum Ca^{2+} ATPase), RyR (ryanodine receptor), IP_3R (IP_3 receptor), TPC (two-pore channels).

1.3.1.1 Intracellular [Ca^{2+}] raising mechanisms

1.3.1.1.1 Ca^{2+} entry

Ca^{2+} entry into the cell is mediated by ion channels located on the plasma membrane, which open in response to distinct stimuli (Taylor, 2002). Voltage-gated Ca^{2+} channels (VGCCs) activate in response to membrane depolarisation and are therefore important transducers of electrical signals, into Ca^{2+} influx (Catterall, 2011). There are 10 members of VGCCs which can be divided into 3 families (Ca_v1-3) and have distinct physiological roles. Broadly, the Ca_v1 family is involved in excitation-contraction coupling of skeletal, smooth and cardiac muscle, the Ca_v2 family contributes to neurotransmitter release at synapses and the Ca_v3 family is involved in rhythmic action potential firing. Antagonists of Ca_v1 (also termed L-type) channels such as verapamil and nifedipine are widely used therapies to treat cardiac arrthymias and hypertension.

Another calcium channel facilitating calcium entry at the plasma membrane is Orai1. This channel contributes to a phenomenon known as store-operated calcium entry, whereby depletion of intracellular calcium stores, activates Orai1. The current generated by Orai1 is known as I_{CRAC} (calcium release-activated Ca^{2+} current). This intricate feedback mechanism is facilitated by stromal-interacting molecule 1 (STIM1) which is located within the ER membrane and has a specialised Ca^{2+} binding, EF-hand domain which can sense the depletion of calcium stores. When stores are depleted, STIM1 relocates near the plasma membrane and activates Orai1, permitting Ca^{2+} entry (Derler et al., 2016). Many physiological functions of Orai1 have been identified including skeletal muscle development and lymphocyte activation in the immune system (Wei-LaPierre et al., 2013, Feske, 2007). Orai1 or STIM1 deficiency results in patients with muscle hypotonia and severe combined immunodeficiency (SCID) (Lacruz and Feske, 2015).

Ligand-gated ion channels are activated by binding of a particular molecule. The P2X receptors are examples of ligand-gated calcium channels, activated by the binding of ATP. They have wide tissue distribution with roles in contraction of smooth muscle, initiating action potentials in sensory cells and inflammation (North, 2016). Other Ca^{2+} permeable channels include the TRP and Piezo families which have been described earlier on in this chapter.

1.3.1.1.2 Ca^{2+} release from internal stores

However, it is not just Ca^{2+} permeable channels located on the cell membrane which contribute to raising intracellular Ca^{2+} concentration. Ca^{2+} release from the ER stores can be mediated by both ryanodine receptors (RyRs) and the IP_3 receptor (IP_3R) (Berridge et al., 2003). Ryanodine receptors are extremely large tetrameric ion channels, primarily located in skeletal muscle, the heart and the brain. The channels are activated by an influx of Ca^{2+}, resulting in an amplification of this original Ca^{2+} signal, via Ca^{2+} release from the ER, a process known as Ca^{2+}-induced Ca^{2+} release (CICR). The RyRs are mostly known for their involvement in excitation-contraction coupling in muscle (Van Petegem, 2012). The IP_3R receptor facilitates Ca^{2+} release from the ER when its ligand IP_3 binds to the receptor. The production of IP_3 occurs via upstream activation of receptors at the plasma membrane and the hydrolysis of signalling molecule PIP_2 by phospholipase C (PLC). IP_3Rs are involved in multiple cell signalling events including fertilisation, apoptosis, synaptic plasticity and gene expression (Mikoshiba, 2015).

Ca^{2+} can also be released from other stores in acidic organelles such as lysosomes and endosomes. Despite receiving less attention that the ER stores, it is emerging that the Ca^{2+} content in endolysosomal stores is significant and its release mediates distinct cellular responses (Morgan et al., 2015). Nicotinic acid adenine dinucleotide phosphate (NAADP) mobilises these Ca^{2+} stores and mediates many physiological process across body systems (Galione, 2015). Several ion channels have been proposed as the Ca^{2+} release channel from these stores, but two-pore channels (TPCs) have emerged as the favoured candidate (Morgan et al., 2011).

1.3.1.2 Ca^{2+} extrusion and re-uptake into stores

Removing Ca^{2+} from the cytoplasm following signalling events is crucial for Ca^{2+} homeostasis, allowing the cell to be sensitive to the next stimulus and preventing excessive Ca^{2+} levels. Reducing cytoplasmic Ca^{2+} levels can be achieved via extrusion from the cell via pumps and transporters at the cell membrane, or via reuptake into the stores (Berridge et al., 2003).

Ca^{2+} extrusion at the plasma membrane occurs via the plasma membrane Ca^{2+} ATPase (PMCA) and the Na^+/Ca^{2+} exchanger (NCX). PMCA pumps one Ca^{2+}

molecule from the cell, for each molecule of ATP hydrolysed. On the other hand, NCX utilises the electrochemical gradient of Na^+ to exchange three extracellular Na^+ ions for one intracellular Ca^{2+} ion. The affinity of PMCA for Ca^{2+} is extremely high meaning it can bind calcium even when concentrations in the cell are low, helping maintain baseline levels. The affinity of the NCX transporter for Ca^{2+} is much lower but it acts at a much faster rate than PMCA, allowing rapid extrusion of Ca^{2+} following a large increase in intracellular Ca^{2+} concentration. Therefore, the properties of these two proteins are complementary (Brini and Carafoli, 2011).

The reuptake up of Ca^{2+} into the ER is mediated by the sarco/endoplasmic reticulum ATPase (SERCA). Similarly to PMCA, it pumps Ca^{2+} against its concentration gradient via the hydrolysis of ATP (Clapham, 2007). When intracellular calcium concentrations are high, Ca^{2+} uptake into mitochondrial stores can occur via a Ca^{2+} uniporter (Marchi and Pinton, 2014).

1.4 Summary

In summary, Piezo1 is a global mechanosensor, with varied physiological functions across multiple body systems, predominantly mediated by Ca^{2+} entry. Increased knowledge of the channel is occurring at an astounding rate and research in this area is dynamic and exciting, uncovering new importance for mechanosensation within biology. The intricacies of Piezo1 gating and structures that enable the channel to sense mechanical force are still to be elucidated but are required if therapeutic channel modulation is to be possible. Pharmacological tools with activity against the channel remain limited and as yet lack drug-like properties necessary for *in vivo* studies.

The more that is discovered about Piezo1, the more dichotomies arise including the seemingly opposing functions of the channel within vascular biology and in different cancers. Additionally, within pathophysiology, mutations that result in either gain or loss of Piezo1 function, result in diseases which share phenotypes, suggesting that normal physiology requires a fine balance of Piezo1 channel activity. Investigation into the effect of Piezo1 disease-causing mutations in native cells will help determine the true effect on channel gating and identify whether this varies between different cell types and body systems.

1.5 Aims and Objectives

Aims

The global aim of my thesis was to better understand the effects of Piezo1 GOF. This was achieved using a genetic approach by studying the effects of a disease-causing, GOF Piezo1 mutation on mouse physiology. The mutation, M2225R, has been shown to delay channel inactivation after mechanical stimulation in overexpressed channel constructs. This global mouse model was designed to provide a unique opportunity to study the effects of altered Piezo1 gating in its native state. It will be possible to determine the physiological effects of Piezo1 GOF to decipher important roles of Piezo1 channel gating.

Interestingly, humans with this mutation do not report any other symptoms other than anaemia. However, the widespread role of Piezo1 in mammalian physiology raises the possibility that patients might have previously unrecognised disease or disease predisposition. This mouse model also provides an important resource for testing this hypothesis.

To modulate Piezo1 activity pharmacologically to attempt to replicate channel GOF chemically, or indeed reduce activity to target diseases like DHS, additional chemical tools against Piezo1 are required. Therefore, knowledge of the Piezo1 agonist structure-activity relationship was sought with the hope of finding chemicals with activity against the channel. New synthetic small molecules with structural similarity to existing Piezo1 agonist, Yoda1, were developed by the School of Chemistry and tested for Piezo1 activity.

Objectives

1. Generate a construct of the mouse equivalent of Piezo1 M2225R and check that the mutation causes GOF in the murine channel.
2. Determine whether mice harbouring the equivalent of the Piezo1 M2225R mutation (Piezo1 M-R) exhibit symptoms of DHS, like humans.
3. Investigate the effects of the Piezo1 M-R mutation on channel gating in RBCs.
4. Investigate additional cardiometabolic effects of Piezo1 GOF to determine the physiological importance of Piezo1 inactivation.

5. Determine the structure-activity relationship of Yoda1-mediated Piezo1 activation by testing modified Yoda1 analogues in HEK-293 cells overexpressing the channel.
6. Test whether the Yoda1 analogues have improved activation or an inhibition compared to Yoda1.
7. Determine potency and selectivity of any hit compounds.
8. Test that hit compounds have activity against the endogenous Piezo1 channel in endothelial cells.

Chapter 2 Materials and Methods

2.1 Ionic solutions

2.1.1 Standard bath solution (SBS)

SBS contained (mM): NaCl 134, KCl 5, $MgCl_2$ 1.2, $CaCl_2$ 1.5, HEPES 10, D-Glucose 8. pH was titrated to 7.4 with 4 M NaOH. Ca^{2+} free SBS had the same components but lacked $CaCl_2$ and contained 0.4 mM EGTA.

2.1.2 Dulbecco's Phosphate Buffered Saline (DPBS)

DPBS without Mg^{2+} and Ca^{2+} (Sigma-Aldrich) contained (mM): KCl 2.68, KH_2PO_4 1.47, NaCl 136.89 and Na_2HPO_4-$7H_2O$ 8.06. DPBS was used for cell culture and for washing cells. Ca^{2+} and Mg^{2+} can inhibit trypsin activity so it was important to use DPBS lacking these ions.

2.2 Chemicals and reagents

All general salts and reagents were purchased from Sigma. Other chemicals are presented in Table 2-1.

2.2.1 Yoda1 analogues

Yoda1 analogues were synthesised by Kevin Cuthbertson in the School of Chemistry, University of Leeds. All synthesised chemicals were purified by column chromatography or trituration and determined as >97% pure by ^{1}H NMR (proton NMR) and ^{13}C NMR (carbon-13 NMR). All Yoda1 analogues were stored as 10 mM stocks in DMSO at -20ºC. The structure of the compounds are presented in the results chapters for easy comparison of structure-activity relationships.

Chemical	Supplier	Solvent	Storage	Description
Yoda1	Tocris	DMSO	10 mM, -20ºC	Piezo1 activator
ATP	Sigma	H_2O	20 mM, -20ºC	P2X receptor agonist
(-)-Englerin A	PhytoLab	DMSO	20 mM, -80ºC	TRPC4/5 activator
Gadolinium chloride	Sigma	H_2O	100 mM, Room Temp	Non-selective cation channel blocker
4α-phorbol 12,13-decanoate	Sigma	DMSO	10 mM, -20 ºC	TRPV4 activator
Phenylephrine	Sigma	H_2O	100 mM, -20 ºC	α_1- receptor agonist
Pluronic Acid (F-127)	Sigma	DMSO	10% w/v, Room Temp	Dispersing agent
Mannitol	Sigma	H_2O	0.5 M, Room Temp	Osmolarity raising agent
Thapsigargin	Sigma	DMSO	2 mM, -20ºC	SERCA pump inhibitor
Fura-2 AM	Invitrogen	DMSO	1 mM, -20ºC Protected from light	Ca^{2+} indicator dye
Fluo-4	Invitrogen	DMSO	1 mM, -20ºC Protected from light	Ca^{2+} indicator dye
Probenecid	Sigma	0.5 M NaOH	1 M, prepared fresh	Inhibitor of plasma membrane anion transport
FluxOR™	Thermo Fisher	DMSO	1 mM, -20ºC Protected from light	Tl^{+} indicator dye

Table 2-1 List of reagents. List of reagents used throughout the thesis presented with their supplier, solvent/storage information and a description of their action.

2.3 Cell culture

2.3.1 Cell lines

2.3.1.1 HEK293 derived cell lines

The tetracycline inducible Piezo1 cell line (Piezo1 T-REx) was generated in house by stably transfecting human Piezo1 into T-REx™-293 cells as previously described (Rode et al., 2017). Plain T-REx cells without the Piezo1 plasmid were used as controls. Each cell line was validated by RT-PCR and western blotting. HEK293 cells stably expressing tetracycline-regulated human TRPC4 and TRPC5 have been described (Akbulut et al., 2015). Selection was achieved by including 200 $\mu g.mL^{-1}$ (Piezo1 T-REx) or 400 $\mu g.mL^{-1}$ (TRPC4/TRPC5) zeocin (Invitrogen) and 5 $\mu g.mL^{-1}$ blasticidin (Invitrogen) in the cell medium. Expression was induced by treating the cells for 24 hours with 10 ng/mL tetracycline (Sigma).

The Piezo1 M-R cell line was generated in house by stably transfecting mouse Piezo1 with the M-R mutation into T-REx™-293 cells. Cells were transfected with pcDNA4/TO-mPiezo1M-R using Lipofectamine 2000 (Thermo Fisher Scientific). Subsequently cells were treated with 200 µg.mL-1 zeocin and 10 µg.mL-1 blasticidin to select stably transfected cells. Single cell clones were isolated and analysed individually.

All HEK293 cells were maintained in Dulbecco's Modified Eagle's medium (DMEM) GlutaMAX (Gibco) containing 4.5 $g.L^{-1}$ D-glucose and pyruvate. Media was supplemented with 10% foetal calf serum and 1% Penicillin/Streptomycin (Sigma-Aldrich).

2.3.1.2 Human Umbilical Vein Endothelial Cells (HUVECs)

HUVEC (human umbilical vein endothelial cells) from pooled donors were purchased from Lonza and were maintained in Endothelial Cell Basal Medium (EBM-2). This media was supplemented with a bullet kit (Cell Media and Bullet Kit, Lonza) containing the growth factors: 10 ng.ml-1 vascular endothelial growth factor, 5 ng.ml-1 human basic fibroblast growth factor, 1 µg.ml-1 hydrocortisone, 50 ng.ml-1 gentamicin, 50 ng.ml-1 amphotericin B and 10 µg.ml-1 heparin, in

addition to 2% foetal calf serum (Sigma). Experiments were performed on HUVECs passaged 2-6 times.

2.3.1.3 Chinese Hamster Ovary (CHO) cells stably expressing TRPV4

CHO K1 cells stably expressing human TRPV4 were maintained in Ham's F12 (ThermoFisher Scientific) in the presence of 1 mg.mL-1 G418 (Sigma-Aldrich).

2.3.2 Primary cells

2.3.2.1 Mouse liver sinusoidal endothelial cell (mLSEC) isolation

mLSECs were isolated using an immunomagnetic separation technique. A mouse liver was thoroughly minced using scalpel blades and resuspended in a dissociation solution containing 9 ml 0.1% collagenase II, 1 ml 2.5 U ml^{-1} dispase, 1 µM $CaCl_2$ and 1 µM $MgCl_2$ in Hanks Buffer solution. The tissue-dissociation mix was incubated at 37ºC for 50 mins in a MACSMix Tube rotator (Miltenyi Biotech) to provide continuous agitation. Following this enzymatic digestion, the mix was passed through 100 and 40 µm cell strainers to remove undigested tissue. Cells were washed twice in PEB buffer containing PBS, EDTA 2mM and 0.5% BDA, pH 7.2. The washed pellets were resuspended in 1 ml PEB buffer and 30 µl CD146 microbeads (Miltenyi Biotech) at 4ºC for 15 min under continuous agitation. CD146 is a membrane protein marker for endothelial cells and is highly expressed in mLSECs. Following incubation, the solution was passed through an MS column primed with PEB buffer. CD146 positive cells were retained in the column and flushed into a separate tube away from the CD146 negative eluate. Cells were diluted in 1 ml warm Promega media and plated on Poly-D-lysine - coated plates at 100,000 cells/well for a 96-well plate and grown in a 5% CO_2 incubator at 37ºC. Media was changed following 2 h and then every 24 h until confluent.

mLSECs were maintained in Promega media containing the Supplement Pack Endothelial Cell GM2 and 1% antibiotic-antimycotic.

Cells were grown at 37°C and 5% CO_2 in a humidified incubator. Cells were passaged every 2-4 days when 80-90% confluency was reached. For passaging, cells were rinsed with PBS, covered with 1 ml 0.05% Trypsin-EDTA to encourage cell detachment. After 5 min incubation at 37°C, 5% CO_2, cells were resuspended in media to inactivate the trypsin. The cell suspension was centrifuged at 100g

for 5 min and fresh media added. Cells were either seeded into a new flask for growth or plated for experimentation. If required for plating, cells were counted on a haemocytometer before centrifugation. For use in the FlexStation experiments, cells were seeded at a density of 5 x 10^4 (HEK-293), 2 x 10^4 (HUVECs), 10 x 10^4 (mLSEC) cells/well in 100 µl media into black, clear-bottomed 96-well Poly-D-lysine plates (Grenier), 24 h before experimentation.

For the cells used for RT-PCR and Western blot, cells were seeded at a density of 1 x 10^6 cells/well in 2 ml of media in clear, 6-well plates (Corning). These cells were either lysed 24 h after plating for Western blotting or suspended in 1ml Tri-reagent and kept at -80°C until RNA isolation.

2.4 Molecular Biology

2.4.1 mPiezo1-MR plasmid generation

Mouse Piezo1 cDNA was cloned into pcDNA4/TO as described (Blythe et al., 2019b). The mPiezo1 M-R mutant was made using site-directed mutagenesis using primers containing the desired mutation. The primers were designed using PrimerX software and were as follows. M2241R (F: CCACTGTTCACCAGGAGCGCCCAGCAG; R: CTGCTGGGCGCTCCTGGT

GAACAGTGG).

The mutagenesis reaction mix was composed of 1 x Buffer, 50 ng template (mPiezo1), 125 ng forward and reverse primers, 200 µM dNTP, 1.25 U of PrimeSTAR HS DNA polymerase (TaKaRa) and H_2O with a final volume of 50 µL. The thermal cycling was set as follows:

98ºC	2mins	
98ºC	10 secs	⎫
58ºC	5 secs	⎬ x18
72ºC	2mins 30 secs	⎭
72ºC	5mins	
4ºC	hold	

The input template was then degraded by addition of 15 U Dpn1 (NEB) at 37 °C for 2 hours. The restriction enzyme was denatured by 10 min incubation at 80 °C prior to transformation in bacteria.

2.4.2 Plasmid DNA transfection

HEK293 cells were transfected using Lipofectamine™ 2000 transfection reagent (Thermo Fisher Scientific) according to the manufacturer's guidelines. Cells were transfected when ~70% confluent on a 6-well plate. 3 µl Lipofectamine was incubated with 1 µg plasmid DNA in 200 µl Opti-MEM 1 Reduced Serum Media (Thermo Fisher Scientific) for 20 min to allow for complexes to form. After incubation, 200 µl of the complexes were added to the cells containing 1.8 ml media. Medium was changed after 6 h and experiments were performed 48 h after transfection.

2.4.3 Transformation

mPiezo1-M-R DNA was transformed into Stellar chemically competent cells (Clontech). 0.5 µg DNA was added to 45 µl bacteria and the combination was left on ice for 30 minutes. Following this, the preparation was heat shocked at 42°C for 45 seconds before being returned to ice for 2 minutes. 250 µl SOC media was added and the tube was incubated for 1 hour at 37°C under continuous agitation. 50 µl of this reaction was spread onto LB agar (Sigma) supplemented with kanamycin (50 µg/ml) and the plates were incubated overnight at 37°C. Single colonies were picked the following day and inoculated in 5 ml LB broth (Sigma) supplemented with kanamycin (50 µg/ml). These cultures were incubated overnight at 37°C under continuous shaking at 220 rpm.

2.4.4 Mini prep and maxi prep

Mini preps were performed as per the manufacturer's protocol using the Spin Miniprep Kit (Qiagen). DNA concentration was measured using a Nanodrop (Thermo Fisher Scientific) and sequencing was outsourced to Genewiz. After correct sequencing was confirmed, maxi preps were performed as per the manufacturer's protocol using the Plasmid Maxi Kit (Qiagen).

2.5 RNA isolation, cDNA preparation and quantitative polymerase chain reaction (qPCR)

2.5.1 RNA isolation from Trizol

Total RNA was isolated from tissue samples and cells by a phase-separation technique using TRI-reagent (Sigma Aldrich). Cells were grown to confluence in

a 6-well plate prior to lysis with 1 ml ice-cold TRI-reagent and subsequently stored at -80°C. For tissue samples, the organs were harvested from the mice and were immediately snap-frozen in liquid nitrogen, before being stored at -80°C. 1 ml TRI-reagent was added to the tissue samples before mechanical homogenisation using the TissueLyserII (Qiagen). All steps were performed in a clean area, prepared with RNAase away using sterile, filter tips and autoclaved plastics.

200 µl chloroform was added to all samples and the tubes were vigorously shaken for 15 seconds and left to settle for 3 minutes at room temperature. Following this, the samples underwent centrifugation (12000g, 15 minutes, 4°C) to separate the phases; RNA found in the top aqueous layer, DNA found in the middle layer and protein in the bottom layer. The RNA-containing top aqueous layer was carefully transferred into a new Eppendorf tube and the RNA precipitated with 500 µl isopropanol and gently inverted to encourage formation of RNA strands. After 10 minute incubation at room temperature, the samples underwent centrifugation (12000g, 15 minutes, 4°C) to pellet the RNA, followed by two washes with 75% ethanol. The samples were vortexed and centrifuged (12000g, 5 minutes, 4°C) following each wash step. After the final wash step, the ethanol was carefully removed and the pellet was air dried for 5 minutes. The RNA was dissolved in 30 µl nuclease-free water and the RNA concentration was measured using a Nanodrop (Thermo Fisher Scientific).

2.5.2 Reverse transcription

Reverse transcription of mRNA was performed using Superscript® III Reverse Transcriptase (Invitrogen) in the presence of random primers (Promega) and RNase OUT™ (Invitrogen). 1 µg of total RNA from each sample was used with 2 µL of random Hexamers (20 µmol.L-1) and 0.5 µL of RNase OUT. After 8 min of incubation at 70 °C to inactivate DNase, 100 units of M-MLV transcriptase (Invitrogen) were added and the mixture was incubated at 75 °C for 7 min, 10 min at room temperature and then at 37 °C for 1 h. The RT reaction was ended by heating the mixture at 95 °C for 5 min. It was stored at -20 °C until use where the sample was diluted 1:3 in nuclease free water.

2.5.3 Real-time quantitative polymerase chain reaction

Real-time quantitative PCR analysis was performed using SYBR Green I Master (Roche) on LightCycler® 480 Real-Time PCR System (Roche). SYBR Green1

binds to double-stranded DNA products and fluoresces when excited at 470 nm allowing for detection and quantification. Emission of light is significantly enhanced in the DNA bound state compared to the free state. PCR reactions were run in a 384-well format with 10 µL reaction mixture containing 5 µl SYBR Green I Master (Biorad) (containing antibody-mediated hot-start iTaq DNA polymerase, dNTPs, $MgCl_2$, SYBR® Green I dye, enhancers and stabilizers), 0.75 µl (0.375 µM) of forward and reverse primers respectively, 1 µl cDNA from the RT reaction and 2.5 µl nuclease- free water. Reactions were run with a 2-step cycling program as follows: 95 °C for 10 minutes followed by 40 cycles of : 95 °C for 10 seconds and 60 °C for 40 seconds. mRNA abundance of target genes was calculated relative to the housekeeping gene. Primer sequences and information are displayed in Table 2-2.

Target Gene	Primer sequence (5' to 3')
18S (housekeeper for WAT samples)	F: CGGCGACGACCCATTCGAAC R: GAATCGAACCCTGATTCCCCGTC
Acta1	F: CGTGAAGCCTCACTTCCTACC R: AGAGCCGTTGTCACACACAA
Adiponectin	F: GCAGAGATGGCACTCCTGGA R: CCCTTCAGCTCCTGTCATTCC
ANP	F: AGGCCATATTGGAGCAAATC R: CTCCTCCAGGTGGTCTAGCA
ApoB100	F: AAGCACCTCCGAAAGTACGTG R: CTCCAGCTCTACCTTACAGTTGA
BNP	F: ATGGATCTCCTGAAGGTGCTG R: GTGCTGCCTTGAGACCGAA
CD36	F: GAGCAACTGGTGGATGGTTT R: GCAGAATCAAGGGAGAGCAC
CD68	F: CCAATTCAGGGTGGAAGAAA R: CTCGGGCTCTGATGTAGGTC
CHOP	F: CTGGAAGCCTGGTATGAGGAT R: CAGGGTCAAGAGTAGTGAAGGT
ChREBP	F: TGCTTGAGCCTGGCTTACAGTG R: AGGCCTTTGAAGTTCTTCCACTTG
Col1a1	F: GCTCCTCTTAGGGGCCACT R: CCACGTCTCACCATTGGGG
Col3a1	F: CTGTAACATGGAAACTGGGGAAA R: CCATAGCTGAACTGAAAACCACC
Cyp7a1	F: CAGGGAGATGCTCTGTGTTCA R: AGGCATACATCCCTTCCGTGA
DGAT2	F: GCGCTACTTCCGAGACTACTT R: GGGCCTTATGCCAGGAAACT

ELOVL6	F: GAAAAGCAGTTCAACGAGAACG R: AGATGCCGACCACCAAAGATA
F4/80	F: CTTTGGCTATGGGCTTCCAGTC R: GCAAGGAGGACAGAGTTTATCGTG
FAS	F: TCCTGGGAGGAATGTAAACAGC R: CACAAATTCATTCACTGCAGCC
GAPDH (housekeeper for HEK T-REx cells)	F: AGGTCGGTGTGAACGGATTTG R: TGTAGACCATGTAGTTGAGGTCA
Glut2	F: TCTTCACCAACTGGCCCTTGTC R: TAAAGCTGAGGCCAGCAATCTGAC
Hif1α	F: ACCTTCATCGGAAACTCCAAAG R: CTGTTAGGCTGGGAAAAGTTAGG
HMGCoAR	F: AGCTTGCCCGAATTGTATGTG R: TCTGTTGTGAACCATGTGACTTC
HSL	F: GGGCCTGGCAGTGGTGTGTAAC R: TGAGAACGCTGAGGCTTTGATCTTG
IL-1b	F: TGGTGTGTGACGTTCCCATT R: CAGCACGAGGCTTTTTTGTTG
Leptin	F: TGCTGCAGATAGCCAATGAC R: GAGTAGAGTGAGGCTTCCAGGA
Lipocalin2	F: TGGAAGAACCAAGGAGCTGT R: GGTGGGGACAGAGAAGATGA
LPL	F: GGGAGTTTGGCTCCAGAGTTT R: TGTGTCTTCAGGGGTCCTTAG
MCP1	F: CCCAATGAGTAGGCTGGAGA R: TCTGGACCCATTCCTTCTTG
MMP9	F: TAAGGACGGCAAATTTGGTT R: CTTTAGTGGTGCAGGCAGAG
MTTP	F: ATACAAGCTCACGTACTCCACT R: TCCACAGTAACACAACGTCCA
Myh6	F: GCCCAGTACCTCCGAAAGTC R: GCCTTAACATACTCCTCCTTGTC
Myh7	F: CTACAGGCCTGGGCTTACCT R: TCTCCTTCTCAGACTTCCGC
PGC1a	F: AGCCGTGACCACTGACAACGAG R: GCTGCATGGTTCTGAGTGCTAAG
Piezo1	F: CACAAAGTACCGGGCG R: AAAGTAAATGCACTTGACG
PPARα	F: TATTCGGCTGAAGCTGGTGTAC R: CTGGCATTTGTTCCGGTTCT
PPARγ	F: CACAATGCCATCAGGTTTGG R: GCTGGTCGATATCACTGGAGATC
RPL32 (housekeeper for heart tissue samples)	F: GCTGCTGATGTGCAACAAA R: GGGATTGGTGACTCTGATGG
RPS29 (housekeeper for liver tissue samples)	F: GTCTGATCCGCAAATACGGG R: AGCCTATGTCCTTCGCGTACT
Scd1	F: AAAGCCGAGAAGCTGGTGAT R: TACAAAAGTCTCGCCCCAGC

Serca2a	F: CACACCGCTGAATCTGAC R: GGAAGCGGTTACTCCAGT
SREBP-1c	F: GATGTGCGAACTGGACACAG R: CATAGGGGGCGTCAAACAG
TNFα	F: CAACCTCCTCTCTGCCGTCAA R: TGACTCCAAAGTAGACCTGCCC
VLDLr	F: TCCTGATTGCGAAGACGGTTCTG R: ATGCGGCATGTTCTCATATGGC

Table 2-2 List of primer sequences used for qPCR. Table includes forward (F) and reverse (R) primers used to amplify genes of interest and relevant housekeeping genes.

2.6 Intracellular Ca^{2+} measurement

2.6.1 Fura-2

Fura-2 AM (Invitrogen, USA) is a ratiometric, sensitive Ca^{2+} indicator dye that can be used for measuring intracellular calcium (Ca^{2+}_i). Being able to make ratiometric measurements makes this probe attractive to use as measuring by ratio reduces the effects of unequal dye loading, variation in cell thickness, dye leakage and photobleaching, thereby providing robust and reproducible results.

The –AM form of Fura-2 is membrane permeable, allowing the dye to enter the cell, yet is Ca^{2+} insensitive. Once inside the cell, the AM group is cleaved by intracellular esterases, producing a charged form, Fura-2, which binds Ca^{2+} with high affinity. Fura-2 can be excited by two wavelengths and the peak of excitation shifts depending on whether it is bound to Ca^{2+}; highest peak at 340nm for Ca^{2+} bound Fura-2 and 380nm for unbound Fura-2. Both emit light at 510nm. Upon calcium flux, intracellular calcium rises and emission at 340nm increases, whilst emission at 380nm decreases (Figure 2-1). Fura-2 fluorescence is recorded as a ratio of the emission at 340/380. Therefore, an overall increase in the ratio represents an increase in intracellular calcium.

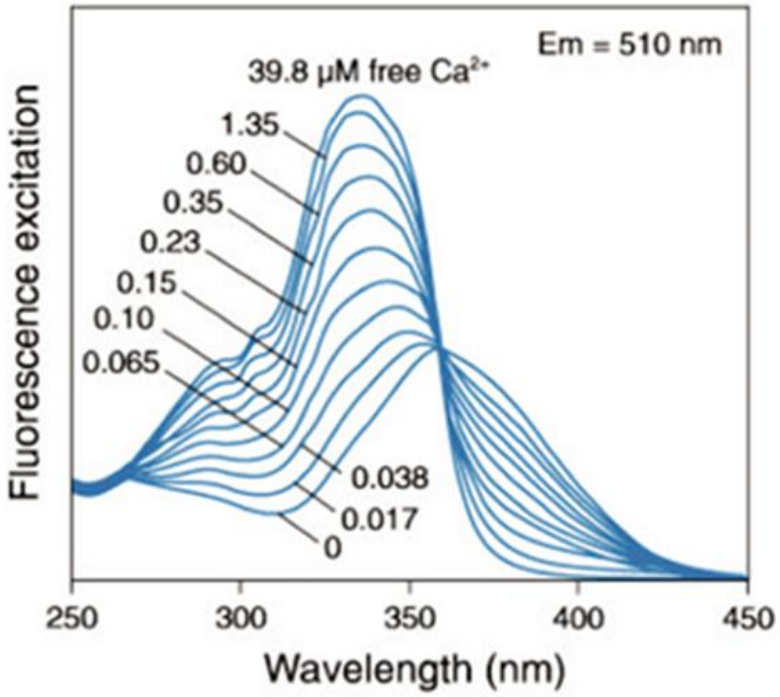

Figure 2-1 Fluorescence excitation spectra for Fura-2 in solutions containing increasing concentrations of free Ca^{2+}. Increasing Ca^{2+} concentrations will cause the emission intensity at 510nm to rise at excitation wavelength 340nm and decrease at 380nm. Image taken from www.moleculardevices.com.

2.6.2 Fluo-4

Fluo-4 is a non-ratiometric Ca^{2+} indicator dye, so unlike Fura-2, measurements can be affected by unequal dye loading. It is excited at 485nm and emits light at 525nm; the intensity of emission is much greater when bound to Ca^{2+} so can effectively indicate increases in intracellular Ca^{2+}. It is useful in cases where certain cell types do not effectively take up Fura-2 or when compounds interfere with the wavelengths of Fura-2 emission.

2.6.3 Experimental protocol

To measure changes in intracellular calcium, cells were loaded with calcium indicator dye Fura-2-AM (Molecular Probes™). Cells were incubated with 50 µL/well 2µM Fura-2-AM in 1.5 mM Ca^{2+} SBS with 0.01% pluronic acid to allow complete dissolution of the dye, for 1 hour at 37°C, protected from light. This solution was then removed and the cells were washed with 100 µL SBS for 30 minutes and kept at room temperature to allow for cleavage of the –AM group. If inhibitors were being tested, then these were added at this time, immediately after

an SBS wash. Prior to measurement, SBS was removed and 100 µL recording buffer added, containing SBS, 0.01% pluronic acid and 0.2% DMSO.

Measurements were made at room temperature (unless otherwise stated) using a FlexStation (Molecular Devices) controlled by Softmax Pro software v5.4.5. The system allows automated fluid transfer from a compound plate to an assay plate, whilst making continuous fluorescence readings. 100 µl was transferred from the compound plate into the assay plate containing 100 µl. The concentration of compounds in the assay plate were calculated to allow for this 1:1 dilution. The change (Δ) in intracellular calcium was indicated as the ratio of Fura-2 emission (510nm) intensities for 340 and 380nm excitation. 'Zero baseline' traces are displayed where pre-incubation steps were not performed and so the baseline Ca^{2+} levels were the same. 'Absolute' Ca^{2+} traces are displayed following pre-incubation steps to determine whether the baseline Ca^{2+} level was affected by the compound.

2.6.3.1 Washout protocol

Cells underwent normal Fura-2 loading and SBS wash step, followed by 30 minute incubation with inhibitor (10 µM) or vehicle control (DMSO) at room temperature. After this incubation, the inhibitor was washed off half of the wells (3x washes in 1.5 mM Ca^{2+} SBS). The cells in these 'washout' wells were maintained in 1.5 mM Ca^{2+} SBS containing vehicle only. The assay plate was then placed immediately onto the FlexStation after washout and Ca^{2+} measurements were obtained. 2 µM Yoda1 was added during the recording in combination with 10 µM inhibitor for non-washout wells, or DMSO for washout wells.

2.6.3.2 Temperature comparison assay

Cells underwent normal Fura-2 loading and SBS wash step. The 30 minute incubation with inhibitor or vehicle control was carried out at 37°C, rather than room temperature. The recording was carried out on the FlexStation which was set at 37°C. These measurements were compared to experiments with a normal room temperature pre-incubation and recordings on the FlexStation at room temperature.

2.6.3.3 Ca^{2+} addback (SOCE)

In order to deplete endoplasmic reticulum (ER) Ca^{2+} stores, cells were pre-treated with 1 µM thapsigargin in 0 mM Ca^{2+} SBS for 30 minutes, immediately following the Fura-2 wash step. If pre-treatment with a test compound was required, this was also added at this stage. 1.5 mM Ca^{2+} SBS was used in the compound plate to enable store-operated Ca^{2+} entry (SOCE) following Ca^{2+} addback.

2.7 Intracellular Tl^{+} measurement

2.7.1 FluxOR™

FluxOR™ reagent is a non-ratiometric, fluorescent Tl^{+} sensitive indicator dye. Like Fura-2 and Fluo-4 the dye is loaded into cells as a membrane-permeable AM ester before cleavage by intracellular esterases to produce the Tl^{+} sensitive form. It is excited at 490 nm and emits light at 525 nm; the intensity of emission is much greater when bound to Tl^{+} so can effectively indicate increases in intracellular Tl^{+}.

2.7.2 Experimental protocol

Cells were loaded with 2 mM FluxOR™ dye for 1 h at room temperature, protected from light, before being transferred to assay buffer (consisting of (mM): 136.9 NaCl, 0.33 Na_2HPO, 4.17 NaHCO3, 5.33 KCl, 0.44 KH_2PO_4, 0.49 $MgCl_2$, 0.41 $MgSO_4$, 5.55 D-glucose, and 20 HEPES (pH titrated to 7.4 using NaOH) for 20 min. If inhibitors were being tested, these were added at this time and maintained for the duration of the experiment. Cells were stimulated with a Tl^{+}-containing K^{+}-free solution consisting of (mM): 140 sodium gluconate, 2.5 potassium gluconate, 1 magnesium gluconate, 1.5 calcium gluconate, 2 thallium sulphate and 20 HEPES (pH titrated to 7.4 with NaOH) 20 s into the recording. Measurements were made at room temperature using a FlexStation (Molecular Devices) controlled by Softmax Pro software v5.4.5. FluxOR™ was excited at 485nm, emitted light collected at 520nm and measurements were expressed as a ratio increase over baseline (F/F_0).

2.8 Cell alignment

Endothelial cells were plated on a 12-well plate. At 100% confluency, cells were subjected to shear stress for 24 hours via an orbital shaker (SSM1, Stuart) rotating at 210 rpm. Cells were then imaged using the Incucyte Imaging System (Essen Bioscience).

To quantify the orientation of mLSECs relative to flow, ImageJ software (NIH) was used. Phase contrast images were processed using a 'Difference of Gaussian' operator accessed via the ImageJ plugin from the University of Sussex, to highlight the edge of individual cells. The settings used were Sigma1: 20, Sigma2: 1.5 and Enhance Contrast was applied. Quantification of cell orientation relative to flow was calculated by an ImageJ plugin, OrientationJ, which produced a histogram of local angles for each cell. Using OriginPro 2017 Gauss distribution curves were fitted to the histograms. The baseline-adjusted frequency at the mode of each curve compared between experimental groups. The protocol for analysis is depicted in Figure 2-2.

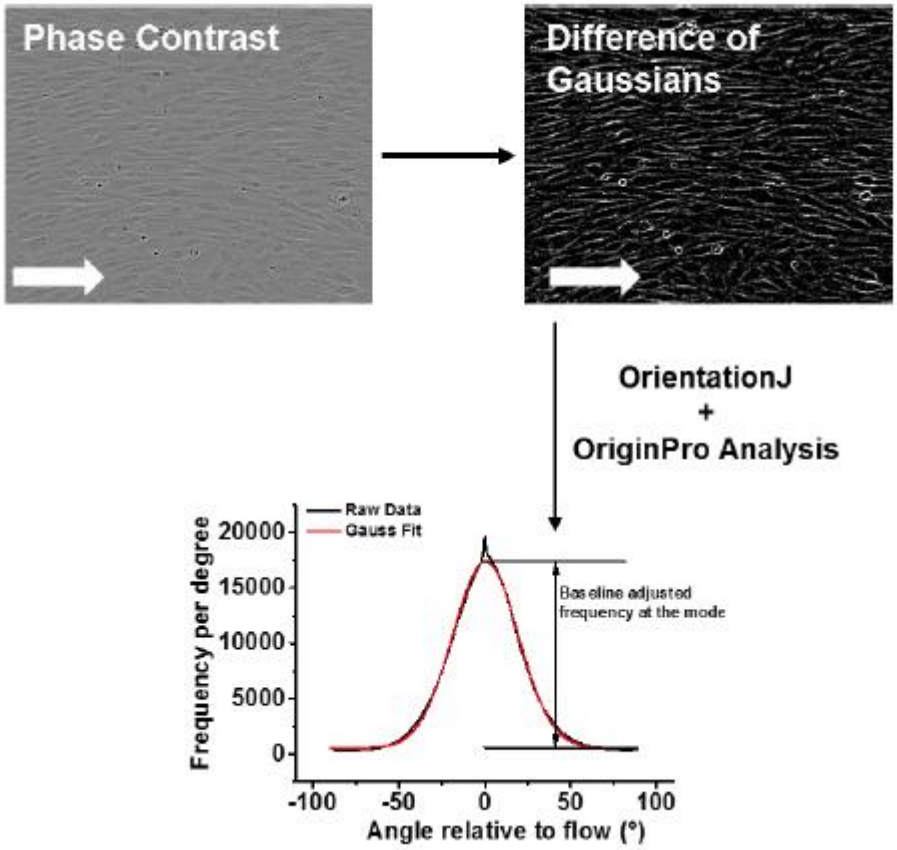

Figure 2-2 Cell alignment analysis method. Phase-contrast images are processed using the Difference of Gaussians function to define cell edges. Cell orientation was determined using OrientationJ, a plugin for ImageJ. The software returns the frequency of cells at each degree. The frequency of the aligned edges in the direction of flow are used for comparison.

2.9 Western blotting

2.9.1 Solutions

2.9.1.1 Lysis buffer

Lysis buffer contained 10 mM Tris, pH7.4, 150 mM NaCl, 0.5 mM EDTA, 0.5% NP-40. Minutes iComplete protease inhibitors (Roche 1:500) and PhosSTOP phosphatase inhibitors (Roche 1:500) were added just before lysing.

2.9.1.2 Sample (loading) buffer (4x)

Sample buffer contained 200 mM Tris pH 6.8, 8% SDS, 40% glycerol, 8% mercaptoethanol, 0.1% bromophenol blue.

2.9.1.3 Running (electrophoresis) buffer

Running buffer was purchased from BioRad and comprised of 25 mM Tris, 192 mM glycine and 0.1% SDS, pH 8.3.

2.9.1.4 Semi-dry transfer buffer

Semi-dry transfer buffer contained 48 mM Tris, 39 mM glycine and 20% methanol.

2.9.1.5 TBS-T

TBS-T contained 145 mM NaCl, 20 mM Tris-base, 0.5% Tween 20, pH 7.5.

2.9.2 Cell lysis and protein quantification

Cells were grown to confluence in a 6-well plate and harvested in lysis buffer. Cells were washed twice in PBS and 80 µl cold lysis buffer was then added to each well. Cells were scraped off the dish and the lysate was left on ice for 30 minutes prior to centrifugation at 10000xg for 20 minutes at 4°C. The soluble protein was kept for experimentation and the pellet containing cell debris and nuclei was disposed of.

Protein quantification was performed using the DC Protein Quantification kit (BioRad). Absorbance was measured in a microtiter plate reader at 570 nm wavelength. Comparison was made to a BSA standard curve and the samples protein concentrations were derived from this.

2.9.3 Western blotting and protein visualisation

20 µg of protein sample was mixed with sodium dodecyl sulphate (SDS) reducing sample buffer and heated at 90°C for 5 minutes to ensure complete protein denaturation. Samples were loaded along with molecular weight markers (BioRad) onto a 4-20% gradient SDS polyacrylamide gel (BioRad) and resolved by electrophoresis for 60-90 minutes at 175 volts. SDS is an anionic detergent which disrupts the secondary structure of proteins to produce linear, negatively charged structures. Application of electrical charge throughout the gel, causes negatively charged proteins to move towards the positively charged electrode. The distance travelled by proteins is inversely proportional to their size, so smaller proteins travel further down the gel.

Samples were transferred to a polyvinylidene fluoride (PVDF) membrane (Immobilon) by semi-dry transfer at constant current of 50 mA per membrane, for 90 minutes in transfer buffer. The membrane was then incubated for 1 hour in TBS-T containing 5% milk to block non-specific background binding. Membranes were then labelled overnight with primary antibody BEEC-4 (1:1000, Cambridge Biosciences) in TBS-T containing 5% milk, at 4°C. Following four 10 minute washes with TBS-T, the membrane was incubated with secondary horse radish-peroxidase (HRP)- donkey, anti-rabbit antibody (1:5000, Jackson ImmunoResearch) in TBS-T containing 5% milk for 1 hour at room temperature, followed by final washes with TBS-T.

SuperSignal Femto detection reagents (Pierce Science) were used to detect protein bands. Membranes were imaged using a G:BOX (Syngene) with genesis software.

2.10 Generation of Piezo1 M-R mice

The Piezo1 M-R GOF mice (M2240R), equivalent to human M2225R, were generated by CRISPR/Cas9. The gRNA was designed to direct Cas9-mediated cleavage of Piezo1 6 bp upstream of the target methionine codon and possesses no off-target sites with less than 3 mismatches elsewhere in the genome (binding sequence 5’ GGGCGCUCAUGGUGAACAG 3’).

A 120 nucleotide single-stranded homology directed repair (ssHDR) template was designed to incorporate the methionine to arginine missense mutation, in addition to silent mutations introducing a Mlu1 restriction enzyme recognition site to facilitate genotyping (5’ccacccgtcccctgagcctgaggggctccatgctgagcgtgcttccatcc

ccagccaTTAttTacGCGTagcgcccagcagccatccattgtgccattcacaccccaggcctacgagga g 3’; capital letters denote the mutated bases) (Sigma Aldrich).

The gRNA, delivered as an alt-R crRNA combined with tracrRNA (Integrated DNA Technologies, Illnois, USA), Cas9 protein (Thermo Fisher check) and ssHDR template were microinjected into C57BL/6 mouse zygotes, and implanted into females (Manchester Transgenic Animal Facility). Successful gene editing of pups was identified by Mlu1 digestion of PCR amplicons (F: 5’ TCTGGTTCCCTCTGCTCTTC 3’, R: 5’ TGCCTTCGTGCCGTACTG 3’) and confirmed by DNA sequencing following subcloning into pCRTM-Blunt

(Invitrogen). Further genotypes were determined by real-time PCR with specific probes designed for each gene (Transnetyx, Cordova, TN).

2.11 Generation of CreMyh6-Piezo1$^{-/-}$ mice.

The cardiac myocyte-specific Piezo1 KO mouse model was generated by crossing C57BL/6 mice expressing *Cre* recombinase under a cardiac myocyte specific promoter, Myh6 (CreMyh6 mice, obtained from Jax), with C57BL/6 mice expressing a Piezo1 gene with *loxP* sites flanking exons 19-23 (Piezo1$^{flx/flx}$ mice) (Li et al., 2014). Mice homozygous for Piezo1 floxed alleles but heterozygous for Cre were obtained so litters contained Piezo1 floxed mice either positive (Cre+, experimental) or negative (Cre-, control) for Cre. In this model the Cre is constitutively active and so facilitates *loxP* directed deletion of Piezo1 between exons 19-23 in cardiac myocytes from development.

Initial genotyping was performed using primers for *loxP* (F: 5' GGAGGGTTGCTTGTTGGATA 3', R:5' ACTCATCTGGGTGAGGTTGC 3') and Cre (F:5' ACCACCTGAGAAGTTGTCCC 3', R:5' ACTCATCTGGGTGAGGTTGC 3'). Further genotypes were determined by real-time PCR with specific probes designed for each gene (Transnetyx, Cordova, TN).

2.12 Animal husbandry

Animals were houses in GM500 individually ventilated cages (Animal Care Systems) at 21°C, 50-70% humidity and with a 12 h alternating light/dark cycle. They had ad libitum access to RM1 diet (SpecialDiet Services, Witham, UK) and triple filtered Hydropac water, with bedding from Pure'o Cell (Datesand, Manchester, UK). All animal experiments were authorised by the University of Leeds Animal Ethics Committee and the UK Home Office.

2.13 Haematological tests

2.13.1 Full blood counts

Haematological properties of the mice were analysed by The Blood Sciences Laboratory, Leeds Teaching Hospitals, Leeds, UK. Blood was taken from 8-week old male mice and kept in an EDTA tube. Full blood and reticulocyte counts were analysed by an ADVIA 2120i Haematology System.

2.13.2 Liver function tests and iron levels

Blood was taken from 8-week old mice and kept in a serum tubes, containing a separating gel. Samples were centrifuged at high speed for 10 minutes to separate the serum which was used for analysis. Liver function tests and iron levels were analysed using an ADVIA Chemistry XPT System by The Blood Sciences Laboratory, Leeds Teaching Hospitals, Leeds, UK.

2.13.3 Blood smears

Blood smears were stained with May-Grunwald followed by Giesma and imaged by a Nikon Eclipse E400 light microscope, fitted with a Nikon Digital Camera DXM1200.

2.13.4 Electron microscopy

Clots for scanning electron microscopy (SEM) were prepared by adding 10 µL activation mixture (0.5 $U.mL^{-1}$ murine thrombin [Enzyme Research Laboratories], $CaCl_2$ 5 mM in TBS [0.05 M Tris-Base, 0.1 M NaCl, pH 7.4]) to 100 µL of whole blood. The clotting mixture was immediately transferred to pierced Eppendorf lids. Clots were left to form in a humidified chamber at room temperature for 2 hr. Clots were washed with saline solution to remove excess salt and prepared for microscopy by fixation in 2% glutaraldehyde solution for at least 2 hr. Clots were further washed with sodium cacodylate buffer (67 mM $C_2H_6AsNaO_2$, pH 7.4) and dehydrated in a series of increasing acetone concentrations (30%–100%). Clots were critical-point dried with CO_2, mounted onto stubs, and sputter coated with platinum using a Cressington 208 HR (Cressington Scientific Instruments). Each clot was formed in duplicate and imaged in 5 areas at different magnifications (5000×, 10000×) using a Hitachi SU8230 high-performance cold field emission (CFE) SEM (Chiyoda).

2.13.5 Red blood cell (RBC) osmotic fragility test

Blood was diluted 1:8 into saline containing 2 mM HEPES (pH 7.4). 10 µl of this diluted blood was added to each well on a row of a 96-well U-bottomed plate (8 wells per sample). 225 µl tonicity solutions were added containing saline at concentrations of 0, 20, 25, 30, 35, 40, 45, 50, 55, 60, 80 and 100%, made up in water. The plate was left at room temperature for 5 min before centrifugation for 5 min at 1000xg. 150 µL of the supernatant was transferred into a well of a flat-

bottomed 96-well clear plate. The absorbance was measured at 540 nm using a FlexStation (Molecular Devices).

2.14 Electrophysiology

2.14.1 Isolation of RBCs for patch-clamp studies

Whole blood was collected in EGTA tubes and centrifuged at 10000xg for 10 min at 4 °C. Plasma was removed and RBCs were washed twice with 1 mL PBS followed by 1 min centrifugation under the same conditions. 2 µL of resulting haematocrit was resuspended in 5 mL PBS, plated onto borosilicate glass coverslips and left to settle for 30 min before recordings.

2.14.2 Patch-clamp recordings

Experiments were conducted in standard perforated-patch whole-cell (current- and voltage-clamp modes) configuration. All recordings were made using AXOpatch 200B amplifier (Axon Instruments, Inc., USA) equipped with Digidata 1550B hosted by a PC running pClamp 10.6 software (Molecular Devices, USA) at room temperature. Current records were analogue filtered at 2-5 kHz and digitally acquired at 5-20 kHz. Perforated-patch whole-cell transmembrane ionic currents were measured at a holding potential of −80 mV and cell-attached experiments were performed at a holding potential of +80 mV. RBCs were maintained during the experiment in an external solution of the following composition (mM): 135 NaCl, 4 KCl, 2 CaCl2, 1 MgCl2, 10 D-glucose and 10 HEPES (pH 7.4, NaOH). 10 mM NaCl was equimolarly replaced with TEA-Cl in voltage-clamp experiments. Patch pipettes had a resistance of 20–25 MΩ when filled with pipette solution. The pipette solution for the perforated-patch whole-cell experiments contained (mM): 145 KCl, 1 MgCl2, 0.5 EGTA, 10 HEPES (pH 7.2, KOH) and was supplemented with freshly prepared amphotericin B (300 µg.mL^{-1}) before each experiment. For application of fluid flow, membrane patches were manoeuvred to the exit of a capillary tube with tip diameter of 350 µm, out of which ionic (bath) solution flowed at 20 µl.s^{-1}.

2.15 Arterial contraction studies

Animals were culled by CO_2 inhalation, according to Schedule 1 procedure approved by the UK Home Office. Thoracic aorta or mesenteric artery was

dissected out and immediately placed into ice-cold Krebs solution (125 mM NaCl, 3.8 mM KCl, 1.2 mM $CaCl_2$, 25 mM $NaHCO_3$, 1.2 mM KH_2PO_4, 1.5 mM $MgSO_4$, 0.02 mM EDTA and 8 mM D-glucose, pH 7.4). Connective tissue and fat were carefully removed under a dissection microscope. 1 mm length segments were mounted in an isometric wire myograph system (Multi Wire Myograph System, 620M, Danish Myo Technology) with two 40 µm stainless steel wires, bathed in Krebs solution at 37°C and bubbled with 95% O_2, 5% CO_2. The segment was then stretched stepwise to its optimum resting tension to a 90% equivalent transmural pressure of 100 mmHg and equilibrated for 1 h prior to experiments. The stretch was approximately equal to that expected at diastolic blood pressure (Rode et al., 2017). Arteries were only used for investigation if they constricted in response to phenylephrine (PE) and dilated in response to acetylcholine (ACh).

2.16 Metabolic tests

2.16.1 Insulin and glucose tolerance tests (ITT and GTT)

For insulin tolerance tests, mice were fasted for 2 h before injection with 0.75 units.kg-1 recombinant human insulin i.p. (Actrapid; Novo Nordisk). For glucose tolerance tests mice were fasted overnight before injection with 1 mg.kg-1 glucose i.p. Blood was collected from the tail vein at time 0 and 30, 60, 90 and 120 min after injection for determination of glucose levels. Blood glucose was measured with a portable glucometer.

2.16.2 Plasma lipid analysis

Total cholesterol, triglycerides (TGs) and HDL cholesterol concentrations were measured from plasma using commercially available colourmetric kits (CHOD-PAP for cholesterol #87656, GPO-PAP for TGs #87319 and Cholesterol HDL-PTA for HDL cholesterol #86516; BIOLABO SA, Maizy, France). All samples were performed in duplicate and absorbance was measured on the FlexStation.

2.16.3 Indirect calorimetry

Mice were placed in individual cages in the Oxymax Comprehensive Laboratory Animal Monitoring System (CLAMS, Columbus Instruments) for 3 consecutive days, with access to a running wheel. The data from the first day was disregarded to allow for acclimatisation of the animals and an identical 24-hour period for each animal was chosen for analysis. The Oxymax system is an open-circuit indirect

calorimeter for lab animal research allowing the measurement of oxygen consumption (VO_2), respiratory exchange ratio (RER) and activity levels of mice. Oxygen consumption (VO_2) is a measure of the volume of oxygen used to convert energy substrate into ATP. Respiratory exchange ratio (RER) is the ratio of carbon dioxide production (VCO_2) divided by O_2 consumption, and can be used to estimate the fuel source for energy production based on the difference in the number of oxygen molecules required for the oxidation of glucose versus fatty acids. An RER of 0.7 indicates that fatty acids are the primary substrate for oxidative metabolism, while an RER of 1.0 indicates that carbohydrate is the primary energy substrate. Food intake and activity levels of mice can also be measured using the CLAMs system.

2.17 Tissue histology

Tissue samples were fixed for 48 h in 4% PFA at 4°C prior to processing on a Leica ASP 200 and embedding in CellWax (Cellpath) on a Leica EG1150H embedding system. Sections of 4 µm were cut on a Leica RM2235 microtome on Plus Frost slides (Solmedia) and allowed to dry at 37°C overnight prior to staining. Slides were de-waxed in xylene and rehydrated in ethanol. H&E was performed by staining in Mayer's Haematoxylin for 2 min and eosin for 2 min. Slides were imaged on an Aperio AT2 (Leica Biosystems) high definition digital pathology slide scanner with a maximal magnification of x20. Tissue processing and imaging were performed at the Section of Pathology and Tumour Biology, Leeds Institute of Cancer and Pathology.

2.17.1 Calculating adipocyte cell area

Adipocyte size was measured using ImageJ software. Between 414-967 adipocytes were measured per sample. The background was subtracted, noise removed and the contrast uniformly enhanced to improve membrane definition. The threshold was set to highlight the membranes, whilst leaving empty space and the image was converted to a binary image. Adiposoft was then used to measure adipocyte area (Galarraga et al., 2012).

2.18 Blood pressure recordings from tail cuff

Blood pressure was measured non-invasively using the CODA tail-cuff system which uses Volume Pressure Recording (VPR) to measure blood pressure by

determining the tail blood volume. Mice were placed into a holder to restrict movement and allow access to the tail. The “Occlusion Cuff” was placed and fastened onto the base of the tail, followed by the “VPR Cuff”. The mice were placed into an incubator set at 36ºC and left for 15 min to thermoregulate and acclimatise to the holder. The recording sessions were conducted by the CODA software and consisted of 28 cycles (10 of which were Acclimation Cycles) with 5 seconds between each cycle. The Maximum Occlusion Pressure was 250 mmHg, Deflation Time, 20 seconds and Minimum Volume, 15 µl. 8 week old mice were used for the recordings.

2.19 Echocardiography

Animals were maintained under steady-state isoflurane anaesthesia and placed on a heated platform with ECG and respiration monitoring. Echocardiography was performed using a Vevo2100 high resolution, pre-clinical *in vivo* ultrasound system (Visual Sonics) with the MS-550D transducer at 40 MHz frequency and 100% power. Imaging was performed on a layer of aquasonic gel after the pre-cordial skin had been removed with cream (Veet). Short-axis view (SAX) images were obtained in M-mode which displays the cardiac cross-section image data during the cardiac cycle. The IVS (interventricular septum), LVID (left ventricular internal diameter) and LVPW (posterior wall of the left ventricle) were traced from the same images in systole and diastole. Ejection fraction (%) and fractional shortening (%) were calculated with the Vevo LAB cardiac package software using the following formulas FS: 100*({LVIDd–LVIDs}/LVIDd), EF: 100*({LV vol d–LV vol s}/LV vol d).

2.20 Data analysis

Data are presented as mean ± SEM. Data were analysed and figures presented using OriginPro 2018 software (OriginLab Corporation). Paired data were compared statistically using a two-tailed Students’ *t*-test. Data sets with more than 2 groups were compared using a one-way ANOVA with Tukey’s *post hoc* test. Statistical significance is indicated by * ($p<0.05$), ** ($p<0.01$) and *** ($p<0.001$) and **** ($p<0.0001$). n represents the number of independent experiments for a given result and N indicates the total number of replicates between the independent experiments. For IC_{50}/EC_{50} determination, curves were fitted using the Hill1 (Origin Pro 2018) equation.

Chapter 3 Characterising the Piezo1 M-R mouse model

3.1 Introduction

Gain-of-function (GOF) Piezo1 mutations have been linked to dehydrated hereditary stomatocytosis (DHS), a form of anaemia (Iolascon et al., 2019). Over 10 Piezo1 mutations have been associated with DHS (Figure 1-4), one of the first ones observed being missense mutation M2225R, located in the extracellular cap domain (Zarychanski et al., 2012).

Studies in heterologous expression systems determined that the cause of GOF in M2225R and many other Piezo1, DHS-causing mutations is a prolonging of channel inactivation (Bae et al., 2013a). However, the effects of the mutation on Piezo1 gating have not been determined in the native red blood cells (RBCs) and there is growing evidence that Piezo1 channel kinetics are vastly different in studies of the endogenous channel, compared to heterologous expression systems (Beech and Kalli, 2019). Therefore it is important to study the effects of Piezo1 mutations in isolated cells. Additionally, it is not known whether the mutation can cause GOF of Piezo1 in cells other than RBCs.

The aim of this chapter was to determine whether the murine equivalent of the DHS-causing Piezo1 M2225R (Piezo1 M-R) mutation caused GOF in the mouse channel. The mutation was recapitulated into a CRISPR/Cas9-edited mouse model and the resulting Piezo1 M-R mice were tested for signs of DHS. The effects of the mutation on channel gating in RBCs was investigated before examining whether Piezo1 M-R also caused GOF in endothelial cells; the cells of interest in our laboratory, with important Piezo1 activity.

3.2 Results

3.2.1 The M-R mutation causes gain-of-function in response to pharmacological activation in the murine Piezo1 channel

In order to verify that the murine equivalent of M2225R (M2240R), hereby referred to as Piezo1 M-R, caused GOF properties in the Piezo1 channel, the mutation was generated in a mouse Piezo1 clone and transiently transfected into HEK 293 cells. Intracellular Ca^{2+} entry to Piezo1 agonist Yoda1, was investigated

in these cells using the FlexStation. The response to 10 μM Yoda was potentiated in the Piezo1 M-R expressing cells by 1.6 fold (Figure 3-1A-B).

To test further properties of the channel, the murine Piezo1 M-R mutant was stably incorporated into HEK T-REx cells and the cell line mPiezo1 M-R was achieved. The potency of Yoda1 in this mutant clone was investigated by generating concentration-effect curves. The Yoda1 dose-response was left-shifted in mPiezo1 M-R compared to wild-type mouse Piezo1 (mPiezo1) with EC_{50} values of 0.12 μM (mPiezo1) and 0.04 μM (mPiezo1 M-R) (Figure 3-2A-C). The amplitude of the Yoda1 response was increased at lower concentrations, but not at higher concentrations, likely due to a saturation of the Fura-2 response (Figure 3-2C). Analysis of EC_{50} values from concentration-effect curves generated for each individual experiment were also reduced in the mPiezo1 M-R cells (Figure 3-2D). Overall, the murine equivalent of the Piezo1 M2225R channel demonstrated increased function in response to pharmacological activation by Yoda1.

To determine that the GOF effects of murine Piezo1 M-R were not specific to pharmacological activation by Yoda1, mPiezo1 M-R cells were tested against their response to Yoda1 analogue, KC159, which has been identified as a Piezo1 agonist in our laboratory (Figure 3-3A). Similarly to the results observed for Yoda1 activation, the KC159 concentration-effect was left-shifted in the mPiezo1 M-R cells compared to WT mouse Piezo1, with EC_{50} values of 0.21 μM (mPiezo1) and 0.06 μM (mPiezo1 M-R) (Figure 3-3B-D). Additionally the average EC_{50} values generated from each individual experiment were reduced in the mPiezo1 M-R cells (Figure 3-3E). Overall, these experiments show that pharmacological activation of the murine Piezo1 M-R channel cause augmented, more sensitive responses suggesting that the M-R mutation in the mouse is GOF. This suggests the mutation affects mouse Piezo1 in a similar manner to the human channel, indicating that murine Piezo1 is a suitable model for the human condition.

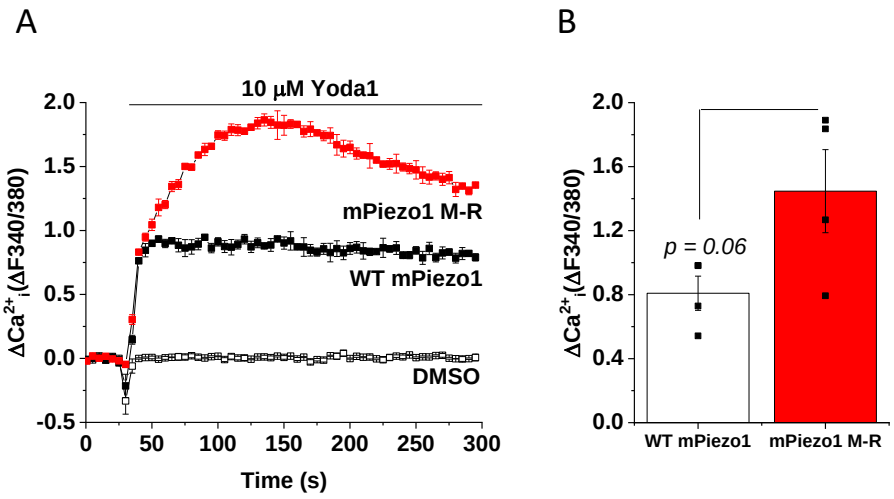

Figure 3-1 The Piezo1 M-R mutation potentiates the Yoda1 response. (A) FlexStation intracellular Ca^{2+} measurement data for HEK293 cells transiently transfected with WT murine Piezo1 (mPiezo1) or murine Piezo1 with the M-R mutation (mPiezo1 M-R) and exposed to 10 µM Yoda1 or vehicle only. Error bars indicate SEM (N=3, in-plate replicates). (B) Summary of experiments of the type shown in (A) measured between 60-90 s after Yoda1 application. All individual data points are shown with mean ± SEM (n=4).

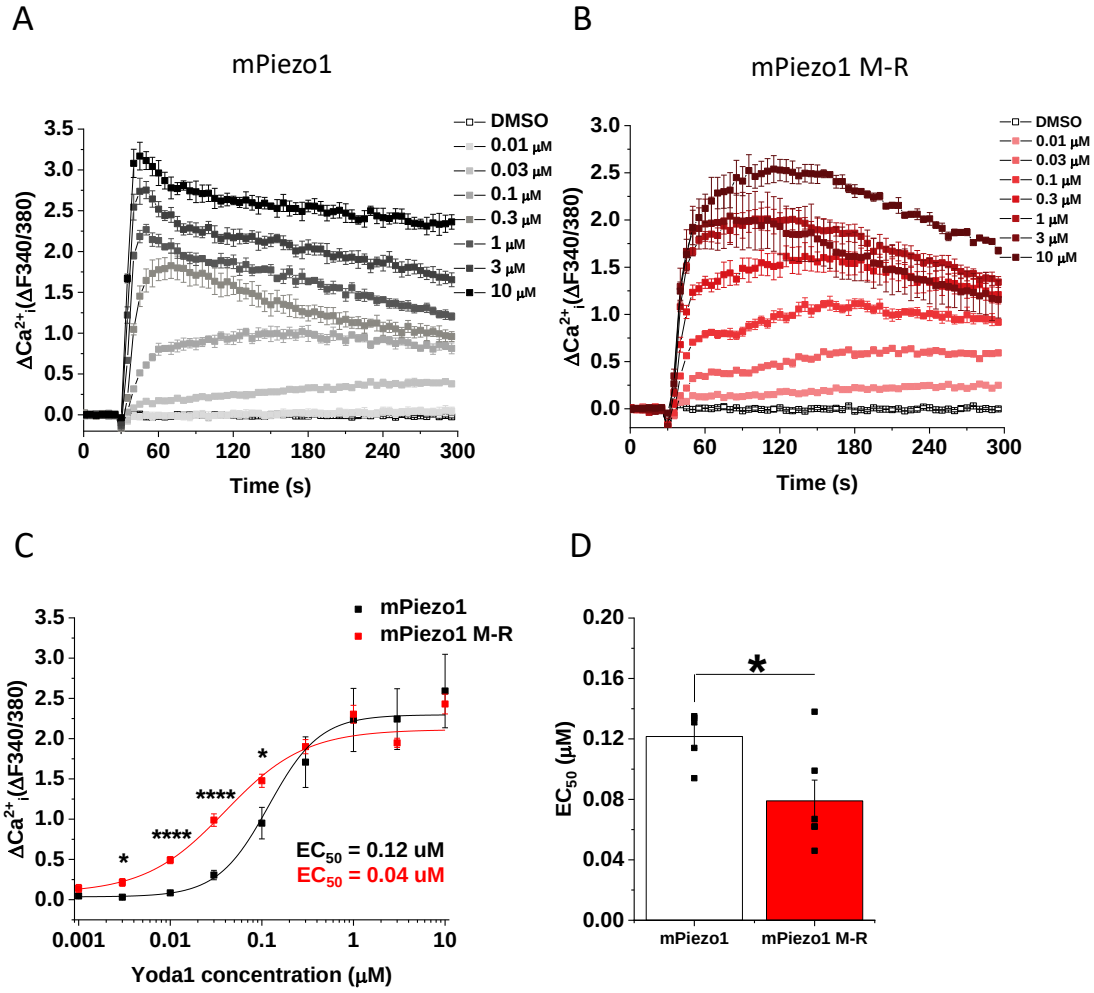

Figure 3-2 The Piezo1 M-R mutation causes increased sensitivity to Yoda1. (A-B) FlexStation intracellular Ca^{2+} measurement data for mPiezo1 (A) or mPiezo1 M-R (B) cells exposed to Yoda1 at the specified concentrations or exposed to the vehicle only. Error bars indicate SEM (N = 3, in-plate replicates). (C) Mean data ± SEM for the type of experiments shown in (A-B). The fitted curve is the Hill equation with EC_{50}s of 0.12 μM (mPiezo1), 0.04 μM (mPiezo1 M-R) (n=5, mPiezo1; n=6 mPiezo1 M-R). (D) Average EC_{50} values from individual fitted dose response curves (as C), for separate experiments such as in (A-B). Mean data ± SEM. Each square represents results from an individual experiment (n=5 mPiezo1, n=6 mPiezo1 M-R). * (p<0.05), ** (p<0.01), *** (p<0.001), **** (p<0.0001).

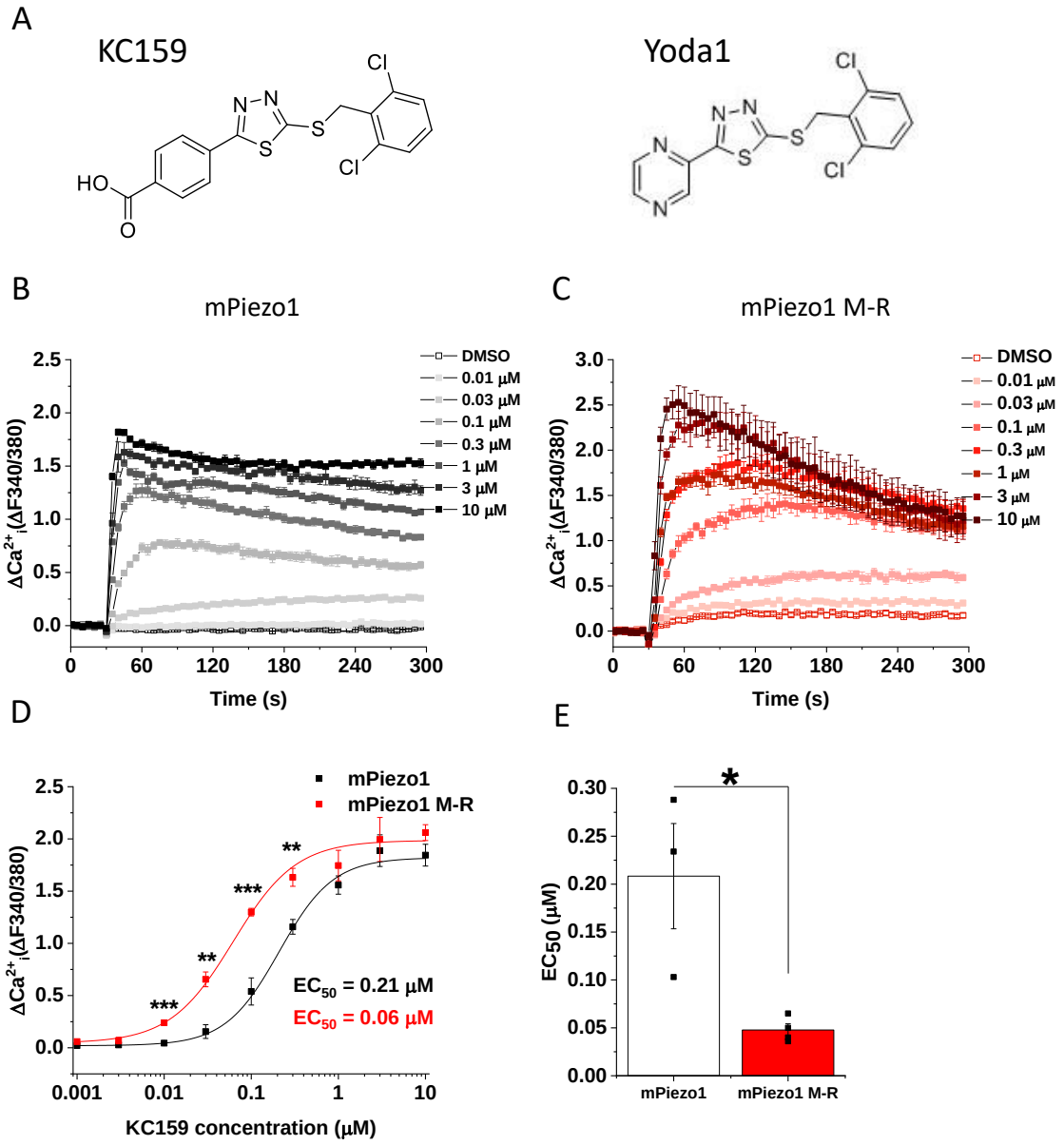

Figure 3-3 The Piezo1 M-R mutation causes increased sensitivity to Yoda1 analogue, KC159. (A) Structure of KC159 (left) with structure of Yoda1 (right) for comparison. (B-C) FlexStation intracellular Ca^{2+} measurement data for mPiezo1 (B) or mPiezo1 M-R (C) cells exposed to KC159 at the specified concentrations or exposed to the vehicle only. Error bars indicate SEM (N = 3, in-plate replicates). (D) Mean data ± SEM for the type of experiments shown in (B-C). The fitted curve is the Hill equation with EC_{50}s of 0.21 µM (mPiezo1) and 0.06 µM (mPiezo1 M-R) (n=3 mPiezo1, n=4, mPiezo1 M-R). (E) Average EC_{50} values from individual fitted dose response curves (as D), for separate experiments such as in (B-C). Mean data ± SEM. Each square represents results from an individual experiment (n=3 mPiezo1, n=4 mPiezo1 M-R). * ($p<0.05$), ** ($p<0.01$), *** ($p<0.001$), **** ($p<0.0001$). Dr Kevin Cuthbertson (University of Leeds) designed and synthesised KC159.

3.2.2 Generation of Piezo1 M-R (M2240R) mouse model

After establishing that the Piezo1 M-R mutation also affects murine channel function, it was suitable to generate a mouse model of the mutation, in order to model the human condition. A Piezo1 M-R mouse line was generated by CRISPR/Cas9 technology, resulting in expression of the mutation globally in all cell types, therefore mirroring human patients. A homology directed repair (HDR) approach was used to introduce the exact point mutation (M-R) at amino acid residue M2240R (Figure 3-4) located in the C-terminal extracellular domain, of the channel, above the pore (Figure 3-5A). Successful incorporation of the HDR template was confirmed by Sanger sequencing, revealing the expected silent and M-R mutated residues (Figure 3-5B). The mice appeared superficially normal and bred well with Mendelian inheritance (Figure 3-6A). Mice homozygous for the mutation did not demonstrate any difference in body weight compared to WT mice (Figure 3-6B). Overall, the results show successful generation of a homozygote Piezo1 M-R mouse model, to be used in further studies of the effects of Piezo1 GOF.

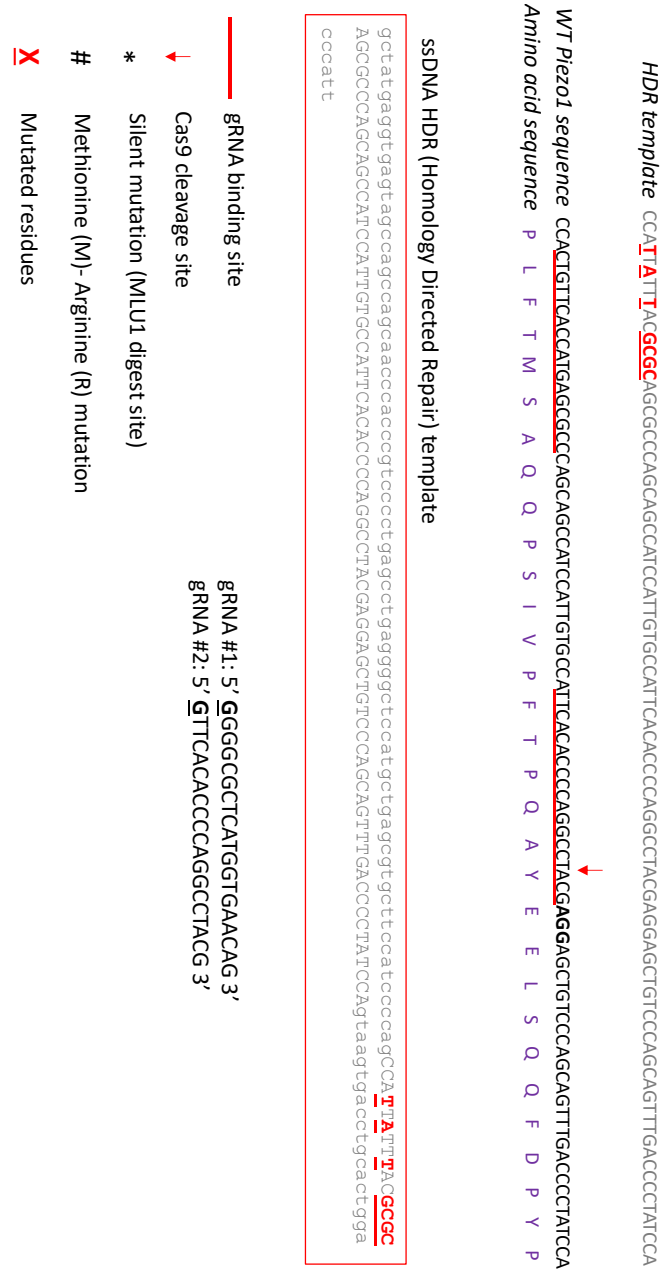

Figure 3-4 Piezo1 M-R mouse generation by CRISPR/Cas9. Schematic showing the strategy for CRISPR/Cas9 editing to produce Piezo1 M-R mutation in mice via homology directed repair (HDR). Two guide RNAs (gRNAs) were designed to target the Piezo1 sequence close to amino acid residue 2240. The red bars on the Piezo1 sequence denote where the gRNAs bind. The red arrow indicates the site of the double stranded DNA break via Cas9 cleavage, upstream of the PAM sequence in bold. A 200 base pair HDR template was introduced (shown in full in the red box) which included silent mutations (indicated by *) to incorporate an MLU1 digest site for selection and the M-R mutation (indicated by #). All mutations introduced indicated in red and underlined. gRNAs and HDR template designed by Dr Melanie Ludlow (University of Leeds). Dr Neil Humphries and Dr Anthony Adamson (University of Manchester) generated the mouse at the Manchester Transgenic Animal Facility.

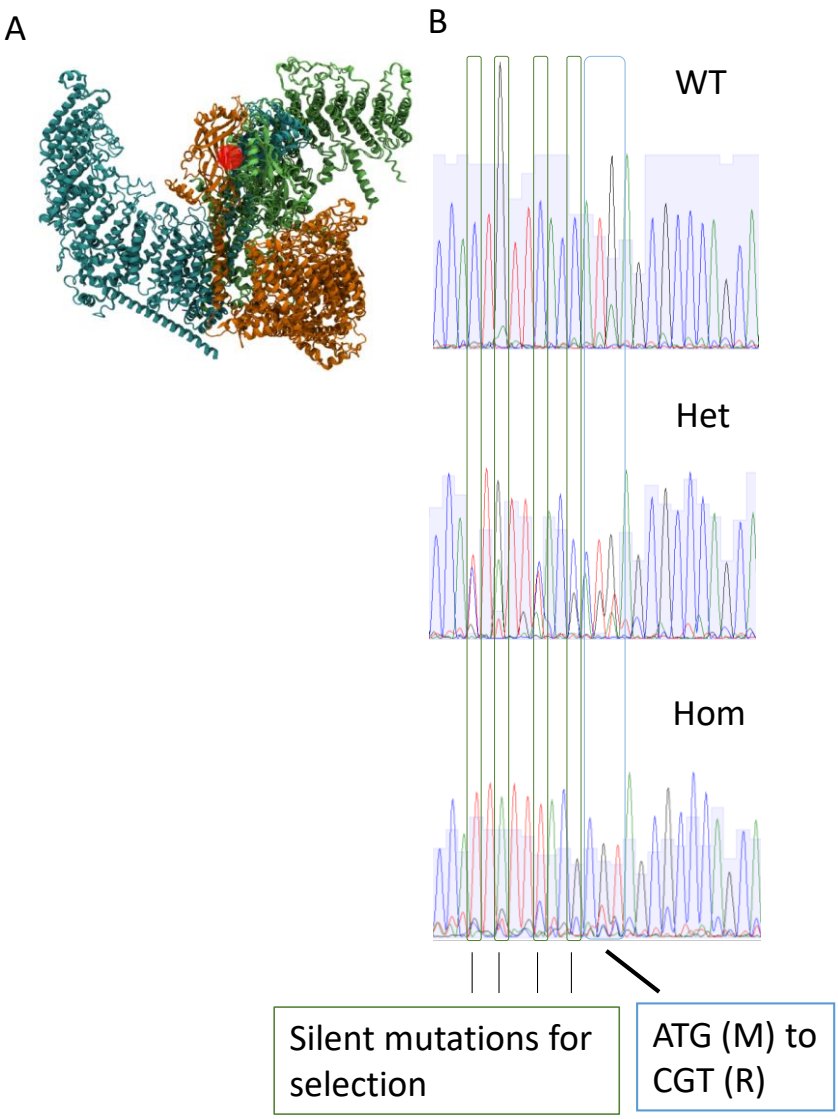

Figure 3-5 Sequence analysis of Piezo1 M-R mice. (A) Molecular model of mouse Piezo1. The channel comprises 3 Piezo1 proteins, shown in different colours. The red dot indicates the region of the M2240R mutation in the C-terminal extracellular domain. Model produced by Dr Dario De Vecchis (University of Leeds). (B) Sanger sequencing indicating CRISPR-generated mutations by homology-directed repair. DNA sequence encoding methionine (ATG) to arginine (CGT) mutation are highlighted by the blue box. Silent mutations for MLU1 selection are highlighted by the green boxes. In the sequencing trace, blue = cysteine, green = adenine, red = thymine, black = guanine.

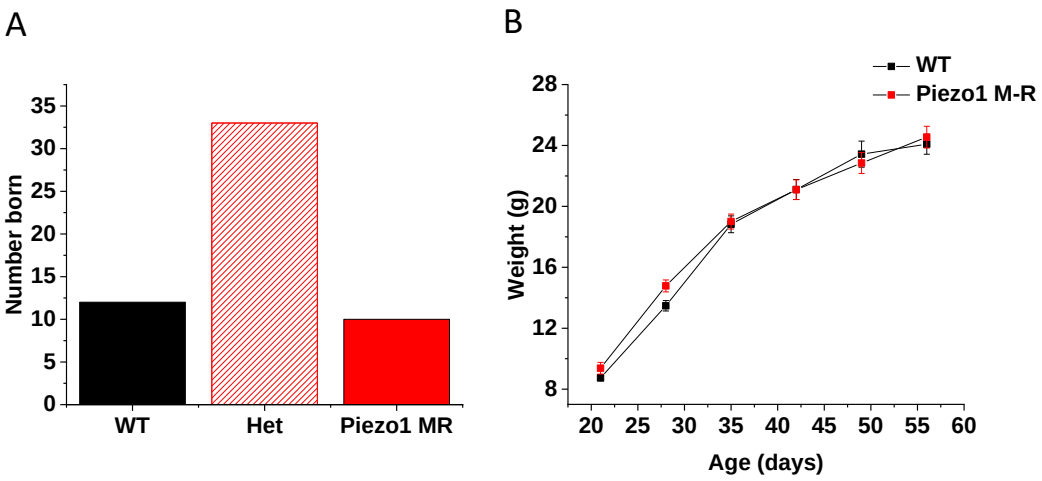

Figure 3-6 Piezo1 M-R mice are viable and appear normal. (A) Numbers of mice born with the indicated genotypes after mating of mice heterozygous for Piezo1 M-R mutation. (B) Mean ± SEM comparison of body weights of wildtype (WT) and Piezo1 M-R mice between 3-8 weeks of age (n=5 WT, n=7 Piezo1 M-R).

3.2.3 Piezo1 M-R mice display features of DHS

Next, it was important to determine whether Piezo1 M-R caused an anaemia like phenotype in mice, like humans with the mutation. Blood was collected in EDTA tubes to prevent clotting and the samples were analysed by the Blood Sciences Laboratory at Leeds General Infirmary. The haematological properties from these mice demonstrated signs of anaemia normally observed in patients with DHS, with a decrease in haemoglobin and increase in reticulocytes (Figure 3-7). Mean red cell distribution (RDW) and haemoglobin width (HDW), which measure the heterogeneity of cell size and haemoglobin concentrations respectively, were also increased in the M-R mice, indicating the differing sizes of red blood cells (RBCs) from haemolytic anaemia. Patients with DHS are expected to exhibit increased mean corpuscular volume (MCV) and haemoglobin (MCH) indicating increased RBC size and haemoglobin mass per RBC (Albuisson et al., 2013, Zarychanski et al., 2012), however these differences were not observed. This anaemia phenotype was not due to altered iron levels or liver function (Figure 3-8). Splenomegaly which is often reported in human patients with DHS was emerging in some mice at 8 weeks, but became more evident at 22 weeks of age (Figure 3-9).

Importantly, the properties of the RBCs matched well with the human condition and showed evidence of being dehydrated. Blood films and scanning electron microscopy of RBCs from the mice demonstrated the presence of deformed stomatocytes with the distinctive ‘coffee bean’ appearance which is observed in human patients (Figure 3-10). Another hallmark of DHS is reduced osmotic fragility of RBCs. To investigate this RBCs were exposed to solutions of different tonicity’s, ranging from isotonic saline, to water and the degree of haemolysis was elucidated by measuring absorbance at a red wave length, 540 nm. RBCs from the Piezo1 M-R mice demonstrated reduced osmotic fragility as shown by a leftward shift in the osmotic fragility curve (Figure 3-11A) and a reduced tonicity at which 50% haemolysis was achieved (Figure 3-11B). In other words, RBCs from Piezo1 M-R can withstand more hypotonic solutions before bursting. Overall, the data show the GOF Piezo1 M-R mutation alone is able to produce an anaemia-like phenotype in mice which matches many of the clinical properties observed in human patients.

	Mean ± SEM		p-value
	WT	Piezo1 M-R	
HGB	*129.60 ± 1.03*	*121.50 ± 1.32*	*0.002***
WBC	2.50 ± 0.27	2.945 ± 0.60211	0.50
WBCP	2.39 ± 0.23	2.81 ± 0.62	0.50
PLT	861.20 ± 48.59	861.50 ± 53.42	0.99
MCV	50.64 ± 0.42	49.90 ± 0.54	0.31
HCT	*0.45 ± 0.004*	*0.41 ± 0.01*	*0.003***
RBC	*8.88 ± 0.06*	*8.32 ± 0.22*	*0.03**
MCH	14.60 ± 0.08	14.63 ± 0.37	0.94
MCHC	288.24 ± 3.70	293.18 ± 5.25	0.45
CHCM	282.40 ± 3.98	292.50 ± 4.57	0.14
RDW	*11.74 ± 0.12*	*14.18 ± 0.22*	*0.00002****
HDW	*16.56 ± 0.44*	*19.40 ± 0.66*	*0.007***
%RETIC	*4.27 ± 0.39*	*7.33 ± 0.39*	*0.002***

Figure 3-7 Haematological analysis of Piezo1 M-R mice reveals signs of anaemia. (A) Mean ± SEM data and p-values for haematological parameters for WT (n=4) and Piezo1 M-R mice (n=5). HGB: Haemoglobin, WBC: White blood cells, WBCP: White Blood Cells Count from the Peroxidase Method, PLT: Platelet Count, MCV: Mean Corpuscular Volume, HCT: Haematocrit, RBC: Red Blood Cells, MCH: Mean Corpuscular Haemoglobin, MCHC: Mean Corpuscular Haemoglobin Concentration, CHCM: Cellular Haemoglobin Concentration Mean, RDW: Red Blood Cell Distribution Width, HDW: Haemoglobin Concentration Distribution Width, %RETIC: % of Reticulocytes. * ($p<0.05$), ** ($p<0.01$), *** ($p<0.001$), **** ($p<0.0001$).

	Mean ± SEM		p-value
	WT	Piezo1 M-R	
ALBP (g/L)	13.04 ± 0.74	13.22 ± 0.22	0.82
ALP_2c (U/L)	146.68 ± 9.94	127.36 ± 10.53	0.24
ALT_c (U/L)	33.84 ± 3.19	32.10 ± 3.70	0.73
IRON_2 (µmol/L)	18.98 ± 1.61	20.02 ± 1.77	0.68
TIBC (µmol/L)	21.72 ± 12.37	38.46 ± 9.04	0.39

Figure 3-8 Anaemia observed in Piezo1 M-R mice is not due to altered liver function. Liver function tests: ALBP, albumin; ALP_2c, alkaline phosphatase; ALT-c, alanine aminotransferase; TIBC, total iron binding capacity. Data are shown as mean ± SEM (n=5 mice in each group).

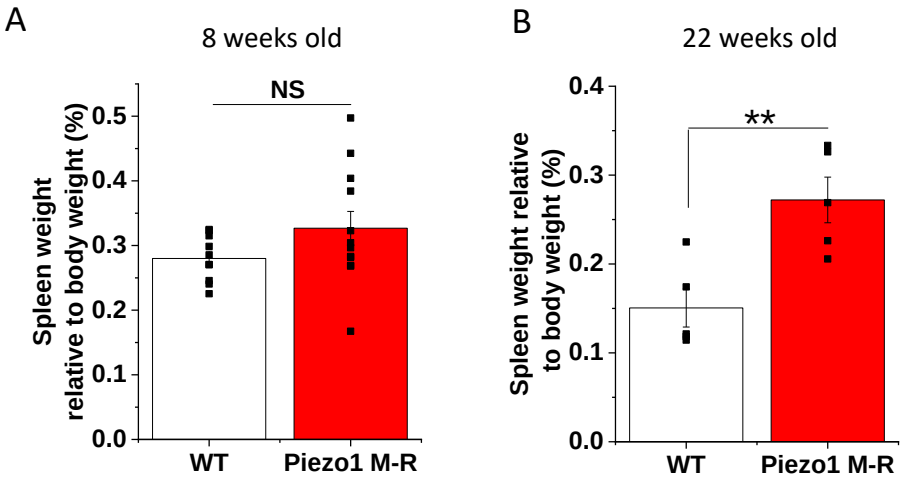

Figure 3-9 Older Piezo1 M-R mice exhibit splenomegaly. Mean ± SEM weight of spleen as % of total body weight in 8 week-old (A) (WT: n=10, Piezo1 M-R: n=12) and 22 week-old mice (B) (n=5 both genotypes). Each square represents a value from an independent experiment. * ($p<0.05$), ** ($p<0.01$), *** ($p<0.001$), **** ($p<0.0001$).

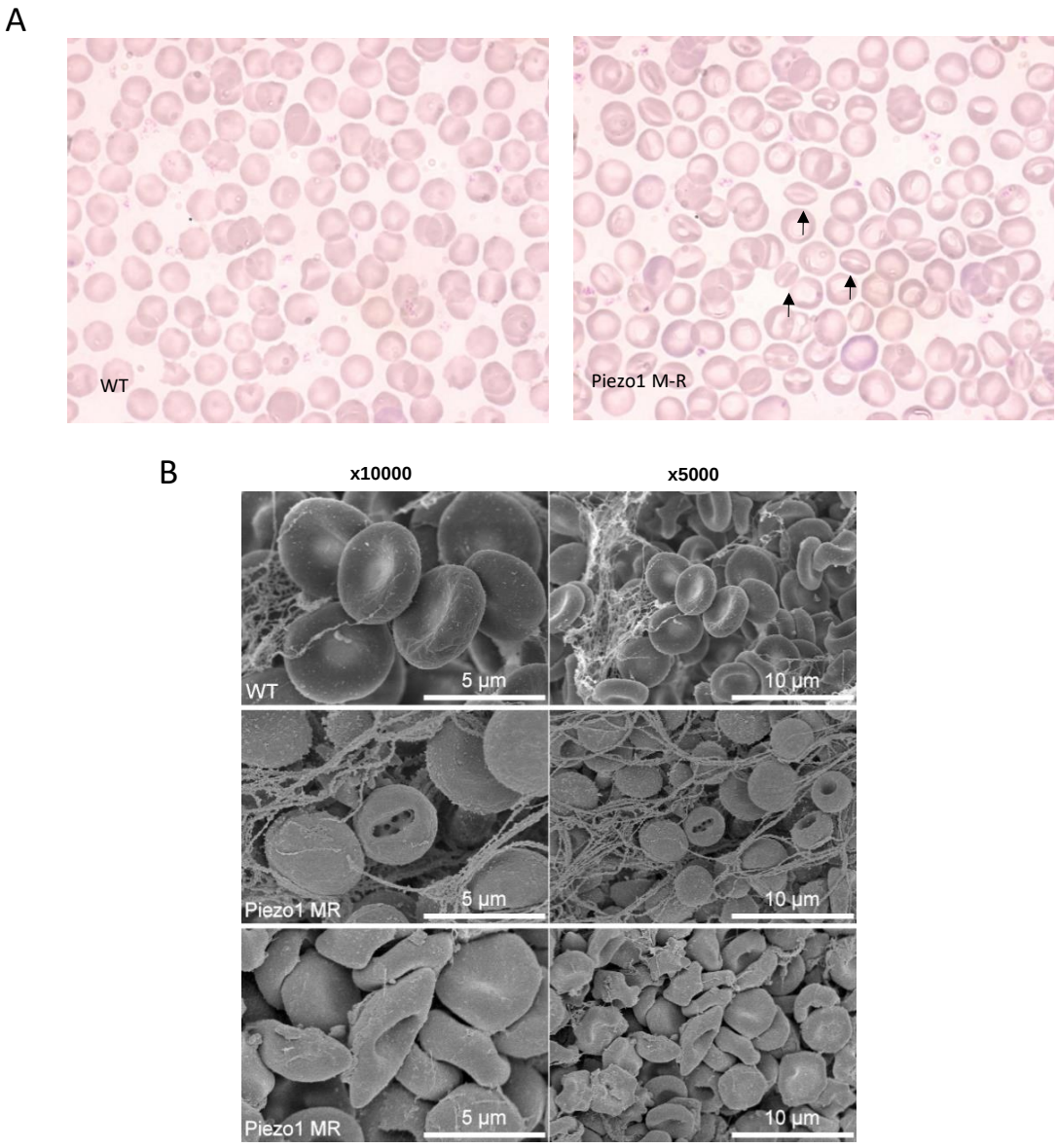

Figure 3-10 Piezo1 M-R mice have stomatocytes. (A) Red blood cells from WT (left) or Piezo1 M-R (right) mice stained with May-Grunwald followed by Giesma stain. Magnification is 100x. The presence of stomatocytes is indicated by the black arrows pointing to cells with the appearance of coffee beans. (B) Scanning electron microscopy images of red blood cells from WT (1 example at 2 magnifications) and Piezo1 (2 example at 2 magnifications) mice, showing presence of stomatocytes in Piezo1 M-R mice. Representative of 2 independent experiments. Scanning electron microscopy performed by Dr Fraser Macrae (University of Leeds).

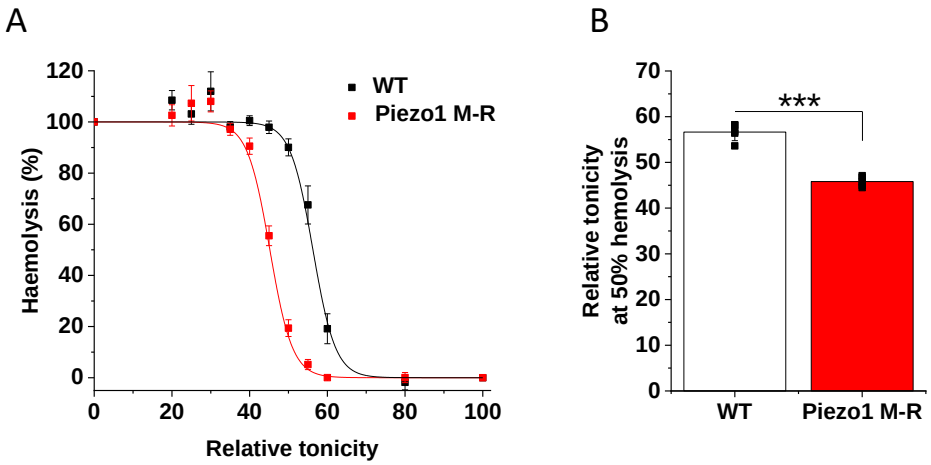

Figure 3-11 RBCs from Piezo1 M-R mice have reduced osmotic fragility. (A) Osmotic fragility test in RBCs from WT and Piezo1 M-R mice. Data are shown as mean ± SEM (n=5). The fitted curves are the function Dose response. (B) Quantification of the experiments shown on the left indicated the relative tonicity at which 50% of the RBCs are lysed, calculated from each individual curve. Each data point represents a value from an independent experiment with mean values and error bars representing SEM (n=5). * ($p<0.05$), ** ($p<0.01$), *** ($p<0.001$), **** ($p<0.0001$).

3.2.4 Piezo1 M-R causes a slowed deactivation in affected RBCs

To investigate how the Piezo1 M-R mutation alters channel function in the affected RBCs, electrophysiological experiments were performed on RBCs freshly isolated from the mice. Perforated-patch technique was used to measure whole-cell membrane potential and constant current was injected to adjust the resting membrane potential to -80mV. For a mechanical stimulus which was physiologically relevant, fluid flow was applied to the cells at a similar magnitude to that which occurs *in vivo* in mice (Rode et al., 2017). Fluid flow caused a small depolarisation in WT RBCs, expected for the opening of Piezo1 channels (Figure 3-12A-B). After cessation of fluid flow, the membrane potential quickly returned to resting levels (Figure 3-12A-B). The depolarisation in Piezo1 M-R RBCs was larger and particularly striking was the failure of the membrane potential to recover after removal of fluid flow (Figure 3-12A-B).

To further investigate the effect of the Piezo1 M-R mutation, voltage-clamp mode was utilised to maintain the membrane potential at -80mV and measure changes in membrane current. Application of fluid flow resulted in inward current in WT RBCs as expected for activation of Piezo1 channels. The current decayed whilst still in the presence of the mechanical stimulus, suggesting channel inactivation (Figure 3-12C-D). The current amplitude returned to pre-stimulus values, during or shortly after cessation of fluid flow, suggesting full inactivation or recovery. In RBCs from Piezo1 M-R mice, a similar current amplitude was observed in response to fluid flow, but little or no current decay occurred whilst fluid flow was maintained, suggesting an absence or dramatic slowing of inactivation (Figure 3-12C-D). Similar to the membrane potential recordings, the current amplitude failed to recover after cessation of fluid flow (Figure 3-12C-D). Taken together the data suggest that the effect of the Piezo1 M-R mutation is prevention of recovery after activation by mechanical stimulus. It would appear that the Piezo1 M-R mutation has a different mechanism in physiological cells, rather than the delayed inactivation previously observed in overexpression systems. It agrees with a prolonged activated state but indicates that channel deactivation is affected more so than inactivation in the presence of a stimulus.

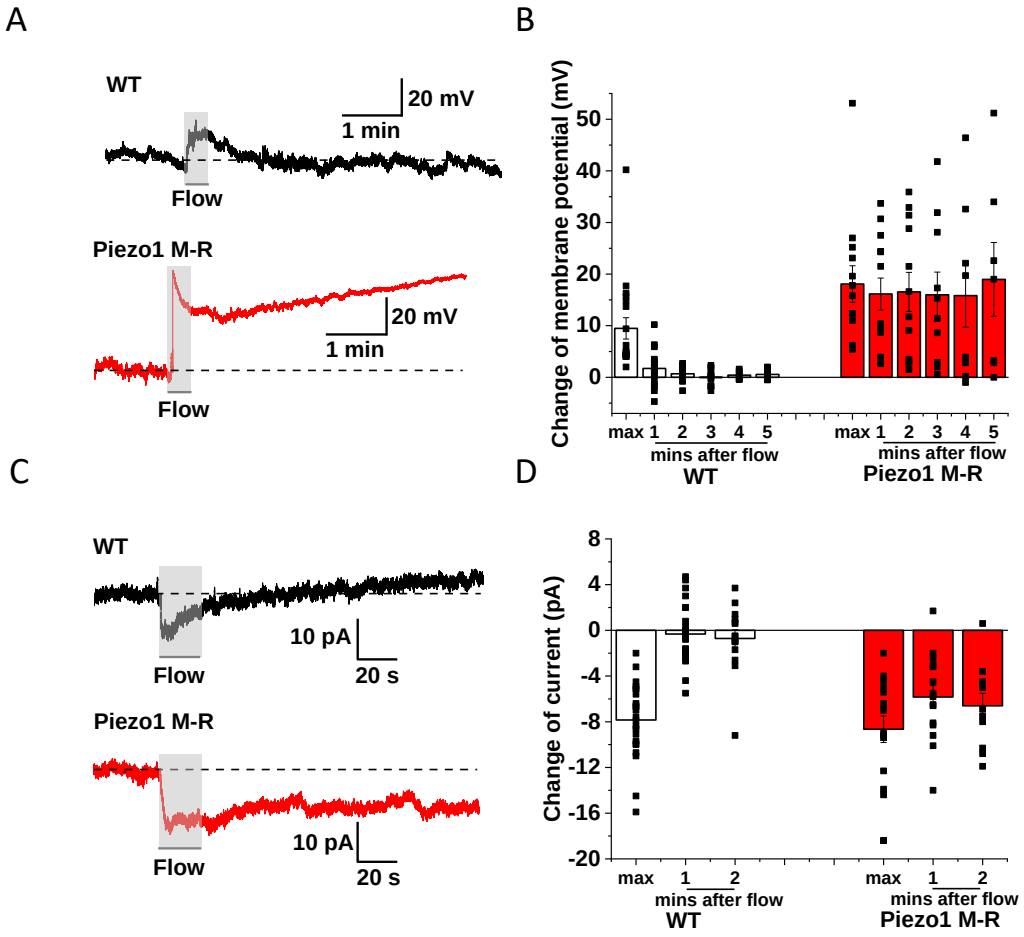

Figure 3-12 RBCs of Piezo1 M-R mice fail to recover resting membrane potential and maintain current entry after fluid flow. (A-B) Membrane potential (V_m) recordings obtained using perforated-patch whole-cell mode applied to freshly-isolated RBCs from wildtype (WT) (top) or Piezo1 M-R mice (bottom). RBCs were exposed to 20 µL.s^{-1} fluid flow for 20 s as indicated by the shaded area. (B) Summary data for experiments of the type shown in (A). Presented is the peak (maximum) change in V_m of WT and Piezo1 M-R RBCs after exposure to flow and then the V_m at 1-5 min after flow. Averaged data are displayed as mean ± SEM and each individual data point (WT; n= 18 {max, 1 min, 2 min}, 15 {3 min}, 12 {4 min}, 8 {5 min}; Piezo1 M-R; n= 13 {max, 1 min, 2 min}, 12 {3 min}, 10 {4 min}, 8 {5 min}). (C-D) Ionic current recordings obtained using perforated-patch technique in whole-cell voltage-clamp mode applied to freshly-isolated RBCs from wildtype (WT) (top) or Piezo1 M-R mice (bottom). RBCs were exposed to 20 µL.s^{-1} fluid flow for 20 s as indicated by the shaded area. Holding voltage was -80 mV. (D) Summary data for experiments of the type shown in (C). Presented is the peak (maximum) change in current (DI) of WT and Piezo1 M-R RBCs after exposure to flow and then the DI at 1 and 2 min after flow. Averaged data are displayed as mean ± SEM and each individual data point (WT; n= 23 {max, 1 min}, 15 {2 min}; Piezo1 M-R; n= 18 {max}, 15 {1 min}, 11 {2 min}). Patch-clamp recordings performed by Dr Oleksandr Povstyan (University of Leeds).

3.2.5 Piezo1 M-R also causes GOF in endothelial cells

Piezo1 is a global mechanotransducer and the channel has been shown to have a particularly important role within endothelial cells, contributing to vascular development, angiogenesis and blood pressure (Li et al., 2014, Kang et al., 2018, Wang et al., 2016, Rode et al., 2017, Zeng et al., 2018). Therefore it was important to determine whether the Piezo1 M-R mutation also caused GOF in these specialised cells.

To test this, liver sinusoidal endothelial cells (mLSECs) were isolated from WT and Piezo1 M-R mice. Intracellular Ca^{2+} entry to Piezo1 agonist Yoda1, was investigated in these cells using the FlexStation. The response to 2 μM Yoda was potentiated in the Piezo1 M-R cells by 1.3 fold (Figure 3-13A,C), but Ca^{2+} entry to ATP was unaffected (Figure 3-13B,D) suggesting the GOF effect was specific to activation of Piezo1.

Next, it was suitable to determine whether the increase in Ca^{2+} signal possible in the Piezo1 M-R cells resulted in a change to endothelial cell function. Alignment of endothelial cells in the direction of fluid flow is a well-known phenomenon and is important to maintain a healthy vasculature. Piezo1 has been demonstrated to mediate endothelial cell alignment as mice lacking the protein have disorganised endothelial cells which cannot align to fluid flow (Li et al., 2014). To investigate whether the Piezo1 M-R mutation affected the alignment of endothelial cells, mLSECs were subjected to 24 hours of 10 $dyn.cm^{-2}$ flow using an orbital shaker to induce alignment in the direction of flow, compared to cells maintained in static conditions. As expected, mLSECs from WT mice aligned in the direction of flow (Figure 3-14A-C). mLSECs from Piezo1 M-R mice appeared to exhibit a subtle trend for increased alignment (*p* value = 0.19), perhaps expected if the mutation caused channel GOF, but increased sample sizes are required for a definitive conclusion (14 samples in each group are required to detect a 20% difference with 80% power). Overall, the data suggest that the Piezo1 M-R mutation may cause GOF effects in cells other than RBCs; in this case, endothelial cells, but the physiological relevance of this remains to be proved.

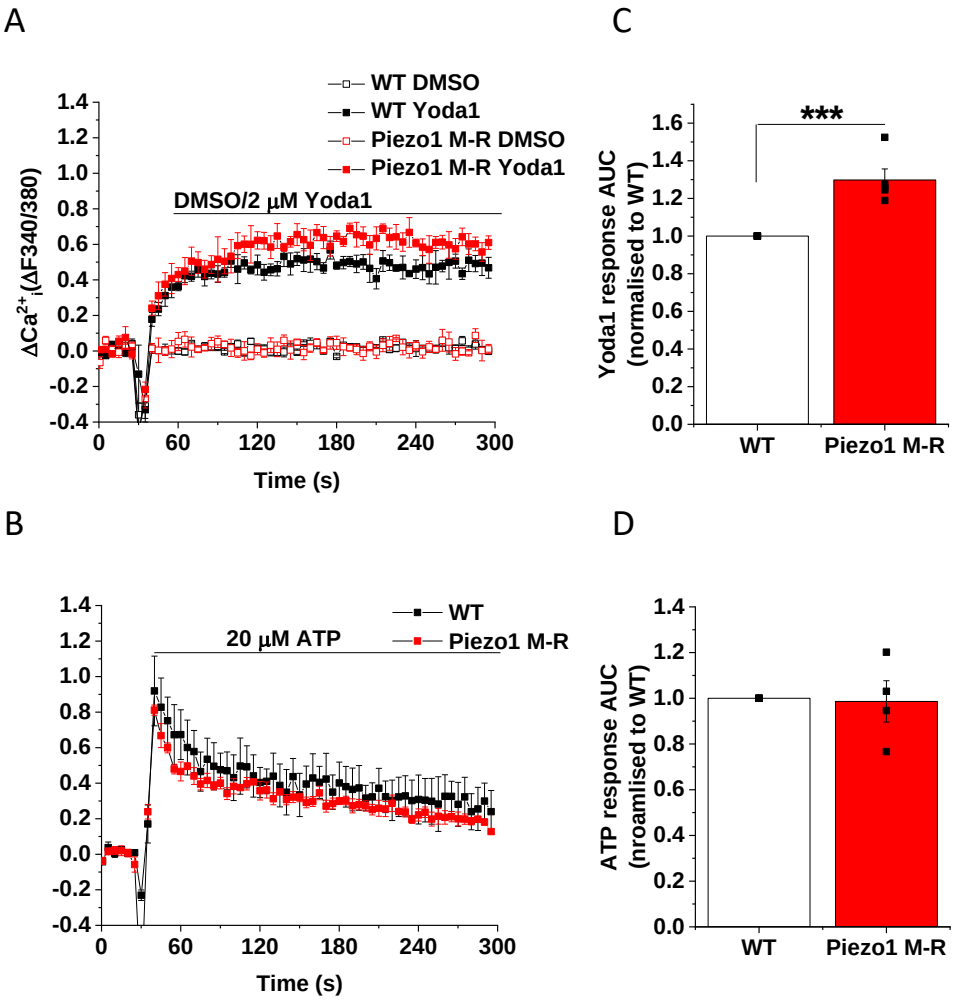

Figure 3-13 - Response to Yoda1 is increased in isolated mLSECs from Piezo1 M-R mice. (A-B) FlexStation intracellular Ca^{2+} measurement data for mLSECs exposed to 2 µM Yoda1 (A), vehicle only (A) or 20 µM ATP (B). Error bars indicate SEM (N = 4, in-plate replicates). (C-D) Summary for experiments of the type shown on the left measured by AUC from 30-300s and normalised to the AUC values for WT mice. Each data point represents a value from an independent experiment with mean values and error bars representing SEM (n=4). * (p<0.05), ** (p<0.01), *** (p<0.001), **** (p<0.0001).

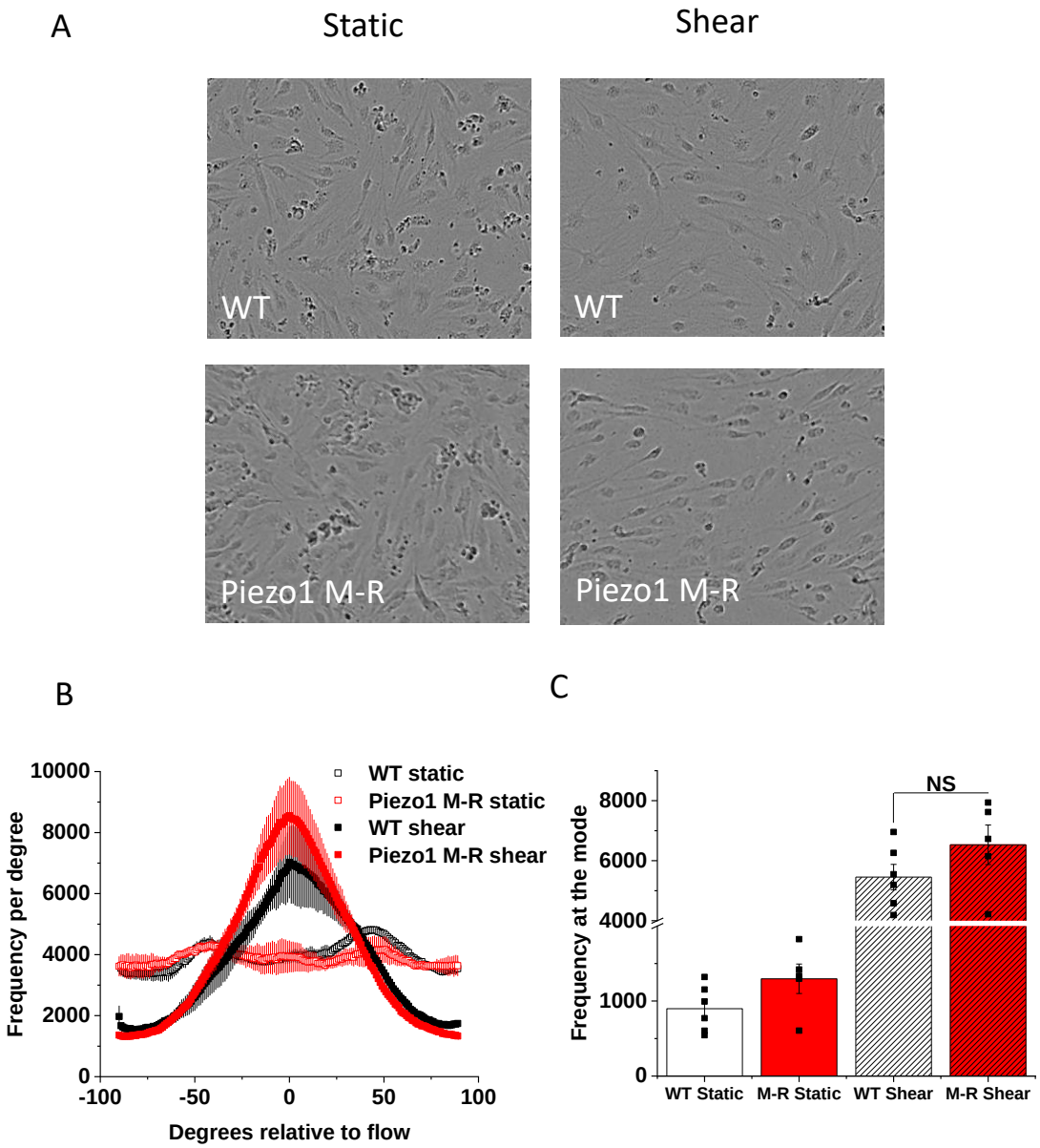

Figure 3-14 Endothelial cells from Piezo1 M-R may align better to shear stress. (A) Example phase contrast images of mLSECs from WT (top) or Piezo1 M-R mice (bottom) subjected to 10 dyn.cm^{-2} shear stress for 24 hours (shear, right) or not (static, left). (B) Mean distribution ± SEM from the type of experiments in (A) of alignment of mLSECs after exposure to 24 hours shear stress. Alignment was measured by the height of the peak at the mode of the Gaussian distribution curve (WT: n=6, Piezo1 M-R: n=5 with N=3 images used per analysis per well). (C) Average height of the Gaussian distribution from the type of experiments in (A) and (B). Each data point represents a value from an independent experiment with mean values and error bars representing SEM (WT: n=6, Piezo1 M-R: n=5).

3.2.6 The Piezo1 M-R mutation affects Yoda1 responses in aorta and mesenteric artery

As the Piezo1 M-R mutation affected Ca^{2+} responses in endothelial cells it was investigated whether the mutation could affect vascular responses in mouse thoracic aortic rings, to Piezo1 agonist Yoda1, measured via isometric tension recordings. It has been shown by our laboratory previously using this method that Yoda1 causes relaxation of the vessels after pre-constriction with phenylephrine (PE) and that this effect is dependent on endothelial cells (Evans et al., 2018).

To examine this, aorta were pre-constricted with PE. 5 μM Yoda1 caused a modest contractile response followed by relaxation in the WT vessel (Figure 3-15A-B). Both of these contractile and relaxation responses were dramatically enhanced in the Piezo1 M-R aortas, clearly demonstrating effects of the mutation in whole vessel (Figure 3-15A-B). The existence of these two opposite mechanisms is consistent with the dichotomy of endothelial Piezo1, as described previously.

Endothelial Piezo1 function has been shown to be vascular bed specific (Rode et al., 2017). To determine whether the effect of Piezo1 M-R was specific to responses in aorta, Yoda1 responses were measured in resistance vessels from mesenteric artery. Similarly, vessels were pre-constricted with PE before application of 5 μM Yoda1. The amplitude of relaxation mediated by Yoda1 was unaffected by the Piezo1 M-R mutation, but quite striking was the faster responses in vessels from the mutant mice (Figure 3-15C-D). Taken together, the data show that the Piezo1 M-R mutation affects vascular function in response to Piezo1 activation and in general this is GOF, either increasing the amplitude or kinetics of the response. It shows that the mutation affects vascular beds in different ways.

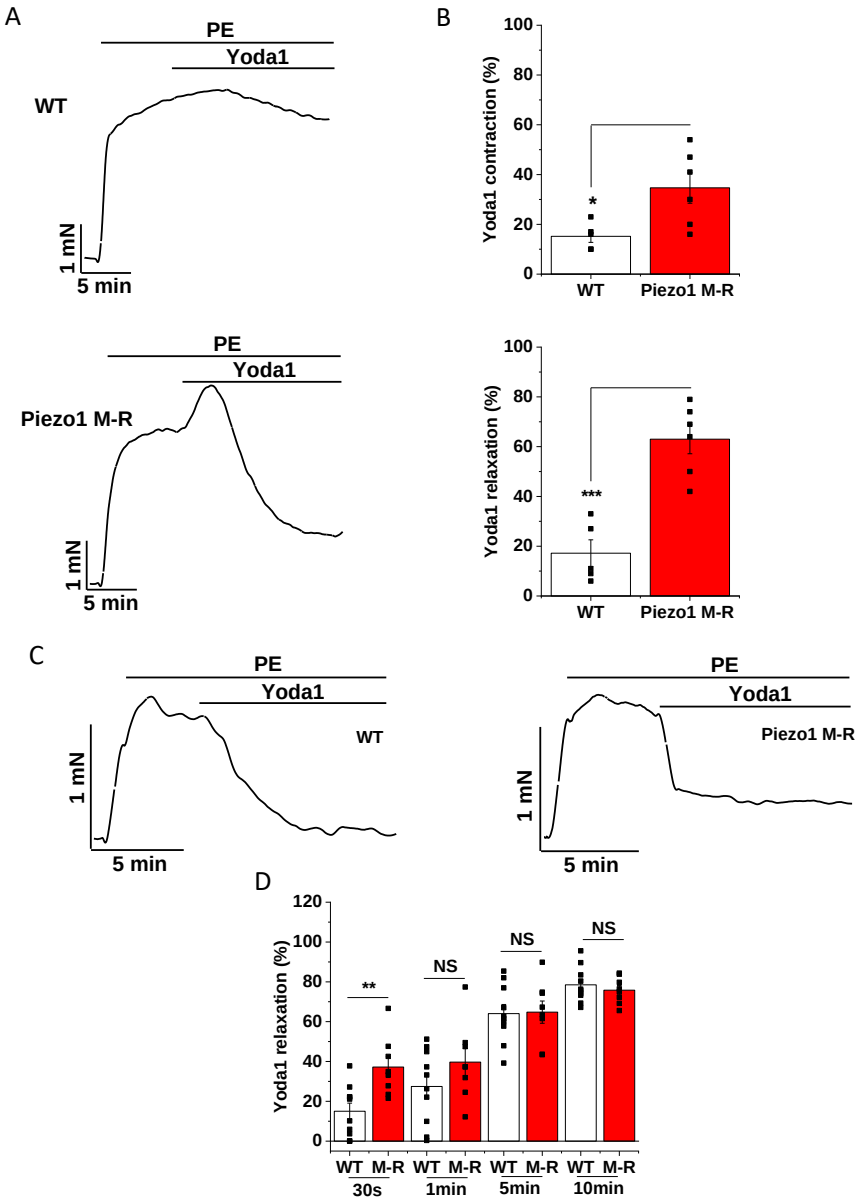

Figure 3-15 Yoda1-induced vascular responses are affected in Piezo1 M-R mice. (A,C) Isometric tension recordings from mouse thoracic aorta (A)(WT, top and Piezo1 M-R, bottom) or mouse mesenteric artery (C) (WT, left and Piezo1 M-R, right) pre-constricted with 0.3 μM phenylephrine (PE) and exposed to 5 μM Yoda1. (B) Mean data for experiments of the type shown in (A) expressed as % contraction (top) and % relaxation (bottom) evoked by Yoda1. Each data point represents a value from an independent experiment with mean values and error bars representing SEM (n = 5 WT, n = 6 Piezo1 M-R). (D) Mean data for experiments of the type shown in (C) expressed as % relaxation of WT and Piezo1 M-R vessels after exposure to Yoda1 at 30s, 1, 5 and 15 min following application (n = 10 WT, n = 8 Piezo1 M-R). * ($p<0.05$), ** ($p<0.01$), *** ($p<0.001$), **** ($p<0.0001$). Wire myography was performed by Dr Naima Endesh (University of Leeds).

3.2.7 Blood pressure is unaffected in Piezo1 M-R at rest

The role of Piezo1 in blood pressure control has been demonstrated, athough as yet a clear consensus as to the channel's function in this complex system has not yet been reached (Wang et al., 2016, Rode et al., 2017, Zeng et al., 2018). As the Piezo1 M-R mutation affected vascular reponses it was hypothesised that this may be observed in Piezo1 M-R mice *in vivo* via alterations to blood pressure. To investigate this, blood pressure measurements were made in awake animals via the tail cuff technique in 8-week old mice. Neither systolic, diastolic or mean blood pressures were changed in the Piezo1 M-R mice (Figure 3-16). The data suggest that although alterations to vascular functions are possible due to the Piezo1 M-R mutation, this does not result in changes in blood pressure, at least in a rested state.

In order to achieve stable blood pressure recordings when the mice are at rest, an acclimitisation run is performed to give the mice chance to adjust to the holder and become used to the pressure applied through the tail cuff. During these recordings, the mice are stressed after having been handled and placed into a different environment. Therefore, to achieve a preliminary idea of whether blood pressure could be affected in Piezo1 M-R mice in stressed conditions, the results of this 1st acclimitisation run were investigated. As expected, all blood pressure parameters were raised during this 1st run, indicative of a stressed condition (Figure 3-17). However, neither systolic, diastolic or mean blood pressures were changed in the Piezo1 M-R mice (Figure 3-17A-C), giving an early indication that blood pressure is also unaffected in Piezo1 M-R mice under stress.

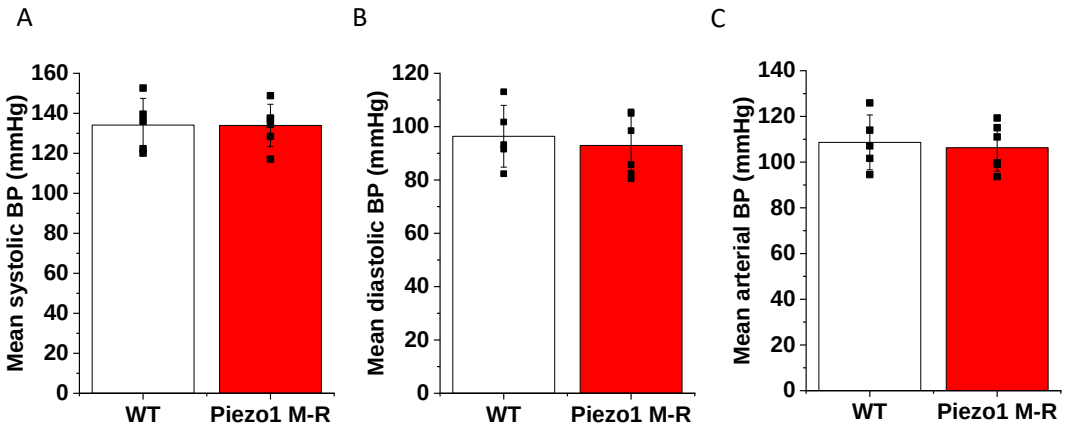

Figure 3-16 Blood pressure is normal in Piezo1 M-R mice. Mean diastolic (A), systolic (B) and arterial (C) blood pressures of 8-week old mice, measured by tail cuff. All individual data points are shown with mean ± SEM (n = 5 WT, n = 6 Piezo1 M-R).

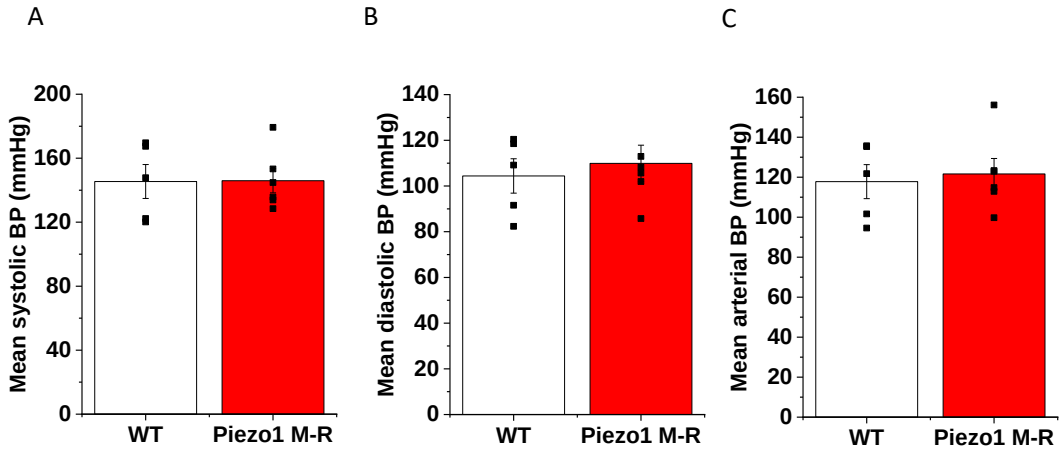

Figure 3-17 Blood pressure is normal in stressed Piezo1 M-R mice. Mean diastolic (A), systolic (B) and arterial (C) blood pressures of 8-week old mice, measured by tail cuff, prior to acclimatisation. All individual data points are shown with mean ± SEM (n = 5 WT, n = 6 Piezo1 M-R).

3.3 Discussion

This chapter has characterised the murine equivalent of the Piezo1 M2225R mutation which causes DHS in humans. It has shown that M2240R (Piezo1 M-R) causes GOF in the murine channel and that mice with the mutation have many clinical signs of DHS. An important finding has been that studying the effects of native Piezo1 M-R on channel function in RBCs revealed that the mutation affects the channel by a delayed deactivation mechanism, more so than inactivation which has been reported in studies using over-expression systems. Additionally, it has demonstrated that Piezo1 M-R can affect cells other than RBCs and GOF effects of the mutation can be observed in endothelial cells and whole vessel, indicating that additional physiological effects of Piezo1 GOF are possible.

Yoda1 has previously been shown to cause increased calcium responses in the M2225R mutant human channel in overexpression systems (Syeda et al., 2015). The results from transient transfection with the mutant mouse clone demonstrate that the same is true for the murine channel as Ca^{2+} influx in response to Yoda1 was augmented. The stable cell line with the Piezo1 M-R mutation did not show increased amplitude of Ca^{2+} responses to Yoda1 at the higher concentrations, likely due to saturation of the assay, but instead showed an increase in sensitivity to the agonist, with a leftward shift in the dose-response curves. This was confirmed using another Piezo1 agonist generated within our laboratory, KC159, showing that the increased sensitivity was not specific to channel activation by Yoda1.

By generating the CRISPR/Cas9 edited Piezo1 M-R mouse model, global for the mutation, it was possible to demonstrate that the presence of this mutation alone is sufficient to cause DHS-like symptoms in the mouse. Piezo1 M-R mice exhibited reduced haemoglobin, increased reticulocytes, the presence of stomatocytes, reduced RBC osmotic fragility and splenomegaly; all hallmarks of the human condition (Delaunay, 2004, Archer et al., 2014). Despite these similarities, the symptoms observed were not identical to those found in humans. Typically patients exhibit increased mean corpuscular volume (MCV), a measure of RBC size and increased mean corpuscular haemoglobin (MCH), the average amount of haemoglobin per RBC (Albuisson et al., 2013, Zarychanski et al., 2012). Whilst increases in MCV or MCH were not observed, there were increases in red cell distribution width (RDW) and haemoglobin distribution width (HDW) in

the Piezo1 M-R mice, which measure the heterogeneity of RBC size and haemoglobin concentration. These slight differences may reflect species-specific effects of the mutation or possibly that the machines used to measure haematological properties are calibrated to human samples. Another DHS-causing mutation has previously been replicated in mice and also did not report all the symptoms of the human condition (Ma et al., 2018). Importantly, both showed the most significant, diagnostic clinical features, to be confident that the mutations in Piezo1 are disease-causing.

Previous studies of the effects of Piezo1 M-R mutation on channel function have used cloned mutants and over-expression systems. Here, electrophysiological recordings on native Piezo1 channels in RBCs with the Piezo1 M-R mutation activated by physiological force in the form of fluid flow revealed much different channel kinetics. RBCs from wild-type mice exhibited much slower Piezo1 kinetics than those observed in overexpression studies, which matches with the biology of RBCs. RBCs are constantly exposed to some mechanical force and changes to this force such as squeezing into narrow capillaries are likely to be slower than the abrupt mechanical force applied in studies of the channel, therefore it is likely not physiologically advantageous for Piezo1 to inactivate quickly in these cells. In fact, inactivation in the WT cells was slow and incomplete during the 20 seconds of fluid flow. This inactivation was further slowed by the presence of the Piezo1 M-R mutation consistent with previous studies of the mutation. However, the greatest effect of the mutation was failure of the channels to deactivate following cessation of the stimulus, suggesting a prolonging or stabilisation of channel opening. Previous electrophysiological experiments of RBCs from patients with DHS are limited and do not involve mechanical stimulation, but are consistent with these results as they too demonstrate constitutively active Piezo1 channels from these cells, suggesting Piezo1 is unable to switch off (Andolfo et al., 2013, Shmukler et al., 2014, Rapetti-Mauss et al., 2017). It is likely this characteristic would be detrimental to RBC function, as excess ion flux would be mediated for long durations. From studies of DHS and Piezo1 function in RBCs it is known that increased ion flux through Piezo1 results in RBC dehydration through activation of the downstream Ca^{2+}-activated K^{+} (Gardos) channel (Cahalan et al., 2015, Rapetti-Mauss et al., 2017).

The observations from freshly isolated RBCs add to a growing body of evidence that distinct Piezo1 properties are exhibited from the native channel compared to cell lines. Patch-clamp experiments with isolated renal tubule epithelial cells or endothelial cells show that Piezo1 channels appear to adopt an inactivating state and only partial inactivation is observed in arterial myocytes (Peyronnet et al., 2013, Martins et al., 2016, Rode et al., 2017, Retailleau et al., 2015). The reason for distinct channel gating remains unknown, but is a necessary avenue for investigation in order to fully understand Piezo1 function in physiology. It is possibly affected by the lipid composition of the cell membranes or perhaps the presence of an interacting partner which is as yet undiscovered (Romero et al., 2019).

Investigating the effect of Piezo1 M-R in endothelial cells has shown that the Piezo1 channel response can be affected by the mutation in cells other than RBCs. The Yoda1 response was increased in mLSECs from Piezo1 M-R mice with increased Ca^{2+} influx. It would be important in future studies to determine whether this increased Ca^{2+} entry granted by the M-R mutation has an effect on downstream, Piezo1 mediated effects in endothelial cells, such as eNOS phosphorylation and nitric oxide production (Wang et al., 2016). Additionally, endothelial cell alignment revealed hints at being increased by the Piezo1 M-R mutation, suggesting the mutation can impact endothelial cell function, but statistical significance was not achieved in the experiments. It is possible that this could be due to the incomplete alignment observed under the experimental conditions, preventing full sensitivity of the assay.

The wire myography experiments provide convincing evidence of Piezo1 GOF within the endothelium. The much larger relaxation in response to Yoda1 in aorta from Piezo1 M-R mice does suggest that increased nitric oxide production in these vessels is likely. Whilst the amplitude of Yoda1-induced relaxation was unchanged in mesenteric arteries harbouring the Piezo1 M-R mutation, the time course of relaxation was strikingly reduced. It is as yet unknown how this faster response is mediated as it does not correlate with the latency of activation observed in overexpression studies of the M-R mutation. It suggests gating of Piezo1 is different between vascular beds. Whilst the Yoda1 experiments are convincing, it would also be beneficial to perform the isometric tension recordings with a mechanical stimulus, such as flow, to determine whether the same

augmented relaxation responses are observed when other pressure-sensitive proteins are also activated in conjunction with Piezo1. This would be more representative of the physiological condition.

Despite Piezo1 effects observed in both aorta and mesenteric artery from Piezo1 M-R mice, the mutation did not affect blood pressure. This is perhaps not surprising due to the multi-factorial control of blood pressure, with many feedback systems in place to carefully regulate this important physiological parameter. Blood pressure regulation has both central and peripheral control centres which exert short and long term control, as detailed in the following review article (Dampney et al., 2002). In summary, short term control is primarily mediated by the baroceptor response, sensing acute changes in blood pressure and adjusting cardiac output and vasomotor tone via the automatic nervous system, to restore normal blood pressure. Longer term control is provided via an orchestra of endocrine factors including the renin-angiotensin-aldosterone system (RAAS) mediated by the kidneys and anti-diuretic hormone (ADH) released from the hypothalamus, both managing blood volume. In addition a balance of vasoactive factors contribute to blood pressure such as nitric oxide, a vasorelaxing factor synthesised by endothelial cells.

The role of Piezo1 in these control mechanisms has only been reported for nitric oxide production and the baroreceptor response and the channel is dispensable for basal myogenic tone (Wang et al., 2016, Zeng et al., 2018, Retailleau et al., 2015). Therefore, Piezo1 may have little role in long-term control of blood pressure, which would have been measured in the mice at rest. The resistance vessels have an important role in blood pressure regulation by adjusting the resistance to the blood, and although faster responses to Yoda1 were observed in the Piezo1 M-R mice in mesenteric arteries, the overall amplitude of relaxation was unchanged. This may help to explain why differences were not observed between the mice under these conditions.

The initial, acclimatisation blood pressure measurements suggested that blood pressure of Piezo1 M-R mice was also the same under stress. However, these are very preliminary experiments, showing acute stress which would vary between mice i.e. some mice went into the holders much more easily than others. Also, the nature of the experiments is that the mice calm down during the recordings so the ‘stressed’ state is not maintained. The final blood pressures,

although raised compared to recordings following acclimatisation, were not vastly different suggesting the stress response was mild. Therefore, differences in blood pressure due to the Piezo1 M-R mutation could still be identified following a more constant stress to the regulatory control systems, such as during exercise. Blood pressure has to increase by 15-20% during physical activity, granting increased blood flow and suitable supply to the skeletal muscles (Delp and Laughlin, 1998). It has already been shown that endothelial Piezo1 contributes to elevate blood pressure during exercise as mice lacking the channel from these cells cannot adjust blood pressure effectively, resulting in a decreased physical performance (Rode et al., 2017). Further experiments investigating acute changes to blood pressure are required, such as telemetry recordings with a running wheel, before an effect of Piezo1 M-R on blood pressure can be ruled out.

3.4 Summary

Overall the findings from this chapter support the conclusion that Piezo1 GOF mutations are a cause of DHS and present validation of a new Piezo1 M-R mouse model which can be used for further studies of native cells with the mutation, or for developing therapeutic strategies with which to treat DHS. The results reveal that in affected RBCs, the M-R mutation has the greatest effect via disruption of deactivation, rather than delayed inactivation, which is an important new discovery for the role of Piezo1 in disease and endogenous channel kinetics. It adds to observations that the native channel can behave distinctly from overexpressed channels, which is important for designing future therapeutics to target Piezo1 gating. This mouse model now provides a platform for additional Piezo1 gating studies using physiologically relevant cells and allows for further phenotyping the effects of Piezo1 GOF. This work has been started in this chapter showing that endothelial cells and whole vessels from Piezo1 M-R mice can exhibit Piezo1 GOF, which may yet have undiscovered physiological relevance.

Chapter 4 Cardiometabolic effects of Piezo1 M-R

4.1 Introduction

Despite the global nature of the Piezo1 M-R mutation, humans with this defect do not report symptoms other than a mild to moderate anaemia. However, the widespread role of Piezo1 in mammalian physiology indicates that patients may have unrecognised disease or disease predisposition. This is important and relevant to investigate as the incidence of Piezo1 GOF mutations is high, harboured by 1/3 of the African population, due to a protection against malaria (Ma et al., 2018). Additionally, potential findings could also reveal previously unknown functions of Piezo1 in physiology, particularly the importance of Piezo1 channel gating.

The Piezo1 M-R mouse model, validated in Chapter 3, allows for further phenotyping the effects of Piezo1 GOF. Like humans, Piezo1 M-R mice develop a DHS-like phenotype, suggesting the model is relevant for human translation. Hints at additional, non-RBC Piezo1 M-R effects have also been demonstrated, showing that Piezo1 in endothelial cells can exhibit GOF properties. The physiological relevance of this remains unknown.

The aim of this chapter was to establish whether there are additional physiological effects of Piezo1 GOF, using the validated Piezo1 M-R mouse model. Investigations focused on cardiometabolic features of the mice, as governed by early findings. Research involved gene expression analysis of heart, white adipose tissue and liver, cardiac function by echocardiography, histology and global tests of metabolic state. Piezo1 M-R mice were then challenged by high fat diet (HFD) to discover whether the stress induced by HFD feeding was dealt with differently due to Piezo1 GOF.

4.2 Results

4.2.1 Piezo1 M-R have gross anatomical differences

As a starting point to uncover additional effects of the Piezo1 M-R mutation, organ weights were measured in 8-week old mice to determine whether there were gross anatomical changes present, which may indicate underlying changes to

physiology (Figure 4-1A). The weights of heart, kidney, epididymal white adipose tissue (eWAT) and brown adipose tissue (BAT) were all unexpectedly increased by at least 10% in Piezo1 M-R mice compared to wild-type (WT) controls. Next, organ weights of older Piezo1 M-R mice at 22 weeks were compared to determine whether additional anatomical effects developed over time (Figure 4-1B). At this older time point, changes in weight to the heart, kidney and eWAT were lost, but an increase in BAT remained, in addition to an increase in liver and spleen weight (presented in Chapter 3). Overall the results suggest that the Piezo1 M-R mutation can cause gross changes in murine anatomy, hinting at additional physiological effects of the mutation.

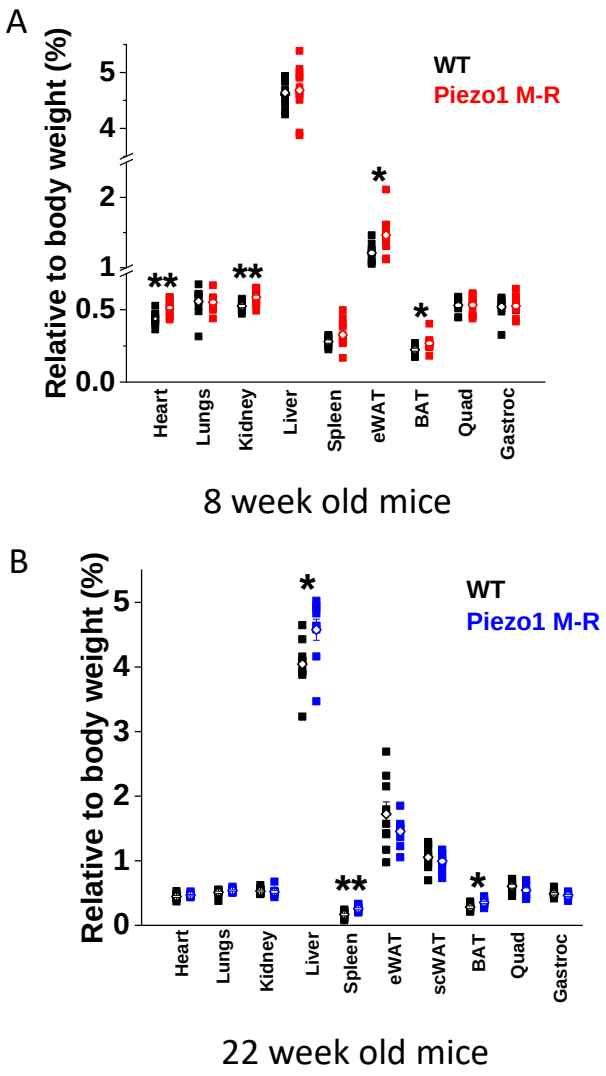

Figure 4-1 Changes to organ weights in Piezo1 M-R mice. (A) Weights of heart, lungs, kidney, liver, spleen, epididymal white adipose tissue (eWAT), brown adipose tissue (BAT), quadriceps (Quad) and gastrocnemius (Gastroc) as % of body weight in 8-week old mice (red) (n=10, WT; n=12, Piezo1 M-R). (B) Same as (A) including subcutaneous white adipose tissue (scWAT), in 22-week old mice (blue) (n=9 for both genotypes). * ($p<0.05$), ** ($p<0.01$), *** ($p<0.001$), **** ($p<0.0001$).

4.2.2 Cardiac differences in Piezo1 M-R mice

As a 15% increase in heart weight was observed in 8-week old Piezo1 M-R mice, the effect of the mutation on cardiac gene expression was investigated (Figure 4-2). A brief description of the genes studied is provided in Table 4-1. A mild hypertrophic gene expression profile was revealed in 8-week old Piezo1 M-R mice, with a trend for increased *Anp* (atrial natriuretic peptide) and *Acta1* (skeletal muscle alpha-actin) mRNA expression ($p \leq 0.1$) and an increase in *Myh7* (myosin heavy chain β). These changes matched well with the documented increase in heart weight and further suggest that cardiac differences exist in Piezo1 M-R mice of this age.

To determine whether there were any effects on cardiac function, echocardiography was performed on 8-week old mice (Figure 4-3). Cardiac performance as measured by % ejection fraction (Figure 4-3B) and % fractional shortening (Figure 4-3C) was comparable between the two genotypes, suggesting that cardiac function was unaffected. Echocardiography can also be used to measure the size of the heart by investigating the left ventricular internal diameter (LVID) and the thickness of the left ventricular posterior wall (LVPW) during systole and diastole (Figure 4-3D-G). These were also identical, contradicting the increase in heart weight and hypertrophic gene expression, although it is possible the technique is not sensitive enough to detect subtle changes. Overall the results suggest that a mild hypertrophic phenotype may exist in 8-week old Piezo M-R mice, but that this has not impacted cardiac function.

As subtle differences were observed in 8-week old mice, the experiments were repeated in older 22-week old mice, to determine whether a phenotype developed with age. The mild hypertrophic gene expression profile was lost in the older mice (Figure 4-4) which fitted with the heart weight data, which were unchanged at this age. Instead, there was a reduction in *Acta1*, suggesting reduced smooth muscle in the hearts and a trend for lowering of inflammatory markers *Il-1b* (interleukin-1 beta) and *Mmp9* (matrix metalloproteinase 9) ($p \leq 0.1$).

Cardiac function in older Piezo1 M-R mice was slightly improved with increased ejection fraction (Figure 4-5B) fractional shortening (Figure 4-5C), or rather maintained compared to WT mice who had a deficit in cardiac function at this age, compared to 8 weeks (Figure 4-5). No change was observed in the LVID

during diastole, but was decreased in the Piezo1 M-R mice during systole (Figure 4-5E), suggesting improved cardiac muscle contraction. Overall, the results from both age groups indicate that Piezo1 GOF mutations can impact on cardiac gene expression and at 22 weeks can impact cardiac function, although the contradictory results between the age groups make it difficult to determine the true relevance of Piezo1 in the heart.

Target gene	Function	Ref
Anp (atrial natriuretic peptide)	Continually secreted from the heart- acts to decrease cardiac load. Expression is upregulated during cardiac pathologies such hypertrophy, congestive heart failure and myocardial infarction. Plasma levels can be useful diagnostic markers of disease.	(Chopra et al., 2013)
Bnp (brain natriuretic peptide)	As *ANP*.	(Chopra et al., 2013)
Acta1 (skeletal muscle alpha-actin)	Upregulated in human hypertrophic cardiomyopathy.	(Lim et al., 2001)
Serca2a	Cardiac sarcoplasmic reticulum (SR), Ca^{2+} -ATPase pump (SERCA) - removes Ca^{2+} from the cytosol following contraction, by facilitating uptake into the SR. During heart failure, expression of SERCA2a is reduced.	(Gianni et al., 2005)
Col1a1 Collagen 1α1	Upregulated during cardiac remodelling, leading to pathological cardiac fibrosis; a stiffening of the heart.	(Hinderer and Schenke-Layland, 2019)
Col3a1 Collagen 3α1	As for *Col1a1*.	(Hinderer and Schenke-Layland, 2019)
Myh6 myosin heavy chain (MHC)-α	Replaces MHC-β as predominant isoform postnatally. Decreased in heart failure.	(Harada et al., 1999)
Myh7 MHC-β	Predominant foetal isoform. Switch to foetal gene expression pattern in heart failure. Increased Myh7 can also indicate cardiac hypertrophy.	(Harada et al., 1999) (Jones et al., 1996b)
Chop (C/EBP homologous protein)	Pro-apoptotic transcription factor, induced during endoplasmic reticulum (ER) stress. Can contribute to apoptosis, hypertrophy and heart failure.	(Wang et al., 2018a)
Il-1b (interleukin-1 beta)	Inflammatory cytokine- contributes to cardiac disease severity.	(Szekely and Arbel, 2018)
Mmp-9 (matrix metalloproteinase 9)	Degrades the myocardial extracellular matrix. Contributes to adverse cardiac remodelling.	(Halade et al., 2013)

Table 4-1 Brief description of cardiac genes measured by qPCR.

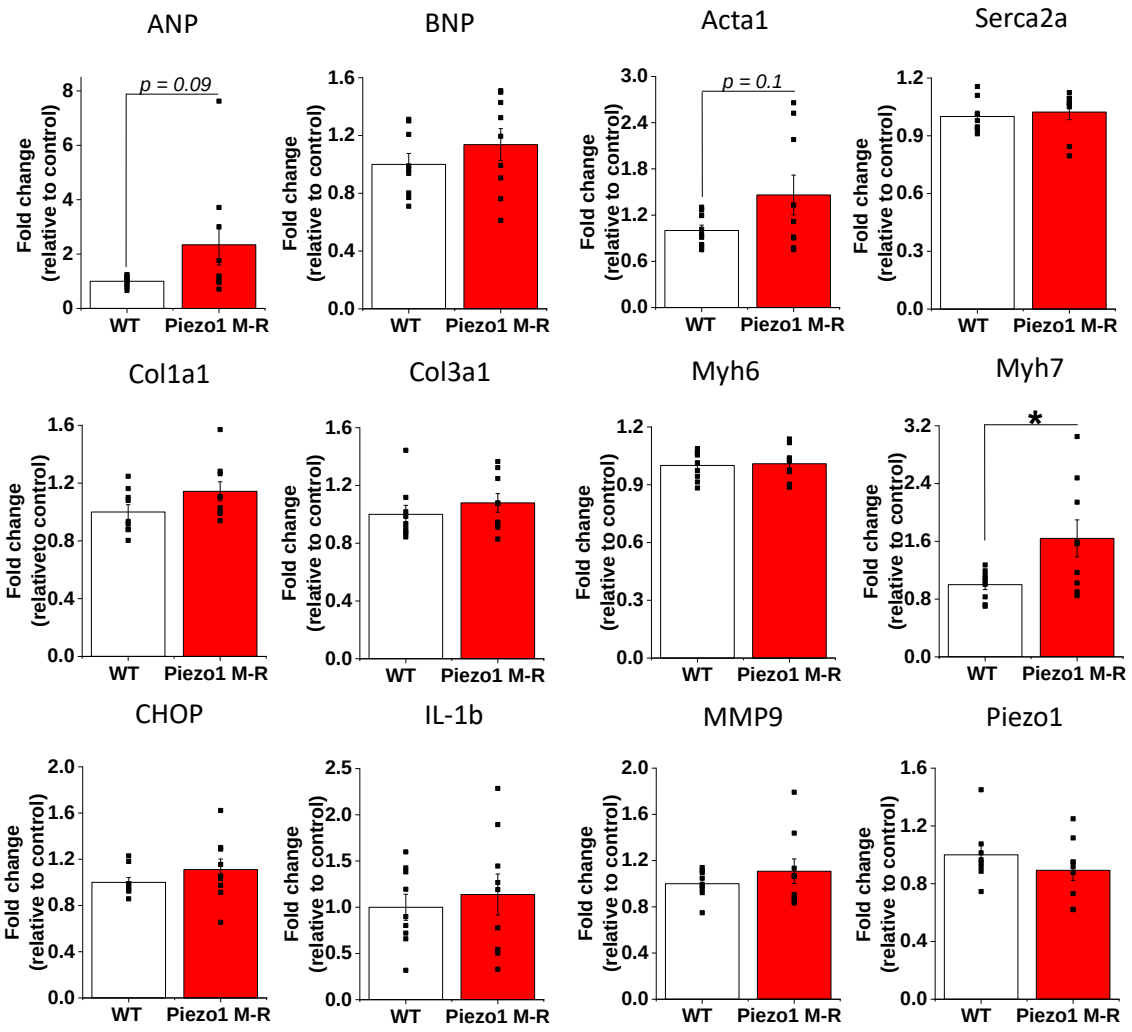

Figure 4-2 Mild hypertrophic cardiac gene expression profile in 8-week old Piezo1 M-R mice. Real-time PCR showing the fold-change in mRNA expression of cardiac genes in Piezo1 M-R mice relative to control (WT). Each data point represents a value from an independent experiment with mean values and error bars representing SEM indicated by the open (WT) or red (Piezo1 M-R) bars (n=10). *Anp*: atrial natriuretic peptide, *Bnp*: brain natriuretic peptide, *Acta1*: skeletal muscle actin, *Col1a1*: Collagen Type 1 alpha 1, *Col3a1*: Collagen Type 3 alpha 1, *Myh6*: myosin heavy chain α, *Myh7*: myosin heavy chain β, *Chop*: C/EPB homologous protein, *Il-1b*: interleukin 1 beta, *Mmp9*: matrix metalloproteinase 9.

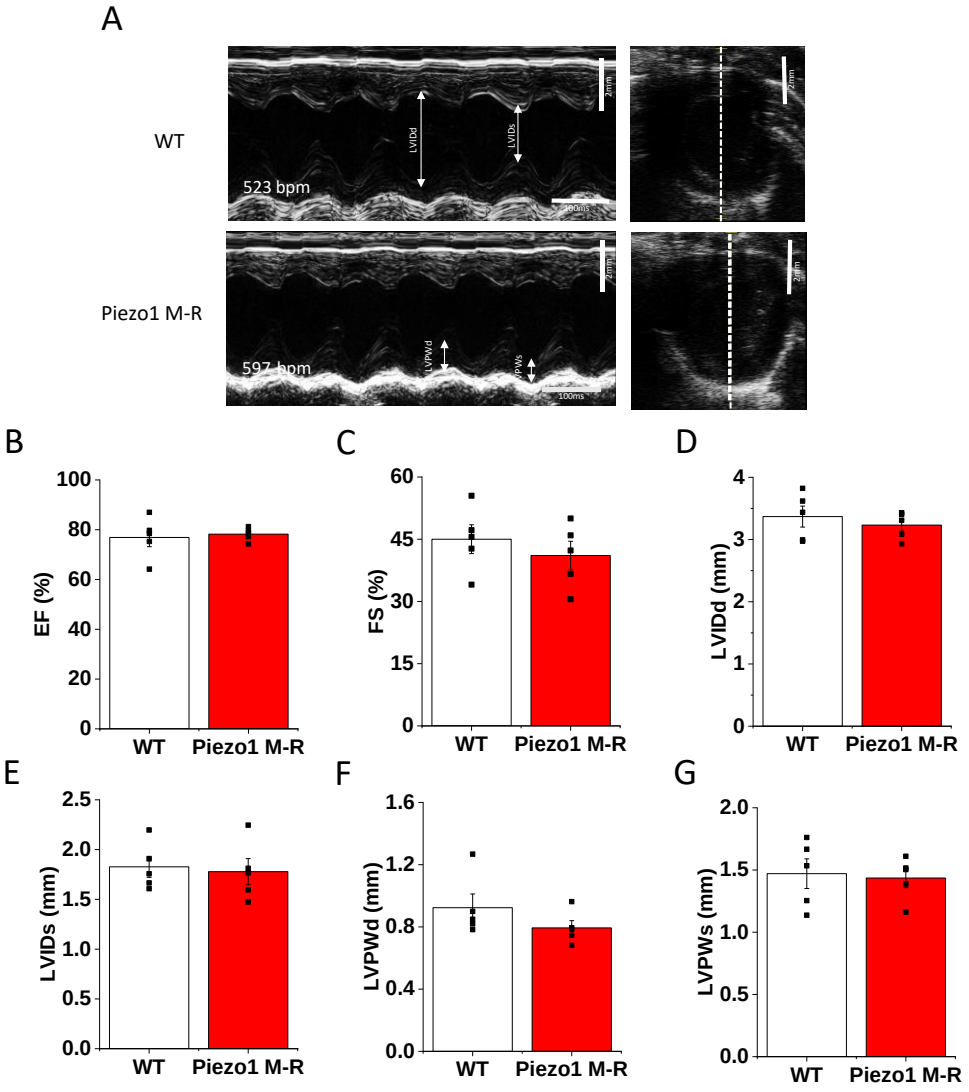

Figure 4-3 Cardiac function is normal in 8-week old Piezo1 M-R mice. (A) Example M-mode echocardiography recordings from WT (top) and Piezo1 M-R mice (bottom). The axis used for M-mode measurement is denoted by the white dashed line through the short axis image (right). Arrows denote measurements made for analysis. (B-F) Mean data for experiments of the type shown in (A) showing % ejection fraction (EF) (B), % fractional shortening (FS) (C), left ventricular internal diameter (LVID) during diastole (D) and systole (E), left ventricular posterior wall thickness during diastole (F) and systole (G) (n=5).

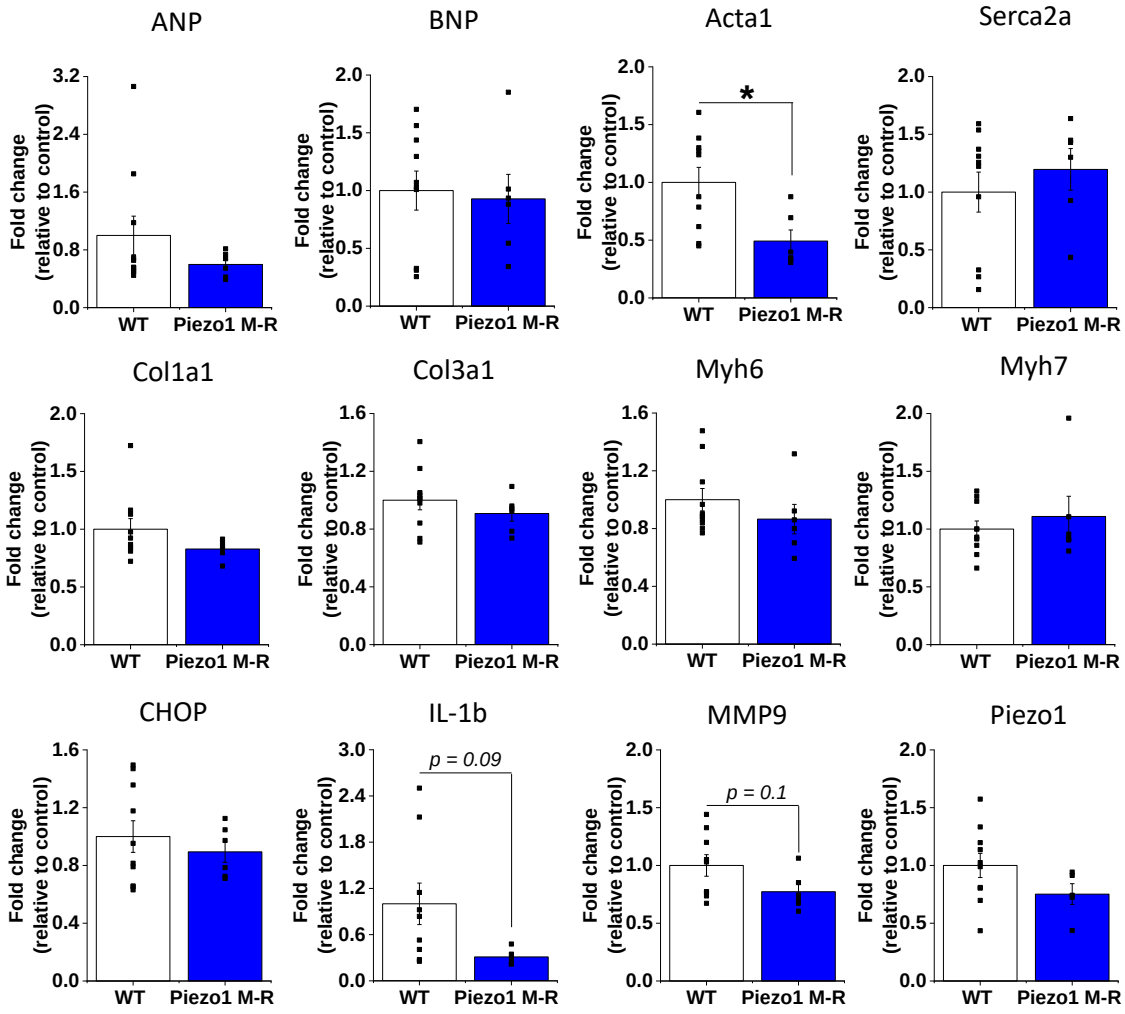

Figure 4-4 Hypertrophic cardiac gene expression profile absent in 22-week old Piezo1 M-R mice. Real-time PCR showing the fold-change in mRNA expression of cardiac genes in Piezo1 M-R mice relative to control (WT). Each data point represents a value from an independent experiment with mean values and error bars representing SEM indicated by the open (WT) or blue (Piezo1 M-R) bars (n=10, WT; n=6 Piezo1 M-R {n=5 *Piezo1, IL-1b*}). * (p<0.05), ** (p<0.01), *** (p<0.001), **** (p<0.0001). *Anp*: atrial natriuretic peptide, *Bnp*: brain natriuretic peptide, *Acta1*: skeletal muscle actin, *Col1a1*: Collagen Type 1 alpha 1, *Col3a1*: Collagen Type 3 alpha 1, *Myh6*: myosin heavy chain α, *Myh7*: myosin heavy chain β, *Chop*: C/EPB homologous protein, *Il-1b*: interleukin 1 beta, *Mmp9*: matrix metalloproteinase 9.

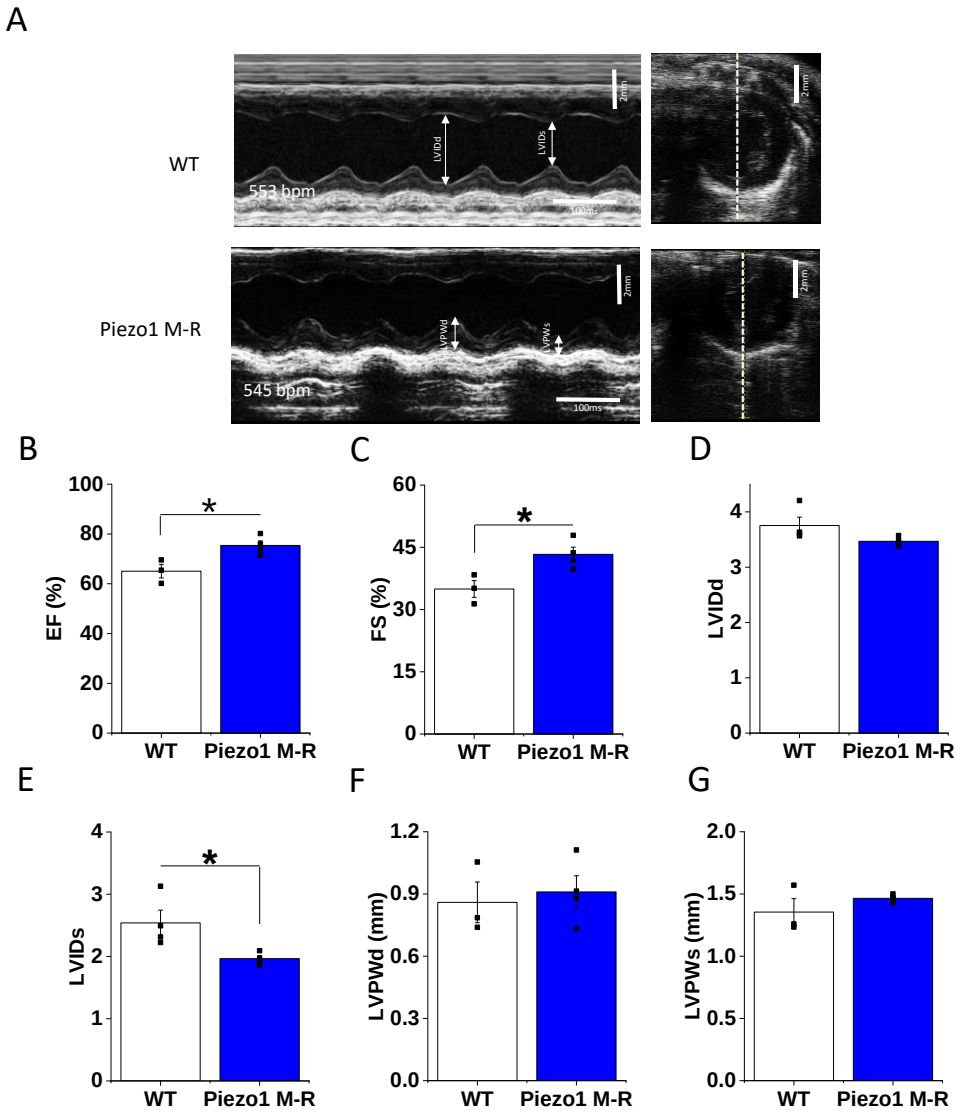

Figure 4-5 Cardiac function is improved in 22-week old Piezo1 M-R mice. (A) Example M-mode echocardiography recordings from WT (top) and Piezo1 M-R mice (bottom). The axis used for M-mode measurement is denoted by the white dashed line through the short axis image (right). Arrows denote measurements made for analysis. (B-F) Mean data for experiments of the type shown in (A) showing % ejection fraction (EF) (B), % fractional shortening (FS) (C), left ventricular internal diameter (LVID) during diastole (D) and systole (E), left ventricular posterior wall thickness during diastole (F) and systole (G) (n=4). * ($p<0.05$), ** ($p<0.01$), *** ($p<0.001$), **** ($p<0.0001$).

4.2.3 Deletion of Piezo1 from cardiomyocytes appears detrimental

Anaemia itself can impact on cardiac function (Coats, 2004), so it is difficult to determine whether any cardiac effects observed in the Piezo1 M-R mice are in fact Piezo1 dependent, or secondary to anaemia. The role of Piezo1 in the heart remains fairly unknown, particularly in the cardiac myocytes, the muscle cells of the heart. In order to investigate the role of the channel in this important organ myocyte-specific Piezo1 knockout mouse (CreMyh6-Piezo1$^{-/-}$) was generated by Dr Jing Li by crossing Piezo1 flox/flox mice to CreMyh6 mice. The Myh6 promoter drives the expression of Cre, which is constitutively active in this model, resulting in Piezo1 deletion specifically in cardiac myocytes.

Firstly, gross anatomical differences in the heart were investigated by measuring heart weight relative to body weight and tibia length at 8 weeks (Figure 4-6). Heart weight was comparable between Cre- and Cre+ mice under both measurements, suggesting lack of Piezo1 in cardiac myocytes does not cause cardiac hypertrophy. The expression of the same cardiac genes investigated in the Piezo1 M-R mice, were measured in the CreMyh6-Piezo1$^{-/-}$ mouse model for comparison (Figure 4-7). The mice exhibited increased mRNA expression of *Bnp* (brain natriuretic peptide), reduced *Serca2a* and increased *Col1a1* indicating a heart failure gene expression profile. This appeared to correlate with a trend for decreased cardiac function as indicated by a tendency of reduction in ejection fraction and fractional shortening ($p \leq 0.1$) (Figure 4-8B-C). A reduction in *Piezo1* mRNA expression was not observed in Cre+ mice in whole heart, however Piezo1 expression in cardiac myocytes is extremely low compared to other cardiac cells, so specific cardiac myocyte deletion may be masked by the relatively high expression in fibroblasts and endothelial cells (Blythe et al., 2019a).

Cardiac weight and gene expression in CreMyh6-Piezo1$^{-/-}$ 6 month old mice were investigated to determine whether the indications of heart failure changed with age. Heart weight relative to body weight and tibia length were comparable between genotypes (Figure 4-9), however the gene expression heart failure profile was more pronounced (Figure 4-10). In addition to the same changes in *Serca2a* and *Col1a1*, with a trend for reduced *Bnp* ($p = 0.07$), Cre+ mice also had increased *Anp*, *Col3a1*, *Myh7* and a trend for increased inflammatory markers, in addition to a decrease in *Myh6* (myosin heavy chain α); all these changes are

observed during heart failure. The results suggest that loss of Piezo1 from cardiac myocytes is detrimental to the heart causing a heart failure gene expression profile which may well correlate with a decreased cardiac function. Overall the use of this mouse model supports the hypothesis that Piezo1 does have a role in normal heart function, indicating changes observed in the Piezo1 M-R mice could in fact be due directly to channel effects within the cardiac myocyte, rather than secondary to anaemia.

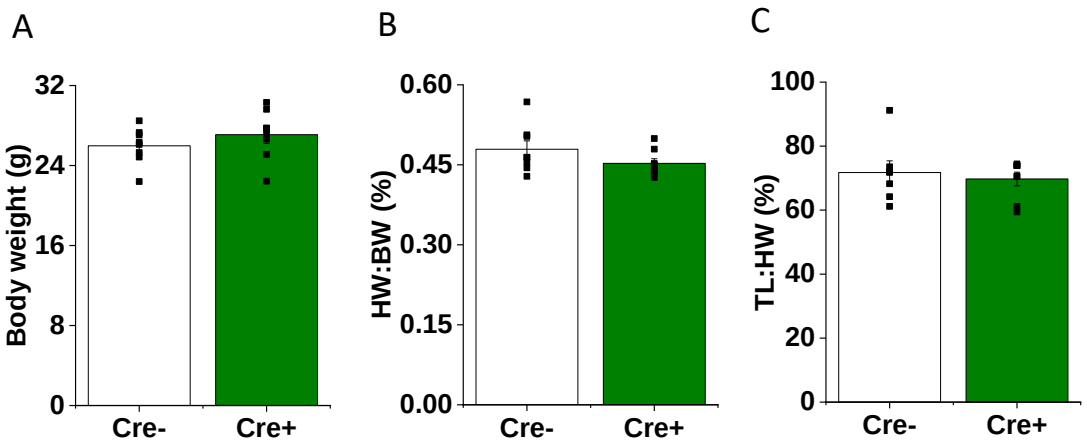

Figure 4-6 Heart size is normal in 8-week old CreMyh6-Piezo1$^{-/-}$ mice. (A) Body weights of Cre- and Cre+ 8-week old mice. (B) Heart weight expressed as a percentage body weight. (C) Heart weight expressed as a percentage of tibia length (mm). Each data point represents a value from an independent experiment with mean values and error bars representing SEM indicated by the open (Cre-) or green (Cre+) bars (n=8).

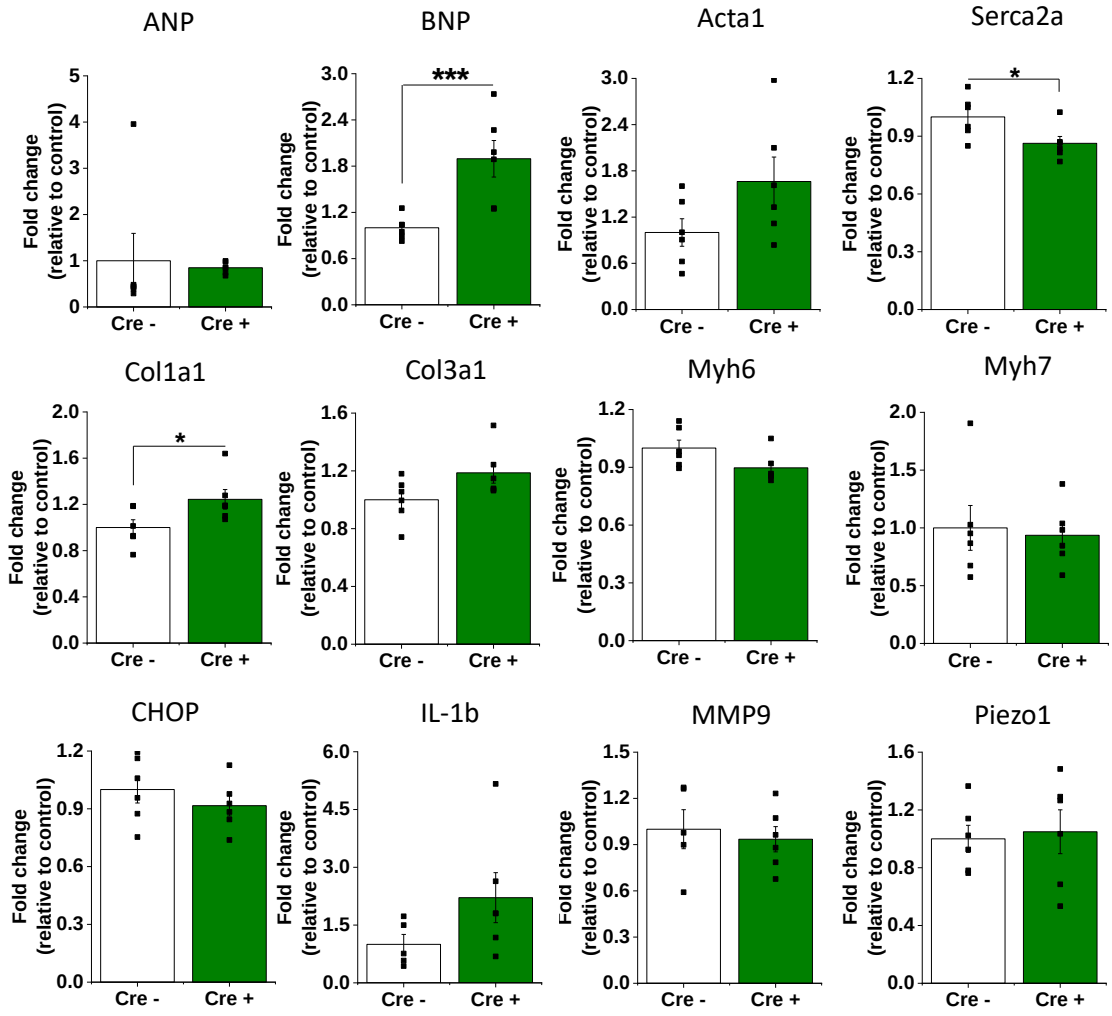

Figure 4-7 Mild heart failure gene expression profile is evident in 8-week old CreMyh6-Piezo1$^{-/-}$ mice. Real-time PCR showing the fold-change in mRNA expression of cardiac genes in Cre+ mice relative to control (Cre -). Each data point represents a value from an independent experiment with mean values and error bars representing SEM indicated by the open (Cre-) or green (Cre+) bars (n=6, Cre- {n=5 *Il-1b* and *Mmp9*}; n=6 Cre+). * (p<0.05), ** (p<0.01), *** (p<0.001), **** (p<0.0001). *Anp*: atrial natriuretic peptide, *Bnp*: brain natriuretic peptide, *Acta1*: skeletal muscle actin, *Col1a1*: Collagen Type 1 alpha 1, *Col3a1*: Collagen Type 3 alpha 1, *Myh6*: myosin heavy chain α, *Myh7*: myosin heavy chain β, *Chop*: C/EPB homologous protein, *Il-1b*: interleukin 1 beta, *Mmp9*: matrix metalloproteinase 9.

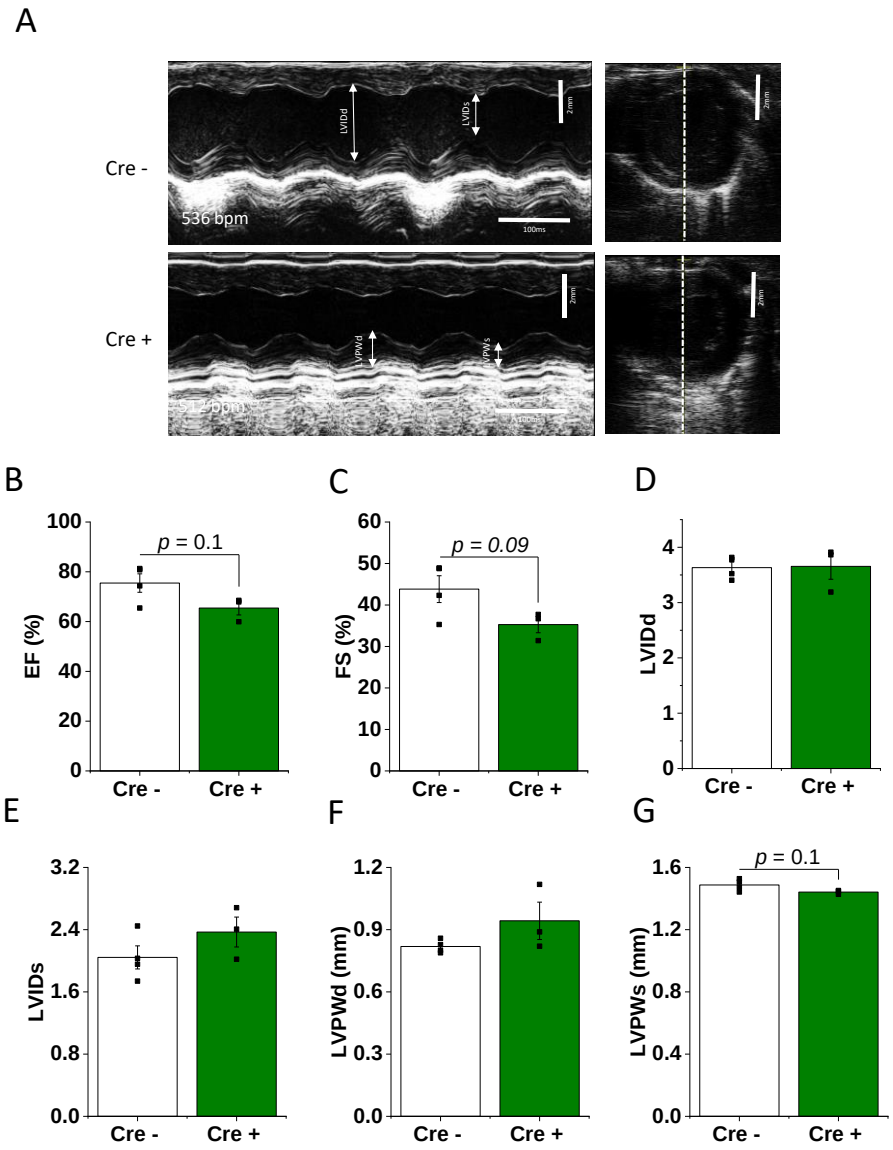

Figure 4-8 Cardiac function exhibits a trend for being reduced in 8-week old CreMyh6-Piezo1$^{-/-}$ mice. (A) Example M-mode echocardiography recordings from Cre- (top) and Cre+ mice (bottom). The axis used for M-mode measurement is denoted by the white dashed line through the short axis image (right). Arrows denote measurements made for analysis. (B-F) Mean data for experiments of the type shown in (A) showing % ejection fraction (EF) (B), % fractional shortening (FS) (C), left ventricular internal diameter (LVID) during diastole (D) and systole (E), left ventricular posterior wall thickness during diastole (F) and systole (G) (n=4, Cre-; n=3, Cre+).

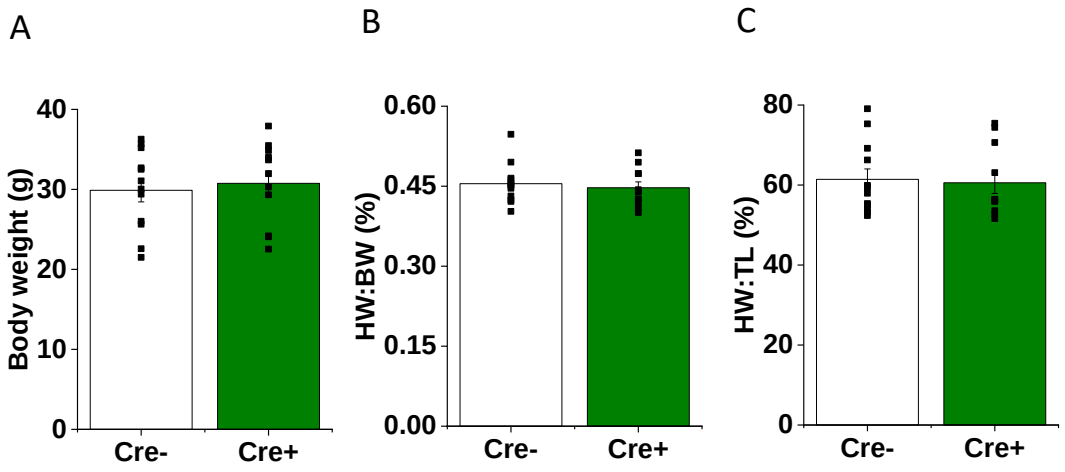

Figure 4-9 Heart size is normal in 6-month old CreMyh6-Piezo1$^{-/-}$ mice. (A) Body weights of Cre- and Cre+ 8 week old mice. (B) Heart weight expressed as a percentage body weight. (C) Heart weight expressed as a percentage of tibia length (mm). Each data point represents a value from an independent experiment with mean values and error bars representing SEM indicated by the open (Cre-) or green (Cre+) bars (n=12, Cre-; n=11, Cre+).

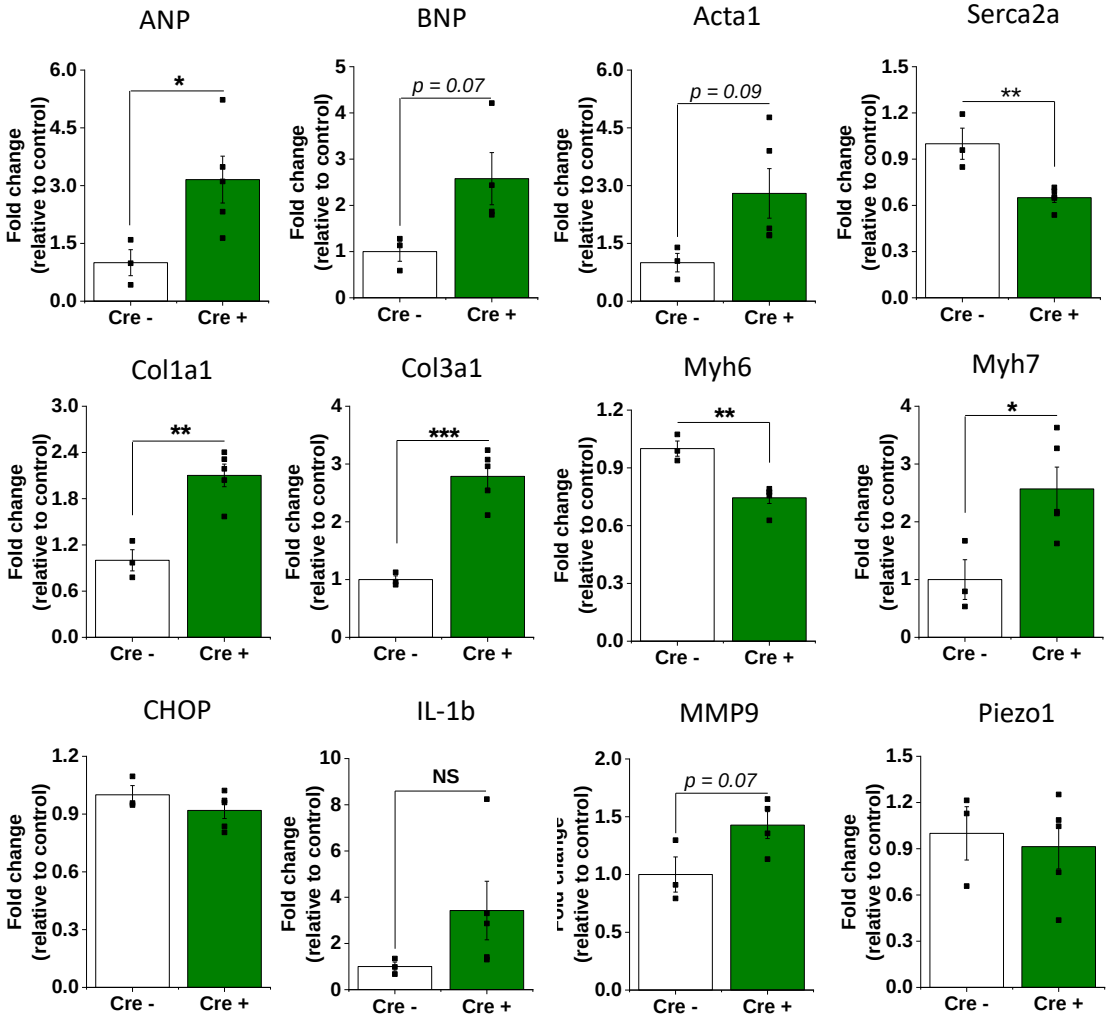

Figure 4-10 Heart failure gene expression phenotype is more pronounced in 6-month old CreMyh6-Piezo1$^{-/-}$ mice. Real-time PCR showing the fold-change in mRNA expression of cardiac genes in Cre+ mice relative to control (Cre -). Each data point represents a value from an independent experiment with mean values and error bars representing SEM indicated by the open (Cre-) or green (Cre+) bars (n=3, Cre-; n=5, Cre+ {n=4 *Bnp* and *Mmp9*}). * ($p<0.05$), ** ($p<0.01$), *** ($p<0.001$), **** ($p<0.0001$). *Anp*: atrial natriuretic peptide, *Bnp*: brain natriuretic peptide, *Acta1*: skeletal muscle actin, *Col1a1*: Collagen Type 1 alpha 1, *Col3a1*: Collagen Type 3 alpha 1, *Myh6*: myosin heavy chain α, *Myh7*: myosin heavy chain β, *Chop:* C/EPB homologous protein, *Il-1b*: interleukin 1 beta, *Mmp9* matrix metalloproteinase 9.

4.2.4 Piezo1 M-R mice exhibit increased expression of lipogenic genes in eWAT

As an increase in eWAT mass was observed in 8-week old Piezo1 M-R mice (Figure 4-1), the expression of a selection of genes involved in energy balance was investigated (Figure 4-11). A brief description of the genes measured is provided in Table 4-2; these broadly fall into the categories of adipokines, enzymes involved in de novo lipogenesis which produces fatty acids from excess carbohydrates, transcription factors, factors involved in fatty acid breakdown, or inflammation.

Apart from a trend for a reduction in *Il-1b* expression ($p = 0.09$), gene expression was broadly unchanged (Figure 4-11). A number of the genes involved in lipogenesis, notably *Dgat2* (diacylglycerol acyltransferase-2), *Cd36*, *Fas* (fatty acid synthase), *Lpl* (lipoprotein lipase), *Elovl6* (fatty acid elongase 6) and *Scd1* (stearoyl-CoA desaturase) were increased in a number of samples, perhaps indicative of the increase in eWAT mass, although this was not the case for all mice and a large spread in expression was observed.

To investigate whether the increase in fat mass was due to an increase in adipocyte size, adipocyte area was measured from H&E stained eWAT tissue sections (Figure 4-12). Deletion of Piezo1 from adipocytes has previously been shown to reduce average adipocyte size (Zhao et al., 2019). The average adipocyte area was comparable (Figure 4-12B). In case Piezo1 M-R mice had a shift in the amount of larger adipocytes which could not be detected by average size, the frequency distribution of adipocyte size, separated into 500 mm^2 bins from 0-5000 mm^2 was investigated (Figure 4-12C). The frequency distribution curve of adipocyte size did not reveal any differences between WT and Piezo1 M-R mice.

Next the same analysis was performed on 22-week old Piezo1 M-R mice. Here, the qPCR results showed distinct upregulation of lipogenic genes; *Dgat2*, *Cd36*, *Fas*, *Elovl6* with a trend for increased *Lpl* and *Scd1* ($p \leq 0.09$) (Figure 4-13). Measurement of adipocyte size did not reveal corresponding increases in average area or changes in frequency distribution (Figure 4-14), however in these data there were clear trends for increased adipocyte size which may emerge through larger sample sizes (18 samples per group are required to detect a 20% change at 80% power). Overall the results show that eWAT gene expression is altered in older Piezo1 M-R mice, with a global increase in lipogenic genes suggesting that metabolic differences due to Piezo1 GOF mutations are possible.

Target gene	Function	Ref
Leptin	Pro-inflammatory adipokine, regulates feeding behaviour. Plasma levels correlate with adipose mass.	(Ouchi et al., 2011)
Adiponectin	Anti-inflammatory adipokine. Protective roles against metabolic dysfunction. Plasma levels negatively correlate with adipose mass.	(Ouchi et al., 2011)
Dgat2 (diacylglycerol acyltransferase-2)	Catalyses final reaction in triglyceride synthesis from fatty acids.	(Liu et al., 2012)
Cd36	Fatty acid transporter- facilitates uptake of fatty acids.	(Goldberg et al., 2009)
Fas (fatty acid synthase)	Catalyses formation of palmitate (fatty acid).	(Strable and Ntambi, 2010)
Lpl (lipoprotein lipase)	Hydrolyses triglyceride-rich lipoproteins and can mediate uptake of lipoproteins.	(Goldberg et al., 2009)
Elovl6 (fatty acid elongase 6)	Elongates long-chain saturated and unsaturated fatty acids.	(Strable and Ntambi, 2010)
Scd1 (stearoyl-CoA desaturase)	Catalyses formation of monounsaturated fatty acids (MUFAs).	(Strable and Ntambi, 2010)
Pparγ (peroxisome proliferator-activated receptor γ)	Transcriptional regulator with critical roles in adipogenesis and adipocyte function. Up-regulates genes involved in lipogenesis.	(Sharma and Staels, 2007)
Pgc1a (PPARγ coactivator 1-alpha)	Transcriptional regulator which interacts with PPARγ and contribute to mitochondrial biogenesis.	(Austin and St-Pierre, 2012)
Hsl (hormone sensitive lipase)	Involved in lipid breakdown. Responsible for hydrolysis of stored triglycerides into free fatty acids.	(Kraemer and Shen, 2002)
Hif1α (hypoxia-inducible factor 1 alpha)	Transcription factor, activated by hypoxia. Facilitates adaptation to low oxygen levels, by promoting glycolysis and opposing hypoxia-induced inflammation and insulin resistance.	(Gaspar and Velloso, 2018)
Tnfα	Pro-inflammatory cytokine.	(Rodríguez-Hernández et al., 2013)
Il-1b	Pro-inflammatory cytokine.	(Bremer et al., 2011)
Mcp1	Recruits macrophages into adipose tissue.	(Bremer et al., 2011)

Table 4-2 Brief description of WAT genes measured by qPCR.

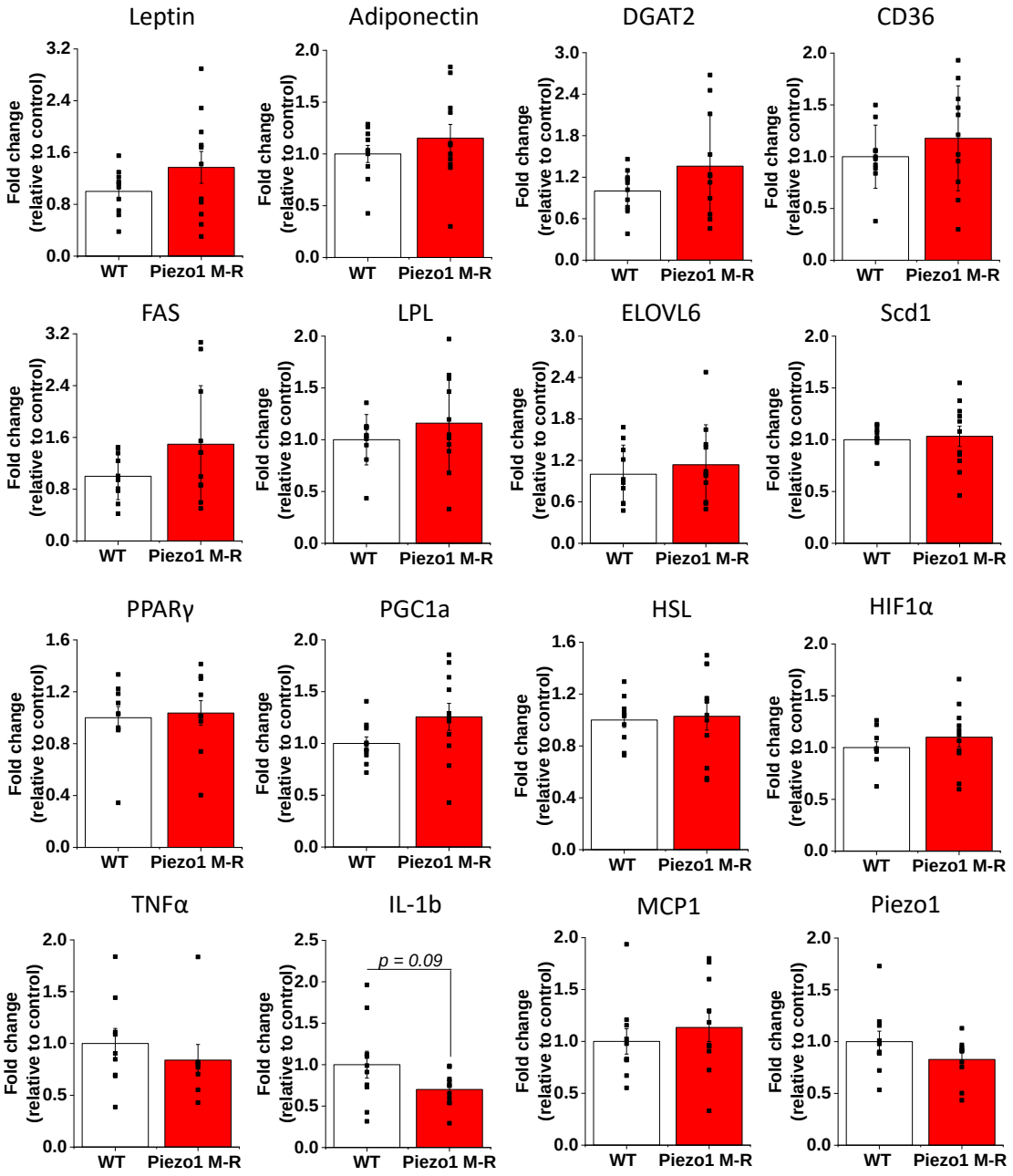

Figure 4-11 Expression of lipid homeostasis genes in eWAT of 8-week old Piezo1 M-R mice. Real-time PCR showing the fold-change in mRNA expression in eWAT of *Leptin, Adiponectin, Dgat2, Cd36, Lpl, Fas, Elovl6, Scd1, Pparγ, Pgc1a, Hsl, Hif1α, Tnfα, Il-1b, Mcp1* and *Piezo1* in Piezo1 M-R mice relative to control (WT). Error bars indicate SEM (n=10, WT; n=11, Piezo1 M-R). *Dgat2*: Diacylglycerol O-Acyltransferase 2, *Lpl*: lipoprotein lipase, *Fas*: fatty acid synthase, *Elovl6*: Fatty acid elongase 6, *Scd1*: stearoyl-CoA desaturase1, *Pparγ*: peroxisome proliferator activated receptor gamma, *Hsl*: hormone-sensitive lipase, *Hif1α*: hypoxia-inducible factor 1-alpha, *Tnfα*: tumour necrosis factor alpha, *Il-1b*: interleukin 1 beta, *Mcp1*: monocyte chemoattractant protein-1.

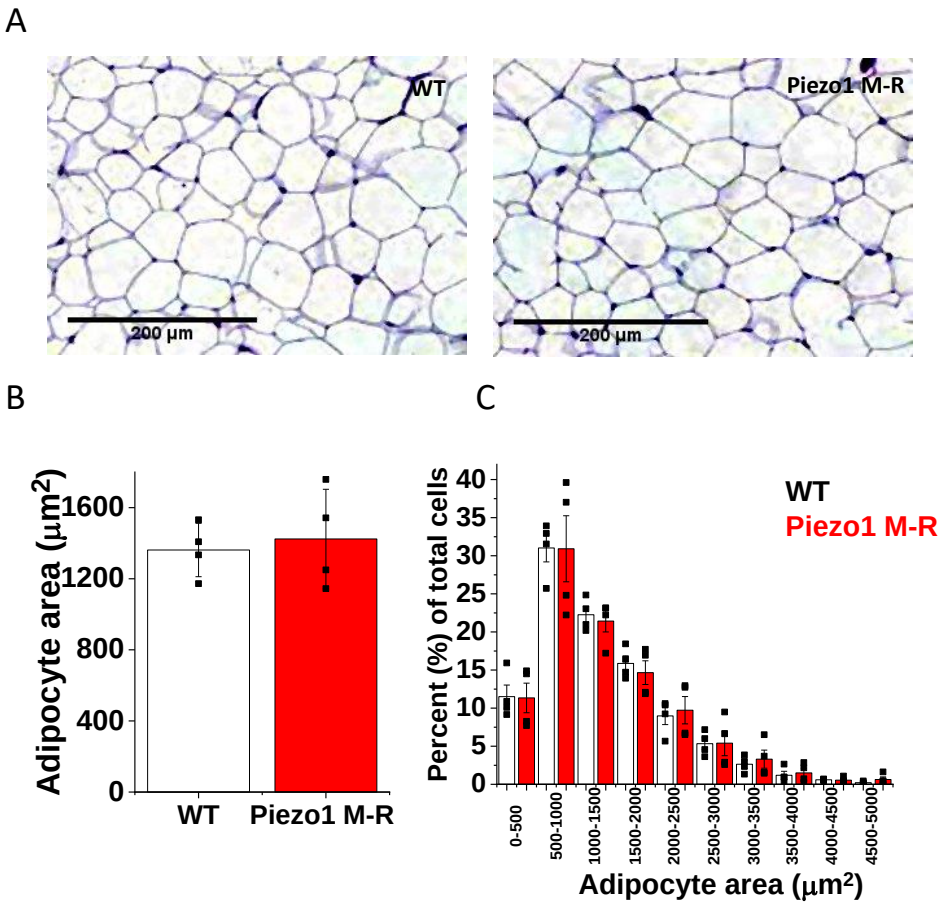

Figure 4-12 Adipocyte size is unchanged in eWAT from 8-week old Piezo1 M-R mice. (A) H&E staining of eWAT. Scale bar 200 µm. (B) Average adipocyte area of eWAT. Error bars indicate SEM (n=4). (C) Frequency distribution of adipocyte cell size expressed as a percentage of total cells. Error bars indicate SEM (n=4).

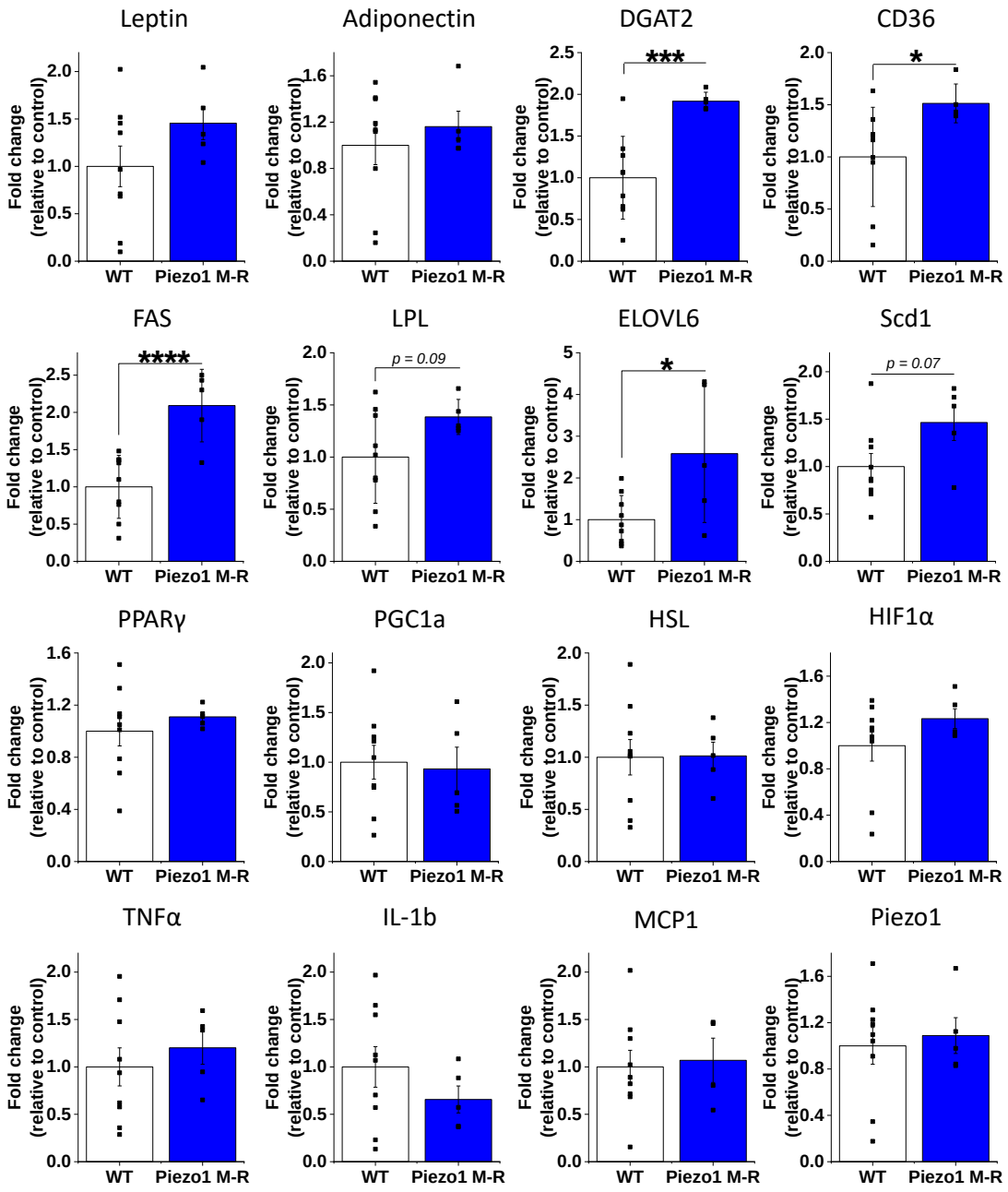

Figure 4-13 Lipogenic genes are upregulated in eWAT of 22-week old Piezo1 M-R mice. Real-time PCR showing the fold-change in mRNA expression in eWAT of *Leptin, Adiponectin, Dgat2, Cd36, Lpl, Fas, Elovl6, Scd1, Pparγ, Pgc1a, Hsl, Hif1α, Tnfα, Il-1b, Mcp1* and *Piezo1* in Piezo1 M-R mice relative to control (WT). Error bars indicate SEM (n=9, WT; n=5, Piezo1 M-R). * ($p<0.05$), ** ($p<0.01$), *** ($p<0.001$), **** ($p<0.0001$). *Dgat2*: Diacylglycerol O-Acyltransferase 2, *Lpl*: lipoprotein lipase, *Fas*: fatty acid synthase, *Elovl6*: Fatty acid elongase 6, *Scd1*: stearoyl-CoA desaturase1, *Pparγ*: peroxisome proliferator activated receptor gamma, *Hsl*: hormone-sensitive lipase, *Hif1α*: hypoxia-inducible factor 1-alpha, *Tnfα*: tumour necrosis factor alpha, *Il-1b*: interleukin 1 beta, *Mcp1*: monocyte chemoattractant protein-1.

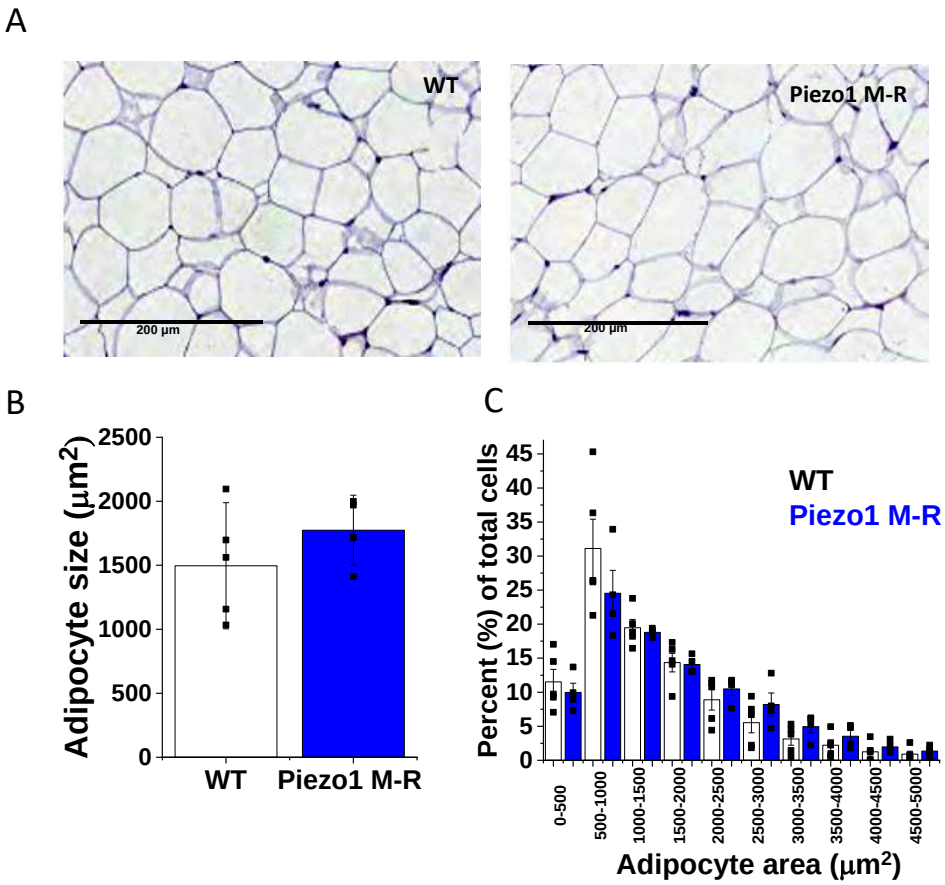

Figure 4-14 Trend for increased adipocyte size in eWAT of 22-week old Piezo1 M-R mice. (A) H&E staining of eWAT. Scale bar 200 µm. (B) Adipocyte area of eWAT. Error bars indicate SEM (n=5, WT; n=4 Piezo1 M-R). (C) Frequency distribution of adipocyte cell size expressed as a percentage of total cells. Error bars indicate SEM (n=5, WT; n=4 Piezo1 M-R).

4.2.5 Increased lipogenic gene expression is not due to an increase in expression of transcription factors, SREBP-1c or ChREBP

As there was blanket upregulation of lipogenic genes; *Dgat2, Cd36, Fas* and *Elovl6* with a trend for increased *Lpl* and *Scd1* in older Piezo1 M-R mice, it was important to investigate the possible mechanism involved. The synthesis of lipids and the regulation of genes involved in this pathway are broadly controlled by two transcription factors; SREBPs (sterol regulatory element binding protein) and ChREBP (carbohydrate response element-binding protein). Within the SREBP family, *SREBP-1c* is highly expressed in adipose tissue. Both are activated in the fed state; SREBP-1c via insulin levels and ChREBP via metabolites of glucose (Ferré and Foufelle, 2007, Abdul-Wahed et al., 2017). *Dgat2, Scd1, Elovl6, Cd36, Fas* and *Lpl* are all targets of these transcription factors so it was conceivable that Piezo1 M-R mice had higher expression levels. As an initial investigation, gene expression was investigated although, it would also be important to measure protein expression and activity levels. mRNA of *SREBP-1c* and *ChREBP* in eWAT of 8 week-old and 22-week old Piezo1 M-R mice were comparable (Figure 4-15). The results suggest that altered mRNA expression of lipogenic transcription factors does not account for the increase in mRNA expression of lipogenic genes.

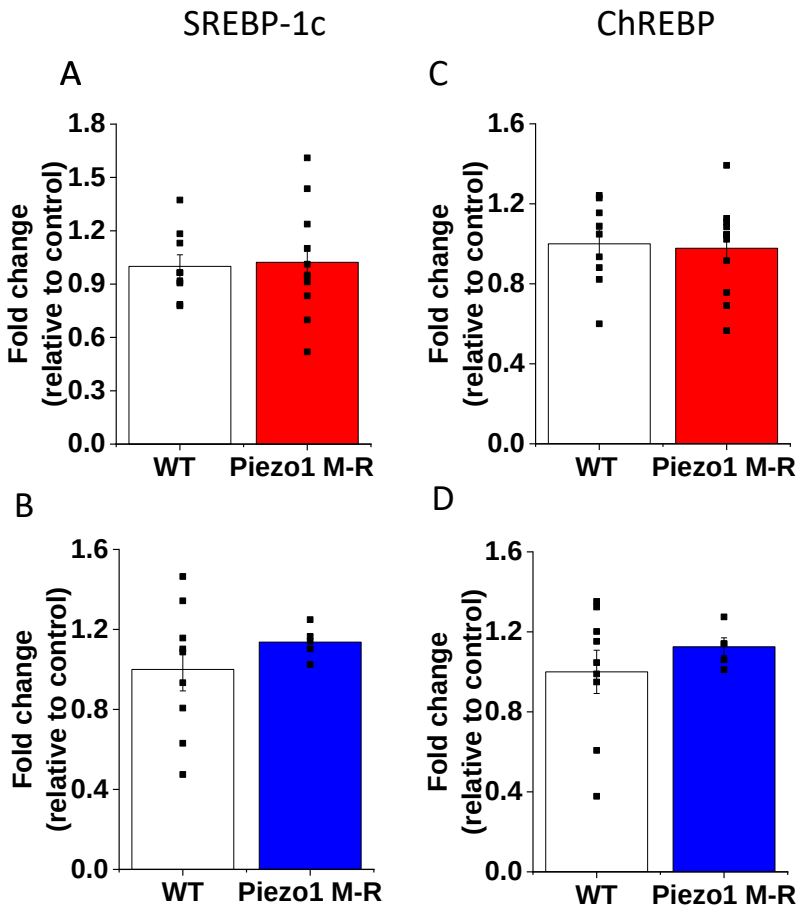

Figure 4-15 Lipogenic transcription factor expression in eWAT is unchanged in Piezo1 M-R mice. (A, C) Experiments performed on 8-week old mice (red). (B, D) Experiments performed on 22-week old mice (blue). Real-time PCR showing the fold-change in mRNA expression of *SREBP-1c* (A, B) and *ChREBP* (C, D) in Piezo1 M-R mice relative to control (WT). Error bars indicate SEM ({A, C} n=9, WT; n=11 Piezo1 M-R: {B, D} n=10, WT; n=5, Piezo1 M-R).

4.2.6 Expression of lipogenic genes is unchanged in scWAT

White adipose tissue depots exhibit functional differences; eWAT is more metabolically active, compared to subcutaneous fat (scWAT) and is associated with more negative effects on health (Sackmann-Sala et al., 2012, Wajchenberg et al., 2002). To determine whether lipogenic genes in scWAT were also altered in 22-week old Piezo1 M-R mice, the expression of *Dgat2, Cd36, Fas, Lpl* and *Elovl6* was measured in scWAT, in addition to *Piezo1* levels (Figure 4-16). The expression of all genes was similar, suggesting that changes to lipogenic gene expression are specific to eWAT.

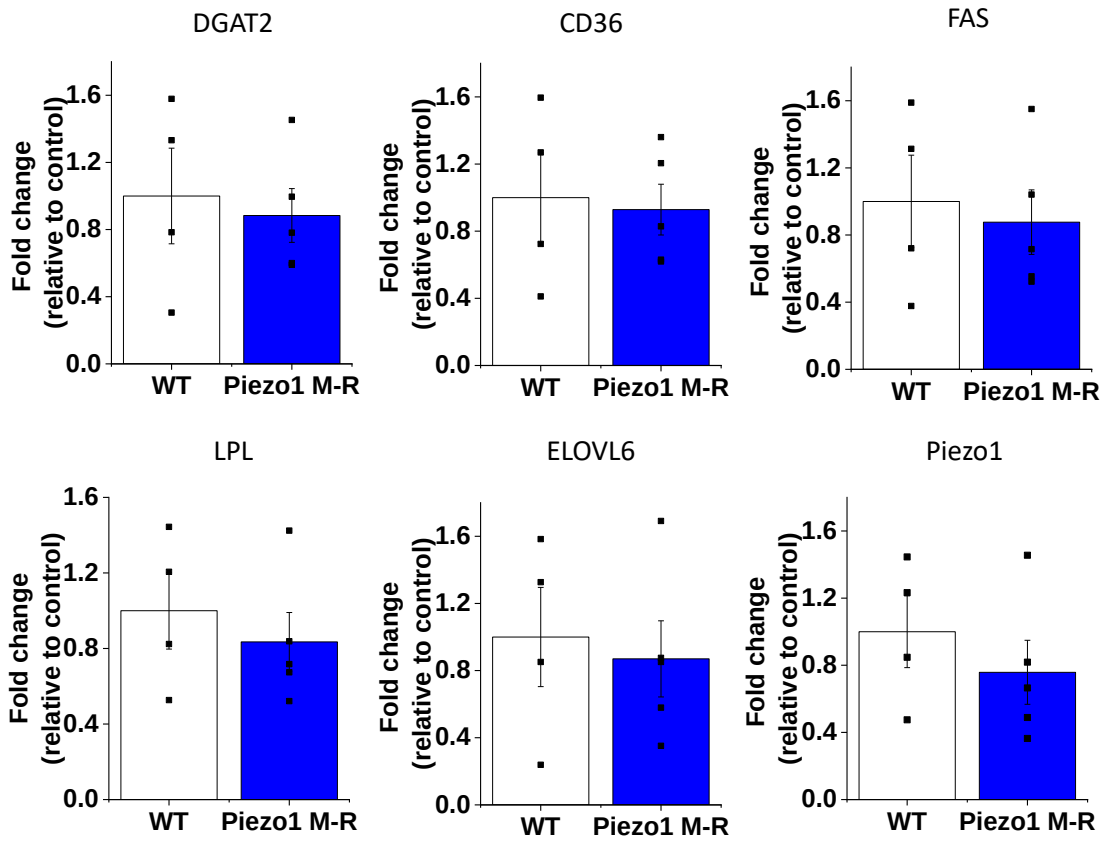

Figure 4-16 Lipogenic genes are unchanged in scWAT of 22 week old Piezo1 M-R mice. Real-time PCR showing the fold-change in mRNA expression in scWAT of *Dgat2, Cd36, Lpl, Fas, Elovl6* and *Piezo1* in Piezo1 M-R mice relative to control (WT). Error bars indicate SEM (n=4, WT; n=5, Piezo1 M-R. *Dgat2*: Diacylglycerol O-Acyltransferase 2, *Lpl*: lipoprotein lipase, *Fas*: fatty acid synthase, *Elovl6*: Fatty acid elongase 6.

4.2.7 Gene expression changes are also evident in livers from Piezo1 M-R mice

De novo lipogenesis also occurs in the liver so it was important to investigate metabolic genes in this organ. Additionally, an increase in liver mass was observed in older Piezo1 M-R mice (Figure 4-1) indicating differences may be present. The genes spanned across lipogenesis, cholesterol and bile acid synthesis, fibrosis, macrophage infiltration and inflammation. A brief description of these genes is provided in Table 4-3.

In 8-week old Piezo1 M-R mice, there were trends for increased *Fas* and *Col1a1* ($p \leq 0.09$), and reduced *Piezo1* mRNA expression ($p = 0.07$), perhaps indicating compensation (Figure 4-17). By 22 weeks of age, the increase in *Fas* mRNA expression was more evident and *lipocalin2* expression was reduced (Figure 4-18). Piezo1 mRNA expression was normal. Taken together, both 8 and 22 week data suggest that *Fas* is upregulated in the livers of Piezo1 M-R mice, in keeping with an increased fat or liver mass and an emerging lipogenic phenotype.

To determine whether the increase in *Fas* and liver mass may correlate with increased lipid storage within the liver, H&E stained sections from 22-week old Piezo1 M-R were carefully examined for the presence of lipid droplets (Figure 4-19). Visually, it did appear that in general the livers from Piezo1 M-R had increased presence of fat with some clear evidence of lipid droplets. Overall, analysis from livers coincides with results from eWAT suggesting that aberrant lipid production and ectopic fat storage occurs due to Piezo1 M-R mutation.

Target gene	Function	Ref
Fas (fatty acid synthase)	Catalyses formation of palmitate (fatty acid).	(Strable and Ntambi, 2010)
Dgat2 (diacylglycerol acyltransferase-2)	Catalyses final reaction in triglyceride synthesis from fatty acids.	(Liu et al., 2012)
Cd36	Fatty acid transporter- facilitates uptake of fatty acids.	(Goldberg et al., 2009)
Pparα (peroxisome proliferator-activated receptor α)	Transcription factor- promotes fatty acid metabolism and opposes inflammation.	(Pawlak et al., 2015)
Glut2	Major glucose transporter in the liver. Required for glucose uptake and facilitates glucose homeostasis.	(Thorens, 2015)
HmgCoAr (hydroxyl methylglutaryl-CoA reductase)	Rate limiting enzyme in cholesterol biosynthesis.	(Trapani et al., 2012)
Mttp (microsomal triglyceride transfer protein)	Helps mediate the secretion of lipids from the liver by facilitating transfer of lipids into lipoproteins.	(Trapani et al., 2012)
ApoB100	Helps mediate the secretion of lipids from the liver- primary apolipoproteins in VLDL and LDL.	(Trapani et al., 2012)
VldLr	Responsible for endocytosis of cholesterol-rich VLDL therefore acting to reduce plasma cholesterol.	(Trapani et al., 2012)
Cyp7a1	Rate limiting enzyme converting bile acids from cholesterol.	(Liu et al., 2016)
Col1a1 Collagen 1α1	Upregulated during hepatic fibrosis caused by chronic liver disease.	(Bataller and Brenner, 2005)
CHOP (C/EBP homologous protein)	Pro-apoptotic transcription factor, induced during endoplasmic reticulum (ER) stress.	(Oyadomari and Mori, 2004)
Lipocalin2	Involved in innate immunity. Upregulated in liver disease, inflammation and injury.	(Asimakopoulou et al., 2016)
F4/80	Marker of Kupffer cells, a type of macrophage originating in the liver, upregulation of which can indicate liver injury or disease.	(Movita et al., 2012)
Cd68	As for *F4/80*.	(Movita et al., 2012)

Table 4-3 Brief description of hepatic genes measured by qPCR.

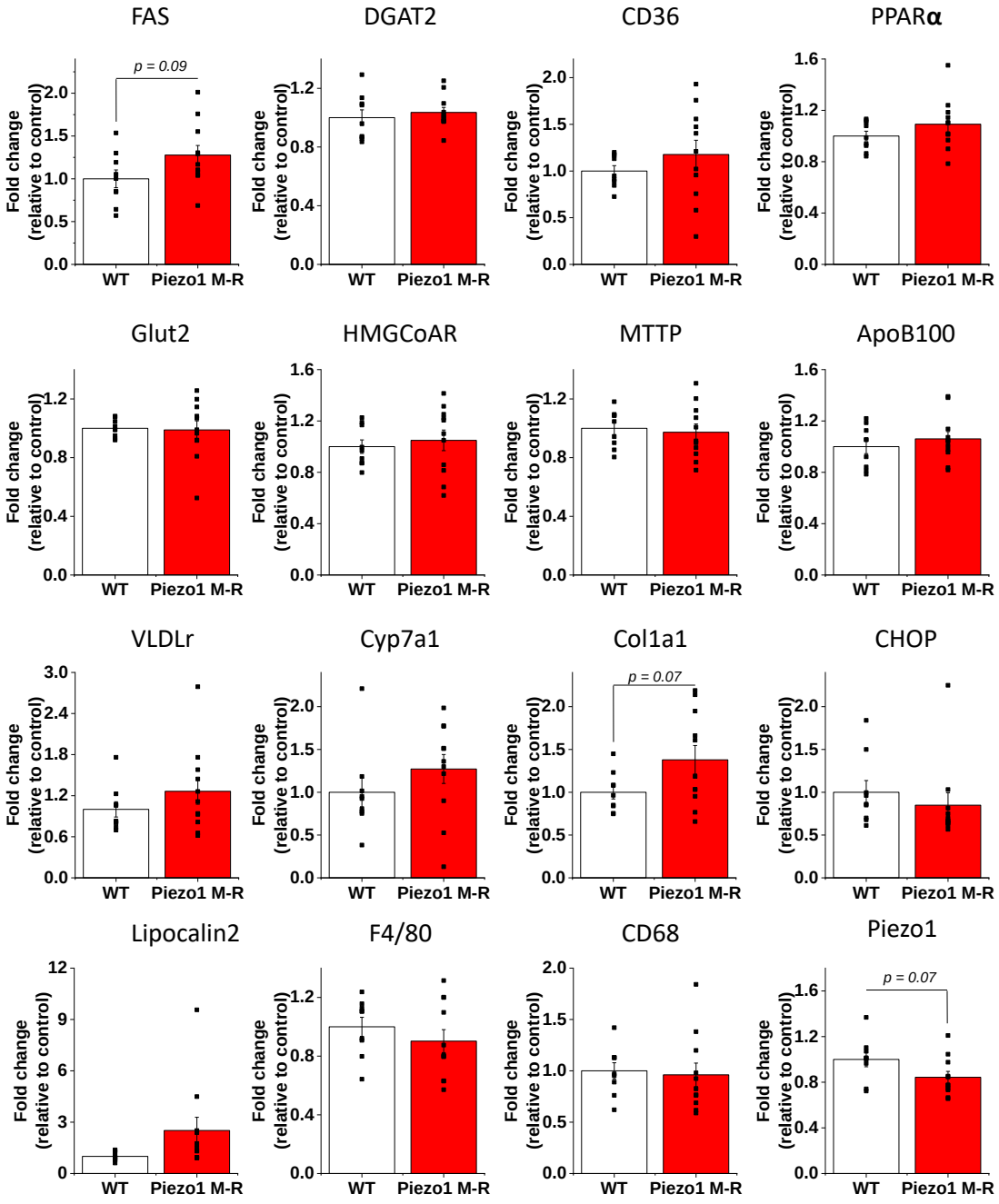

Figure 4-17 Gene expression in liver of 8-week old Piezo1 M-R mice. Real-time PCR showing the fold-change in mRNA expression in liver of *Fas, Dgat2, Pparα, Glut2, HmgCoAr, Mttp, Apob100, VldLr, Cyp7a1, Col1a1, Chop, Lipocalin2, F4/80, Cd68* and *Piezo1* in Piezo1 M-R mice relative to control (WT). Error bars indicate SEM (n=9, WT; n=11, Piezo1 M-R). *Fas*: fatty acid synthase, *Dgat2*: Diacylglycerol O-Acyltransferase 2, *Pparα*: peroxisome proliferator activated receptor alpha, *Glut2*: glucose transporter 2, *HmgCoAr*: HMG-CoA reductase, *Mttp*: microsomal triglyceride transfer protein, *Apob100*: apolipoprotein B, *VldLr*: very low density lipoprotein receptor, *Cyp7a1*: cholesterol 7 alpha-hydroxylase, *Col1a1*: Collagen Type 1 alpha 1, *Chop*: C/EPB homologous protein.

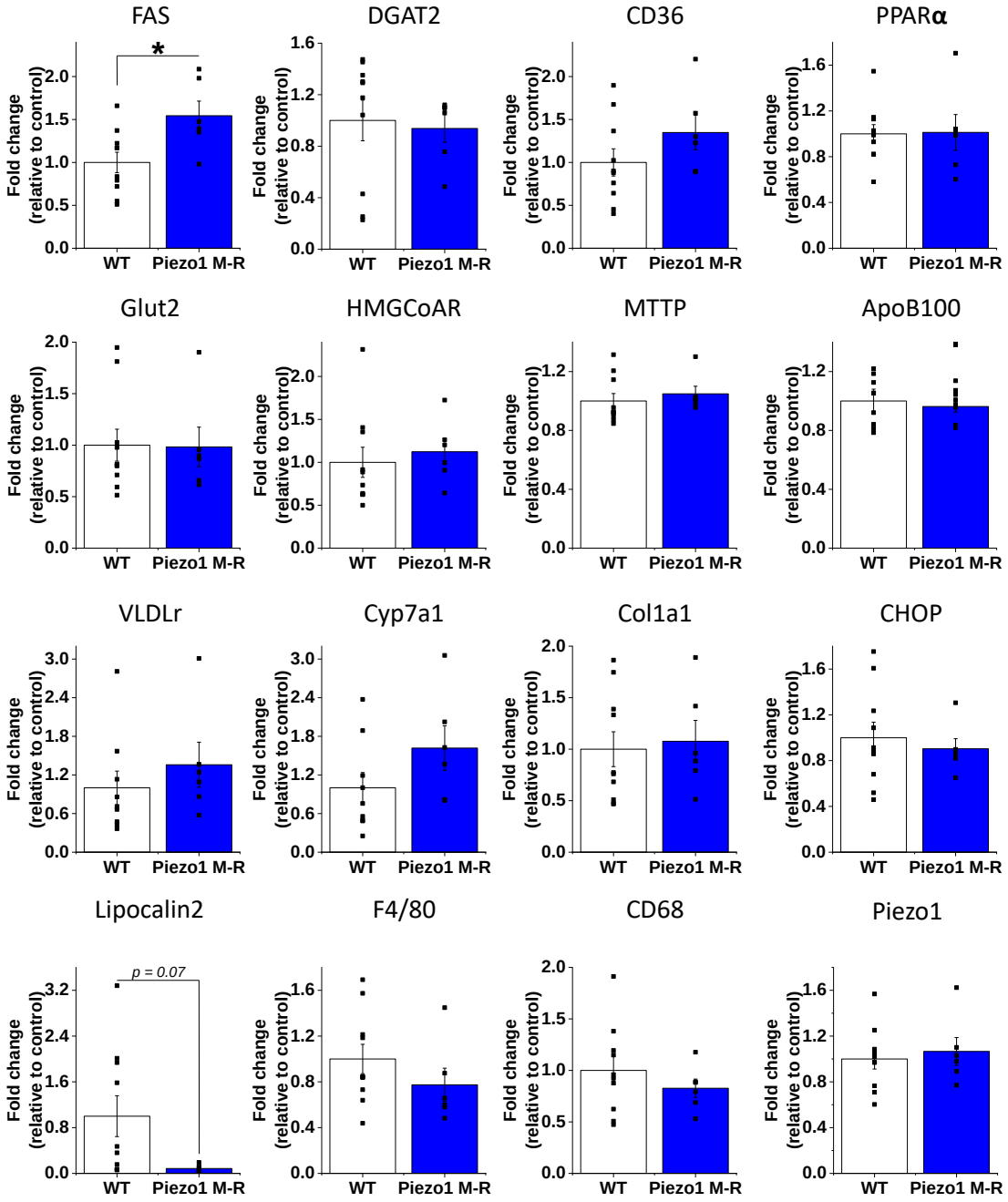

Figure 4-18 Gene expression in liver of 22-week old Piezo1 M-R mice. Real-time PCR showing the fold-change in mRNA expression in liver of *Fas, Dgat2, Pparα, Glut2, HmgCoAr, Mttp, Apob100, VldLr, Cyp7a1, Col1a1, Chop, Lipocalin2, F4/80, Cd68* and *Piezo1* in Piezo1 M-R mice relative to control (WT). Error bars indicate SEM (n=10, WT {9 *Cyp7a1, VldLr, Apob100*}; n=6, Piezo1 M-R). * ($p<0.05$), ** ($p<0.01$), *** ($p<0.001$), **** ($p<0.0001$). *Fas*: fatty acid synthase, *Dgat2*: Diacylglycerol O-Acyltransferase 2, *Pparα*: peroxisome proliferator activated receptor alpha, *Glut2*: glucose transporter 2, *HmgCoAr*: HMG-CoA reductase, *Mttp*: microsomal triglyceride transfer protein, *Apob100*: apolipoprotein B, *VldLr*: very low density lipoprotein receptor, *Cyp7a1*: cholesterol 7 alpha-hydroxylase, *Col1a1*: Collagen Type 1 alpha 1, *Chop*: C/EPB homologous protein.

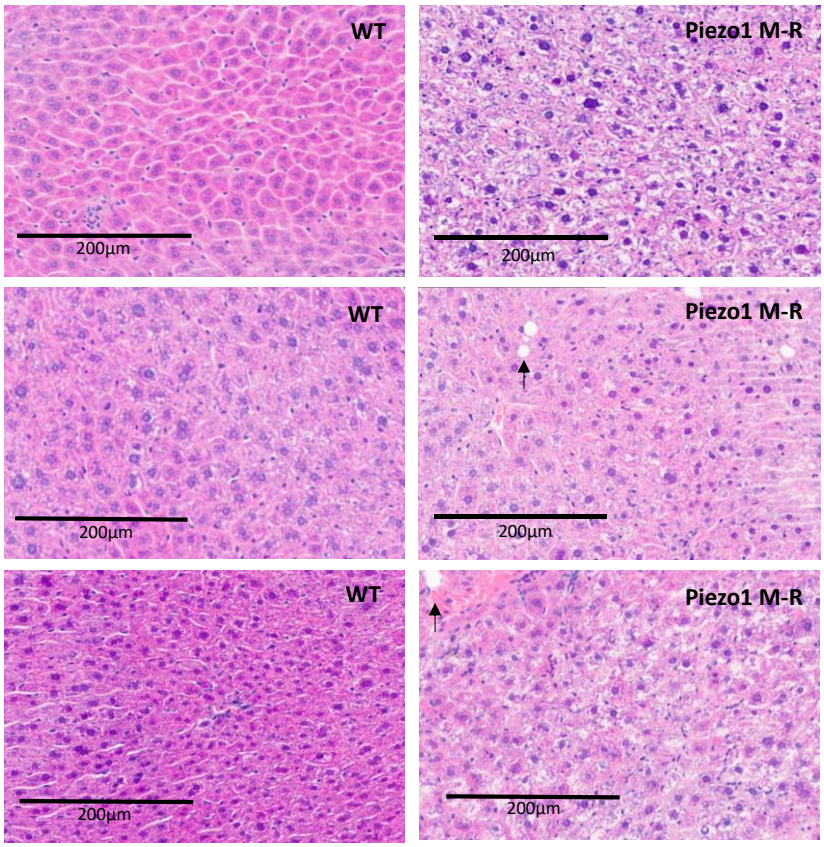

Figure 4-19 Lipid accumulation present in livers of 22-week old Piezo1 M-R mice. H&E staining of liver from WT (left) and Piezo1 M-R mice (right). Each image is representative of a different sample. Examples of lipid droplets highlighted by black arrows. Scale bar 200 µm. Representative of n=5 for WT and Piezo1 M-R.

4.2.8 Metabolic parameters are affected in Piezo1 M-R mice

As metabolic differences were observed in Piezo1 M-R mice at an mRNA level, with changes in organ mass, it was necessary to determine whether this resulted in global metabolic changes in the mice. Indirect calorimetry was used to measure respiratory parameters, energy balance, food intake and activity levels in 22-week old Piezo1 M-R, which exhibited the most profound gene expression changes (Figure 4-20). Mice were placed into individual CLAMs cages and were left to acclimatise for at least 24 hours, before recorded values were used. Data are divided into the 12-hour dark period, the time of activity for nocturnal mice, and the 12-hour light period and were analysed by CalR online calorimetry software (Mina et al., 2018). O_2 consumption, CO_2 production and energy expenditure were all normal (Figure 4-20A-C). Piezo1 M-R mice demonstrated reduced energy balance during the light period (Figure 4-20D) which correlated with a decrease in hourly food intake during this time (Figure 4-20E). However, it is important to note that parameters A-E can all be affected by the weight of the mice (Figure 4-20F) and for energy balance (Figure 4-20D) and hourly food intake (Figure 4-20E), an interaction effect of the mass and group effect was evident, suggesting the changes were not due to phenotype only (*p* values of group and interaction effects presented in the legend). The most interesting finding which was mass independent, was that Piezo1 M-R mice exhibited a reduced respiratory exchange ratio (RER) (Figure 4-20G). The RER is determined by CO_2 production/O_2 uptake and can be used to estimate the fuel source utilised for energy production as a different number of oxygen molecules are required to oxidise carbohydrates vs fatty acids. An RER of 1 indicates that carbohydrates are the primary fuel source, whereas an RER of 0.7 indicates fatty acids are the primary fuel source (Lusk, 1924). The data suggest that Piezo1 M-R mice utilise fatty acids as a fuel source, more so than WT mice, which supports the previous findings that Piezo1 M-R mice are in an increased lipogenic state. Activity levels measured by total wheel counts, locomotor activity and ambulatory activity were not different between groups (Figure 4-20H-J).

Next, insulin and glucose handling were investigated as systemic insulin resistance and therefore impaired glucose tolerance can occur from ectopic fat deposition and is a precursor for type 2 diabetes (Shulman, 2014) (Figure 4-21). Insulin and glucose tolerance tests (ITT and GTT respectively) were performed

on the mice which measure blood glucose levels following an insulin or glucose bolus injection. At 8 weeks old, Piezo1 M-R mice exhibited trends for insulin resistance with glucose levels increasing more rapidly following insulin injection compared to WT (Figure 4-21A). This corresponded with a strong trend for increased area under the curve (AUC) for glucose levels over the course of the experiment (p = 0.06) (Figure 4-21B). Glucose tolerance was unaffected at this age point (Figure 4-21B). Mice were also tested at 16 weeks of age (mice at 22-weeks mice underwent CLAMs measurement so could not be tested). At this older time point, the mice also appeared insulin resistant, recovering much quicker from insulin injection (Figure 4-21C), with a strong trend for increased glucose AUC (p = 0.065) (Figure 4-21D). 22-week old Piezo1 M-R mice did show early signs of reduction in glucose tolerance compared to WT, which occurs after insulin resistance has developed, however this did not reach statistical significance (Figure 4-21CD). Overall, Piezo1 M-R mice show strong trends for signs of insulin resistance.

Metabolic abnormalities including insulin resistance can often cause dyslipidaemia; an abnormal plasma lipid profile. This usually presents as elevated levels of triglycerides and reduced HDL (high density lipoprotein) –cholesterol and increased low (LDL) and very low (VLDL) density lipoproteins (Krauss, 2004). This abnormal lipid profile is associated with an increased cardiovascular risk (Krauss, 1998). To measure the lipid profile of Piezo1 M-R mice, a colorimetric assay was used to determine triglyceride, total cholesterol and HDL-cholesterol levels from plasma samples. Plasma lipid levels were unchanged in 8-week old mice (Figure 4-22). However, older 22-week old mice demonstrated dyslipidaemia, but surprisingly plasma triglyceride levels were reduced compared to controls, with a corresponding increase in HDL-cholesterol. This result was unexpected due to the increased lipogenic profile previously observed, which would normally correlate with the opposite changes to plasma lipids.

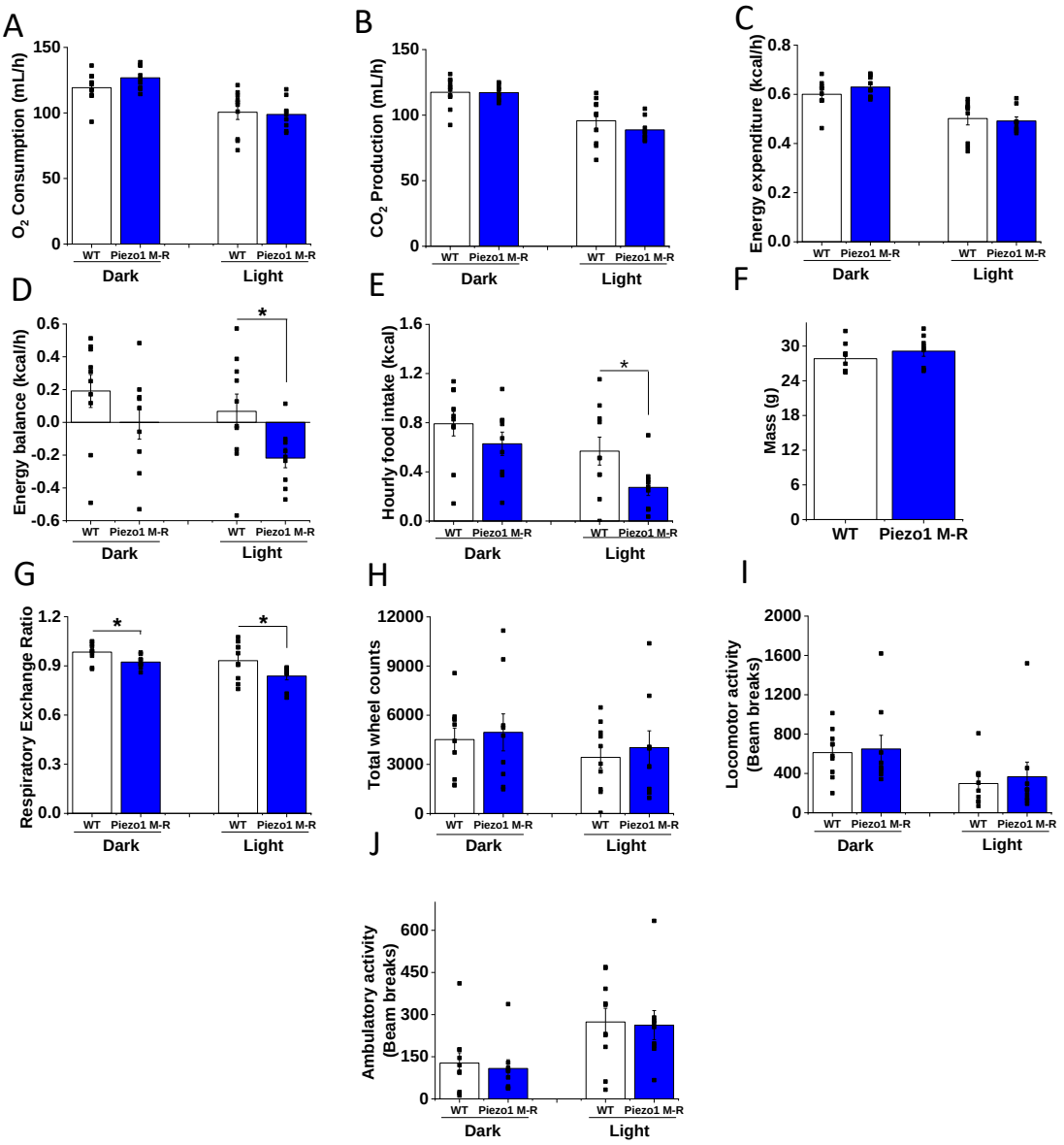

Figure 4-20 Indirect calorimetry for 22 week old Piezo1 M-R mice. Mice were placed into individual cages in the Oxymax Comprehensive Laboratory Animal Monitoring System (CLAMs) with free access to a running wheel. Data taken for a 24 hour period following 24 hour acclimatisation. Results analysed by CalR web-based analysis software for CLAMs. Data are separated into dark and light periods. (A-E) Ancova analysis based on group and mass (F) effect. An interaction effect suggests group effect is also dependent on the mass effect (G-J) Anova analysis only as parameters not affected by mass. (A) Oxygen consumption, (B) Carbon dioxide production, (C) Energy expenditure, (D) Energy balance (Light group *p* value= 0.0224, interaction *p* value= 0.0336) , (E) Average hourly food intake (Light group *p* value= 0.0104, interaction *p* value= 0.0164), (F) Body weight of mice, (G) Respiratory Exchange Ratio (Dark *p* value= 0.0190, light *p* value= 0.0122), (H) Total wheel counts, (I) Locomotor activity, (J) Ambulatory activity (n=10 WT; n=9 Piezo1 M-R). * ($p<0.05$), ** ($p<0.01$), *** ($p<0.001$), **** ($p<0.0001$).

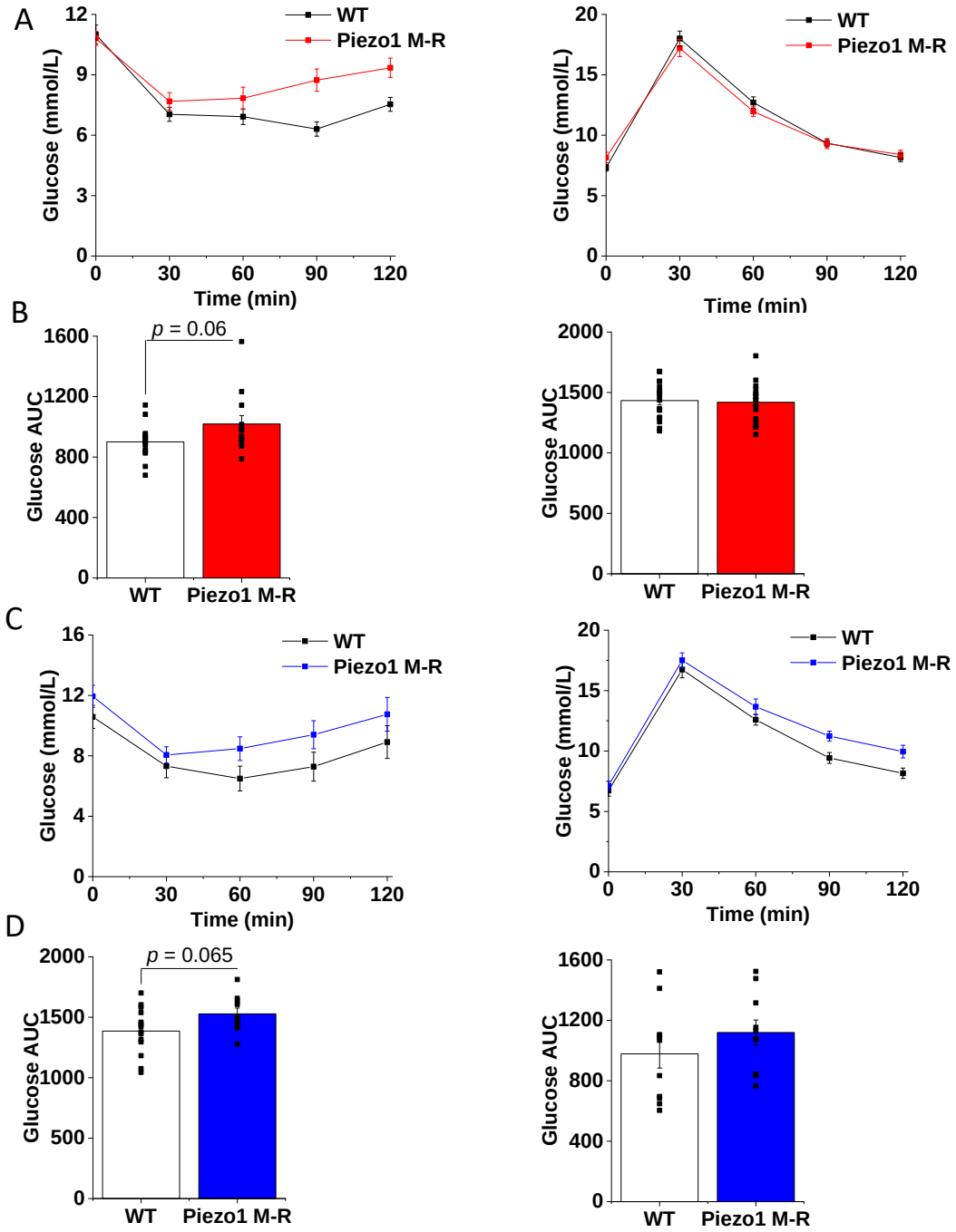

Figure 4-21 Piezo1 M-R mice demonstrate trends for insulin resistance. (A) Mice 8 weeks old. Insulin tolerance test (left) and glucose tolerance test (right) results (n=16, WT; n=15, Piezo1 M-R). (B) Area under the curve for ITT (left) and GTT (right) shown in (A). (C) As for (A) but mice 16 weeks old (n=11, WT; n=14, Piezo1 M-R). (D) Area under the curve for ITT (left) and GTT (right) shown in (C). Error bars indicate SEM.

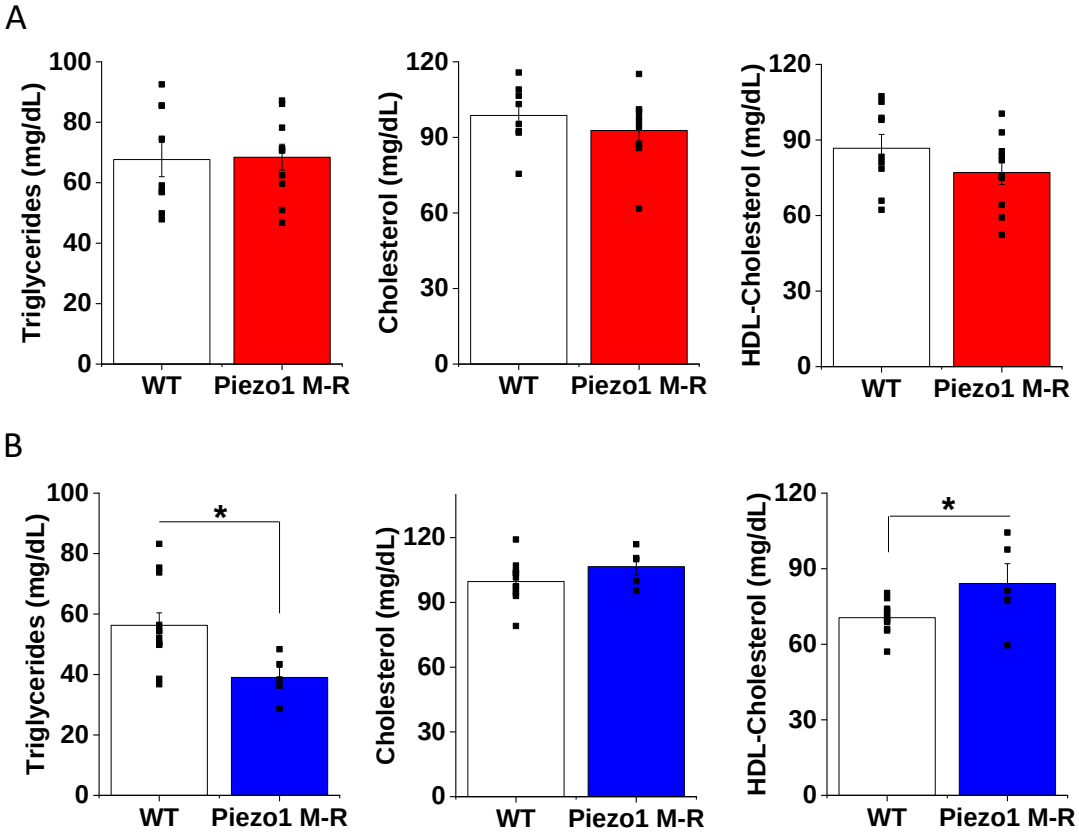

Figure 4-22 Plasma lipid levels are altered in older Piezo1 M-R mice. (A) Plasma lipid concentrations of triglycerides (left), cholesterol (middle) and high-density lipoprotein cholesterol (HDL-Cholesterol) (right) in 8 week old mice (n=9, WT; n=10, Piezo1 M-R). (B) As for (A) but mice were 22 weeks old (n=12, WT; n=5, Piezo1 M-R). * ($p<0.05$), ** ($p<0.01$), *** ($p<0.001$), **** ($p<0.0001$).

4.2.9 High fat diet intervention produced the expected phenotype

As Piezo1 M-R mice on chow diet demonstrated an altered metabolic profile, favouring lipogenesis and lipid storage, with changes to insulin sensitivity, it was investigated whether these differences were exacerbated after stress induced by high fat diet (HFD). Mice were given *ab libitum* access to 60% fat diet from 8 weeks of age, for 14 weeks. Firstly, it was ensured that HFD intervention produced the expected phenotype in WT mice (Figure 4-23). This was confirmed with a substantial increase in body weight, compared to controls observed after 3 weeks of HFD (Figure 4-23A). Additionally, fat depots eWAT and scWAT were much larger in HFD-fed mice (Figure 4-23B) and they were hyperglycaemic (Figure 4-23C). HFD-fed mice also demonstrated expected increase in *leptin* mRNA expression (Figure 4-23D) (Lin et al., 2000) and *Tnfα* mRNA expression in eWAT (Figure 4-23E), indicative of low grade inflammation due to obesity (Wellen and Hotamisligil, 2005). Finally, *Piezo1* has recently been shown to be upregulated in eWAT due to HFD and this was also observed (Figure 4-23F) (Zhao et al., 2019). Overall, the results show that the HFD intervention used produced the expected phenotype.

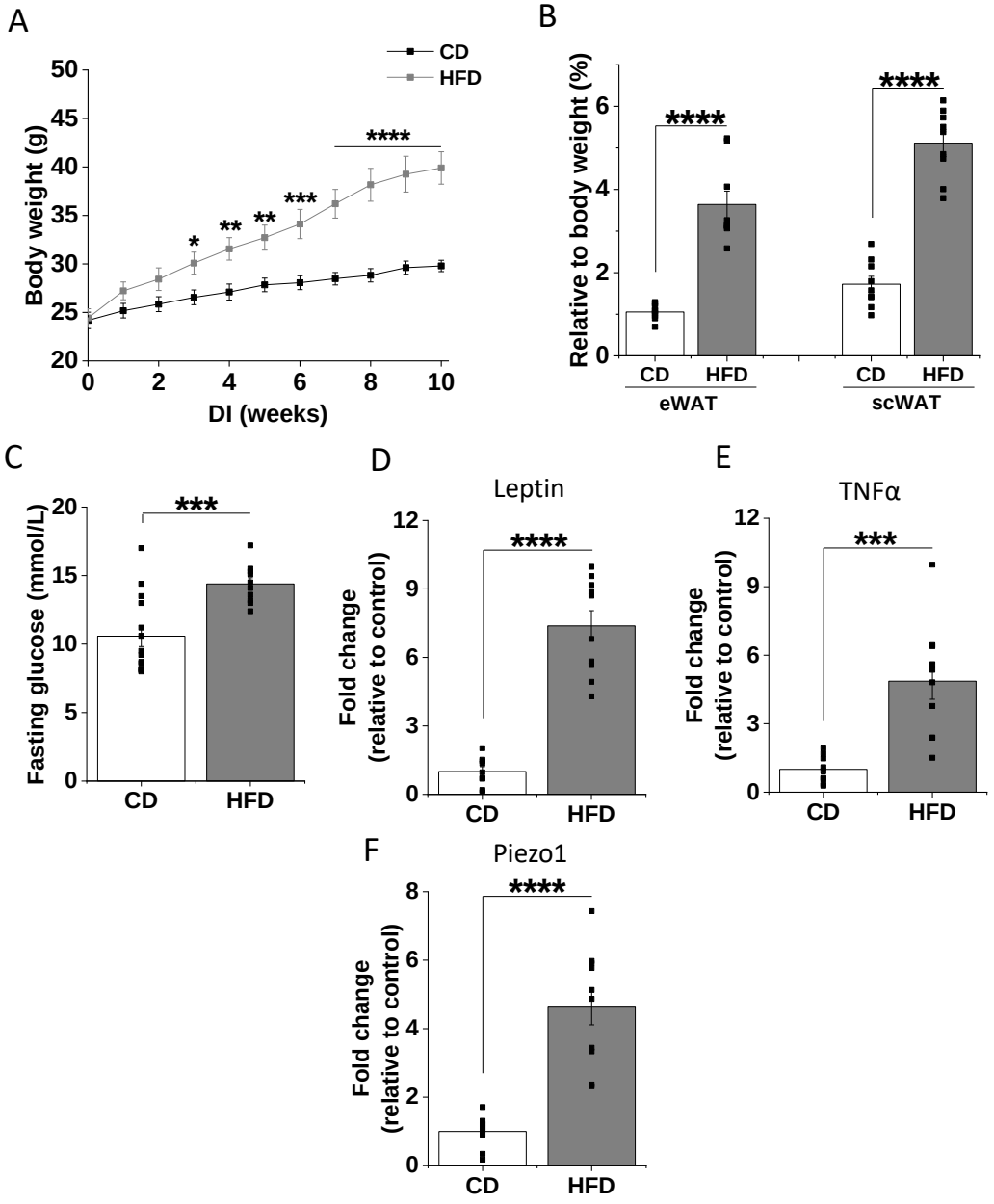

Figure 4-23 HFD intervention caused the expected phenotype. 8 week old mice were fed CD or HFD for 14 weeks until 22 weeks of age. (A) Body weights of mice from 0-10 weeks of CD or HFD feeding (n=14, CD; n=11, HFD). (B) Weights of eWAT and scWAT fat pads relative to body weight (n=14, CD; n=11, HFD). (C) Blood glucose levels of mice fasted for 2 hours (n=14, CD; n=10, HFD). (D-E) Real-time PCR showing the fold-change in mRNA expression in eWAT of *leptin* (D), *Tnfα* (E) and *Piezo1* (F) in HFD fed mice, relative to CD fed mice (n=9, CD; n=10, HFD). * ($p<0.05$), ** ($p<0.01$), *** ($p<0.001$), **** ($p<0.0001$).

4.2.10 Piezo1 M-R mice fed HFD appear normal with no changes in lipogenic gene expression

To investigate gross differences between WT and Piezo1 M-R mice fed HFD, body weights and organ weights were measured. Body weights were the same between genotypes throughout HFD intervention (Figure 4-24A). Additionally, organ weights were generally similar except for a trend for increased spleen weight (p = 0.09), which may reflect the underlying DHS (Figure 4-24B). The weights of the quadriceps and gastrocnemius muscle also had a tendency to be reduced ($p \leq 0.08$). Overall, the data show that broadly HFD Piezo1 M-R mice had no gross anatomical abnormalities and that the increase in fat and liver mass observed on chow diet (CD) were not exacerbated.

Next, the expression of genes examined under CD conditions were investigated in both eWAT (Figure 4-25), scWAT (Figure 4-26) and liver (Figure 4-27). Gene expression in eWAT was comparable between genotypes, including lipogenic genes *Dgat2, Cd36, Fas, Lpl, Elovl6* and *Scd1* which were upregulated in CD-fed Piezo1 M-R mice of the same age. Interestingly, a reduction in *Piezo1* mRNA expression was observed in eWAT, perhaps indicating compensation in this tissue (Figure 4-25). As with CD-fed mice there was also no difference in lipogenic genes in scWAT and interestingly *Piezo1* mRNA expression was also comparable, suggesting only *Piezo1* expression in eWAT was affected by Piezo1 M-R. Gene expression in the liver was also similar between phenotypes, except *Cyp7a1* which was reduced. Overall, the data suggest that Piezo1 M-R mice fed HFD are generally normal and no longer exhibit the altered lipogenic gene expression profile observed under normal diet.

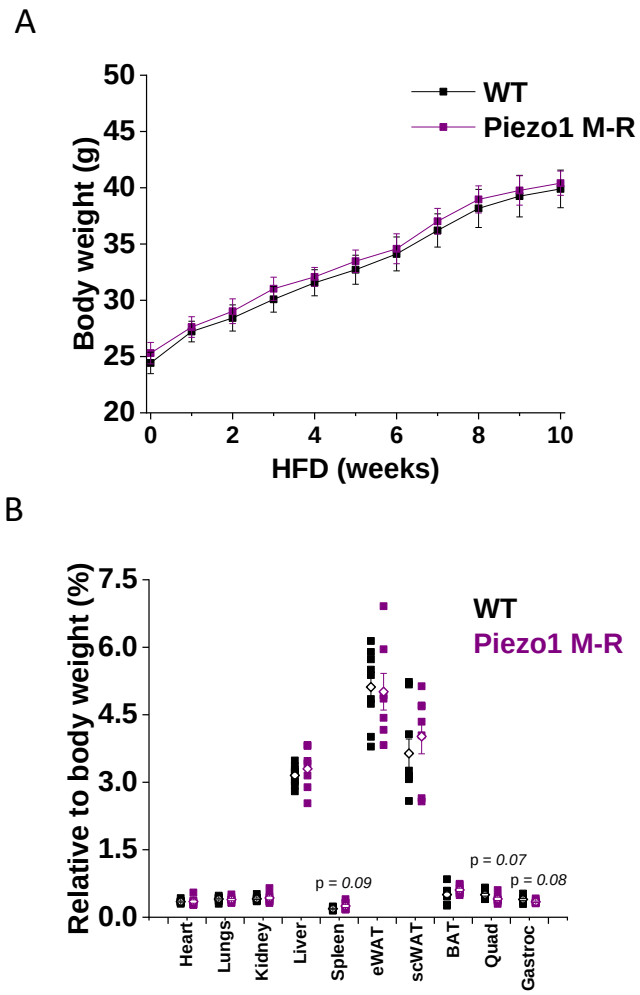

Figure 4-24 Body and organ weights of Piezo1 M-R mice fed HFD. (A) Body weights from WT and Piezo1 M-R mice measured from 8 weeks of age for 10 weeks of HFD feeding (n=11, WT; n=14,Piezo1 M-R). (B) Weights of heart, lungs, kidney, liver, spleen, epididymal white adipose tissue (eWAT), subcutaneous white adipose tissue (scWAT), brown adipose tissue (BAT), quadriceps (Quad) and gastrocnemius (Gastroc) as % of body weight in 22 week old mice following 12 weeks HFD feeding (n=9, WT; n=7, Piezo1 M-R).

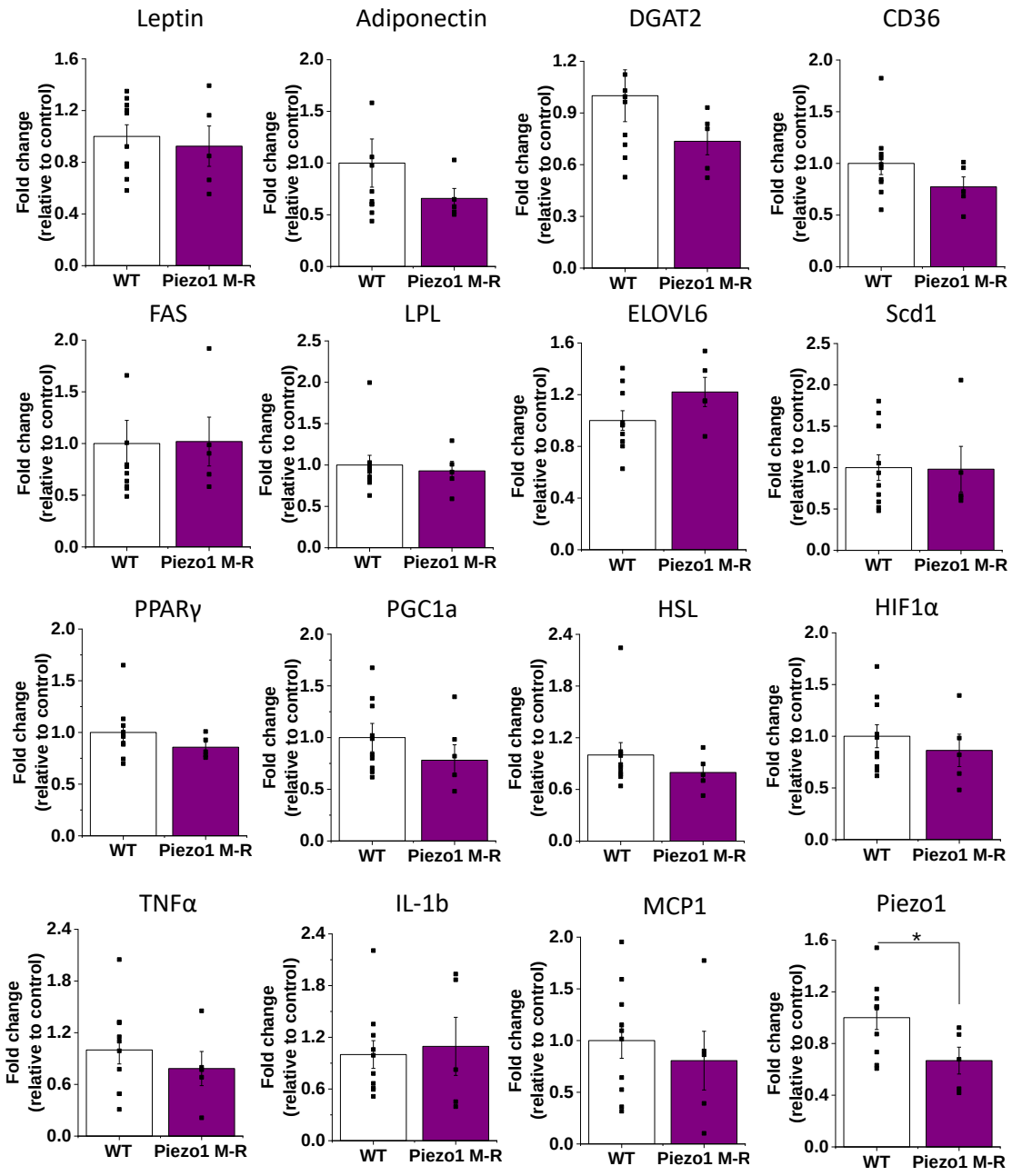

Figure 4-25 Lipogenic genes are unchanged in 22-week old Piezo1 M-R mice fed HFD. Real-time PCR showing the fold-change in mRNA expression in eWAT of *Leptin, Adiponectin, Dgat2, Cd36, Lpl, Fas, Elovl6, Scd1, Pparγ, Pgc1a, Hsl, Hif1α, Tnfα, Il-1b, Mcp1* and *Piezo1* in Piezo1 M-R mice relative to control (WT). Error bars indicate SEM (n=10, WT; n=7, Piezo1 M-R). * ($p<0.05$), ** ($p<0.01$), *** ($p<0.001$), **** ($p<0.0001$).*Dgat2*: Diacylglycerol O-Acyltransferase 2, *Lpl*: lipoprotein lipase, *Fas*: fatty acid synthase, *Elovl6*: Fatty acid elongase 6, *Scd1*: stearoyl-CoA desaturase1, *Pparγ*: peroxisome proliferator activated receptor gamma, *Hsl*: hormone-sensitive lipase, *Hif1α*: hypoxia-inducible factor 1-alpha, *Tnfα*: tumour necrosis factor alpha, *Il-1b*: interleukin 1 beta, *Mcp1*: monocyte chemoattractant protein-1.

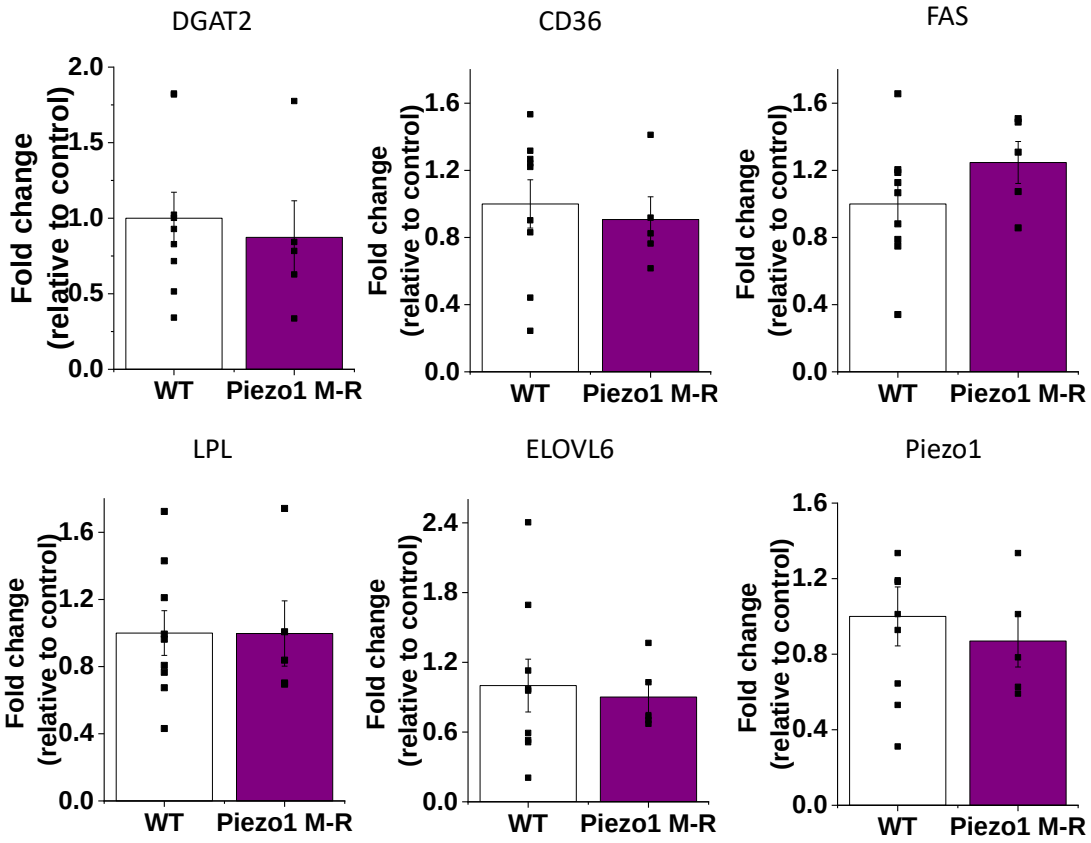

Figure 4-26 Lipogenic genes are unchanged in scWAT of 22 week old Piezo1 M-R mice fed HFD. Real-time PCR showing the fold-change in mRNA expression in scWAT of *Dgat2, Cd36, Lpl, Fas, Elovl6* and *Piezo1* in Piezo1 M-R mice relative to control (WT). Error bars indicate SEM (n=9, WT; n=5, Piezo1 M-R). *Dgat2*: Diacylglycerol O-Acyltransferase 2, *Lpl*: lipoprotein lipase, *Fas*: fatty acid synthase, *Elovl6*: Fatty acid elongase 6.

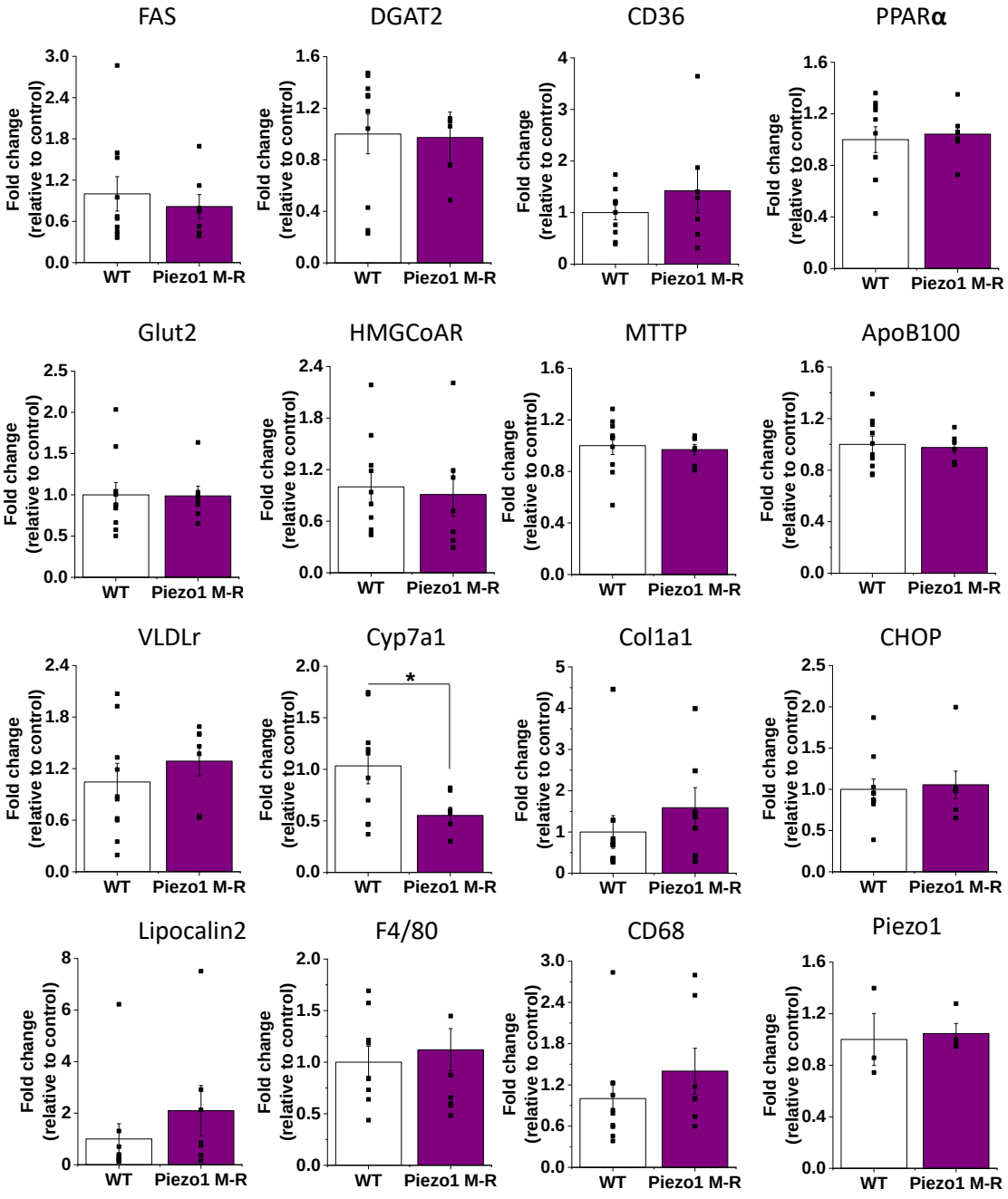

Figure 4-27 Gene expression in liver of 22-week old Piezo1 M-R mice fed HFD. Real-time PCR showing the fold-change in mRNA expression in liver of *Fas, Dgat2, Pparα, Glut2, HmgCoAr, Mttp, ApoB100, Vldlr, Cyp7a1, Col1a1, Chop, Lipocalin2, F4/80, Cd68* and *Piezo1* in Piezo1 M-R mice relative to control (WT). Error bars indicate SEM (n=10, WT; n=7 {n=6 ApoB100} Piezo1 M-R). * (p<0.05), ** (p<0.01), *** (p<0.001), **** (p<0.0001). *Fas*: fatty acid synthase, *Dgat2*: Diacylglycerol O-Acyltransferase 2, *Pparα*: peroxisome proliferator activated receptor alpha, *Glut2*: glucose transporter 2, *HmgCoAr*: HMG-CoA reductase, *Mttp*: microsomal triglyceride transfer protein, *ApoB100*: apolipoprotein B, *Vldlr*: very low density lipoprotein receptor, *Cyp7a1*: cholesterol 7 alpha-hydroxylase, *Col1a1*: Collagen Type 1 alpha 1, *Chop*: C/EPB homologous protein.

4.2.11 HFD-fed Piezo1 M-R mice have comparable metabolic profile, plasma lipids and insulin sensitivity

To investigate additional metabolic changes and to compare to CD-fed Piezo1 M-R mice, HFD-fed mice were analysed by indirect calorimetry (Figure 4-28). O_2 consumption, CO_2 production and energy expenditure were all normal (Figure 4-28A-C). Energy balance showed a trend for being reduced during the light phase and significance may develop with increased sample sizes (*p*-value = 0.11) (20 mice per group are required to detect a 50% reduction at 80% power) (Figure 4-28D). Food intake was increased during both dark and light phases (Figure 4-28E), with no interaction effect in the dark phase suggesting it was a phenotype only effect, independent from any mass effect (Figure 4-28F). Respiratory exchange ratio was unchanged in HFD-fed Piezo1 M-R mice (Figure 4-28G), but was close to the expected value of 0.7 consistent with utilisation of fats as the primary energy source. Total wheel counts were reduced during both dark and light phases (Figure 4-28H), as was locomotor activity during the dark, most active phase (Figure 4-28I). Ambulatory activity was normal (Figure 4-28J). Taken together it appears that the HFD-fed Piezo1 M-R mice utilise the same energy source as WT mice and have comparable respiration, although exhibit increased food intake with a decrease in physical activity, which does not result in an overall difference in energy balance.

ITT and GTTs were performed following 8 weeks of HFD and insulin sensitivity and glucose tolerance were not affected in HFD-fed Piezo1 M-R mice (Figure 4-29). Plasma lipid levels were also the same between phenotypes (Figure 4-30). Overall, the data suggest that HFD-fed Piezo1 M-R exhibit metabolic parameters which are comparable to controls and that previous effects observed on CD are ablated by HFD induced stress.

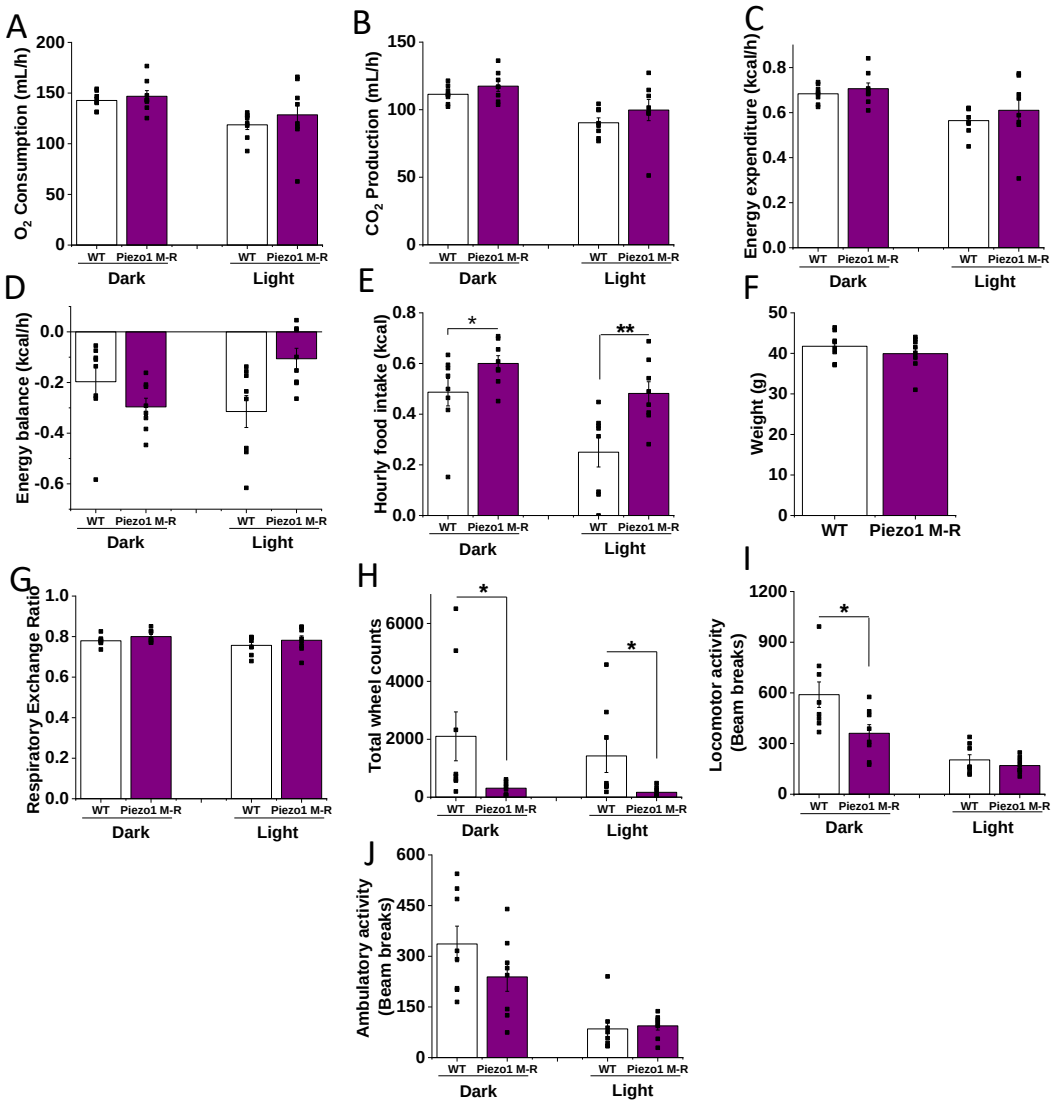

Figure 4-28 Indirect calorimetry for 22 week old Piezo1 M-R mice fed HFD. Mice were placed into individual cages in the Oxymax Comprehensive Laboratory Animal Monitoring System (CLAMs) with free access to a running wheel. Data taken for a 24 hour period following 24 hour acclimatisation. Results analysed by CalR web-based analysis software for CLAMs. Data are separated into dark and light periods. (A-E) Ancova analysis based on group and mass (F) effect. An interaction effect suggests group effect is also dependent on the mass effect (G-J) Anova analysis only as parameters not affected by mass. (A) Oxygen consumption, (B) Carbon dioxide production, (C) Energy expenditure, (D) Energy balance, (E) Average hourly food intake (Dark group p value= 0.0473, no interaction effect, Light group p value= 0.0067, interaction p value= 0.0091), (F) Body weight of mice, (G) Respiratory Exchange, (H) Total wheel counts (Dark p value= 0.0371, light p value= 0.0379), (I) Locomotor activity Ratio (Dark p value= 0.0173), (J) Ambulatory activity (n=8). * ($p<0.05$), ** ($p<0.01$), *** ($p<0.001$), **** ($p<0.0001$).

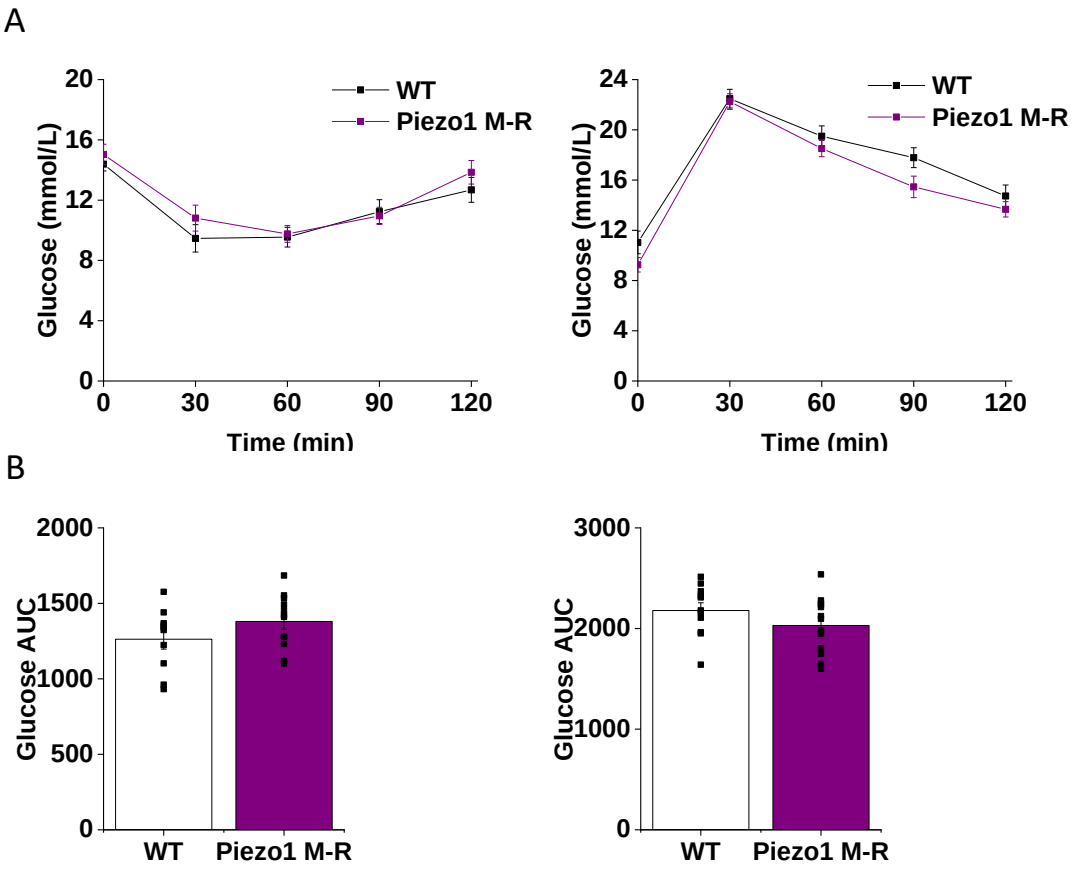

Figure 4-29 Insulin sensitivity is unchanged in Piezo1 M-R mice fed HFD. (A) Insulin tolerance test (left) and glucose tolerance test (right) results following 8 weeks HFD (n=11, WT; n=14, Piezo1 M-R). (B) Area under the curve for ITT (left) and GTT (right) shown in (A). Error bars indicated SEM.

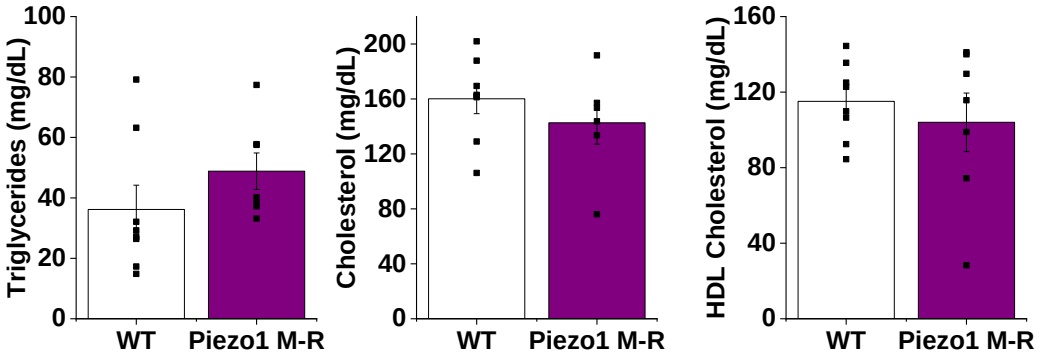

Figure 4-30 Plasma lipid levels are unchanged in Piezo1 M-R mice fed HFD. Plasma lipid concentrations of triglycerides (left), cholesterol (middle) and high-density lipoprotein cholesterol (HDL-Cholesterol) (right) in 8 week old mice (n=8, WT; n=7, Piezo1 M-R {n=6 total cholesterol}).

4.3 Discussion

This chapter has investigated cardiometabolic effects of global Piezo1 GOF due to Piezo1 M-R mutation. It has shown that although humans with the mutation only report signs of anaemia, that a vast array of other effects occur, as summarised in Table 4-4. Notably, a lipogenic phenotype is revealed in chow fed Piezo1 M-R mice, which correlates with a shift in energy utilisation towards fatty acids, ectopic fat deposition and strong trends for insulin resistance. When stressed with HFD, Piezo1 M-R mice seemed able to compensate and the increased lipogenic phenotype was likely masked by the vast increase in lipogenesis, induced by HFD intervention. However, HFD-fed Piezo1 M-R mice exhibited decreased physical activity, suggesting HFD-specific effects of Piezo1 M-R mutation.

Diet	**Age**	**Tissue**	**Result**	**Suggested Physiological Implication**
CD	8- week	Heart	↑ heart weight ↑ mRNA expression of *Myh7*	Mild cardiac hypertrophy
CD	22-week	Heart	↓ *Acta1* mRNA expression ↑ cardiac function	Improved cardiac performance
CD	8-week	eWAT	↑ eWAT mass	Increased fat deposition
CD	22-week	eWAT	↑ mRNA expression of lipogenic genes; *Dgat2, Cd36, Fas, Elovl6.*	Piezo1 M-R mice have a lipogenic disposition.
CD	22-week	Liver	↑ mRNA expression of *Fas*. ↑ liver mass. Evidence of ectopic fat deposition.	Piezo1 M-R mice have a lipogenic disposition.
CD	22-week	N/A	↓ RER	Increased use of fat as an energy source.
CD	8 and 16-week	N/A	Trends for ↓ insulin sensitivity	Metabolic dysfunction.
CD	22-week	Plasma	Dyslipidaemia; ↓ triglycerides and ↑ HDL-cholesterol	Increased triglyceride uptake into tissues.

HFD	22-week	Liver	↓ mRNA expression of *Cyp7a1*	Reduced production of bile salts and therefore poor dietary absorption.
HFD	22-week	N/A	↑ food intake, ↓ physical activity, but no resulting increase in body weight.	HFD-fed Piezo1 M-R mice have reduced physical capability and have to work harder to move.

Table 4-4 Summary of non-RBC differences observed in Piezo1 M-R mice.

The metabolic phenotype of CD-fed Piezo1 M-R mice was convincing with increased expression of genes involved in lipid synthesis within eWAT and liver; the major sites of *de novo* lipogenesis. This also correlated with whole-body measurements of metabolic function including a reduced RER and strong trends for insulin resistance. Typically with this adipogenic phenotype, plasma lipid levels would be expected to exhibit higher triglycerides (TGs) and lower HDL-cholesterol, however older Piezo1 M-R mice had the opposite dyslipidaemia, with favourable plasma lipid analysis. Interestingly, although this result did not match the emerging phenotype, mice with Piezo1 deleted from adipocytes, showed trends of increased TG levels, suggesting the channel may be important for plasma TG control (Zhao et al., 2019). Although Piezo1 M-R mice had reduced circulating TG levels, it is possible that excess TGs were being stored as ectopic fat depots instead. Experiments investigating this hypothesis remain preliminary, but evidence of lipid droplets were observed in livers of older Piezo1 M-R mice and increased mRNA expression of fatty acid transporter, *Cd36*, was apparent in eWAT, which would facilitate uptake of fat into tissues. Additionally, there was a trend for reduced *lipocalin 2* (*Lcn2*) in livers of 22-week old Piezo1 M-R mice and mice lacking *Lcn2* in hepatocytes have demonstrated lipid droplet accumulation (Borkham-Kamphorst et al., 2013).

The mechanism of how global Piezo1 GOF may cause a lipogenic phenotype remains unknown as the role of Piezo1 in metabolism is still being elucidated. The blanket overexpression of genes involved in lipid biogenesis suggest augmented activity of a transcriptional regulator. mRNA expression of the two main lipogenic transcription factors, *ChREBP* and *SREBP-1c*, was unchanged in

eWAT of Piezo1 M-R mice, however an activity assay would be needed before altered function of these regulators could be ruled out. How increased Piezo1 function may cause augmented transcriptional activity would need to be investigated, but interestingly both the activity of ChREBP and SBREP-1c have been shown to be modulated by Ca^{2+} suggesting direct modulation via Piezo1 may be possible (Leclerc et al., 2012, Noordeen et al., 2012, Wang et al., 2017). In fact, ChREBP and SBREP-1c target gene *FAS* is upregulated by increased intracellular Ca^{2+} and was upregulated in Piezo1 M-R mice in both adipose and hepatic tissue (Jones et al., 1996a). Indirect effects on transcriptional regulation may occur through augmented Piezo1 signal pathway activation, such as increased Akt phosphorylation (Han et al., 2019, Wang et al., 2016) which increases SREBP activity (Krycer et al., 2010).

Although clinically relevant, a drawback of using a global mouse model like Piezo1 M-R in elucidating Piezo1 function, is that it is difficult to determine the cellular origin of observed effects. Although seemingly unlikely due to the mild DHS clinical presentation, and metabolic changes in Piezo1 knockout studies, effects observed in Piezo1 M-R mice could be secondary to anaemia. It is possible the lipogenic phenotype revealed in this chapter is due to increased Piezo1 function in the adipocytes or hepatocytes themselves. In order to support this hypothesis, it would be necessary to demonstrate Piezo1 activity in these cells and show that the M-R mutation effects on channel gating are functionally relevant. Alternatively, the phenotype could occur due to increased Piezo1 function in one cell type, such as the endothelium, which then impacts other tissues. Ongoing work in our laboratory has demonstrated that mice lacking endothelial Piezo1 do show some metabolic effects that oppose the results observed due to Piezo1 M-R mutation, including reduced eWAT mass and increased insulin sensitivity, lending weight to this hypothesis. In practice, the phenotype is likely to occur due to a combination of altered Piezo1 function in a number of cells. Overall, the Piezo1 M-R mouse model can be used in combination with tissue specific knockout models, to help elucidate the role of Piezo1 in metabolism.

Despite this drawback, the phenotypic characterisation of Piezo1 M-R is highly important and relevant as the mutation is harboured in humans and so is directly relevant to human health. In this instance the elucidation of specific cellular

mechanisms underlying the phenotype become somewhat secondary to the discovery of altered physiology itself. The findings presented here have heightened relevance due to the high occurrence of similar, Piezo1 GOF mutations in 1/3 of the African population (Ma et al., 2018). It would be important to translate findings from the Piezo1 M-R mouse model back to humans with DHS and determine whether altered plasma lipid levels or insulin resistance are apparent in humans with Piezo1 GOF mutations. Interestingly, African Americans are at increased risk of many metabolic diseases including type II diabetes, obesity and cardiovascular disease compared to Caucasians (Cossrow and Falkner, 2004).

HFD intervention did not exacerbate the CD fed, lipogenic phenotype. In fact, HFD fed Piezo1 M-R mice were broadly similar to WT controls with no evidence of worsened metabolic syndrome. HFD feeding causes a huge stress on normal physiology and it is possible that the dramatic physiological changes incurred by the WT mouse were so strong, that effects of the mild, lipogenic phenotype of Piezo1 M-R was masked. Interestingly, HFD intervention itself does result in increased *Piezo1* expression as observed in eWAT of this study and of others (Zhao et al., 2019). Piezo1 has been shown to form domes in the plasma membrane which can facilitate sensing of lateral membrane tension (Lin et al., 2019). It is possible that increased cholesterol concentration due to HFD could cause stiffening of the membranes, increasing basal tension on the channel, so reducing Piezo1's sensitivity to force.

Expression of Piezo1 in eWAT of Piezo1 M-R mice fed HFD was reduced compared to WT mice, suggesting upregulation of the channel was not as pronounced. It is therefore possible that the GOF effects of Piezo1 M-R were compensated for on HFD due to reduced channel expression, facilitating similar ion flux to WT channels overall, despite fewer ion pores. Alternatively, the increased circulating lipids may in fact correct the altered channel gating observed due to Piezo1 M-R. Treatment of heterologously expressed Piezo1 M2225R with dietary fatty acids produced inactivation times comparable to the WT channel (Romero et al., 2019). In order to decipher whether HFD normalises Piezo1 M-R function, it would be necessary to isolate primary cells and measure electrophysiological properties by patch-clamp to determine the presence of any gating effect and overall effect on mediated current.

However, there were some differences observed with Piezo1 M-R mice fed HFD (Table 4-4). The finding of reduced physical activity was surprising considering a mild decrease in physical performance has been observed in an endothelial specific Piezo1 KO model (Rode et al., 2017) and Piezo1 has important roles in skeletal muscle formation (Tsuchiya et al., 2018), suggesting GOF would be advantageous for physical activity, if it had any effect at all. Interestingly, CD fed Piezo1 M-R mice had normal activity compared to WT mice, suggesting a specific effect of HFD on Piezo1 channel function in Piezo1 M-R, resulting in detrimental effects to physical performance. Not enough is known about the specific effects of excess lipids to Piezo1 function, nor the impact on gating in Piezo1 mutations, but the observations in this chapter suggest that studies investigating HFD on microvascular health supplying skeletal muscle in Piezo1 M-R mice, in addition to the composition of the skeletal muscles following HFD may be important.

In addition, HFD fed Piezo1 M-R mice had reduced hepatic *Cyp7a1* mRNA expression, which is the rate limiting enzyme for the synthesis of bile-acids, which are required for effective absorption of dietary fats (Table 4-4). It would be important to measure bile acid levels in the plasma of HFD-fed Piezo1 M-R mice to determine if levels were reduced, which could perhaps account for similar weight despite increased food intake. Further experiments are required to study the effect of HFD on Piezo1 channel function itself and then relate this to mutant channels.

Investigating the effect of Piezo1 M-R on cardiac gene expression and function resulted in the identification of phenotypic difference, but produced contradicting results, with no marked phenotype at 8-weeks, but increased cardiac function by 22 weeks (Table 4-4). Anaemia itself would be expected to have negative effects on cardiac function if any (Coats, 2004). It is possible the increase in cardiac function could reflect a compensatory state preceding decline, however the gene expression profile does not indicate this and in fact looks favourable with reduced inflammatory markers.

The role of Piezo1 in the heart was further investigated through specific knockout of the gene in cardiomyocytes using a CreMyh6-Piezo1$^{-/-}$ model. Here, a heart failure phenotype was observed at a genetic level, with trends of decreased function at 3 months. By 6 months, the gene expression profile strongly reflected that observed during heart failure. Although it is difficult to compare the two

models, it could be suggested that Piezo1 has an important role in the heart as genetic ablation appears distinctly negative, whereas channel GOF may provide indications of improved function.

Investigation of the role of genes specifically within cardiac myocytes has commonly used Cre expression driven by the Myh6 promoter, as it has proved to be highly effective and specific to cardiac myocytes (Agah et al., 1997). However, the model has come under scrutiny for producing cardiotoxicity in the absence of a floxed gene i.e. the presence of the Cre itself is damaging via off-target effects. 3 month old male Myh6-Cre controls with no floxed gene exhibited gene expression changes, notably an increase in *Anp* and *Bnp.* By 6 months *Myh7* and *Acta1* were also increased and a corresponding decrease in cardiac ejection fraction was observed, in addition to an increase in heart weight. Increases in fibrotic genes *Col1a1, Col3a1, Tnfα and Il-1b* were also noted (Pugach et al., 2015). More recently, the cardiotoxicity of Myh6-Cre has been clearly demonstrated showing complete lethality of Myh6-Cre controls at 11 months of age, with deaths beginning at 7 months due to dilated cardiomyopathy (Rehmani et al., 2019). Therefore, the use of Myh6-Cre mice of controls is recommended (Bhandary and Robbins, 2015).

However, cardiotoxicity of the model is not ubiquitous. In studies of experimental myocardial infarction or pressure overload models, Myh6-Cre positive, floxed-negative controls at 2-4 months age exhibited no negative effects on cardiac function compared to WT (Qi et al., 2014, Fan et al., 2016). Additionally, there have been reports of normal cardiac function up to 6 months (Sanz et al., 2019). The results presented in this chapter do fit with the gene expression profile of Myh6-Cre controls at 3 and 6 months of age, so it is difficult without appropriate controls to elucidate the significance of Piezo1 deletion. However, despite low sample sizes, trends have emerged for reduced cardiac function in Myh6-Cre Piezo1flx/flx mice at 3 months which has not been observed in studies of Myh6-Cre controls of the same age. Overall, coupled with the gene expression and functional changes observed in Piezo1 M-R mice, the results suggest that Piezo1 may have a role in correct functioning of the heart. Work is ongoing to repeat the experiments in Myh6-Cre controls, in addition to increasing the sample sizes in the existing functional experiments in 22-week old Piezo1 M-R mice and including echocardiography data of Myh6-Cre Piezo1 flx/flx mice at 6 months. The results

presented here present a strong case for further investigation of the role of Piezo1 in cardiac function.

4.4 Summary

Overall, the results from this chapter reveal for the first time that there are phenotypic effects of Piezo1 M-R mutation, in addition to DHS. The most striking finding is that Piezo1 M-R mice fed a chow diet exhibit a lipogenic disposition, with increased expression of genes involved in lipid synthesis and storage, early indications of ectopic fat deposition and insulin resistance. This is relevant due to the high occurrence of GOF Piezo1 mutations and reveals that additional disease predisposition may be present in patients with DHS. The work presented here strongly supports a role of Piezo1 in metabolism and will complement ongoing studies using knockout models. The lipogenic phenotype observed on chow diet was completely absent in Piezo1 M-R mice challenged with HFD. However, a different phenotype emerged showing a reduction in physical activity suggesting the gain of function effects on channel gating in Piezo1 M-R are affected differently by HFD. The initial phenotype presented here provides direction for areas that should be investigated in more depth, including cardiac effects of Piezo1 M-R, specific cellular effects of the mutation, effect of HFD on Piezo1 M-R channel gating and the involvement of signalling pathways in creating the observed physiological changes due to Piezo1 GOF.

Chapter 5 Improving Piezo1 Pharmacological Tools

5.1 Introduction

Piezo1 pharmacology is in its infancy. The first agonist of the channel, Yoda1 was identified in 2015 after a screen of 3.25 million compounds (Syeda et al., 2015). The discovery of Yoda1 has aided further Piezo1 studies, by facilitating chemical activation of the channel, without the need for mechanical activation which can be technically more challenging. However, Yoda1 does not have favourable drug-like properties and it has poor solubility which limits its use *in vitro.*

Chemical inhibitors of Piezo1 are limited to pore blockers of non-selective cationic channels, gadolinium chloride and ruthenium red, which are not specific to Piezo1 (Drew et al., 2002). The toxin GSMTx4 provides improved selectivity by only inhibiting mechanically-sensitive ion channels through interactions with the membrane but still does not offer complete specificity (Bae et al., 2011). Therefore, improved pharmacological tools with which to study Piezo1 are necessary.

The aim of this chapter was to address this problem and find improved chemical tools with activity against Piezo1. Analogues of Piezo1 agonist, Yoda1, were designed and synthesised by Kevin Cuthbertson; a PhD student in the School of Chemistry. Intracellular Ca^{2+} measurement assays were performed to examine whether the new compounds had activity against Piezo1 or could inhibit the Yoda1 response. Function of the Yoda1 analogues was confirmed in the endogenous channel and against a physiological response, using isometric tension recordings on murine vessels.

5.2 Results

5.2.1 Yoda1 is indeed a Piezo1 channel activator

In order to study the effects of the Yoda1 analogues on a reliable, overexpression system, human Piezo1 was incorporated into a HEK 293 T-REx™ system designed to stably express Piezo1 after induction with tetracycline. This cell line has been previously described by our group and will be referred to as Piezo1 T-REx cells (Rode et al., 2017). These cells showed Piezo1 protein (Figure 5-1A)

and mRNA (Figure 5-1B) expression after tetracycline induction. This expression was absent or very minimal in the native HEK T-REx cells, lacking the Piezo1 plasmid.

Next, intracellular Ca^{2+} entry in response to Piezo1 agonist Yoda1, was investigated in these cells using the FlexStation. No Ca^{2+} entry was observed in the native T-REx cells in response to 10 μM Yoda1, the highest concentration that can be used in the assay due to solubility limitations (Figure 5-1C). However, in the Piezo1 T-REx cells, concentration dependent increases in intracellular Ca^{2+} were observed upon Yoda1 application (Figure 5-1D). This result is in keeping with the literature that Yoda1 can cause increases in intracellular Ca^{2+} and is specific to Piezo1 activation (Syeda et al., 2015).

The potency of Yoda1 in the Piezo1 T-REx cells was investigated by performing concentration-effect curves, generating an EC_{50} value of 2.51 μM (Figure 5-2A). Solubility limitations, resulting in compound precipitation, prevented the plateau of the concentration-effect curve from being achieved, thus limiting accuracy of the EC_{50} value. This was compared to the EC_{50} value of Yoda1 in HUVECs which endogenously express Piezo1. The EC_{50} was lower at 0.23 μM suggesting that Yoda1 was more potent in these cells, although the order of magnitude remained similar (Figure 5-2B). Overall, these experiments provided a validation of the Piezo1 T-REx line for use in further studies of new Piezo1 pharmacological agents.

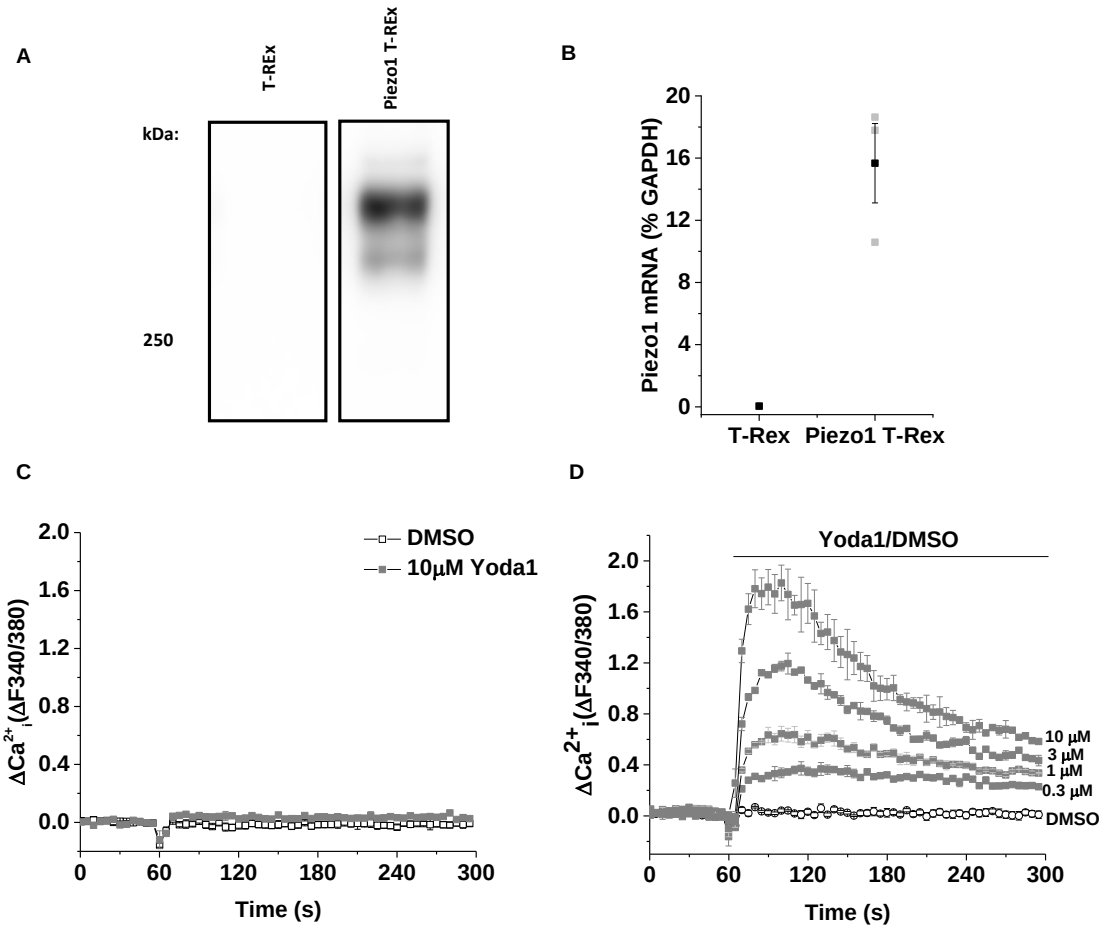

Figure 5-1 Yoda1 is indeed a Piezo1 channel activator. (A) Western blot of control T-REx and Piezo1 T-REx cells with anti-Piezo1 antibody, confirming Piezo1 expression (predicted size, 286 kDa). (B) Real-time PCR of Piezo1 mRNA levels relative to GAPDH mRNA in T-REx and Piezo1 T-REx cells. Error bars indicate SEM (n = 3). (C and D) FlexStation intracellular Ca^{2+} measurement data for T-REx cells (C) and Piezo1 T-REx (D) cells exposed to Yoda1 at the specified concentrations or exposed to the vehicle only (DMSO) (N=3, in-plate replicates).

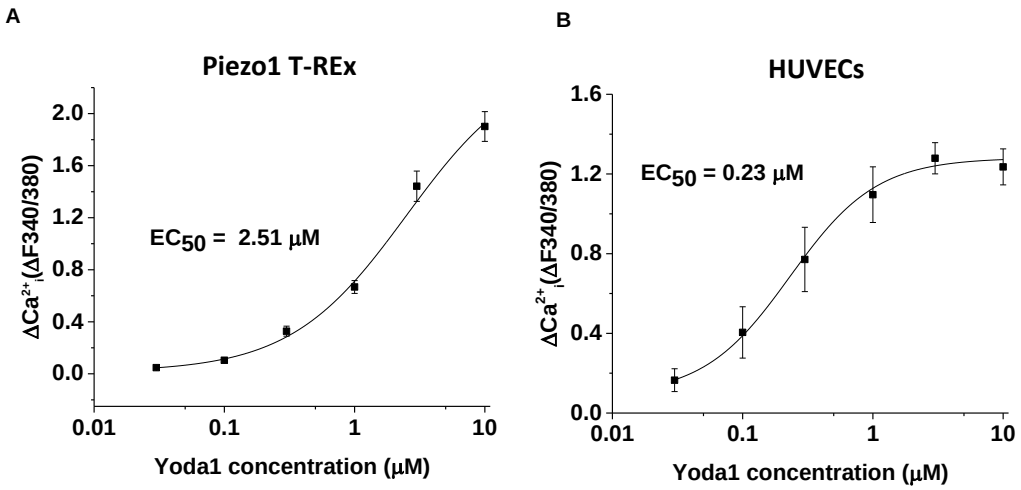

Figure 5-2 Yoda1 is more potent in HUVECs compared to Piezo1 T-REx cells. (A,B) Mean intracellular Ca^{2+} for Piezo1 T-REx cells (A) or HUVECs (B) exposed to the indicated concentrations of Yoda1. The fitted curve is the Hill equation with EC_{50} of 2.51 μM (A) and 0.23 μM (B) (n = 3).

5.2.2 The 2,6-Dichlorophenyl ring is important for Piezo1 activity

A series of Yoda1 analogues were generated by Kevin Cuthbertson using the scaffold-hopping approach, as described (Evans et al., 2018). The first series of compounds had modifications to the 2,6-Dichlorophenyl ring on the right-hand side of the Yoda1 structure (Figure 5-3A).

The analogues were screened at 10 µM for their ability to cause Ca^{2+} entry measured by the FlexStation, in comparison to the Ca^{2+} entry caused by the same concentration of Yoda1. Modifications to this ring on the Yoda1 structure were not tolerated and Ca^{2+} entry was lost, or nearly lost, in each of the compounds tested (Figure 5-3B, C). Compound **2g** exhibited the most Ca^{2+} entry out of all these compounds, but this still showed less than 30% of the Yoda1 response. **2g** was the most similar in structure to Yoda1, with one fluorine replacing one of the chlorines.

The same analogues were then tested for their ability to inhibit the Yoda1 response (Figure 5-4A). Each compound was incubated at 10 µM for 30 min prior to the FlexStation experiment, where 2 µM Yoda1 was applied in the continued presence of the analogue. Pre-treatment with these compounds did not affect the Yoda1 response, apart from compound **2g** which was able to cause 60% inhibition (Figure 5-4B,C). Taken together, these experiments suggest that the 2,6-dichlorophenyl moiety is essential for interaction with the Piezo1 channel and modifications to this ring are to be avoided in order to generate new pharmacological tools.

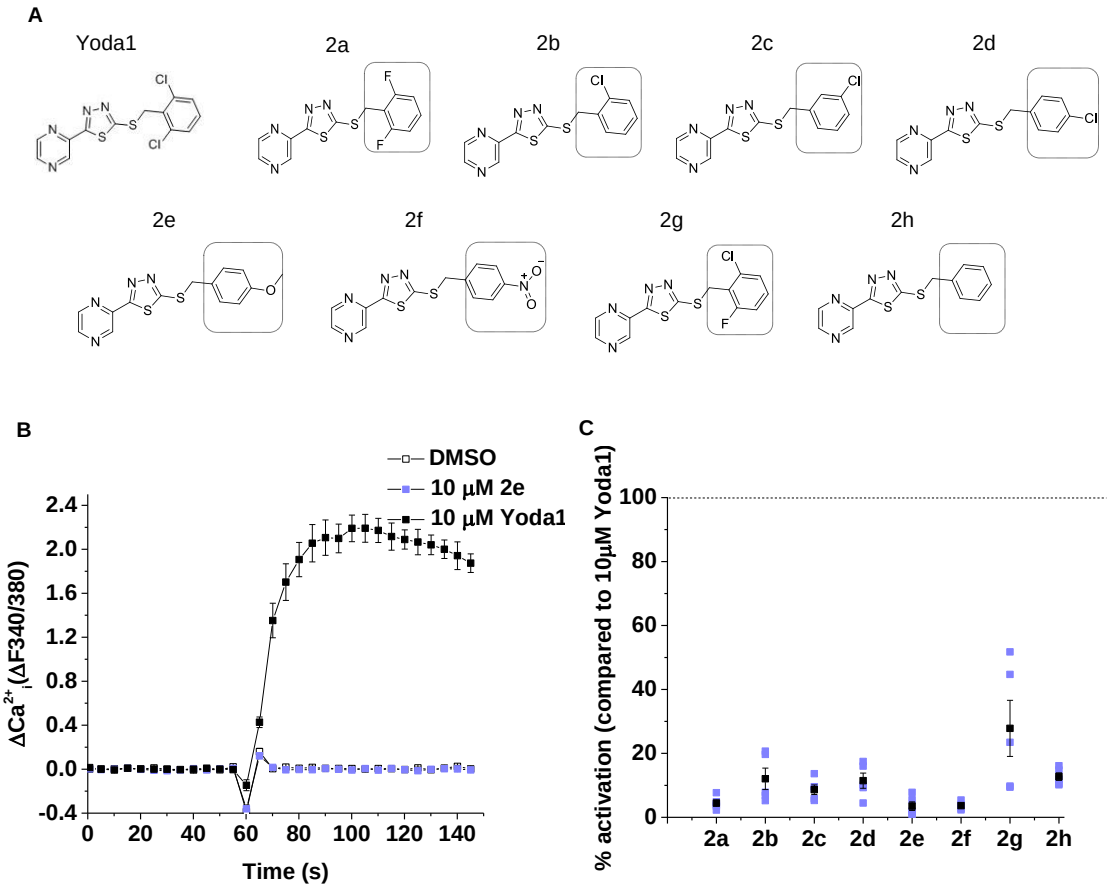

Figure 5-3 The 2,6-dichlorophenyl group of Yoda1 is required for activation of Piezo1. (A) Structures of Yoda1 and analogues. Structural variation to Yoda1 is highlighted by the box outline. (B) FlexStation intracellular Ca^{2+} measurement data for Piezo1 T-REx cells exposed to 10 µM **2e** or exposed to vehicle only (DMSO). Error bars indicate SEM (N = 3, in-plate replicates). (C) Summary for experiments of the type shown on the left measured between 40-60 s after Yoda1 analogue application, expressed as a % of the 10 µM Yoda1 response. Each data point represents a value from an independent experiment with mean values and error bars representing SEM indicated in black (n=5).

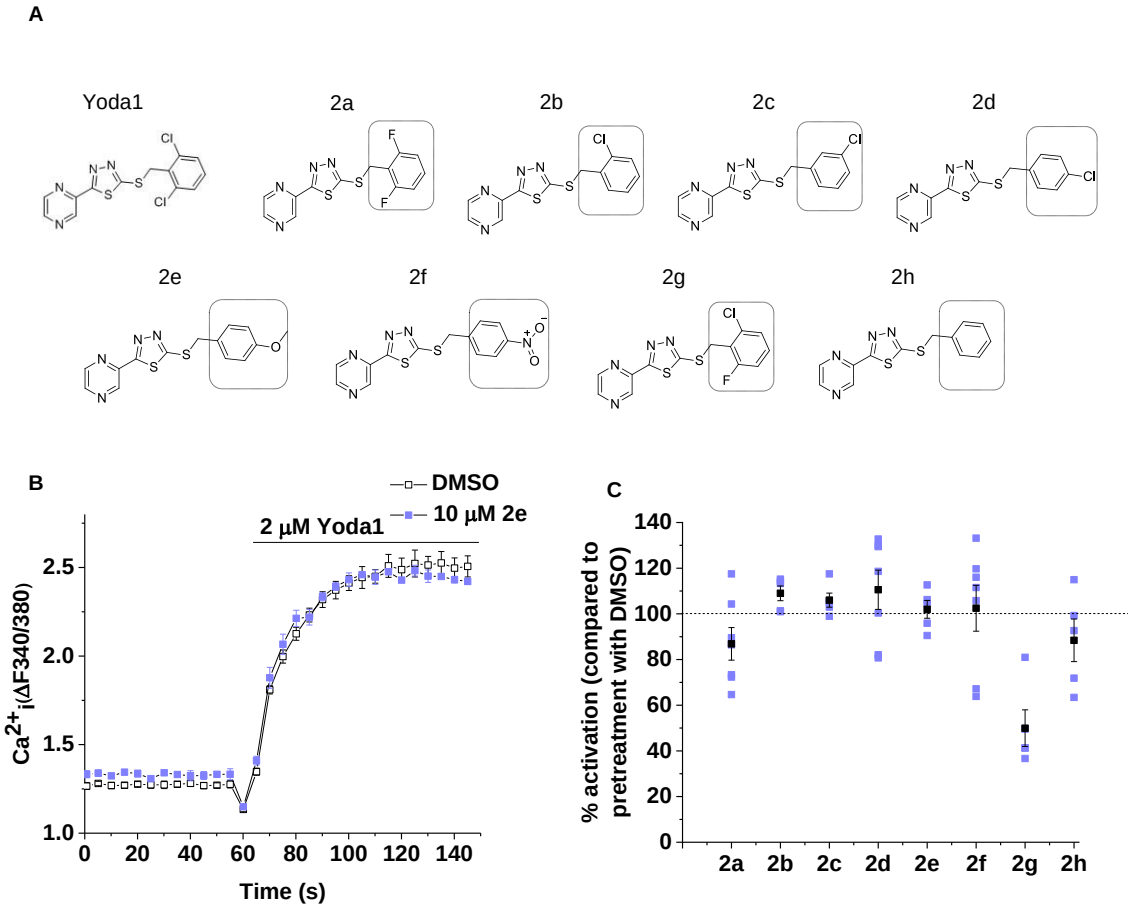

Figure 5-4 The 2,6-dichlorophenyl group of Yoda1 is required for interaction with the Piezo1 channel. (A) Structures of Yoda1 and analogues. Structural variation to Yoda1 is highlighted by the box outline. (B) FlexStation intracellular Ca^{2+} measurement data for Piezo1 T-REx cells exposed to 2 µM Yoda1 after pre-treatment with 10 µM **2e** or vehicle only (DMSO). Error bars indicate SEM (N = 3, in-plate replicates). (C) Summary for experiments of the type shown on the left, as for (F, right) except data are expressed as a % of the Yoda1 response when pre-treated with vehicle only (DMSO) (n=5; **2b**, **2c**, **2e**, **2g**, **2h**, n=7; **2a**, **2d**, **2f**).

5.2.3 Identification of a Yoda1 analogue which can antagonise Yoda1

To further explore the structure-activity relationship for Yoda1, analogues were synthesised with modifications to the pyrazine ring, on the left-hand ring of the Yoda1 structure (Figure 5-5A). They too were screened at 10 µM for their ability to cause Ca^{2+} entry in comparison to Yoda1. Generally, modifications to this ring were not tolerated and Ca^{2+} entry was lost (Figure 5-5B,C). Compound **7a** showed the most activity with 50% of the Yoda1 response and this was the most similar in structure to Yoda1 with a pyridine ring containing one nitrogen, rather than the pyrazine ring.

Next, compounds were made with structural changes to the thiadiazole group of Yoda1 and screened in the same way (Figure 5-6A). The thiadiazole was replaced with an oxadiazole with the aim of increasing compound solubility, if this modification could be tolerated. In general, this could be tolerated, and compound **11**, the most similar in structure to Yoda1 had ~70% activity (Figure 5-6B,C). Still, no compounds were identified that exhibited better activation properties than the existing Piezo1 agonist. These results suggest that activation of Piezo1 is dependent on tight structural requirements, but that successful compounds may be identified by alternative modifications to the pyrazine and thiadiazole rings.

These six compounds were then screened for their ability to inhibit the Yoda1 response, by pre-incubation for 30 min, followed by Yoda1 application (Figure 5-7A-G). All of the compounds were able to reduce the Yoda1 response (Figure 5-7G), most by as much as 50%. However, **2i** (Figure 5-7A) , **2j** (Figure 5-7B), **7a** (Figure 5-7D), **7b** (Figure 5-7E) and **11** (Figure 5-7F) also showed agonist activity as seen by the observed starting baseline Ca^{2+} signal, compared to pre-treatment with vehicle (DMSO) alone. On the other hand, compound **2k** inhibited the Yoda1 response, without any agonist activity (Figure 5-7C), shown by the identical starting baseline Ca^{2+} signal, compared to vehicle.

To investigate the effects of analogue **2k** further, concentration-effect curves were performed. **2k** was incubated for 30 min at a range of concentrations from 0.014 µM to 10 µM, before application of 2 µM Yoda1. A dose-dependent effect of **2k** was observed, with no effects on baseline Ca^{2+} signal, with an IC_{50} value of 1.30 µM (Figure 5-8A,B). The data suggest that **2k** could be a useful antagonist of Yoda1. We named the compound, Dooku1, in keeping with the Star Wars films.

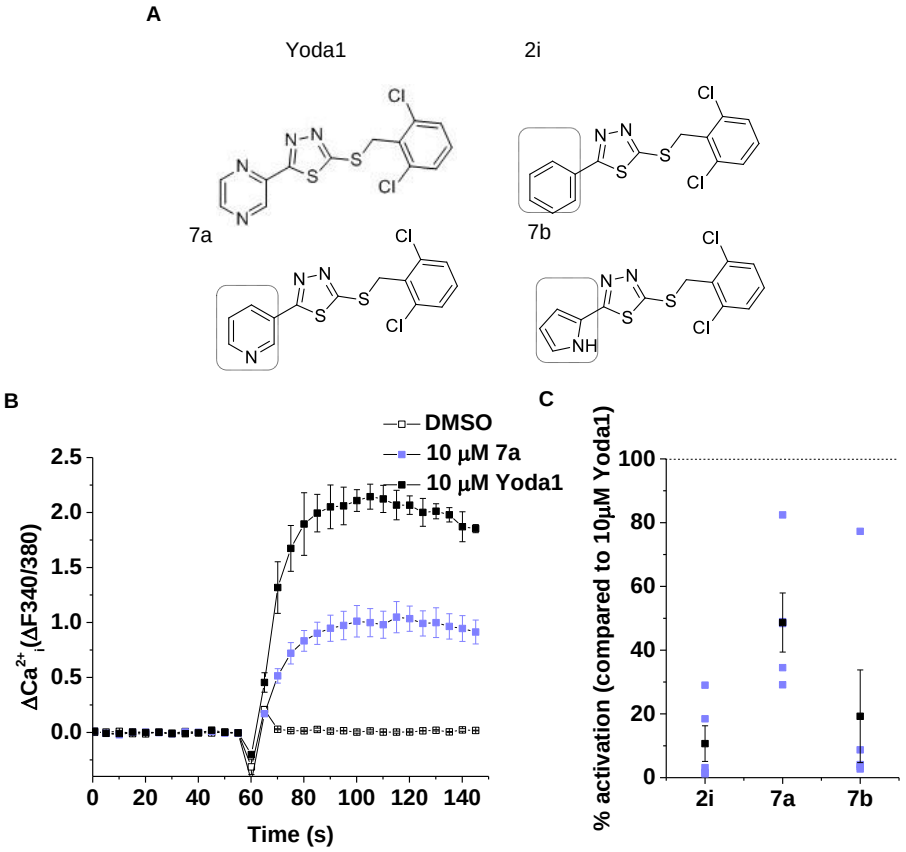

Figure 5-5. Changes to the pyrazine ring gives rise to less active analogues. (A) Structures of Yoda1 and analogues with changes to the pyrazine ring. Structural variation to Yoda1 is highlighted by the box outline. (B) FlexStation intracellular Ca^{2+} measurement data for Piezo1 T-REx cells exposed to 10 µM **7a** or exposed to vehicle only (DMSO). Error bars indicate SEM (N = 3, in-plate replicates). (C) Summary for experiments of the type shown in (B) measured between 40-60 s after Yoda1 analogue application, expressed as a % of the 10 µM Yoda1 response. Each data point represents a value from an independent experiment with mean values and error bars representing SEM indicated in black (n=5).

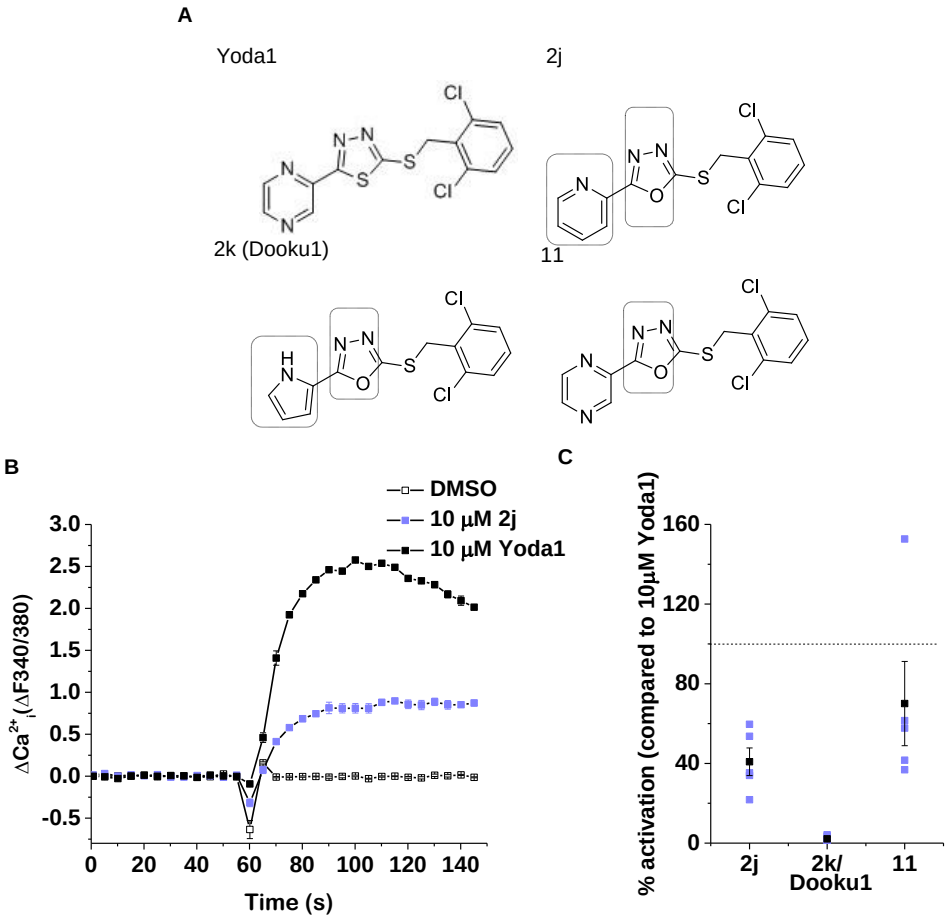

Figure 5-6 Replacing the thiadiazole with an oxadiazole give rise to less active analogues. (A) Structures of Yoda1 analogues with an oxadiazole. Structural variation to Yoda1 is highlighted by the box outline. (B) FlexStation intracellular Ca^{2+} measurement data for Piezo1 T-REx cells exposed to 10 µM **2j** or exposed to vehicle only (DMSO). Error bars indicate SEM (N = 3, in-plate replicates). (C) Summary for experiments of the type shown in (B) measured between 40-60 s after Yoda1 analogue application, expressed as a % of the 10 µM Yoda1 response. Each data point represents a value from an independent experiment with mean values and error bars representing SEM indicated in black (n=5).

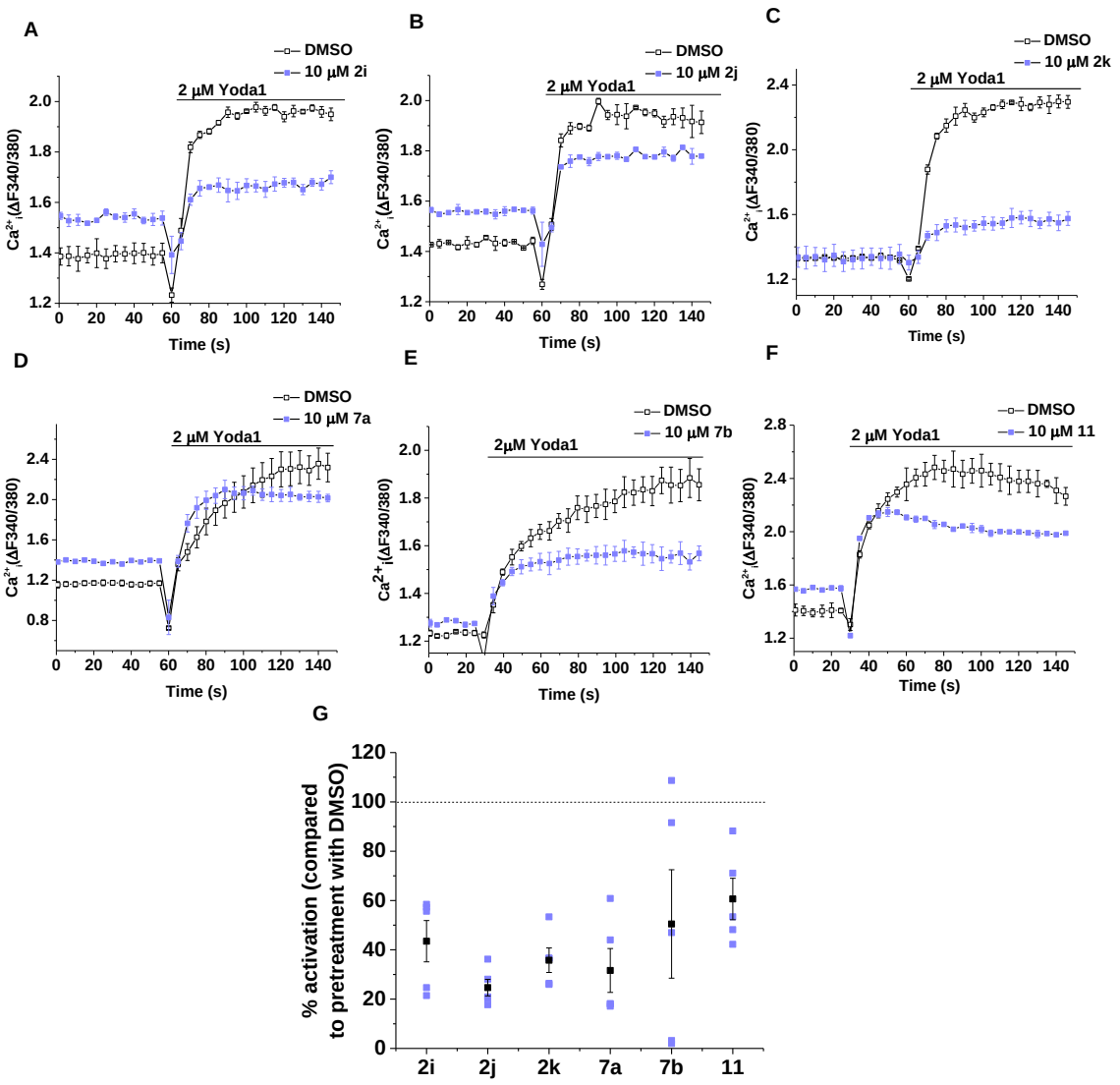

Figure 5-7 Yoda1 analogues are able to inhibit Yoda1-induced Piezo1 activity. (A-F) FlexStation intracellular Ca^{2+} measurement data for Piezo1 T-REx cells exposed to 2 μM Yoda1 after pre-treatment with 10 μM **2i** (A), **2j** (B), **2k** (C), **7a** (D), **7b** (E), **11** (F) or vehicle only (DMSO). Error bars indicate SEM (N = 3, in-plate replicates). (G) Summary for experiments of the type shown in (A-F) measured between 40-60 s after Yoda1 analogue application, expressed as a % of the Yoda1 response when pre-treated with vehicle only (DMSO). Each data point represents a value from an independent experiment with mean values and error bars representing SEM indicated in black (n=5).

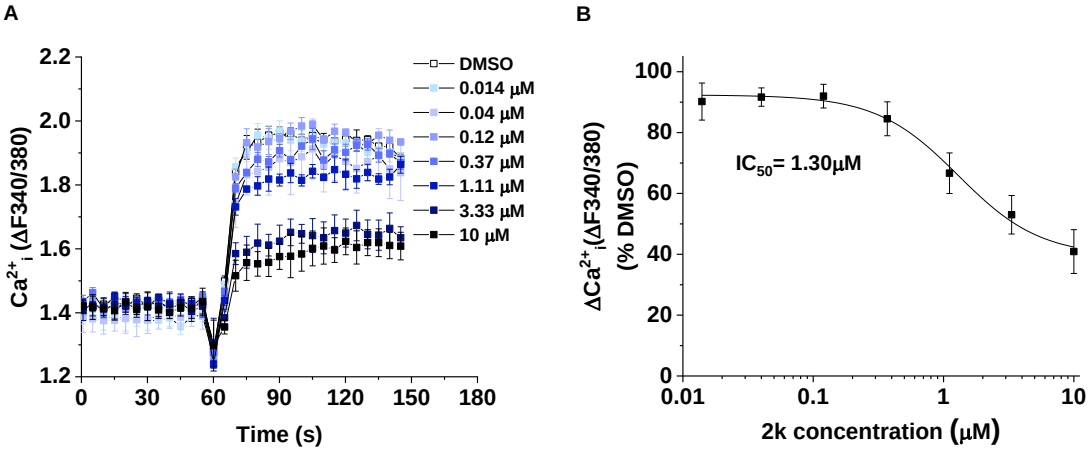

Figure 5-8 Dooku1 inhibits the Yoda1 response. (A) FlexStation intracellular Ca^{2+} measurement data for Piezo1 T-REx cells exposed to 2 µM Yoda1 after pre-treatment with indicted concentration of Dooku1 or vehicle only (DMSO). Error bars indicate SEM (N = 3, in-plate replicates). (B) Mean data for the type of experiment shown in (A) with cells pre-treated with indicated concentrations of **2k**. Expressed as a % of the Yoda1 response when pre-treated with vehicle only (DMSO). The fitted curve is the Hill equation with IC_{50} 1.30 µM (n = 5).

5.2.4 Yoda1 antagonism has tight structural requirements

In order to determine if it was possible to improve on Dooku1 activity, a selection of 8 compounds from internal and external libraries were selected based on their structural similarity to Dooku1 (Figure 5-9A). As with the Yoda1 analogues, they were screened for their ability to induce Ca^{2+} entry at 10 µM compared to 10 µM Yoda1 (Figure 5-9B). As expected due to their sequence similarity to Dooku1, none of the compounds had any agonist activity.

The inhibitory properties of the compounds were then investigated by pre-incubation at 10 µM for 30 min, followed by application of 2 µM Yoda1. Remarkably, only compound **8388-0189** had any Yoda1 inhibitory potential, reducing the Yoda1 response by 25%. All of the rest of the compounds had no effect or in fact seemed to potentiate the Yoda1 response. Many of the compounds did not have the 2,6-Dichlorophenyl ring which seems important for Piezo1 interaction so the lack of inhibitory effect of these compounds is perhaps expected. Compound **8388-0774** was the most structurally similar to Dooku1, however did not show inhibitory potential. The results suggest that as for Yoda1, Dooku1 activity has tight structural requirements.

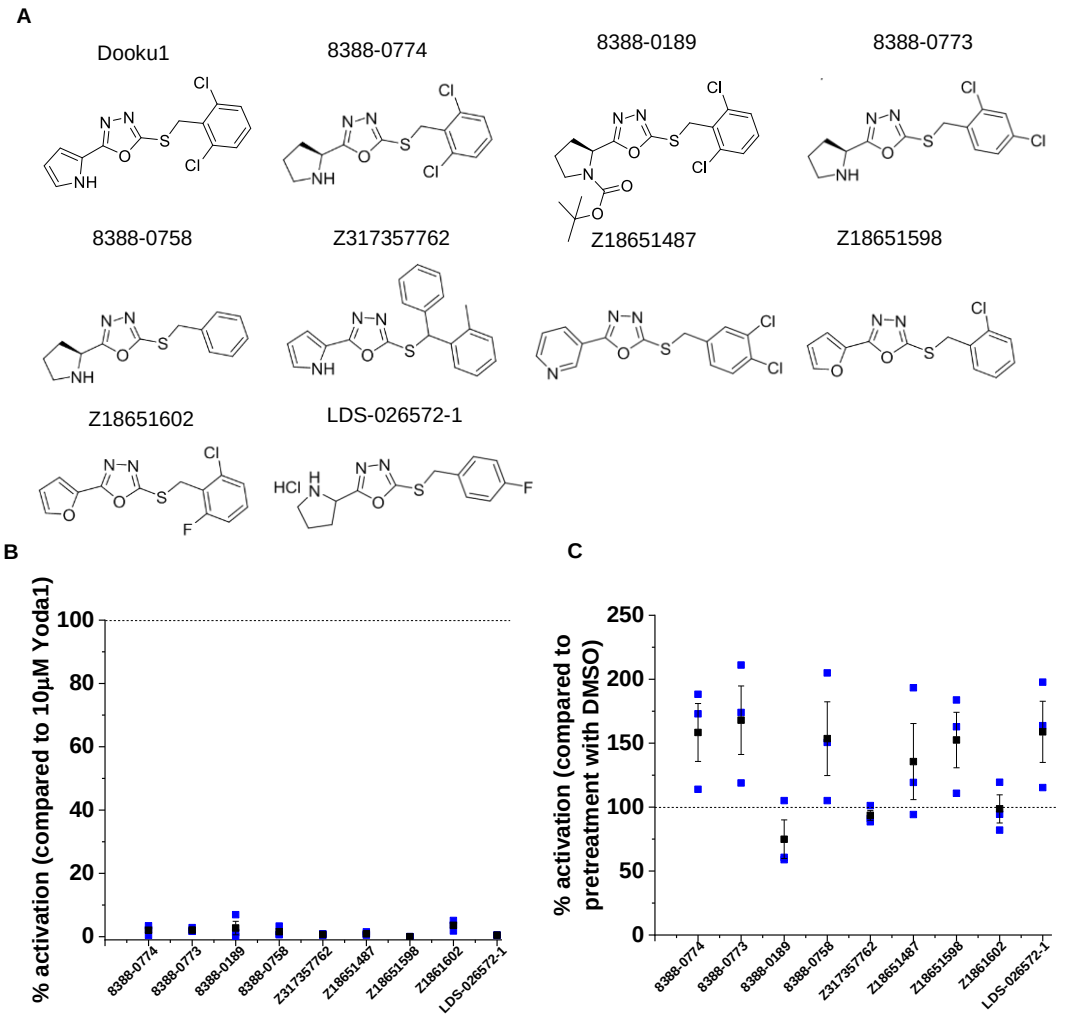

Figure 5-9 Dooku1-like compounds are unable to inhibit the Yoda1 response. (A) Structures of Dooku1-like compounds. (B) Summary of FlexStation intracellular Ca^{2+} data in Piezo1 T-REx cells measured between 40-60 s after Dooku1-like compound application, expressed as a % of the 10 µM Yoda1 response. Each data point represents a value from an independent experiment with mean values and error bars representing SEM indicated in black (n=3). (C) Summary of FlexStation intracellular Ca^{2+} measurement data for Piezo1 T-REx cells exposed to 2 µM Yoda1 after pre-treatment with 10 µM Dooku1-like compound. Measured between 40-60 s after Yoda1 application, expressed as a % of the Yoda1 response when pre-treated with vehicle only (DMSO). Each data point represents a value from an independent experiment with mean values and error bars representing SEM indicated in black (n=3).

5.2.5 Dooku1 effects are reversible

Based on the structural similarity of Yoda1 and Dooku1, it is likely that they interact with the same binding site on Piezo1. The effects of Yoda1 are reversible, which is a property shared by compounds which elicit effects by non-covalent binding to an extracellular site. To determine whether the effect of Dooku1 was also reversible, a washout assay was performed using the FlexStation. All wells were treated with 10 µM Dooku1 for 30 min, after which half the wells were washed out, whereas in the remaining wells, Dooku1 was maintained for the duration of the experiment. 2 µM Yoda1 was added during the FlexStation recording.

In agreement with previous experiments, treatment with Dooku1 inhibited the Yoda1 response by ~50% (Figure 5-10A-E, purple traces). A significant reduction in this inhibitory effect was observed in the washout condition as early as 1 min following washing, as the inhibitory action of Dooku1 was reduced to ~25% (Figure 5-10A). Following 4 min of washout, the level of inhibition was further reduced to less than 20% (Figure 5-10B) and this Ca^{2+} entry signal remained similar following 7 (Figure 5-10C) and 10 min washout (Figure 5-10D). This suggests a rapid, almost complete washout of Dooku1 after 1 min, suggesting it binds extracellularly, which is also predicted for Yoda1.

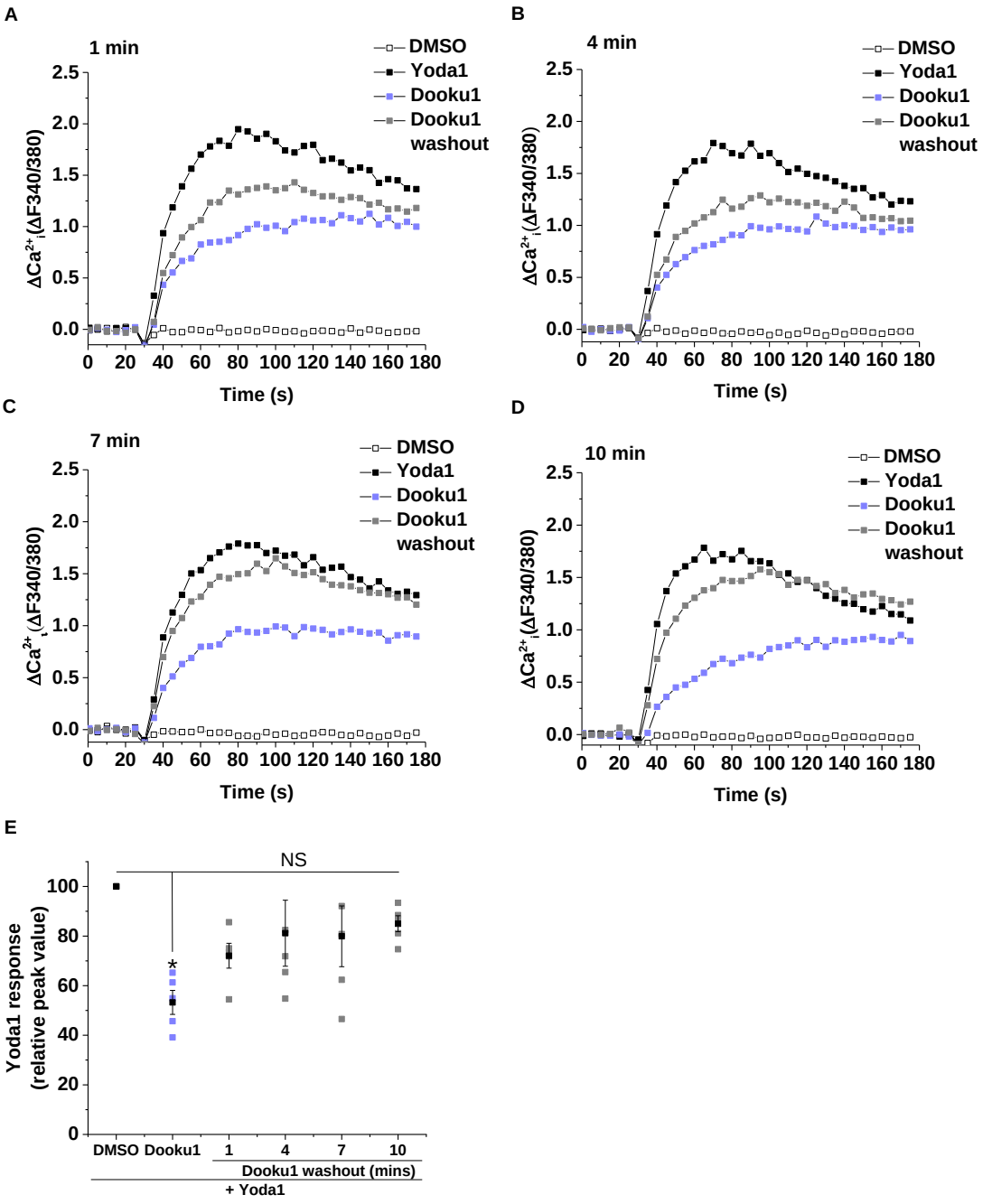

Figure 5-10 The inhibition by Dooku1 is reversible. (A-D) FlexStation intracellular Ca^{2+} measurement data for Piezo1 T-REx cells exposed to 2 μM Yoda1 after pre-treatment with 10 μM Dooku1 or vehicle only (DMSO), showing Yoda1 response after Dooku1 was washed out for 1 (A), 4 (B), 7 (C) or 10 (D) minutes prior to recording. Error bars indicate SEM (N = 3, in-plate replicates). (E) Summary for experiments of the type shown in (A-D) measured between 40-60 s after Yoda1 application, expressed as a % of the Yoda1 response when pre-treated with vehicle only (DMSO). Each data point represents a value from an independent experiment with mean values and error bars representing SEM indicated in black (n=5). * (p<0.05), ** (p<0.01), *** (p<0.001), **** (p<0.0001).

5.2.6 Dooku1 effects are not temperature dependent

For potential use of Dooku1 in *ex vivo* experiments, it is important to investigate whether its inhibitory effects can be modulated by temperature, which could affect solubility or binding of the compound. As such, the effect of Dooku1 was compared on the FlexStation at the usual room temperature (24°C) setting, compared to body temperature (37°C) which is typically used in physiological experiments.

Cells were pre-incubated with Dooku1 for 30 min, prior to exposure to 2 μM Yoda1 at RT or 37°C. Dooku1 effectively inhibited the Yoda1 response at both temperatures to a similar degree, by ~60% (Figure 5-11A-C). The shape of the Yoda1 trace appeared to be effected by temperature, with a much slower peak achieved at RT which was well sustained throughout the recording (Figure 5-11A), as opposed to 37°C in which the peak was achieved rapidly, however decayed (Figure 5-11C). The peak Ca^{2+} signal induced by Yoda1 was also increased at a higher recording temperature (ΔF340/380 1.5 vs 1.1) (Figure 5-11D). The data suggests that the Yoda1 response is affected by temperature, but that Dooku1 is still able to inhibit this response to a similar degree.

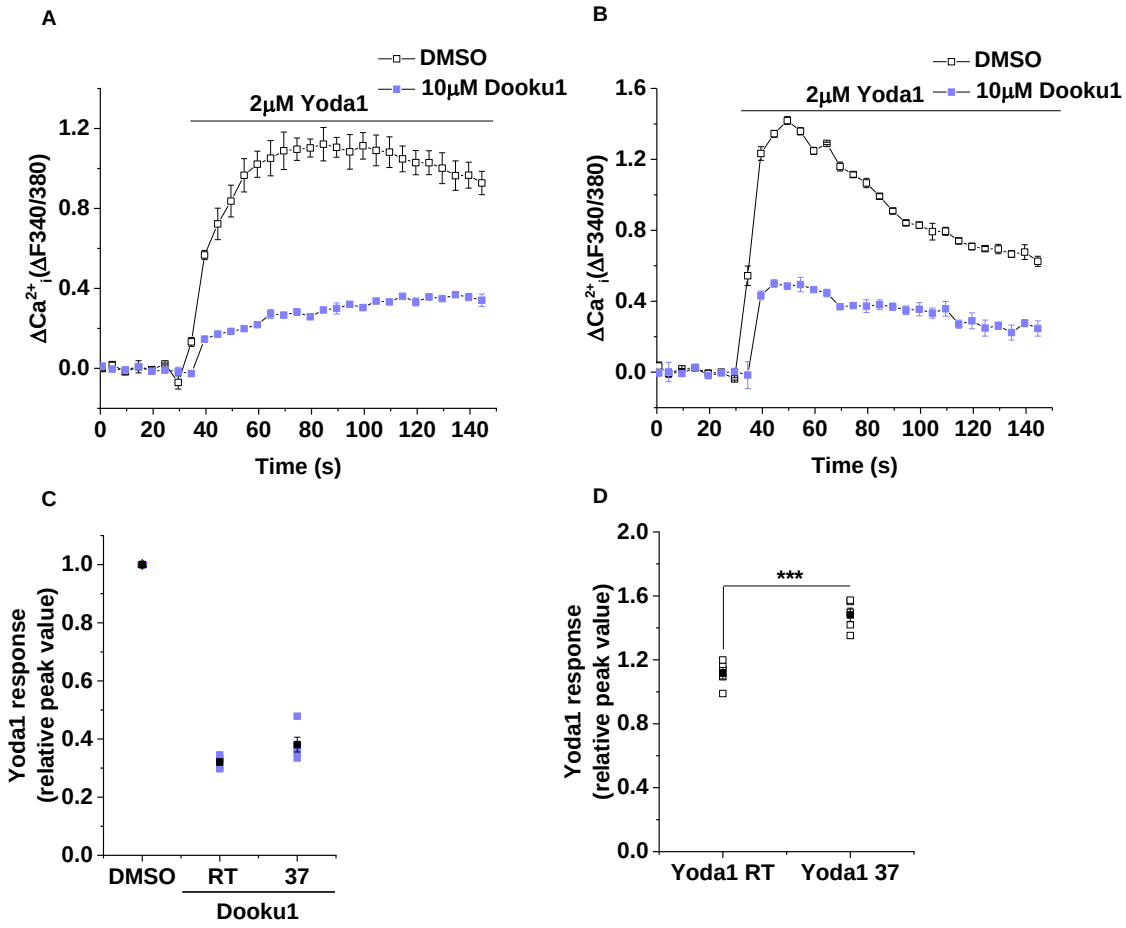

Figure 5-11 The inhibition by Dooku1 is not temperature dependent. (A-B) FlexStation intracellular Ca^{2+} measurement data for Piezo1 T-REx cells exposed to 2 μM Yoda1 after pre-treatment with 10 μM Dooku1 or vehicle only (DMSO) at room temperature (RT) (A) or 37°C (B). Error bars indicate SEM (N = 3, in-plate replicates). (C) Summary for experiments of the type shown in (A, B) measured between 40-60 s after Yoda1 application, expressed as a % of the Yoda1 response when pre-treated with vehicle only (DMSO). Each data point represents a value from an independent experiment with mean values and error bars representing SEM indicated in black (n=5). (D) As for (C) but the raw ΔF340/380 value for the peak Yoda1 response at the two temperatures (n=5). * ($p<0.05$), ** ($p<0.01$), *** ($p<0.001$), **** ($p<0.0001$).

5.2.7 Dooku1 has selectivity for Piezo1

To investigate the selectivity of Dooku1 for Yoda1 antagonist activity, the effect of 30 min pre-treatment of 10 µM Dooku1 was first measured in native HEK 293 cells against response to ATP or store-operated Ca^{2+} entry. Pre-treatment with Dooku1 had no effect on the response to 20 µM ATP (Figure 5-12A). Store-operated Ca^{2+} entry was measured by recording the Ca^{2+} addback response, following depletion of intracellular calcium stores by 30 min pre-treatment with 2 µM thapsigargin. Dooku1 had no effect against this response (Figure 5-12B).

The selectivity of Dooku1 was then investigated against agonist responses in various TRP channels; TRPV4, TRPC4 and TRPC5. 10 µM Dooku1 had no effect on the activity of 5 µM 4α-PDD in TRPV4 channels overexpressed in CHO cells (Figure 5-13A). Neither did 10 µM Dooku1 impact the activation of TRPC4 (Figure 5-13B) or TRPC5 (Figure 5-13C) channels by 100 nM or 10 nM (-)- Englerin A (EA) respectively. The data suggest that the activity of Dooku1 is selective for the Yoda1-induced response through Piezo1 channels.

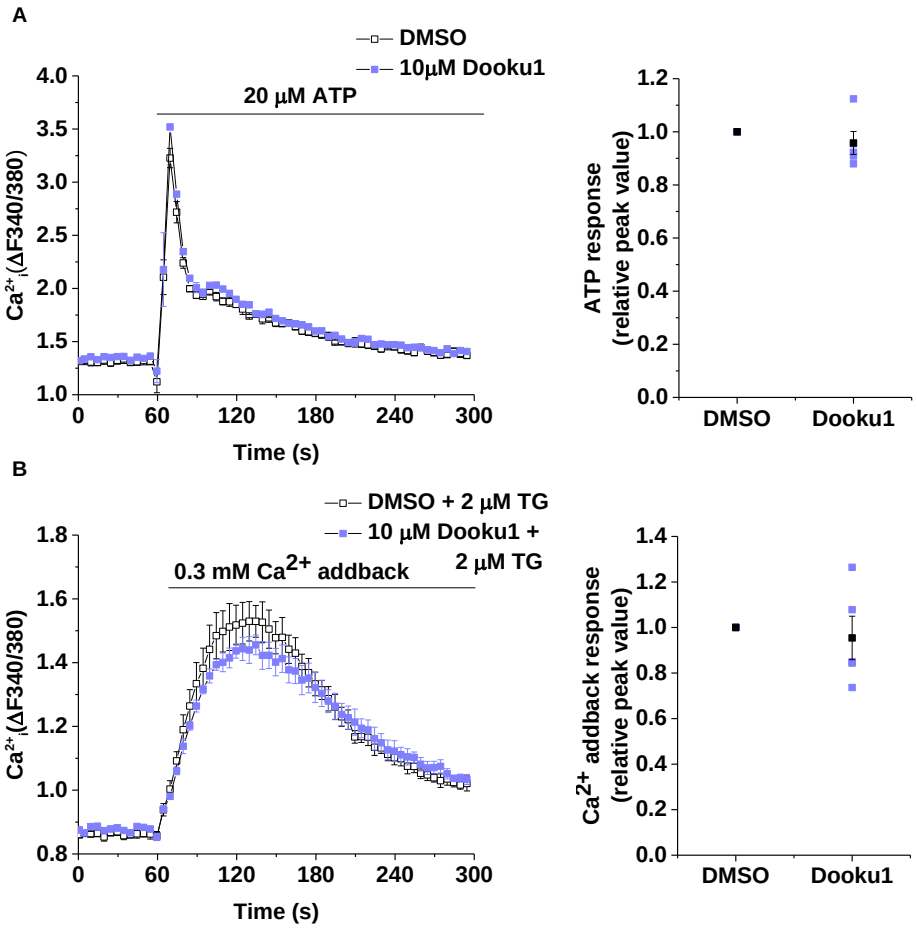

Figure 5-12 The inhibition by Dooku1 does not affect ATP response or store-operated Ca^{2+} entry. Experiments conducted in native HEK 293 cells. Intracellular Ca^{2+} measurement data for cells exposed to 20 μM ATP (A) or 0.3 mM Ca^{2+} addback (B) following pre-treatment with DMSO or 10 μM Dooku1 (left). Error bars indicate SEM (N = 3, in-plate replicates). Summary for experiments of the type shown on the left measured between 10-30s (A), 60-90s (B) after treatment application and normalised to the peak amplitude values for the vehicle only (DMSO) pre-treatment condition (right). Each data point represents a value from an independent experiment with mean values and error bars representing SEM indicated in black (n=5).

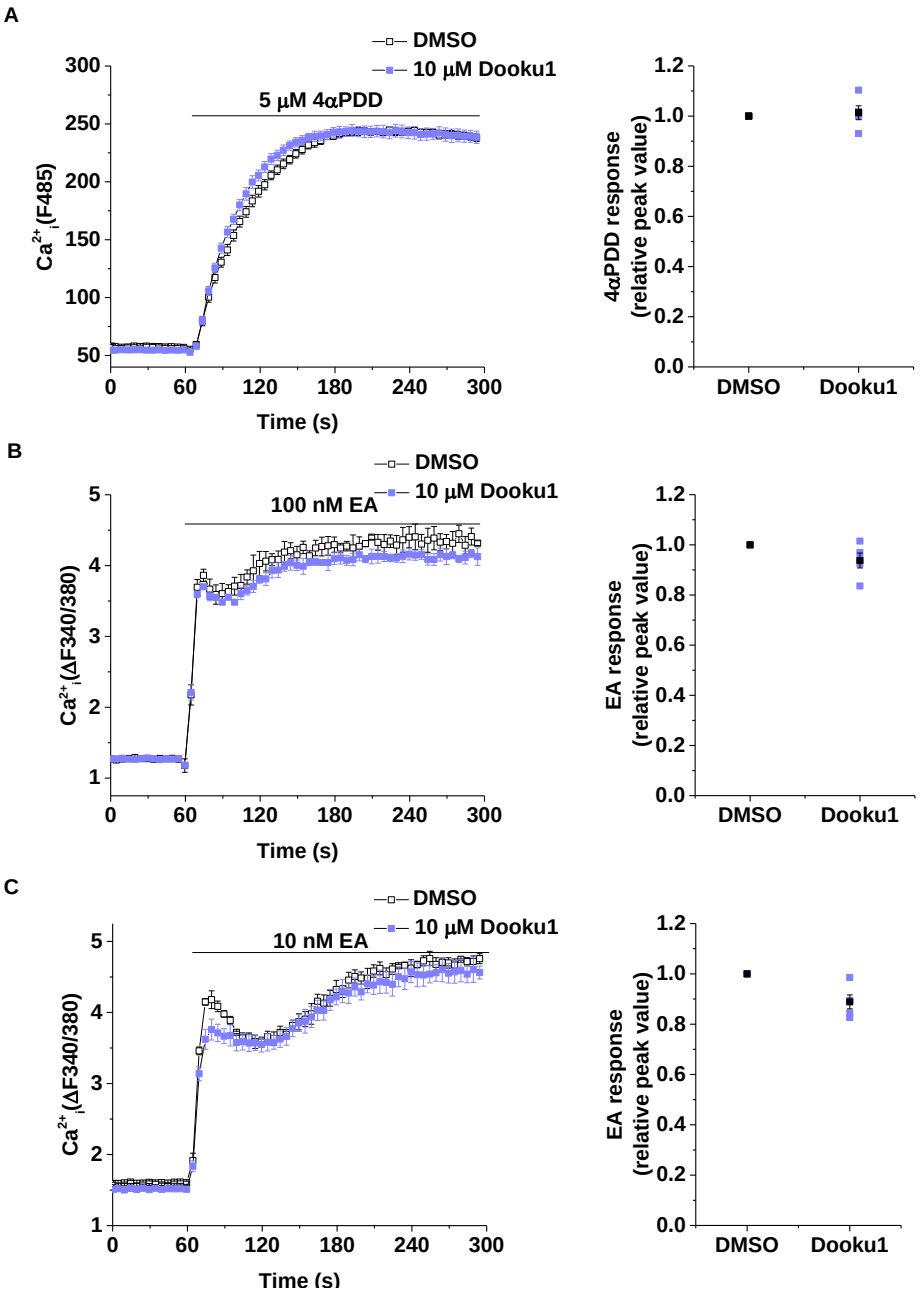

Figure 5-13 The inhibition by Dooku1 does not affect TRP channels. Ca^{2+} indicator dyes were fluo-4 (A) or fura-2 (B, C). Experiments conducted in CHO cells overexpressing TRPV4 (A) or HEK 293 cells overexpressing TRPC4 (B) or TRPC5 (C). Intracellular Ca^{2+} measurement data for cells exposed to 5 μM 4α-phorbol 12,13-didecanoate (4α-PDD) (A),100 nM (B) or 10 nM (C) (-)-Englerin A (EA) following pre-treatment with DMSO or 10 μM Dooku1 (left). Error bars indicate SEM (N = 3, in-plate replicates). Summary for experiments of the type shown on the left measured between 220-240s (A) or 20-60s (B, C) after treatment application and normalised to the peak amplitude values for the vehicle only (DMSO) pre-treatment condition (right). Each data point represents a value from an independent experiment with mean values and error bars representing SEM indicated in black (n=5).

5.2.8 Dooku1 does not affect constitutive Piezo1 activity

To investigate whether Dooku1 can affect the activity of Piezo1, independently of Yoda1, constitutive activity that has been shown to occur in the Piezo1 T-REx cells was recorded (Rode et al., 2017). This constitutive activity is measured by using thallium (Tl^+) sensitive FluxOR™ indicator dye, whereby the entry of Tl^+ ions acts as a surrogate for Na^+ ion entry. Cells are maintained in a Tl^+ ion free solution, until 2 µM Tl^+ is added to the cells 30s into the recording and the resulting intracellular Tl^+ can be detected and recorded by the FlexStation.

This assay measures total cation entry into the cell and is not specific to Piezo1 channel activity. To ensure that constitutive Piezo1 activity was being represented by this method, the Tl^+ entry was compared between Piezo1 T-REx cells induced with tetracycline (Tet+) and Piezo1 T-REx cells where Piezo1 expression was not induced (Tet-) (Figure 5-14A,B). The rate of Tl^+ entry was nearly doubled in the Tet+ cells demonstrating that activity of Piezo1 was being measured by the assay.

Next Tet+ Piezo1 T-REx cells were pre-treated with 10 µM Dooku1 for 30 min, prior to the addition of Tl^+. Incubation with Dooku1 did not affect Tl^+ ion entry compared to vehicle (DMSO) control as shown by comparing the DMSO and Dooku1+DMSO data (Figure 5-14C,D). On the other hand, application of 5 µM Yoda1 in addition to Tl^+ caused a doubling of the Tl^+ entry and this could be reduced by pre-treatment by Dooku1, confirming in an alternative assay to intracellular Ca^{2+} measurement by Fura-2 dye, that Dooku1 can inhibit the Yoda1 response. This can be observed by comparing the Yoda1 and Dooku1+Yoda1 data. These results demonstrate that Dooku1 does not affect constitutive Piezo1 channel activity and that its effect depends on the presence of Yoda1.

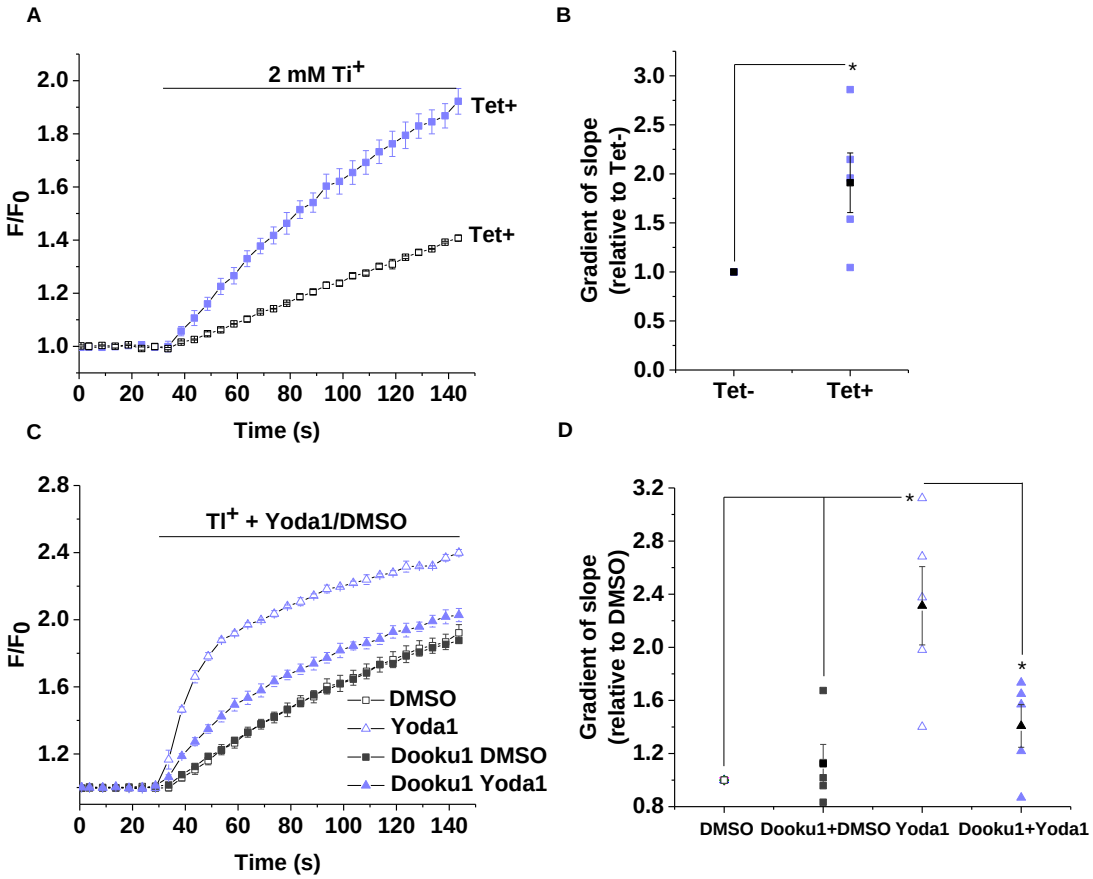

Figure 5-14 Dooku1 does not affect Piezo1 constitutive activity. (A) Intracellular Tl^+ measurement data using FluxOR for Tet+ Piezo1 T-REx cells or control Tet- cells exposed to extracellular Tl^+. The FluxOR measurements are displayed as the fluorescence intensity (F) divided by the initial fluorescence intensity (F_0). Error bars indicate SEM (N = 3, in-plate replicates). (B) Summary for experiments of the type shown in (A) measured between 0-30 s after Tl^+ application, normalised to rate of change of F in the Tet- response. Each data point represents a value from an independent experiment with mean values and error bars representing SEM indicated in black (n=5). (C) Intracellular Tl^+ measurement data for Tet+ Piezo1 T-REx cells exposed to extracellular Tl^+ and 5 μM Yoda1 or vehicle (DMSO), following pre-treatment with 10 μM Dooku1 or vehicle only (DMSO). Error bars indicate SEM (N = 3, in-plate replicates). (D) Summary for experiments of the type shown in (C), as for (B) except data are normalised to the rate of change of the vehicle only (DMSO) control condition (n = 5). * ($p<0.05$), ** ($p<0.01$), *** ($p<0.001$), **** ($p<0.0001$).

5.2.9 Dooku1 inhibits endogenous Yoda1-activated Piezo1 channels

The data presented so far demonstrates the activity of Dooku1 against the Yoda1 response in an overexpressed Piezo1 channel. To determine whether Dooku1 had a similar effect on endogenous Piezo1 channels, the effect of Dooku1 against the Yoda1 response in HUVECs was investigated. Similar to the Piezo1 T-REx cells, application of 10 µM Dooku1 alone was unable to produce an increase in intracellular Ca^{2+} (Figure 5-15A). Pre-treatment with 10 µM Dooku1 for 30 min was able to reduce the response to 2 µM Yoda1 by ~40% (Figure 5-15B,C). Dooku1 exhibited a concentration-dependent inhibitory affect against the Yoda1 response with an IC_{50} value of 1.49 µM (Figure 5-15D). This was comparable to the IC_{50} value observed in Piezo1 T-REx cells (1.30 µM), however the maximum inhibition in HUVECs was less. These data suggest that Dooku1 can also antagonise Yoda1-induced responses in the endogenous Piezo1 channel in endothelial cells.

To investigate whether the effect of Dooku1 could be relevant in a physiological response, isometric tension recordings were made from mouse thoracic aortic rings by Dr Naima Endesh (University of Leeds). After pre-constriction with 0.3 µM phenylephrine (PE), an agonist of α1-adrenoreceptors, the vessels were exposed to 5 µM Yoda1 which caused aortic relaxation (Figure 5-16A). It has been shown by our group that Yoda1 can cause dose-dependent relaxation in these vessels which is mediated by an intact endothelium and nitric oxide (Evans et al., 2018). Pre-treatment with 10 µM Dooku1 for 20 min was able to completely abolish Yoda1-induced relaxation (Figure 5-16B,C). The data suggest that Dooku1 can strongly-inhibit Yoda1-induced relaxation in mouse thoracic aorta by disrupting Yoda1 activity against the Piezo1 channel.

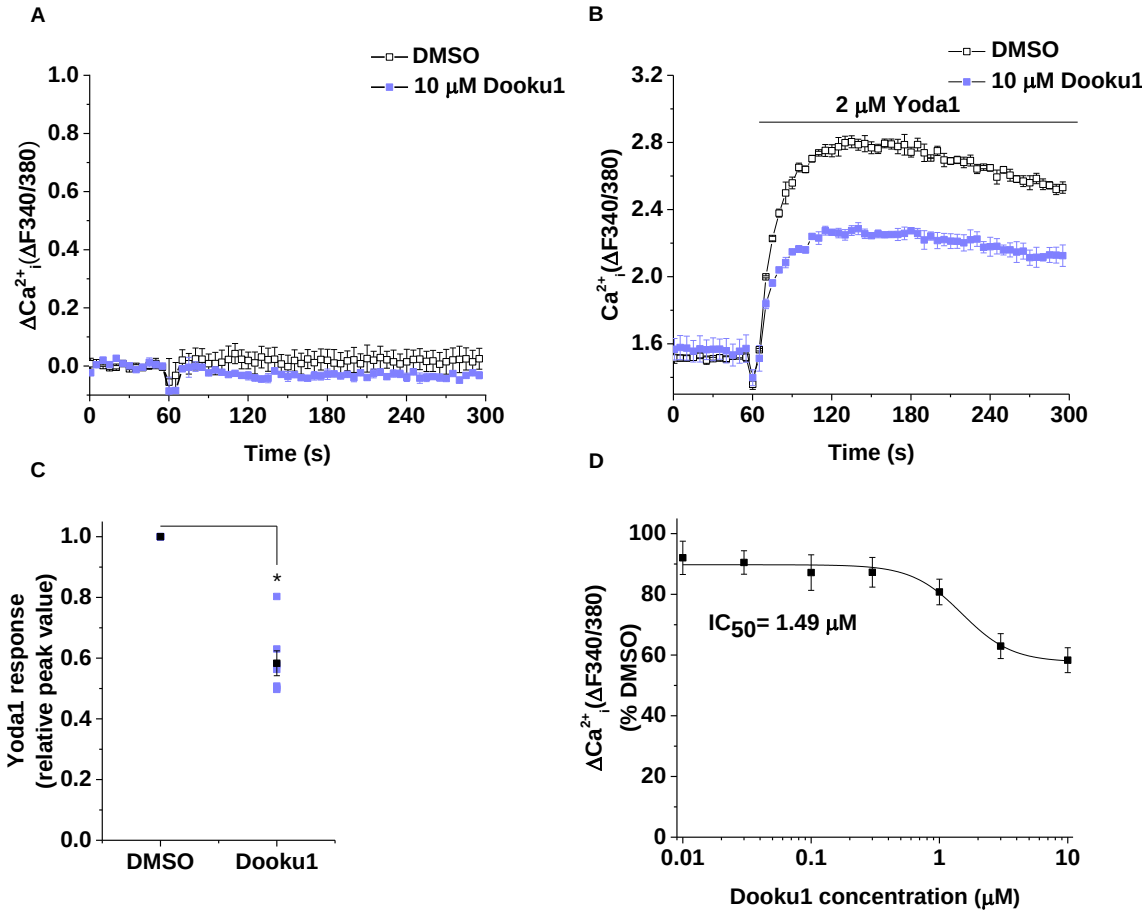

Figure 5-15 Dooku1 is effective against the endogenous Piezo1 channel. (A) Intracellular Ca^{2+} measurement data in HUVECs after exposure to 10 µM Dooku1 or vehicle only (DMSO). Error bars indicate SEM (N = 3, in-plate replicates). (B) Intracellular Ca^{2+} measurement data in HUVECs after exposure to 2 µM Yoda1 after pre-treatment with 10 µM Dooku1 or vehicle only (DMSO). Error bars indicate SEM (N = 3, in-plate replicates). (C) Summary for experiments of the type shown in (B) measured 40-60s after Yoda1 application and normalised to peak amplitudes for the vehicle only group. Each data point represents a value from an independent experiment with mean values and error bars representing SEM indicated in black (n=7). (D) Mean data for the type of experiment shown in (B) with cells pre-treated with indicated concentrations of Dooku1. Data are expressed as a % of the Yoda1 response when pre-treated with vehicle only (DMSO). The fitted curve is the Hill equation with IC_{50} 1.30 µM (n = 5). * ($p<0.05$), ** ($p<0.01$), *** ($p<0.001$), **** ($p<0.0001$).

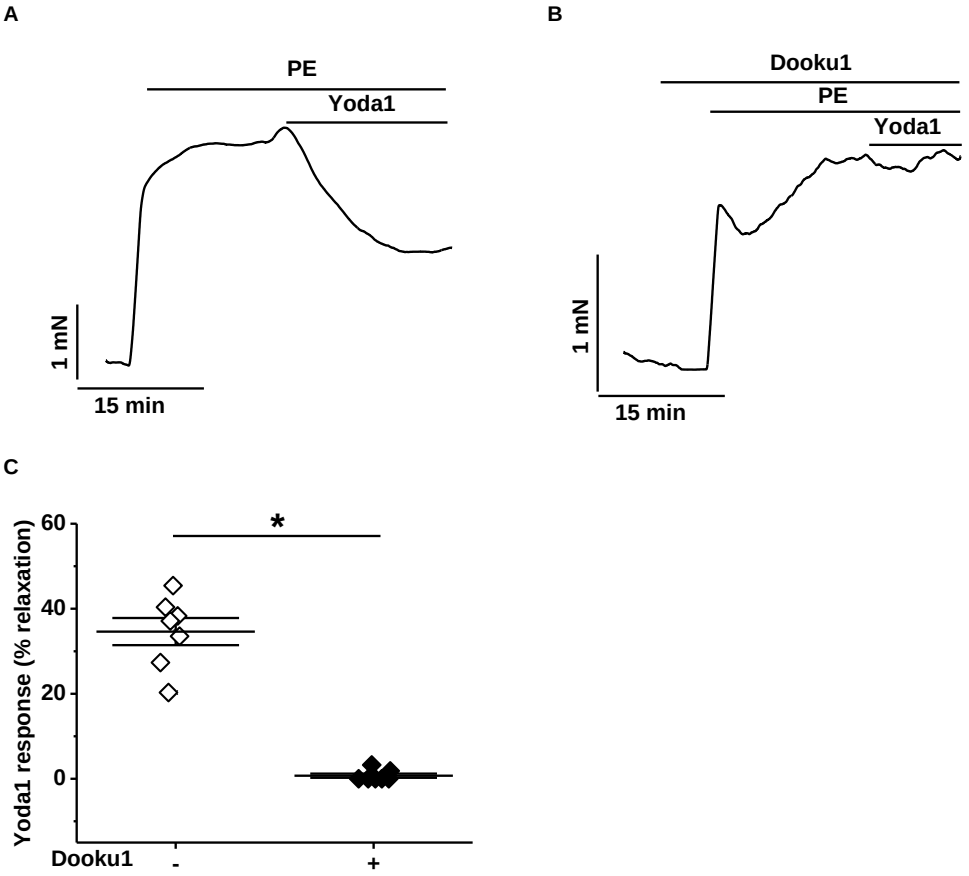

Figure 5-16 Dooku1 inhibits Yoda1-induced dilation in aorta. Isometric tension data from mouse thoracic aorta with intact endothelium. (A) Pre-constricted with PE and exposed to 5 μM Yoda1. (B) As for A but following 30 min pre-incubation with 10 μM Dooku1. (C) Summary data for experiments of the type shown in (A,B) expressed as % relaxation evoked by Yoda1. Each data point represents a value from an independent experiment with mean values and error bars representing SEM indicated by the black lines (n=7). * ($p<0.05$), ** ($p<0.01$), *** ($p<0.001$), **** ($p<0.0001$). Dr Naima Endesh (University of Leeds) performed wire myography experiments.

5.3 Discussion

This chapter aimed to find new pharmacological tools for studying Piezo1 and has added new knowledge to the structure-activity relationship for Piezo1 channel activation. It has been possible to identify an antagonist for Yoda1-induced channel activity, Dooku1, which strongly inhibits physiological responses in aortic rings. Based on the structural similarity of the compounds it is likely Dooku1 competes with Yoda1 at the same binding site, but it has not been possible to rule out the possibility that Dooku1 acts allosterically.

The importance of the 2,6-dichlorophenyl ring of Yoda1 for Piezo1 activity was highlighted during the discovery of the compound (Syeda et al., 2015). The results of this chapter support this finding and demonstrate that even small changes to this ring are catastrophic for Piezo1 modulation. Replacing one [**2g]**, or both, [**2a],** of these chlorines with chemically similar fluorines is enough for Piezo1 activation to be lost or substantially reduced. Removal of one, [**2b],** or both, [**2h]**, of the chlorines or movement of the position of chlorine [**2c**/**2d]** around the ring is also detrimental for pharmacological activity. Investigating the inhibitory potential of the compounds showed that all but **2g** were ineffective at reducing the Yoda1 response. These results imply that the chlorine atoms specifically are important for activity and may interact directly with Piezo1.

Yoda1 analogues with modifications to the pyrazine ring also had less activity than Yoda1 with the most successful compound **7a** showing 50% of Yoda1 activity. This highlights the importance of the nitrogen atom at the 2 position of the pyrazine ring as loss of this atom caused a substantial loss of activity. The other compounds in the series **2i** and **7b** were even less active, suggesting the remaining nitrogen atom of **7a** in the 3 position is also facilitating Piezo1 activation. Substituting the thiadiazole ring for an oxadiazole ring [**11**] was more tolerated as the compound demonstrated 70% of Yoda1 activity. Other analogues with this substitution were not as active. The reduced activity of compound **2j** compared to **11** reinforces the idea that nitrogen in the 3 position of the pyrazine ring on Yoda1 contributes to Piezo1 activity.

Investigating the inhibitory effects of these compounds against Yoda1 provided the most encouraging findings for identifying a new pharmacological tool for studying Piezo1. All compounds were able to reduce Ca^{2+} entry evoked by Yoda1 by at least 40% and inhibition of up to 75% was observed by **2j**. However, all of

these compounds exhibited some partial agonist activity except **2k** (Dooku1) which was able to reduce the Yoda1 response by 60% without causing any activation on its own. Dooku1 also markedly reduced the Yoda1 response in HUVECs and had a strong inhibitory effect against Yoda1 responses in aortic rings. Drawing on the data gathered from all of the Yoda1 analogues suggests that modifications to the pyrazine or thiadiazole ring result in a loss of activity, however these compounds are still able to interact with Piezo1 and can inhibit Yoda1 activity. On the other hand, compounds with modifications to the 2,6-dichlorophenyl ring can neither activate the channels nor inhibit the Yoda1 response. Therefore, it appears that the di-chloro ring is critical for binding to Piezo1, whereas the pyrazine ring is not as required for binding but seems important for activation.

At the time of this study, the only available inhibitors of Piezo1 were not selective and acted against other non-selective cation or mechanosensitive channels (Drew et al., 2002, Bae et al., 2011). Dooku1 is not the perfect Piezo1 inhibitor as it does not reduce constitutive channel activity, but it is a useful tool compound for studying Piezo1 and has since been used in studies investigating Piezo1 function in pancreatic β-cells and cardiac fibroblasts (Deivasikamani et al., 2018, Blythe et al., 2019b). As Dooku1 only inhibits Yoda1-induced Piezo1 activity and not constitutive channel activity, it is likely that it is binding to the same site as Yoda1, thereby preventing Yoda1 from accessing its binding site and activating the channel. Dooku1 is reversible, as is the action of Yoda1 (Rocio Servin-Vences et al., 2017), reinforcing similarities between the compounds. It would have been ideal to perform Schild analysis to determine whether the antagonism by Dooku1 was competitive, but unfortunately solubility limitations prevented these studies. As Dooku1 does not reduce constitutive Piezo1 activity, it suggests that the mechanism of background channel activity, is distinct from the mechanism of Yoda1 activation.

Dooku1 inhibited Yoda1-induced Piezo1 activity, without disrupting Ca^{2+} handling events within the cell, or without inhibiting the activity of a number of TRP channels. This suggests that the activity of Dooku1 is selective, however more investigation is necessary as Dooku1 slightly reduced contraction in response to phenylephrine and also contraction evoked by U44619 (Evans et al., 2018). It is unknown whether this effect is mediated by a Piezo1 mechanism or an alternative

off target effect. One possibility is that Dooku1 is reducing Piezo1 activity in smooth muscle cells of the aortic rings, inhibiting contraction. However, this seems unlikely as it would assume that the channels become activated by a Yoda1-like mechanism during contraction and Piezo1 does not contribute to normal vessel tone (Retailleau et al., 2015).

Dooku1 only partially inhibited the Yoda1 response against the endogenous Piezo1 channel in HUVECs, although strikingly completely abolished Yoda1-induced relaxation in aortic rings. This result was not due to the increased temperature during the isometric tension recordings (37ºC) compared to the intracellular Ca^{2+} measurement recordings (room temperature) as the Dooku1 effect was not temperature dependent (Figure 5-11). Instead, this suggests that a complete reduction in the Ca^{2+} signal is not required for cessation of nitric oxide (NO) production, so that a partial reduction in Ca^{2+} is sufficient to inhibit Yoda1-induced relaxation. Another difference observed in the chapter is that Yoda1 was more potent in HUVECs than in the Piezo1 T-REx cells (EC_{50}'s of 0.23 μM and 2.51 μM respectively) suggesting a difference between endogenous and over-expressed channels. This divergence could be due to a higher basal state of Piezo1 activity in endothelial cells so that they are better primed for opening by Yoda1 activation and therefore more sensitive (Rode et al., 2017).

Since these studies there have been a couple of new developments in the Piezo1 pharmacology field. Enantiomeric amyloid β (Aβ) peptides that are naturally found in the brain and cerebral spinal fluid following traumatic brain injury, have been shown to reduce shear-stress induced intracellular Ca^{2+} entry and decrease cell migration dependent on Piezo1, in Piezo1 overexpressing cell lines at femtomolar to picomolar concentrations (Maneshi et al., 2018). Due to the similar action of both enantiomers, it is unlikely that the effect of Aβ peptides on Piezo1 gating is due to direct peptide-protein interactions. Rather, it is likely that Aβ peptides affect the local bilayer tension surrounding the channel by insertion into the membrane or affecting tension exerted by the cytoskeleton. It has not been investigated whether the effects of Aβ peptides are selective for Piezo1 activity.

Novel Piezo1 agonists, Jedi1 and Jedi2 have been identified in a screen of ~3000 compounds. They are structurally distinct from Yoda1, but like the original agonist can cause increases in intracellular Ca^{2+} and inward currents in Piezo1 expressing cells (Wang et al., 2018b). Studies with mutant Piezo1 channels

showed that the Jedi compounds likely bind to the extracellular blade of the channels, in contrast to Yoda1 which binds to the C-terminal extracellular domain of the pore (Lacroix et al., 2018). However, although these compounds are more water soluble than Yoda1, the potency of the Jedi compounds is much lower (EC50's ~200 μM for intracellular Ca^{2+} entry). Therefore, although progress has been made, there is still the need for more Piezo1 pharmacological tools.

5.4 Summary

Findings from this chapter have provided important insight into the structure-activity requirements for Piezo1 channel chemical modulation and support the concept of a specific chemical binding site present on or near Piezo1 channels. A novel pharmacological tool, Dooku1, has been identified which can inhibit Yoda1-induced Ca^{2+} entry and relaxation in the murine aorta, without effect on constitutive channel activity. The full role of Piezo1 in physiology is yet to be established but the protein may have important clinical significance with function in genetic disease, blood pressure control, exercise capacity, hypertension induced arterial remodelling and pancreatitis (Wang et al., 2016, Zeng et al., 2018, Rode et al., 2017, Retailleau et al., 2015, Romac et al., 2018). Presently, it is not known whether activation or inhibition of Piezo1 would be clinically advantageous but increased pharmacological knowledge in addition to physiological knowledge is required if therapeutic potential of the channel is to be harnessed in the future. Learning more about the interaction of small molecules with Piezo1 is likely to be paramount in the effort to fully understand and utilise Piezo1 biology.

Chapter 6 Summary and Future Direction

6.1 Summary of results

Chapter 3

- Transient transfection of the murine equivalent of human M2225R (M2240R) in HEK293 cells results in potentiation of the Yoda1 response compared to WT mouse Piezo1.
- Stable HEK T-REx cell lines of Piezo1 M2240R (Piezo1 M-R) have increased sensitivity to Yoda1 and Yoda1 analogue KC159, compared to WT mouse Piezo1 cell line.
- Piezo1 M-R mice homozygous for the mutation were successfully generated by CRISPR-Cas9 and were viable and appeared normal.
- Piezo1 M-R mice displayed clinical features of DHS, including reduced haemoglobin, increased reticulocytes, splenomegaly, and evidence of stomatocytes.
- RBCs from Piezo1 M-R mice showed the expected reduced osmotic fragility.
- RBCs from Piezo1 M-R mice failed to recover resting membrane potential and maintained current entry after activation by fluid flow, suggesting a delayed deactivation mechanism was disease-causing.
- Response to Yoda1 was increased in mLSECs isolated from Piezo1 M-R mice with trends for increased alignment to shear stress.
- Responses to Yoda1 were potentiated in aorta from Piezo1 M-R mice.
- Relaxation to Yoda1 was faster in mesenteric arteries from Piezo1 M-R mice.
- Blood pressure was normal in 8-week old Piezo1 M-R mice under resting conditions and under mild stress.

Chapter 4

- 8-week old Piezo1 M-R mice have a mild hypertrophic profile with increased heart weight and mRNA expression of *Myh7* with trends of increased *Anp* and *Acta1.*
- 22-week old Piezo1 M-R mice have favourable cardiac parameters, with reduced *Acta1* mRNA expression, trends for decreased inflammatory markers; *Il-1b* and *Mmp9* and increased cardiac function.

- Heart weight is normal in 8-week old CreMyh6-Piezo1$^{-/-}$ mice, but gene expression reflects a heart failure profile with increased *Bnp, Col1a1* and reduced *Serca2a.*
- 8-week old CreMyh6-Piezo1$^{-/-}$ mice show trends for reduced cardiac function.
- Heart weight is normal in 6 month old CreMyh6-Piezo1$^{-/-}$ mice, but gene expression reflects an advanced heart failure phenotype with increased *Anp, Col1a1, Col3a1* and *Myh7,* decreased *Serca2a* and *Myh6,* with trends for increased *Bnp, Acta1* and *Mmp9*.
- 8 week-old CD fed Piezo1 M-R mice have increased eWAT mass, but lipogenic gene expression and adipocyte size are normal.
- 22-week old CD fed Piezo1 M-R mice have increased expression of lipogenic genes in eWAT; *Dgat2, Cd36, Fas, Elovl6* with trends in increased *Lpl* and *Scd1.*
- Adipocyte size in 22-week old Piezo1 M-R mice shows upward trends.
- mRNA expression of transcription factors *Srebp-1c* or *Chrebp* is unchanged in eWAT from Piezo1 M-R mice.
- Lipogenic gene expression in scWAT of Piezo1 M-R mice is normal.
- BAT mass is increased in both 8 and 22 week old CD fed Piezo1 M-R mice.
- 8-week old CD fed Piezo1 M-R mice have trends for increased mRNA expression of *Fas* and *Col1a1* and reduced mRNA expression of Piezo1 in liver.
- 22-week old CD fed Piezo1 M-R mice have increased mRNA expression of *Fas* and reduced mRNA expression of *lipocalin2* in liver.
- 22-week old CD fed Piezo1 M-R mice have heavier livers with evidence of ectopic fat deposition.
- 22-week old CD fed Piezo1 M-R mice have reduced RER and trends for reduced food intake and energy balance in the light phase.
- Piezo1 M-R mice have strong trends for reduced insulin sensitivity.
- 22-week old Piezo1 M-R mice are dyslipidaemic, with decreased triglycerides and increased HDL-cholesterol.
- Piezo1 M-R mice fed HFD have comparable body weights but trends for increased spleen and decreased skeletal muscle weights.
- HFD fed Piezo1 M-R mice have no altered gene expression of metabolic genes in eWAT, but do have reduced Piezo1 expression.
- HFD fed Piezo1 M-R mice have a reduced mRNA expression of *Cyp7a1* in liver.
- Piezo1 M-R mice fed HFD eat more, but move less with no resulting increase in body weight.

- HFD fed Piezo1 M-R mice have normal insulin and glucose sensitivity and plasma lipid levels.

Chapter 5

- Piezo1 T-REx cells express Piezo1 after induction with tetracycline and show robust, dose-dependent Ca^{2+} entry in response to Piezo1 agonist, Yoda1.
- The 2,6-dichlorophenyl group of Yoda1 is crucial for Piezo1 channel activation or for interaction with the Piezo1 channel.
- Changing the pyrazine ring of Yoda1 or replacing the thiadiazole with an oxadiazole is tolerated, but produces less active analogues.
- Identification of Yoda1 analogue, Dooku1, which can inhibit Yoda1-induced Piezo1 activity in Piezo1 T-REx cells, without activation.
- Structural requirements of Yoda1 antagonism are tight and compounds structurally similar to Dooku1 are unable to inhibit Yoda1-induced Piezo1 activation.
- Dooku1 effects are reversible and are not temperature dependent.
- Dooku1 has selectivity for Piezo1 and does not affect native ATP or store-operated Ca^{2+} responses in HEK 293 cells or agonist responses of TRP channels; TRPV4, TRPC4 and TRPC5.
- Dooku1 does not affect constitutive Piezo1 activity and only inhibits Yoda1-induced Piezo1 activity.
- Dooku1 inhibits endogenous Yoda1-activated Piezo1 channels in HUVECs and reduces Yoda1-induced relaxation in mouse thoracic aorta.

6.2 Future work

This study has revealed many new findings about the nature of Piezo1, DHS-causing mutations, both on the effect on endogenous channel gating in RBCs, but also the identification of additional phenotypic effects. The work presented has had a broad focus, but can now direct areas for future, more in depth investigation which would be worthwhile and is necessary if the complete effect of Piezo1 GOF mutations on physiology is to be elucidated. Dooku1 is a useful tool compound to study Yoda1-induced Piezo1 activity and the Yoda1 SAR findings will be important in finding future Piezo1 targeting compounds. However, Dooku1 itself is unlikely to be useful in *in vivo* Piezo1 modulation and additional effort into developing Piezo1 pharmacology is required for identification of potential therapeutic agents.

6.2.1 Effect of Piezo1 M-R on channel gating in cell types other than RBCs

The work presented in this study demonstrated that the Piezo1 M-R mutation affects channel gating in RBCs by a dramatic delaying of deactivation after cessation of the stimulus, a finding distinct from overexpression studies in which a modest delay in inactivation was observed. This finding in the endogenous Piezo1 channel in RBCs reflected slow RBC biology in which very fast reactions to mechanical force are likely unnecessary. It would be interesting to investigate whether the Piezo1 M-R mutation affects other cell types in the same way, or in fact whether differences in channel gating are observed at all in other cell types. The Piezo1 M-R mouse model provides the unique opportunity to study effects of the mutation in native cells. It would be interesting to isolate primary cells such as mLSECs or adipocytes and investigate their responsiveness to Yoda1 on the FlexStation to establish if GOF in Ca^{2+} influx is observed. It would also be important to perform electrophysiological experiments to a mechanical stimulus to observe effects on current and membrane potential of Piezo1 M-R in these cells.

6.2.2 Effects of Piezo1 M-R on cellular distribution of Piezo1

Some DHS-associated Piezo1 mutations, which reduce the mechanical threshold for activation have been shown to cause trafficking defects when transfected into HEK293 cells, with colocalisation with the endoplasmic reticulum (ER) and Golgi. However, no trafficking defects were found due to Piezo1 M2225R (M-R) mutation (Glogowska et al., 2017). In our own investigations, attempts were made at performing pressure-activated patch clamp experiments on the generated Piezo1 M-R stable cell line (Evans and Muraki, unpublished observations). However, recordings proved difficult and robust, pressure-activated responses were not observed; a vast difference to the corresponding WT murine Piezo1 (mPiezo1) cell line. Therefore, store-operated Ca^{2+} entry was investigated in these cell lines to determine whether the mutant channels may localise to the ER. Cells were pre-treated with 1 µM thapsigargin for 30 minutes to deplete the intracellular Ca^{2+} stores, prior to application of Yoda1. Yoda1 did not evoke Ca^{2+} entry in HEK T-REx cells as expected (Figure 6-1A). Pre-treatment with thapsigargin did not affect the Yoda1 response in mPiezo1 cells, but surprisingly completely abolished it in the Piezo1 M-R cell line (

Figure 6-1 B-D). This raises the possibility that Piezo1 localisation may be affected by the M-R mutation. In order to investigate this phenomenon further and ensure it is not an artefact of cell line generation, thapsigargin needs to be tested against the endogenous Piezo1 M-R channel, using primary cells like mLSECs, isolated from Piezo1 M-R mice. Antibodies targeted to Piezo1 are still not efficient enough to facilitate staining and imaging to confidently show Piezo1 distribution within the cell.

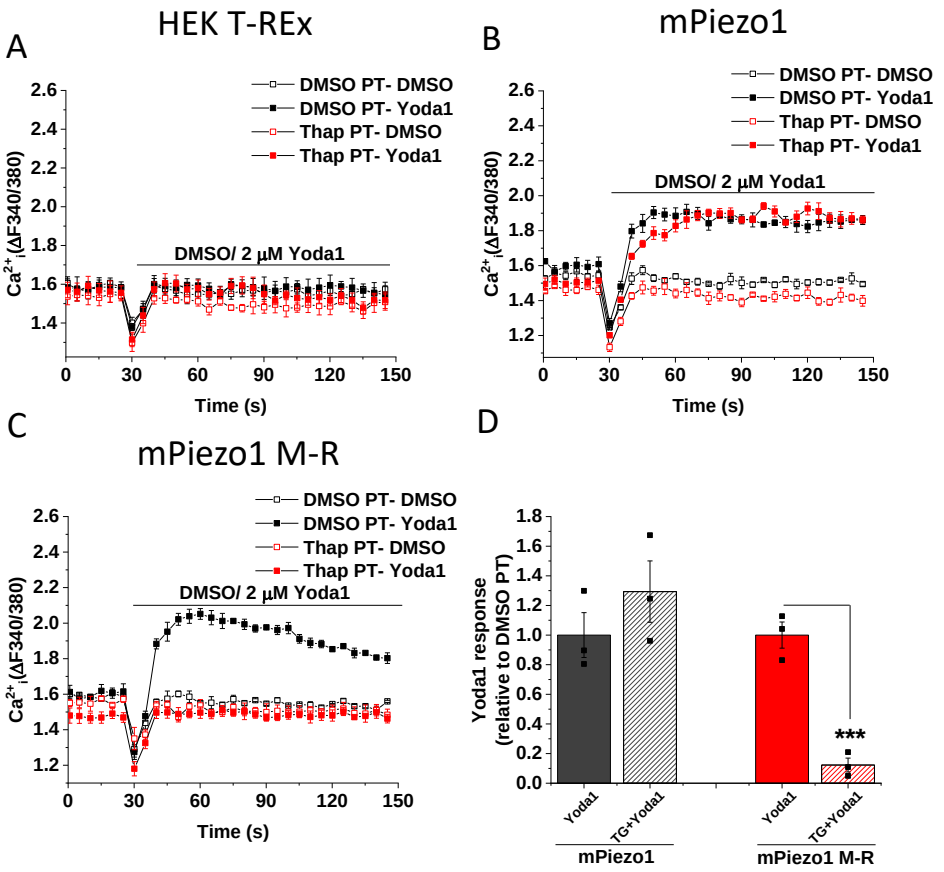

Figure 6-1 Piezo1 M-R response to Yoda1 requires Ca^{2+} stores. (A-C) FlexStation intracellular Ca^{2+} measurement data for HEK T-REx (A), mPiezo1 (B), mPiezo1 M-R (C) cells pre-treated (PT) with 1 µM Thapsigargin (Thap) (red) or DMSO (black) and then exposed to 2 µM Yoda1 (closed squares) or vehicle only (open squares). Error bars indicate SEM (N = 3, in-plate replicates). (D) Mean data for the type of experiments shown in (A-C) comparing peak Yoda1 response measured between 0-30s after Yoda1 application for vehicle pre-treated cells (solid bar) and Thap pre-treated cells (striped bar). Data are normalised to the Yoda1 response following vehicle pre-treatment for each cell type. All individual data points are shown with mean ± SEM (n=3). * ($p<0.05$), ** ($p<0.01$), *** ($p<0.001$), **** ($p<0.0001$).

6.2.3 Translation of Piezo1 M-R phenotyping to humans with Piezo1 GOF mutations

This study has revealed the existence of phenotypic effects, additional to DHS, which occur in mice with Piezo1 M-R mutation. The results suggest a lipogenic phenotype with broadly unfavourable metabolic tendencies, indicating that patients may be at higher risk of conditions such as type 2 diabetes. The relevance of the Piezo1 M-R model to humans was validated by confirmation that the mutations also cause a DHS-like phenotype in the mouse. However, it would be important to confirm the additional findings in patients with DHS arising from Piezo1 mutation. Insulin sensitivity and plasma lipid levels in these patients could be measured simply and non-invasively after seeking appropriate ethical approval, in collaboration with a group researching the genetic basis for Piezo1-causing disease.

6.2.4 Determine the mechanism of the lipogenic phenotype in Piezo1 M-R mice

The mechanism for increased lipogenic phenotype due to Piezo1 M-R was not elucidated during the time frame of this study. However, it is important to decipher, both to relate to human patients with Piezo1 GOF mutations, but also as it may reveal unknown roles of Piezo1 within physiology and metabolism. This is likely to be multifactorial but some suggestions of initial experiments include measuring the activity of transcriptional regulators presented in the study; SREBP-1c and ChREBP within both liver and eWAT; the major sites of *de novo* lipogenesis. Additionally, as the majority of gene expression changes were identified within eWAT it would be interesting to measure Piezo1 activity directly from adipocytes isolated from Piezo1 M-R mice. Functional experiments confirming Piezo1 activity in adipocytes have not yet been published. Experiments on isolated adipocytes could be used to confirm if Piezo1 M-R mutation does in fact result in channel gain of function in these cells. If GOF is observed, it would suggest lipogenic changes could originate from the adipocytes themselves so it would be relevant to treat isolated WT adipocytes with Piezo1 agonist Yoda1 to determine whether changes in adipocyte gene expression can occur directly from Piezo1 activation.

6.2.5 Role of Piezo1 in cardiac function

Evidence of a possible role for Piezo1 in cardiac function was presented in this study, using the global gain of function Piezo1 M-R mouse, in addition to a cardiac myocyte specific Piezo1 knockout model, CreMyh6-Piezo1$^{-/-}$. The results hinted that Piezo1 deletion may be detrimental, whereas Piezo1 GOF may provide functional benefits, but more experiments are necessary to form proper conclusions. It will be essential to investigate cardiac gene expression and function in CreMyh6 control mice lacking Piezo1 flox to determine whether previous findings with the model are Piezo1 dependent. The experiments with Piezo1 M-R mice will need repeating with larger sample sizes, in addition to staining to look for changes in cardiac histology. If the role of Piezo1 in normal cardiac function is proved, then it would be interesting to induce heart failure in the mouse models and investigate whether Piezo1 deletion of GOF is advantageous in this disease state.

6.2.6 Determine the structural basis for Piezo1 M-R gain-of-function

It still remains unknown specifically how Piezo1 M-R mutation, and other DHS-causing mutations, result in Piezo1 GOF. It seems that the mutation affords a stabilisation of the open state or that it delays conformational changes that result in pore closure. Understanding the mechanism for altered Piezo1 gating is important if modulation of channel kinetics is to be utilised for therapeutics. It is possible the methionine to positively charged arginine, amino acid substitution generates a charge effect which may stabilise the open state. Molecular dynamic simulations allow modelling of Piezo1 in which the structure is given freedom to move within the simulation and the interaction between different amino acids can be conferred. Necessary cryo-EM structures exist for the relevant region of the channel to facilitate modelling of Piezo1 M-R to determine if this results in the generation of additional interactions around the pore. This can be used in combination with traditional mutagenesis approaches, to determine the relevance of different combinations of amino acid substitution on channel function.

6.2.7 Identify additional Piezo1 pharmacological tools

The work in this study was able to identify important structural requirements for Piezo1 interaction, including confirming the importance of the di-chloro ring on the Yoda1 structure. Dooku1 can be used in studies of Piezo1 but does not affect

constitutive channel activity so it is unlikely to be useful *in vivo,* therefore additional pharmacological modulators are still needed. Using the knowledge acquired in this study, more Yoda1 analogues can be designed and synthesised, strictly maintaining the di-chloro ring but modulating areas of the structure which can be changed and tolerated. The overall aim would be to identify a Yoda1 analogue with improved solubility and half-life which could be used in pilot murine *in vivo* studies to investigate the effects of global Piezo1 activation. This would be important to determine whether pharmacological modulation of the channel could be tolerated and would be therapeutically beneficial. It would be interesting to test partial inhibitors, if and when they are developed, in Piezo1 M-R mice to see if they can protect against anaemia.

6.3 Conclusions

My thesis presents the first investigation of the effects of DHS-causing Piezo1 mutations on endogenous channel gating in RBCs. It has also shown that non-RBC phenotypic effects of Piezo1 gain-of-function are possible, despite humans with DHS only reporting mild to moderate anaemia. These results have relevance for patients with Piezo1 mutations suggesting additional disease predisposition and are also important in helping to uncover unknown roles of Piezo1 function in physiology. The work has added knowledge to the Piezo1 pharmacology field and discovered a new tool compound, Dooku1, with which to study the channel. These efforts can contribute to the identification of future Piezo1 modulators which may be useful to treat disease caused by Piezo1 mutations.

References

ABDUL-WAHED, A., GUILMEAU, S. & POSTIC, C. 2017. Sweet Sixteenth for ChREBP: Established Roles and Future Goals. *Cell Metabolism,* 26**,** 324-341.

AGAH, R., FRENKEL, P. A., FRENCH, B. A., MICHAEL, L. H., OVERBEEK, P. A. & SCHNEIDER, M. D. 1997. Gene recombination in postmitotic cells. Targeted expression of Cre recombinase provokes cardiac-restricted, site-specific rearrangement in adult ventricular muscle in vivo. *The Journal of clinical investigation,* 100**,** 169-179.

AKBULUT, Y., GAUNT, H. J., MURAKI, K., LUDLOW, M. J., AMER, M. S., BRUNS, A., VASUDEV, N. S., RADTKE, L., WILLOT, M., HAHN, S., SEITZ, T., ZIEGLER, S., CHRISTMANN, M., BEECH, D. J. & WALDMANN, H. 2015. (−)-Englerin A is a Potent and Selective Activator of TRPC4 and TRPC5 Calcium Channels. *Angewandte Chemie International Edition,* 54**,** 3787-3791.

ALBUISSON, J., MURTHY, S. E., BANDELL, M., COSTE, B., LOUIS-DIT-PICARD, H., MATHUR, J., FENEANT-THIBAULT, M., TERTIAN, G., DE JAUREGUIBERRY, J. P., SYFUSS, P. Y., CAHALAN, S., GARCON, L., TOUTAIN, F., SIMON ROHRLICH, P., DELAUNAY, J., PICARD, V., JEUNEMAITRE, X. & PATAPOUTIAN, A. 2013. Dehydrated hereditary stomatocytosis linked to gain-of-function mutations in mechanically activated PIEZO1 ion channels. *Nat Commun,* 4**,** 1884.

AMI, O., PICONE, O., GARÇON, L., CASTEL, C., GUITTON, C., DELAUNAY, J., FRYDMAN, R. & SENAT, M. V. 2009. First-trimester nuchal abnormalities secondary to dehydrated hereditary stomatocytosis. *Prenatal Diagnosis,* 29**,** 1071-1074.

ANDERSON, E. O., SCHNEIDER, E. R., MATSON, J. D., GRACHEVA, E. O. & BAGRIANTSEV, S. N. 2018. TMEM150C/Tentonin3 Is a Regulator of Mechano-gated Ion Channels. *Cell Reports,* 23**,** 701-708.

ANDOLFO, I., ALPER, S. L., DE FRANCESCHI, L., AURIEMMA, C., RUSSO, R., DE FALCO, L., VALLEFUOCO, F., ESPOSITO, M. R., VANDORPE, D. H., SHMUKLER, B. E., NARAYAN, R., MONTANARO, D., D'ARMIENTO, M., VETRO, A., LIMONGELLI, I., ZUFFARDI, O., GLADER, B. E., SCHRIER, S. L., BRUGNARA, C., STEWART, G. W., DELAUNAY, J. & IOLASCON, A. 2013. Multiple clinical forms of dehydrated hereditary stomatocytosis arise from mutations in PIEZO1. *Blood,* 121**,** 3925.

ANDOLFO, I., DE ROSA, G., ERRICHIELLO, E., MANNA, F., ROSATO, B. E., GAMBALE, A., VETRO, A., CALCATERRA, V., PELIZZO, G., DE FRANCESCHI, L., ZUFFARDI, O., RUSSO, R. & IOLASCON, A. 2019. PIEZO1 Hypomorphic Variants in Congenital Lymphatic Dysplasia Cause Shape and Hydration Alterations of Red Blood Cells. *Frontiers in Physiology,* 10**,** 258.

ANDOLFO, I., MANNA, F., DE ROSA, G., ROSATO, B. E., GAMBALE, A., TOMAIUOLO, G., CARCIATI, A., MARRA, R., DE FRANCESCHI, L., IOLASCON, A. & RUSSO, R. 2018a. PIEZO1-R1864H rare variant accounts for a genetic phenotype-modifier role in dehydrated hereditary stomatocytosis. *Haematologica,* 103**,** e94-e97.

ANDOLFO, I., RUSSO, R., GAMBALE, A. & IOLASCON, A. 2016. New insights on hereditary erythrocyte membrane defects. *Haematologica,* 101**,** 1284-1294.

ANDOLFO, I., RUSSO, R., ROSATO, B. E., MANNA, F., GAMBALE, A., BRUGNARA, C. & IOLASCON, A. 2018b. Genotype-phenotype correlation and risk stratification in a cohort of 123 hereditary stomatocytosis patients. *American Journal of Hematology,* 93**,** 1509-1517.

ARCHER, N., SHMUKLER, B. E., ANDOLFO, I., VANDORPE, D. H., GNANASAMBANDAM, R., HIGGINS, J. M., RIVERA, A., FLEMING, M. D., SACHS, F., GOTTLIEB, P. A., IOLASCON, A., BRUGNARA, C., ALPER, S. L. & NATHAN, D. G. 2014. Hereditary Xerocytosis Revisited. *American journal of hematology,* 89**,** 1142-1146.

ASIMAKOPOULOU, A., WEISKIRCHEN, S. & WEISKIRCHEN, R. 2016. Lipocalin 2 (LCN2) Expression in Hepatic Malfunction and Therapy. *Frontiers in physiology,* 7**,** 430-430.

AUSTIN, S. & ST-PIERRE, J. 2012. PGC1α and mitochondrial metabolism – emerging concepts and relevance in ageing and neurodegenerative disorders. *Journal of Cell Science,* 125**,** 4963-4971.

BAE, C., GNANASAMBANDAM, R., NICOLAI, C., SACHS, F. & GOTTLIEB, P. A. 2013a. Xerocytosis is caused by mutations that alter the kinetics of the mechanosensitive channel PIEZO1. *Proceedings of the National Academy of Sciences,* 110**,** E1162-E1168.

BAE, C., GOTTLIEB, P. A. & SACHS, F. 2013b. Human PIEZO1: removing inactivation. *Biophysical journal,* 105**,** 880-886.

BAE, C., SACHS, F. & GOTTLIEB, P. A. 2011. The mechanosensitive ion channel Piezo1 is inhibited by the peptide GsMTx4. *Biochemistry,* 50**,** 6295-6300.

BAE, C., SACHS, F. & GOTTLIEB, P. A. 2015. Protonation of the human PIEZO1 ion channel stabilizes inactivation. *The Journal of biological chemistry,* 290**,** 5167-5173.

BASU, A. P., CAREY, P., CYNOBER, T., CHETTY, M., DELAUNAY, J., STEWART, G. W. & RICHMOND, S. 2003. Dehydrated hereditary stomatocytosis with transient perinatal ascites. *Archives of Disease in Childhood - Fetal and Neonatal Edition,* 88**,** F438-F439.

BATALLER, R. & BRENNER, D. A. 2005. Liver fibrosis. *The Journal of Clinical Investigation,* 115**,** 209-218.

BEECH, D. J. & KALLI, A. C. 2019. Force Sensing by Piezo Channels in Cardiovascular Health and Disease. *ATVB,* 0**,** 2228-2239.

BENETEAU, C., THIERRY, G., BLESSON, S., LE VAILLANT, C., PICARD, V., BÉNÉ, M. C., EVEILLARD, M. & LE CAIGNEC, C. 2014. Recurrent mutation in the PIEZO1 gene in two families of hereditary xerocytosis with fetal hydrops. *Clinical Genetics,* 85**,** 293-295.

BERRIDGE, M. J., BOOTMAN, M. D. & RODERICK, H. L. 2003. Calcium signalling: dynamics, homeostasis and remodelling. *Nature Reviews Molecular Cell Biology,* 4**,** 517-529.

BERRIDGE, M. J., LIPP, P. & BOOTMAN, M. D. 2000. The versatility and universality of calcium signalling. *Nature Reviews Molecular Cell Biology,* 1**,** 11-21.

BERTONI, A., ALABISO, O., GALETTO, A. S. & BALDANZI, G. 2018. Integrins in T Cell Physiology. *International journal of molecular sciences,* 19**,** 485.

BHANDARY, B. & ROBBINS, J. 2015. Giving credence to controls: Avoiding the false phenotype. *Journal of Molecular and Cellular Cardiology,* 86**,** 136-137.

BLYTHE, N. M., MURAKI, K., LUDLOW, M. J., STYLIANIDIS, V., GILBERT, H. T. J., EVANS, E. L., CUTHBERTSON, K., FOSTER, R., SWIFT, J., LI, J., DRINKHILL, M. J., VAN NIEUWENHOVEN, F. A., PORTER, K. E., BEECH, D. J. & TURNER, N. A. 2019a. Mechanically activated Piezo1 channels of cardiac fibroblasts stimulate p38 mitogen-activated protein kinase activity and interleukin-6 secretion. *Journal of Biological Chemistry,* 294**,** 17395-17408.

BLYTHE, N. M., STYLIANIDIS, V., LUDLOW, M. J., GILBERT, H. T. J., EVANS, E. L., CUTHBERTSON, K., FOSTER, R., SWIFT, J., LI, J., DRINKHILL, M. J., VAN NIEUWENHOVEN, F. A., PORTER, K. E., BEECH, D. J. & TURNER, N. A. 2019b. Stimulation of cardiac fibroblast Piezo1 channels opposes myofibroblast differentiation and induces IL-6 secretion via Ca2+-mediated p38 MAP kinase activation. *bioRxiv***,** 603456.

BORKHAM-KAMPHORST, E., VAN DE LEUR, E., ZIMMERMANN, H. W., KARLMARK, K. R., TIHAA, L., HAAS, U., TACKE, F., BERGER, T., MAK, T. W. & WEISKIRCHEN, R. 2013. Protective effects of lipocalin-2 (LCN2) in acute liver injury suggest a novel function in liver homeostasis. *Biochimica et Biophysica Acta (BBA) - Molecular Basis of Disease,* 1832**,** 660-673.

BOWMAN, C. L., GOTTLIEB, P. A., SUCHYNA, T. M., MURPHY, Y. K. & SACHS, F. 2007. Mechanosensitive Ion Channels and the Peptide Inhibitor GsMTx-4: History, Properties, Mechanisms and Pharmacology. *Toxicon : official journal of the International Society on Toxinology,* 49**,** 249-270.

BREMER, A. A., DEVARAJ, S., AFIFY, A. & JIALAL, I. 2011. Adipose Tissue Dysregulation in Patients with Metabolic Syndrome. *The Journal of Clinical Endocrinology & Metabolism,* 96**,** E1782-E1788.

BRINI, M. & CARAFOLI, E. 2011. The Plasma Membrane Ca2+ ATPase and the Plasma Membrane Sodium Calcium Exchanger Cooperate in the Regulation of Cell Calcium. *Cold Spring Harbor perspectives in biology,* 3**,** a004168.

BROHAWN, S. G., SU, Z. & MACKINNON, R. 2014. Mechanosensitivity is mediated directly by the lipid membrane in TRAAK and TREK1 K+channels. *Proceedings of the National Academy of Sciences,* 111**,** 3614-3619.

CAHALAN, S. M., LUKACS, V., RANADE, S. S., CHIEN, S., BANDELL, M. & PATAPOUTIAN, A. 2015. Piezo1 links mechanical forces to red blood cell volume. *Elife,* 4**,** e07370.

CARELLA, M., STEWART, G., AJETUNMOBI, J. F., PERROTTA, S., GROOTENBOER, S., TCHERNIA, G., DELAUNAY, J., TOTARO, A., ZELANTE, L., GASPARINI, P. & IOLASCON, A. 1998. Genomewide Search for Dehydrated Hereditary Stomatocytosis (Hereditary Xerocytosis): Mapping of Locus to Chromosome 16 (16q23-qter). *The American Journal of Human Genetics,* 63**,** 810-816.

CATTERALL, W. A. 2011. Voltage-gated calcium channels. *Cold Spring Harbor perspectives in biology,* 3**,** a003947-a003947.

CHOPRA, S., CHERIAN, D., VERGHESE, P. P. & JACOB, J. J. 2013. Physiology and clinical significance of natriuretic hormones. *Indian journal of endocrinology and metabolism,* 17**,** 83-90.

CINAR, E., ZHOU, S., DECOURCEY, J., WANG, Y., WAUGH, R. E. & WAN, J. 2015. Piezo1 regulates mechanotransductive release of ATP from human RBCs. *Proceedings of the National Academy of Sciences,* 112**,** 11783-11788.

CLAPHAM, D. E. 2007. Calcium Signaling. *Cell,* 131**,** 1047-1058.

COATS, A. J. S. 2004. Anaemia and heart failure. *Heart (British Cardiac Society),* 90**,** 977-979.

CONNELL, F. C., GORDON, K., BRICE, G., KEELEY, V., JEFFERY, S., MORTIMER, P. S., MANSOUR, S. & OSTERGAARD, P. 2013. The classification and diagnostic algorithm for primary lymphatic dysplasia: an update from 2010 to include molecular findings. *Clinical Genetics,* 84**,** 303-314.

COSSROW, N. & FALKNER, B. 2004. Race/Ethnic Issues in Obesity and Obesity-Related Comorbidities. *The Journal of Clinical Endocrinology & Metabolism,* 89**,** 2590-2594.

COSTE, B., HOUGE, G., MURRAY, M. F., STITZIEL, N., BANDELL, M., GIOVANNI, M. A., PHILIPPAKIS, A., HOISCHEN, A., RIEMER, G., STEEN, U., STEEN, V. M., MATHUR, J., COX, J., LEBO, M., REHM, H., WEISS, S. T., WOOD, J. N., MAAS, R. L., SUNYAEV, S. R. & PATAPOUTIAN, A. 2013. Gain-of-function mutations in the mechanically activated ion channel PIEZO2 cause a subtype of Distal Arthrogryposis. *Proceedings of the National Academy of Sciences of the United States of America,* 110**,** 4667-4672.

COSTE, B., MATHUR, J., SCHMIDT, M., EARLEY, T. J., RANADE, S., PETRUS, M. J., DUBIN, A. E. & PATAPOUTIAN, A. 2010. Piezo1 and Piezo2 are essential components of distinct mechanically-activated cation channels. *Science (New York, N.Y.),* 330**,** 55-60.

COSTE, B., MURTHY, S. E., MATHUR, J., SCHMIDT, M., MECHIOUKHI, Y., DELMAS, P. & PATAPOUTIAN, A. 2015. Piezo1 ion channel pore properties are dictated by C-terminal region. *Nature Communications,* 6**,** 7223.

COSTE, B., XIAO, B., SANTOS, J. S., SYEDA, R., GRANDL, J., SPENCER, K. S., KIM, S. E., SCHMIDT, M., MATHUR, J., DUBIN, A. E., MONTAL, M. & PATAPOUTIAN, A. 2012. Piezo proteins are pore-forming subunits of mechanically activated channels. *Nature,* 483**,** 176-81.

DALGHI, M. G., CLAYTON, D. R., RUIZ, W. G., AL-BATAINEH, M. M., SATLIN, L. M., KLEYMAN, T. R., RICKE, W. A., CARATTINO, M. D. & APODACA, G. 2019. Expression and distribution of PIEZO1 in the mouse urinary tract. *American Journal of Physiology-Renal Physiology,* 317**,** F303-F321.

DAMPNEY, R., COLEMAN, M., FONTES, M., HIROOKA, Y., HORIUCHI, J., LI, Y.-W., POLSON, J., POTTS, P. & TAGAWA, T. 2002. Central Mechanisms Underlying Short- And Long-Term Regulation Of The Cardiovascular System. *Clinical and Experimental Pharmacology and Physiology,* 29**,** 261-268.

DAVIS, M. J. & HILL, M. A. 1999. Signaling Mechanisms Underlying the Vascular Myogenic Response. *Physiological Reviews,* 79**,** 387-423.

DECAEN, P. G., DELLING, M., VIEN, T. N. & CLAPHAM, D. E. 2013. Direct recording and molecular identification of the calcium channel of primary cilia. *Nature,* 504**,** 315.

DEIVASIKAMANI, V., DHAYALAN, S., MUGHAL, R., VISNAGRI, A., CUTHBERTSON, K., SCRAGG, J. L., MUNSEY, T. S.,

VISWAMBHARAN, H., FOSTER, R., SIVAPRASADARAO, A., KEARNEY, M. T., BEECH, D. J. & SUKUMAR, P. 2018. Piezo1 channel agonist mimics high glucose as a stimulator of insulin release. *bioRxiv***,** 455832.

DEL MÁRMOL, J. I., TOUHARA, K. K., CROFT, G. & MACKINNON, R. 2018. Piezo1 forms a slowly-inactivating mechanosensory channel in mouse embryonic stem cells. *eLife,* 7**,** e33149.

DELAUNAY, J. 2004. The hereditary stomatocytoses: genetic disorders of the red cell membrane permeability to monovalent cations. *Seminars in Hematology,* 41**,** 165-172.

DELLE VEDOVE, A., STORBECK, M., HELLER, R., HÖLKER, I., HEBBAR, M., SHUKLA, A., MAGNUSSON, O., CIRAK, S., GIRISHA, K. M., O'DRISCOLL, M., LOEYS, B. & WIRTH, B. 2016. Biallelic Loss of Proprioception-Related PIEZO2 Causes Muscular Atrophy with Perinatal Respiratory Distress, Arthrogryposis, and Scoliosis. *American journal of human genetics,* 99**,** 1206-1216.

DELP, M. D. & LAUGHLIN, M. H. 1998. Regulation of skeletal muscle perfusion during exercise. *Acta Physiologica Scandinavica,* 162**,** 411-419.

DERLER, I., JARDIN, I. & ROMANIN, C. 2016. Molecular mechanisms of STIM/Orai communication. *American Journal of Physiology-Cell Physiology,* 310**,** C643-C662.

DREW, L. J., WOOD, J. N. & CESARE, P. 2002. Distinct Mechanosensitive Properties of Capsaicin-Sensitive and -Insensitive Sensory Neurons. *The Journal of Neuroscience,* 22**,** RC228-RC228.

DRUMMOND, H. A., PRICE, M. P., WELSH, M. J. & ABBOUD, F. M. 1998. A Molecular Component of the Arterial Baroreceptor Mechanotransducer. *Neuron,* 21**,** 1435-1441.

DUBIN, ADRIENNE E., SCHMIDT, M., MATHUR, J., PETRUS, MATTHEW J., XIAO, B., COSTE, B. & PATAPOUTIAN, A. 2012. Inflammatory Signals Enhance Piezo2-Mediated Mechanosensitive Currents. *Cell Reports,* 2**,** 511-517.

DYRDA, A., CYTLAK, U., CIURASZKIEWICZ, A., LIPINSKA, A., CUEFF, A., BOUYER, G., EGÉE, S., BENNEKOU, P., LEW, V. L. & THOMAS, S. L. Y. 2010. Local Membrane Deformations Activate Ca2+-Dependent K+ and Anionic Currents in Intact Human Red Blood Cells. *PLOS ONE,* 5**,** e9447.

EARLEY, S., WALDRON BRIAN, J. & BRAYDEN JOSEPH, E. 2004. Critical Role for Transient Receptor Potential Channel TRPM4 in Myogenic Constriction of Cerebral Arteries. *Circulation Research,* 95**,** 922-929.

EISENHOFFER, G. T., LOFTUS, P. D., YOSHIGI, M., OTSUNA, H., CHIEN, C.-B., MORCOS, P. A. & ROSENBLATT, J. 2012. Crowding induces live cell extrusion to maintain homeostatic cell numbers in epithelia. *Nature,* 484**,** 546-549.

ENTEZAMI, M., BECKER, R., MENSSEN, H. D., MARCINKOWSKI, M. & VERSMOLD, H. T. 1996. Xerocytosis with concomitant intrauterine ascites: first description and therapeutic approach [letter]. *Blood,* 87**,** 5392-5393.

ERNSTROM, G. G. & CHALFIE, M. 2002. Genetics of Sensory Mechanotransduction. *Annual Review of Genetics,* 36**,** 411-453.

EVANS, E. L., CUTHBERTSON, K., ENDESH, N., RODE, B., BLYTHE, N. M., HYMAN, A. J., HALL, S. J., GAUNT, H. J., LUDLOW, M. J., FOSTER, R. & BEECH, D. J. 2018. Yoda1 analogue (Dooku1) which antagonizes

Yoda1-evoked activation of Piezo1 and aortic relaxation. *British journal of pharmacology,* 175**,** 1744-1759.

FAN, D., TAKAWALE, A., LEE, J. & KASSIRI, Z. 2012. Cardiac fibroblasts, fibrosis and extracellular matrix remodeling in heart disease. *Fibrogenesis & tissue repair,* 5**,** 15-15.

FAN, D., TAKAWALE, A., SHEN, M., SAMOKHVALOV, V., BASU, R., PATEL, V., WANG, X., FERNANDEZ-PATRON, C., SEUBERT, J. M., OUDIT, G. Y. & KASSIRI, Z. 2016. A Disintegrin and Metalloprotease-17 Regulates Pressure Overload;Induced Myocardial Hypertrophy and Dysfunction Through Proteolytic Processing of Integrin. *Hypertension,* 68**,** 937-948.

FAUCHERRE, A., KISSA, K., NARGEOT, J., MANGONI, M. E. & JOPLING, C. 2014. Piezo1 plays a role in erythrocyte volume homeostasis. *Haematologica,* 99**,** 70-75.

FAUCHERRE, A., MOHA OU MAATI, H., NASR, N., PINARD, A., THERON, A., ODELIN, G., DESVIGNES, J. P., SALGADO, D., COLLOD BEROUD, G., AVIERINOS, J. F., LEBON, G., ZAFFRAN, S. & JOPLING, C. 2019. Piezo1 is required for outflow tract and aortic valve development. *bioRxiv***,** 528588.

FERMO, E., VERCELLATI, C., MARCELLO, A. P., ZANINONI, A., VAN WIJK, R., MIRRA, N., CURCIO, C., CORTELEZZI, A., ZANELLA, A., BARCELLINI, W. & BIANCHI, P. 2017. Hereditary Xerocytosis due to Mutations in PIEZO1 Gene Associated with Heterozygous Pyruvate Kinase Deficiency and Beta-Thalassemia Trait in Two Unrelated Families. *Case reports in hematology,* 2017**,** 2769570-2769570.

FERRÉ, P. & FOUFELLE, F. 2007. SREBP-1c Transcription Factor and Lipid Homeostasis: Clinical Perspective. *Hormone Research in Paediatrics,* 68**,** 72-82.

FESKE, S. 2007. Calcium signalling in lymphocyte activation and disease. *Nature Reviews Immunology,* 7**,** 690-702.

FOLGERING, J. H. A., SHARIF-NAEINI, R., DEDMAN, A., PATEL, A., DELMAS, P. & HONORÉ, E. 2008. Molecular basis of the mammalian pressure-sensitive ion channels: Focus on vascular mechanotransduction. *Progress in Biophysics and Molecular Biology,* 97**,** 180-195.

FOTIOU, E., MARTIN-ALMEDINA, S., SIMPSON, M. A., LIN, S., GORDON, K., BRICE, G., ATTON, G., JEFFERY, I., REES, D. C., MIGNOT, C., VOGT, J., HOMFRAY, T., SNYDER, M. P., ROCKSON, S. G., JEFFERY, S., MORTIMER, P. S., MANSOUR, S. & OSTERGAARD, P. 2015. Novel mutations in PIEZO1 cause an autosomal recessive generalized lymphatic dysplasia with non-immune hydrops fetalis. *Nat Commun,* 6**,** 8085.

FRIEDRICH, E. E., HONG, Z., XIONG, S., ZHONG, M., DI, A., REHMAN, J., KOMAROVA, Y. A. & MALIK, A. B. 2019. Endothelial cell Piezo1 mediates pressure-induced lung vascular hyperpermeability via disruption of adherens junctions. *Proceedings of the National Academy of Sciences,* 116**,** 12980-12985.

GALARRAGA, M., CAMPIÓN, J., MUÑOZ-BARRUTIA, A., BOQUÉ, N., MORENO, H., MARTÍNEZ, J. A., MILAGRO, F. & ORTIZ-DE-SOLÓRZANO, C. 2012. Adiposoft: automated software for the analysis of white adipose tissue cellularity in histological sections. *Journal of lipid research,* 53**,** 2791-2796.

GALIONE, A. 2015. A primer of NAADP-mediated Ca2+ signalling: From sea urchin eggs to mammalian cells. *Cell Calcium,* 58**,** 27-47.

GASPAR, J. M. & VELLOSO, L. A. 2018. Hypoxia Inducible Factor as a Central Regulator of Metabolism – Implications for the Development of Obesity. *Frontiers in Neuroscience,* 12**,** 813.

GE, J., LI, W., ZHAO, Q., LI, N., CHEN, M., ZHI, P., LI, R., GAO, N., XIAO, B. & YANG, M. 2015. Architecture of the mammalian mechanosensitive Piezo1 channel. *Nature,* 527**,** 64-9.

GIANNI, D., CHAN, J., GWATHMEY, J. K., DEL MONTE, F. & HAJJAR, R. J. 2005. SERCA2a in Heart Failure: Role and Therapeutic Prospects. *Journal of Bioenergetics and Biomembranes,* 37**,** 375-380.

GLOGOWSKA, E. & GALLAGHER, P. G. 2015. Disorders of erythrocyte volume homeostasis. *International journal of laboratory hematology,* 37 Suppl 1**,** 85-91.

GLOGOWSKA, E., SCHNEIDER, E. R., MAKSIMOVA, Y., SCHULZ, V. P., LEZON-GEYDA, K., WU, J., RADHAKRISHNAN, K., KEEL, S. B., MAHONEY, D., FREIDMANN, A. M., ALTURA, R. A., GRACHEVA, E. O., BAGRIANTSEV, S. N., KALFA, T. A. & GALLAGHER, P. G. 2017. Novel mechanisms of PIEZO1 dysfunction in hereditary xerocytosis. *Blood,* 130**,** 1845-1856.

GNANASAMBANDAM, R., BAE, C., GOTTLIEB, P. A. & SACHS, F. 2015. Ionic Selectivity and Permeation Properties of Human PIEZO1 Channels. *PLoS One,* 10**,** e0125503.

GOLDBERG, I. J., ECKEL, R. H. & ABUMRAD, N. A. 2009. Regulation of fatty acid uptake into tissues: lipoprotein lipase- and CD36-mediated pathways. *Journal of lipid research,* 50**,** S86-S90.

GONZALES, E. B., KAWATE, T. & GOUAUX, E. 2009. Pore architecture and ion sites in acid-sensing ion channels and P2X receptors. *Nature,* 460**,** 599-604.

GOTTLIEB, P. A., BAE, C. & SACHS, F. 2012. Gating the mechanical channel Piezo1: a comparison between whole-cell and patch recording. *Channels (Austin),* 6**,** 282-9.

GRIMM, C., KRAFT, R., SAUERBRUCH, S., SCHULTZ, G. & HARTENECK, C. 2003. Molecular and Functional Characterization of the Melastatin-related Cation Channel TRPM3. 278**,** 21493-21501.

GROOTENBOER, S., SCHISCHMANOFF, P.-O., LAURENDEAU, I., CYNOBER, T., TCHERNIA, G., DOMMERGUES, J.-P., DHERMY, D., BOST, M., VARET, B., SNYDER, M., BALLAS, S. K., DUCOT, B., BABRON, M.-C., STEWART, G. W., GASPARINI, P., IOLASCON, A. & DELAUNAY, J. 2000. Pleiotropic syndrome of dehydrated hereditary stomatocytosis, pseudohyperkalemia, and perinatal edema maps to 16q23-q24. *Blood,* 96**,** 2599-2605.

GUDIPATY, S. A., LINDBLOM, J., LOFTUS, P. D., REDD, M. J., EDES, K., DAVEY, C. F., KRISHNEGOWDA, V. & ROSENBLATT, J. 2017. Mechanical stretch triggers rapid epithelial cell division through Piezo1. *Nature,* 543**,** 118-121.

GUHARAY, F. & SACHS, F. 1984. Stretch-activated single ion channel currents in tissue-cultured embryonic chick skeletal muscle. *The Journal of Physiology,* 352**,** 685-701.

GUO, Y. R. & MACKINNON, R. 2017. Structure-based membrane dome mechanism for Piezo mechanosensitivity. *eLife,* 6**,** e33660.

HALADE, G. V., JIN, Y.-F. & LINDSEY, M. L. 2013. Matrix metalloproteinase (MMP)-9: A proximal biomarker for cardiac remodeling and a distal biomarker for inflammation. *Pharmacology & Therapeutics,* 139**,** 32-40.

HALILOGLU, G., BECKER, K., TEMUCIN, C., TALIM, B., KÜÇÜKŞAHIN, N., PERGANDE, M., MOTAMENY, S., NÜRNBERG, P., AYDINGOZ, U., TOPALOGLU, H. & CIRAK, S. 2016. Recessive PIEZO2 stop mutation causes distal arthrogryposis with distal muscle weakness, scoliosis and proprioception defects. *Journal Of Human Genetics,* 62**,** 497-501.

HAMMOUDI, N. & LEBECHE, D. 2015. Calcium Signaling in Cardiovascular Physiology and Pathology. *In:* JAGADEESH, G., BALAKUMAR, P. & MAUNG-U, K. (eds.) *Pathophysiology and Pharmacotherapy of Cardiovascular Disease.* Cham: Springer International Publishing.

HAN, Y., LIU, C., ZHANG, D., MEN, H., HUO, L., GENG, Q., WANG, S., GAO, Y., ZHANG, W., ZHANG, Y. & JIA, Z. 2019. Mechanosensitive ion channel Piezo1 promotes prostate cancer development through the activation of the Akt/mTOR pathway and acceleration of cell cycle. *International journal of oncology,* 55**,** 629-644.

HARADA, K., SUGAYA, T., MURAKAMI, K., YAZAKI, Y. & KOMURO, I. 1999. Angiotensin II Type 1A Receptor Knockout Mice Display Less Left Ventricular Remodeling and Improved Survival After Myocardial Infarction. *Hypertension,* 100**,** 2093-2099.

HEURTEAUX, C., GUY, N., LAIGLE, C., BLONDEAU, N., DUPRAT, F., MAZZUCA, M., LANG-LAZDUNSKI, L., WIDMANN, C., ZANZOURI, M., ROMEY, G. & LAZDUNSKI, M. 2004. TREK-1, a K+ channel involved in neuroprotection and general anesthesia. *EMBO Journal,* 23**,** 2684-2695.

HINDERER, S. & SCHENKE-LAYLAND, K. 2019. Cardiac fibrosis – A short review of causes and therapeutic strategies. *Advanced Drug Delivery Reviews,* 146**,** 77-82.

HOUSTON, B. L., ZELINSKI, T., ISRAELS, S. J., COGHLAN, G., CHODIRKER, B. N., GALLAGHER, P. G., HOUSTON, D. S. & ZARYCHANSKI, R. 2011. Refinement of the hereditary xerocytosis locus on chromosome 16q in a large Canadian kindred. *Blood Cells, Molecules, and Diseases,* 47**,** 226-231.

HOYER, J., DISTLER, A., HAASE, W. & GÖGELEIN, H. 1994. Ca2+ influx through stretch-activated cation channels activates maxi K+ channels in porcine endocardial endothelium. *Proceedings of the National Academy of Sciences,* 91**,** 2367-2371.

HUANG, Z., SUN, Z., ZHANG, X., NIU, K., WANG, Y., ZHENG, J., LI, H. & LIU, Y. 2019. Loss of stretch-activated channels, PIEZOs, accelerates non-small cell lung cancer progression and cell migration. *Bioscience Reports,* 39**,** BSR20181679.

IMASHUKU, S., MURAMATSU, H., SUGIHARA, T., OKUNO, Y., WANG, X., YOSHIDA, K., KATO, A., KATO, K., TATSUMI, Y., HATTORI, A., KITA, S., OE, K., SUEYOSHI, A., USUI, T., SHIRAISHI, Y., CHIBA, K., TANAKA, H., MIYANO, S., OGAWA, S., KOJIMA, S. & KANNO, H. 2016. PIEZO1 gene mutation in a Japanese family with hereditary high phosphatidylcholine hemolytic anemia and hemochromatosis-induced diabetes mellitus. *International Journal of Hematology,* 104**,** 125-129.

IOLASCON, A., ANDOLFO, I. & RUSSO, R. 2019. Advances in understanding the pathogenesis of red cell membrane disorders. *British Journal of Haematology,* 187**,** 13-24.

JANIGRO, D., NGUYEN, T. S., GORDON, E. L. & WINN, H. R. 1996. Physiological properties of ATP-activated cation channels in rat brain microvascular endothelial cells. *American Journal of Physiology-Heart and Circulatory Physiology,* 270**,** H1423-H1434.

JONES, B. H., KIM, J. H., ZEMEL, M. B., WOYCHIK, R. P., MICHAUD, E. J., WILKISON, W. O. & MOUSTAID, N. 1996a. Upregulation of adipocyte metabolism by agouti protein: possible paracrine actions in yellow mouse obesity. *American Journal of Physiology-Endocrinology and Metabolism,* 270**,** E192-E196.

JONES, W. K., GRUPP, I. L., DOETSCHMAN, T., GRUPP, G., OSINSKA, H., HEWETT, T. E., BOIVIN, G., GULICK, J., NG, W. A. & ROBBINS, J. 1996b. Ablation of the murine alpha myosin heavy chain gene leads to dosage effects and functional deficits in the heart. *The Journal of Clinical Investigation,* 98**,** 1906-1917.

KANG, H., HONG, Z., ZHONG, M., KLOMP, J., BAYLESS, K. J., MEHTA, D., KARGINOV, A. V., HU, G. & MALIK, A. B. 2018. Piezo1 mediates angiogenesis through activation of MT1-MMP signaling. *American Journal of Physiology-Cell Physiology,* 316**,** C92-C103.

KAWATE, T., MICHEL, J. C., BIRDSONG, W. T. & GOUAUX, E. 2009. Crystal structure of the ATP-gated P2X4 ion channel in the closed state. *Nature,* 460**,** 592-598.

KNIGHT, T., ZAIDI, A. U., WU, S., GADGEEL, M., BUCK, S. & RAVINDRANATH, Y. 2019. Mild erythrocytosis as a presenting manifestation of PIEZO1 associated erythrocyte volume disorders. *Pediatric Hematology and Oncology,* 36**,** 317-326.

KOSER, D. E., THOMPSON, A. J., FOSTER, S. K., DWIVEDY, A., PILLAI, E. K., SHERIDAN, G. K., SVOBODA, H., VIANA, M., COSTA, L. D. F., GUCK, J., HOLT, C. E. & FRANZE, K. 2016. Mechanosensing is critical for axon growth in the developing brain. *Nat Neurosci,* 19**,** 1592-1598.

KRAEMER, F. B. & SHEN, W.-J. 2002. Hormone-sensitive lipase: control of intracellular tri-(di-)acylglycerol and cholesteryl ester hydrolysis. *Journal of lipid research,* 43**,** 1585-1594.

KRAUSS, R. M. 1998. Triglycerides and atherogenic lipoproteins: rationale for lipid management. *The American Journal of Medicine,* 105**,** 58S-62S.

KRAUSS, R. M. 2004. Lipids and Lipoproteins in Patients With Type 2 Diabetes. 27**,** 1496-1504.

KRYCER, J. R., SHARPE, L. J., LUU, W. & BROWN, A. J. 2010. The Akt–SREBP nexus: cell signaling meets lipid metabolism. *Trends in Endocrinology & Metabolism,* 21**,** 268-276.

LACROIX, J. J., BOTELLO-SMITH, W. M. & LUO, Y. 2018. Probing the gating mechanism of the mechanosensitive channel Piezo1 with the small molecule Yoda1. *Nature Communications,* 9**,** 2029.

LACRUZ, R. S. & FESKE, S. 2015. Diseases caused by mutations in ORAI1 and STIM1. *Annals of the New York Academy of Sciences,* 1356**,** 45-79.

LAU, O.-C., SHEN, B., WONG, C.-O. & YAO, X. 2018. Correspondence: Reply to 'Challenging a proposed role for TRPC5 in aortic baroreceptor pressure-sensing'. *Nature Communications,* 9**,** 1244.

LECLERC, I., RUTTER, G., MEUR, G. & NOORDEEN, N. 2012. Roles of Ca2+ ions in the control of ChREBP nuclear translocation. *The Journal of endocrinology,* 213**,** 115-22.

LEE, W., LEDDY, H. A., CHEN, Y., LEE, S. H., ZELENSKI, N. A., MCNULTY, A. L., WU, J., BEICKER, K. N., COLES, J., ZAUSCHER, S., GRANDL,

J., SACHS, F., GUILAK, F. & LIEDTKE, W. B. 2014. Synergy between Piezo1 and Piezo2 channels confers high-strain mechanosensitivity to articular cartilage. *Proceedings of the National Academy of Sciences,* 111**,** E5114-E5122.

LEWIS, A. H., CUI, A. F., MCDONALD, M. F. & GRANDL, J. 2017. Transduction of Repetitive Mechanical Stimuli by Piezo1 and Piezo2 Ion Channels. *Cell Reports,* 19**,** 2572-2585.

LEWIS, A. H. & GRANDL, J. 2015. Mechanical sensitivity of Piezo1 ion channels can be tuned by cellular membrane tension. *Elife,* 4**,** e12088.

LI, C., REZANIA, S., KAMMERER, S., SOKOLOWSKI, A., DEVANEY, T., GORISCHEK, A., JAHN, S., HACKL, H., GROSCHNER, K., WINDPASSINGER, C., MALLE, E., BAUERNHOFER, T. & SCHREIBMAYER, W. 2015. Piezo1 forms mechanosensitive ion channels in the human MCF-7 breast cancer cell line. *Scientific Reports,* 5**,** 8364.

LI, J., HOU, B., TUMOVA, S., MURAKI, K., BRUNS, A., LUDLOW, M. J., SEDO, A., HYMAN, A. J., MCKEOWN, L., YOUNG, R. S., YULDASHEVA, N. Y., MAJEED, Y., WILSON, L. A., RODE, B., BAILEY, M. A., KIM, H. R., FU, Z., CARTER, D. A., BILTON, J., IMRIE, H., AJUH, P., DEAR, T. N., CUBBON, R. M., KEARNEY, M. T., PRASAD, K. R., EVANS, P. C., AINSCOUGH, J. F. & BEECH, D. J. 2014. Piezo1 integration of vascular architecture with physiological force. *Nature,* 515**,** 279-82.

LIANG, G.-P., XU, J., CAO, L.-L., ZENG, Y.-H., CHEN, B.-X., YANG, J., ZHANG, Z.-W. & KANG, Y. 2019. Piezo1 induced apoptosis of type II pneumocytes during ARDS. *Respiratory Research,* 20**,** 118.

LIANG, J., HUANG, B., YUAN, G., CHEN, Y., LIANG, F., ZENG, H., ZHENG, S., CAO, L., GENG, D. & ZHOU, S. 2017. Stretch-activated channel Piezo1 is up-regulated in failure heart and cardiomyocyte stimulated by AngII. *American journal of translational research,* 9**,** 2945-2955.

LIANG, X. & HOWARD, J. 2018. Structural Biology: Piezo Senses Tension through Curvature. *Current Biology,* 28**,** R357-R359.

LIEDTKE, W., CHOE, Y., MARTÍ-RENOM, M. A., BELL, A. M., DENIS, C. S., SALI, A., HUDSPETH, A. J., FRIEDMAN, J. M. & HELLER, S. 2000. Vanilloid receptor-related osmotically activated channel (VR-OAC), a candidate vertebrate osmoreceptor. *Cell,* 103**,** 525-535.

LIM, D. S., ROBERTS, R. & MARIAN, A. J. 2001. Expression profiling of cardiac genes in human hypertrophic cardiomyopathy: insight into the pathogenesis of phenotypes. *Journal of the American College of Cardiology,* 38**,** 1175-1180.

LIN, S., THOMAS, T. C., STORLIEN, L. H. & HUANG, X. F. 2000. Development of high fat diet-induced obesity and leptin resistance in C57Bl/6J mice. *International Journal of Obesity,* 24**,** 639-646.

LIN, Y.-C., GUO, Y. R., MIYAGI, A., LEVRING, J., MACKINNON, R. & SCHEURING, S. 2019. Force-induced conformational changes in PIEZO1. *Nature,* 573**,** 230-234.

LIU, C. S. C., RAYCHAUDHURI, D., PAUL, B., CHAKRABARTY, Y., GHOSH, A. R., RAHAMAN, O., TALUKDAR, A. & GANGULY, D. 2018. Cutting Edge: Piezo1 Mechanosensors Optimize Human T Cell Activation. *The Journal of Immunology***,** ji1701118.

LIU, H., PATHAK, P., BOEHME, S. & CHIANG, J. Y. L. 2016. Cholesterol 7α-hydroxylase protects the liver from inflammation and fibrosis by

maintaining cholesterol homeostasis. *Journal of lipid research,* 57**,** 1831-1844.

LIU, Q., SILOTO, R. M. P., LEHNER, R., STONE, S. J. & WESELAKE, R. J. 2012. Acyl-CoA:diacylglycerol acyltransferase: Molecular biology, biochemistry and biotechnology. *Progress in Lipid Research,* 51**,** 350-377.

LU, Y., MA, X., SABHARWAL, R., SNITSAREV, V., MORGAN, D., RAHMOUNI, K., DRUMMOND, H. A., WHITEIS, C. A., COSTA, V., PRICE, M., BENSON, C., WELSH, M. J., CHAPLEAU, M. W. & ABBOUD, F. M. 2009. The Ion Channel ASIC2 Is Required for Baroreceptor and Autonomic Control of the Circulation. *Neuron,* 64**,** 885-897.

LUKACS, V., MATHUR, J., MAO, R., BAYRAK-TOYDEMIR, P., PROCTER, M., CAHALAN, S. M., KIM, H. J., BANDELL, M., LONGO, N., DAY, R. W., STEVENSON, D. A., PATAPOUTIAN, A. & KROCK, B. L. 2015. Impaired PIEZO1 function in patients with a novel autosomal recessive congenital lymphatic dysplasia. *Nat Commun,* 6**,** 8329.

LUSK, G. 1924. ANIMAL CALORIMETRY: Twenty-Fourth Paper. ANALYSIS OF THE OXIDATION OF MIXTURES OF CARBOHYDRATE AND FAT. *Journal of Biological Chemistry,* 59**,** 41-42.

MA, S., CAHALAN, S., LAMONTE, G., GRUBAUGH, N. D., ZENG, W., MURTHY, S. E., PAYTAS, E., GAMINI, R., LUKACS, V., WHITWAM, T., LOUD, M., LOHIA, R., BERRY, L., KHAN, S. M., JANSE, C. J., BANDELL, M., SCHMEDT, C., WENGELNIK, K., SU, A. I., HONORE, E., WINZELER, E. A., ANDERSEN, K. G. & PATAPOUTIAN, A. 2018. Common PIEZO1 Allele in African Populations Causes RBC Dehydration and Attenuates Plasmodium Infection. *Cell,* 173**,** 443-455.e12.

MA, Y., ZHAO, Y., CAI, Z. & HAO, X. 2019. Mutations in PIEZO2 contribute to Gordon syndrome, Marden-Walker syndrome and distal arthrogryposis: A bioinformatics analysis of mechanisms. *Experimental and therapeutic medicine,* 17**,** 3518-3524.

MANESHI, M. M., ZIEGLER, L., SACHS, F., HUA, S. Z. & GOTTLIEB, P. A. 2018. Enantiomeric Aβ peptides inhibit the fluid shear stress response of PIEZO1. *Scientific Reports,* 8**,** 14267.

MARCHI, S. & PINTON, P. 2014. The mitochondrial calcium uniporter complex: molecular components, structure and physiopathological implications. *The Journal of physiology,* 592**,** 829-839.

MARTIN-ALMEDINA, S., MANSOUR, S. & OSTERGAARD, P. 2018. Human phenotypes caused by PIEZO1 mutations; one gene, two overlapping phenotypes? *The Journal of Physiology,* 596**,** 985-992.

MARTINO, F., PERESTRELO, A. R., VINARSKÝ, V., PAGLIARI, S. & FORTE, G. 2018. Cellular Mechanotransduction: From Tension to Function. *Frontiers in Physiology,* 9**,** 824.

MARTINS, J. R., PENTON, D., PEYRONNET, R., ARHATTE, M., MORO, C., PICARD, N., KURT, B., PATEL, A., HONORÉ, E. & DEMOLOMBE, S. 2016. Piezo1-dependent regulation of urinary osmolarity. *Pflügers Archiv - European Journal of Physiology,* 468**,** 1197-1206.

MATHIASSEN, O. N., BUUS, N. H., SIHM, I., THYBO, N. K., MØRN, B., SCHROEDER, A. P., THYGESEN, K., AALKJAER, C., LEDERBALLE, O., MULVANY, M. J. & CHRISTENSEN, K. L. 2007. Small artery structure is an independent predictor of cardiovascular events in essential hypertension. *Journal of Hypertension,* 25**,** 1021-1026.

MCHUGH, B. J., MURDOCH, A., HASLETT, C. & SETHI, T. 2012. Loss of the Integrin-Activating Transmembrane Protein Fam38A (Piezo1) Promotes a Switch to a Reduced Integrin-Dependent Mode of Cell Migration. *PLOS ONE,* 7**,** e40346.

MCMILLIN, MARGARET J., BECK, ANITA E., CHONG, JESSICA X., SHIVELY, KATHRYN M., BUCKINGHAM, KATI J., GILDERSLEEVE, HEIDI I. S., ARACENA, MARIANA I., AYLSWORTH, ARTHUR S., BITOUN, P., CAREY, JOHN C., CLERICUZIO, CAROL L., CROW, YANICK J., CURRY, CYNTHIA J., DEVRIENDT, K., EVERMAN, DAVID B., FRYER, A., GIBSON, K., GIOVANNUCCI UZIELLI, MARIA L., GRAHAM, JOHN M., HALL, JUDITH G., HECHT, JACQUELINE T., HEIDENREICH, RANDALL A., HURST, JANE A., IRANI, S., KRAPELS, INGRID P. C., LEROY, JULES G., MOWAT, D., PLANT, GORDON T., ROBERTSON, STEPHEN P., SCHORRY, ELIZABETH K., SCOTT, RICHARD H., SEAVER, LAURIE H., SHERR, E., SPLITT, M., STEWART, H., STUMPEL, C., TEMEL, SEHIME G., WEAVER, DAVID D., WHITEFORD, M., WILLIAMS, MARC S., TABOR, HOLLY K., SMITH, JOSHUA D., SHENDURE, J., NICKERSON, DEBORAH A. & BAMSHAD, MICHAEL J. 2014. Mutations in PIEZO2 Cause Gordon Syndrome, Marden-Walker Syndrome, and Distal Arthrogryposis Type 5. *The American Journal of Human Genetics,* 94**,** 734-744.

MIKOSHIBA, K. 2015. Role of IP3 receptor signaling in cell functions and diseases. *Advances in Biological Regulation,* 57**,** 217-227.

MILLER, D. R., RICKLES, F. R., LICHTMAN, M. A., LA CELLE, P. L., BATES, J. & WEED, R. I. 1971. A New Variant of Hereditary Hemolytic Anemia With Stomatocytosis and Erythrocyte Cation Abnormality. *Blood,* 38**,** 184-204.

MINA, A. I., LECLAIR, R. A., LECLAIR, K. B., COHEN, D. E., LANTIER, L. & BANKS, A. S. 2018. CalR: A Web-Based Analysis Tool for Indirect Calorimetry Experiments. *Cell Metabolism,* 28**,** 656-666.e1.

MIYAMOTO, T., MOCHIZUKI, T., NAKAGOMI, H., KIRA, S., WATANABE, M., TAKAYAMA, Y., SUZUKI, Y., KOIZUMI, S., TAKEDA, M. & TOMINAGA, M. 2014. Functional Role for Piezo1 in Stretch-evoked Ca2+ Influx and ATP Release in Urothelial Cell Cultures. *Journal of Biological Chemistry,* 289**,** 16565-16575.

MOCHIZUKI, T., WU, G., HAYASHI, T., XENOPHONTOS, S. L., VELDHUISEN, B., SARIS, J. J., REYNOLDS, D. M., CAI, Y., GABOW, P. A., PIERIDES, A., KIMBERLING, W. J., BREUNING, M. H., DELTAS, C. C., PETERS, D. J. M. & SOMLO, S. 1996. PKD2; a Gene for Polycystic Kidney Disease That Encodes an Integral Membrane Protein. *Science,* 272**,** 1339-1342.

MONTEITH, G. R., DAVIS, F. M. & ROBERTS-THOMSON, S. J. 2012. Calcium Channels and Pumps in Cancer: Changes and Consequences. *Journal of Biological Chemistry,* 287**,** 31666-31673.

MORGAN, ANTHONY J., DAVIS, LIANNE C., RUAS, M. & GALIONE, A. 2015. TPC: the NAADP discovery channel? *Biochemical Society Transactions,* 43**,** 384-389.

MORGAN, A. J., PLATT, F. M., LLOYD-EVANS, E. & GALIONE, A. 2011. Molecular mechanisms of endolysosomal Ca2+ signalling in health and disease. *Biochemical Journal,* 439**,** 349-378.

MORONI, M., SERVIN-VENCES, M. R., FLEISCHER, R., SÁNCHEZ-CARRANZA, O. & LEWIN, G. R. 2018. Voltage gating of mechanosensitive PIEZO channels. *Nature Communications,* 9**,** 1096.

MOVITA, D., KREEFFT, K., BIESTA, P., VAN OUDENAREN, A., LEENEN, P. J. M., JANSSEN, H. L. A. & BOONSTRA, A. 2012. Kupffer cells express a unique combination of phenotypic and functional characteristics compared with splenic and peritoneal macrophages. *Journal of Leukocyte Biology,* 92**,** 723-733.

MURAKI, K., IWATA, Y., KATANOSAKA, Y., ITO, T., OHYA, S., SHIGEKAWA, M. & IMAIZUMI, Y. 2003. TRPV2 Is a Component of Osmotically Sensitive Cation Channels in Murine Aortic Myocytes. *Circulation Research,* 93**,** 829-838.

MURTHY, S. E., LOUD, M. C., DAOU, I., MARSHALL, K. L., SCHWALLER, F., KÜHNEMUND, J., FRANCISCO, A. G., KEENAN, W. T., DUBIN, A. E., LEWIN, G. R. & PATAPOUTIAN, A. 2018. The mechanosensitive ion channel Piezo2 mediates sensitivity to mechanical pain in mice. *Science Translational Medicine,* 10**,** eaat9897.

NAEINI, R. S., WITTY, M.-F., SÉGUÉLA, P. & BOURQUE, C. W. 2006. An N-terminal variant of Trpv1 channel is required for osmosensory transduction. *Nature Neuroscience,* 9**,** 93-98.

NAULI, S. M., ALENGHAT, F. J., LUO, Y., WILLIAMS, E., VASSILEV, P., LI, X., ELIA, A. E. H., LU, W., BROWN, E. M., QUINN, S. J., INGBER, D. E. & ZHOU, J. 2003. Polycystins 1 and 2 mediate mechanosensation in the primary cilium of kidney cells. *Nature Genetics,* 33**,** 129-137.

NIEUWENHUIS, B., HAENZI, B., ANDREWS, M. R., VERHAAGEN, J. & FAWCETT, J. W. 2018. Integrins promote axonal regeneration after injury of the nervous system. *Biological reviews of the Cambridge Philosophical Society,* 93**,** 1339-1362.

NOËL, J., ZIMMERMANN, K., BUSSEROLLES, J., DEVAL, E., ALLOUI, A., DIOCHOT, S., GUY, N., BORSOTTO, M., REEH, P., ESCHALIER, A. & LAZDUNSKI, M. 2009. The mechano-activated K+ channels TRAAK and TREK-1 control both warm and cold perception. *EMBO Journal,* 28**,** 1308-1318.

NOORDEEN, N. A., MEUR, G., RUTTER, G. A. & LECLERC, I. 2012. Glucose-induced nuclear shuttling of ChREBP is mediated by sorcin and Ca(2+) ions in pancreatic β-cells. *Diabetes,* 61**,** 574-585.

NORTH, R. A. 2016. P2X receptors. *Philosophical transactions of the Royal Society of London. Series B, Biological sciences,* 371**,** 20150427.

NUMATA, T., SHIMIZU, T. & OKADA, Y. 2007. TRPM7 is a stretch- and swelling-activated cation channel involved in volume regulation in human epithelial cells. *American Journal of Physiology-Cell Physiology,* 292**,** C460-C467.

O'CONOR, C. J., LEDDY, H. A., BENEFIELD, H. C., LIEDTKE, W. B. & GUILAK, F. 2014. TRPV4-mediated mechanotransduction regulates the metabolic response of chondrocytes to dynamic loading. *Proceedings of the National Academy of Sciences,* 111**,** 1316-1321.

OANCEA, E., WOLFE JOSHUA, T. & CLAPHAM DAVID, E. 2006. Functional TRPM7 Channels Accumulate at the Plasma Membrane in Response to Fluid Flow. *Circulation Research,* 98**,** 245-253.

ORR, A. W., HELMKE, B. P., BLACKMAN, B. R. & SCHWARTZ, M. A. 2006. Mechanisms of Mechanotransduction. *Developmental Cell,* 10**,** 11-20.

OUCHI, N., PARKER, J. L., LUGUS, J. J. & WALSH, K. 2011. Adipokines in inflammation and metabolic disease. *Nature Reviews Immunology,* 11**,** 85-97.

OYADOMARI, S. & MORI, M. 2004. Roles of CHOP/GADD153 in endoplasmic reticulum stress. *Cell Death & Differentiation,* 11**,** 381-389.

PAESSLER, M. & HARTUNG, H. 2015. Dehydrated hereditary stomatocytosis masquerading as MDS. *Blood,* 125**,** 1841.

PATEL, A. J. & HONORÉ, E. 2001. Properties and modulation of mammalian 2P domain K+ channels. *Trends in Neurosciences,* 24**,** 339-346.

PATHAK, M. M., NOURSE, J. L., TRAN, T., HWE, J., ARULMOLI, J., LE, D. T. T., BERNARDIS, E., FLANAGAN, L. A. & TOMBOLA, F. 2014. Stretch-activated ion channel Piezo1 directs lineage choice in human neural stem cells. *Proceedings of the National Academy of Sciences,* 111**,** 16148-16153.

PAWLAK, M., LEFEBVRE, P. & STAELS, B. 2015. Molecular mechanism of PPARα action and its impact on lipid metabolism, inflammation and fibrosis in non-alcoholic fatty liver disease. *Journal of Hepatology,* 62**,** 720-733.

PEREIRA, V., BUSSEROLLES, J., CHRISTIN, M., DEVILLIERS, M., POUPON, L., LEGHA, W., ALLOUI, A., AISSOUNI, Y., BOURINET, E., LESAGE, F., ESCHALIER, A., LAZDUNSKI, M. & NOËL, J. 2014. Role of the TREK2 potassium channel in cold and warm thermosensation and in pain perception. *PAIN®,* 155**,** 2534-2544.

PEYRONNET, R., MARTINS, J. R., DUPRAT, F., DEMOLOMBE, S., ARHATTE, M., JODAR, M., TAUC, M., DURANTON, C., PAULAIS, M., TEULON, J., HONORÉ, E. & PATEL, A. 2013. Piezo1-dependent stretch-activated channels are inhibited by Polycystin-2 in renal tubular epithelial cells. *EMBO reports,* 14**,** 1143-1148.

PUGACH, E. K., RICHMOND, P. A., AZOFEIFA, J. G., DOWELL, R. D. & LEINWAND, L. A. 2015. Prolonged Cre expression driven by the α-myosin heavy chain promoter can be cardiotoxic. *Journal of Molecular and Cellular Cardiology,* 86**,** 54-61.

QI, D., ATSINA, K., QU, L., HU, X., WU, X., XU, B., PIECYCHNA, M., LENG, L., FINGERLE-ROWSON, G., ZHANG, J., BUCALA, R. & YOUNG, L. 2014. The vestigial enzyme D-dopachrome tautomerase protects the heart against ischemic injury. *The Journal of clinical investigation,* 124**,** 3540-3550.

RANADE, S. S., QIU, Z., WOO, S.-H., HUR, S. S., MURTHY, S. E., CAHALAN, S. M., XU, J., MATHUR, J., BANDELL, M., COSTE, B., LI, Y.-S. J., CHIEN, S. & PATAPOUTIAN, A. 2014a. Piezo1, a mechanically activated ion channel, is required for vascular development in mice. *Proceedings of the National Academy of Sciences,* 111**,** 10347-10352.

RANADE, S. S., SYEDA, R. & PATAPOUTIAN, A. 2015. Mechanically Activated Ion Channels. *Neuron,* 87**,** 1162-1179.

RANADE, S. S., WOO, S.-H., DUBIN, A. E., MOSHOURAB, R. A., WETZEL, C., PETRUS, M., MATHUR, J., BÉGAY, V., COSTE, B., MAINQUIST, J., WILSON, A. J., FRANCISCO, A. G., REDDY, K., QIU, Z., WOOD, J. N., LEWIN, G. R. & PATAPOUTIAN, A. 2014b. Piezo2 is the major transducer of mechanical forces for touch sensation in mice. *Nature,* 516**,** 121-125.

RAPETTI-MAUSS, R., PICARD, V., GUITTON, C., GHAZAL, K., PROULLE, V., BADENS, C., SORIANI, O., GARÇON, L. & GUIZOUARN, H. 2017. Red

blood cell Gardos channel (KCNN4):the essential determinant of erythrocyte dehydration in Hereditary Xerocytosis. *Haematologica,* 102**,** e415-e418.

REHMANI, T., SALIH, M. & TUANA, B. 2019. Cardiac-Specific Cre Induces Age-Dependent Dilated Cardiomyopathy (DCM) in Mice. *Molecules,* 24**,** 1189.

RETAILLEAU, K., DUPRAT, F., ARHATTE, M., RANADE, S. S., PEYRONNET, R., MARTINS, J. R., JODAR, M., MORO, C., OFFERMANNS, S., FENG, Y., DEMOLOMBE, S., PATEL, A. & HONORÉ, E. 2015. Piezo1 in Smooth Muscle Cells Is Involved in Hypertension-Dependent Arterial Remodeling. *Cell Reports,* 13**,** 1161-1171.

RISINGER, M. A., GLOGOWSKA, E., BEGTRUP, A. H., DAGAONKAR, N., CHONAT, S., JOINER, C. H., QUINN, C. T., KALFA, T. A. & GALLAGHER, P. G. 2014. The Novel PIEZO1 Mutation p.L2023V Is Causal for Hereditary Xerocytosis Resulting in Delayed Channel Inactivation and a Dehydrated Red Blood Cell Phenotype. *Blood,* 124**,** 741.

ROCIO SERVIN-VENCES, M., MORONI, M., LEWIN, G. R. & POOLE, K. 2017. Direct measurement of TRPV4 and PIEZO1 activity reveals multiple mechanotransduction pathways in chondrocytes. *eLife,* 6**,** e21074.

RODE, B., SHI, J., ENDESH, N., DRINKHILL, M. J., WEBSTER, P. J., LOTTEAU, S. J., BAILEY, M. A., YULDASHEVA, N. Y., LUDLOW, M. J., CUBBON, R. M., LI, J., FUTERS, T. S., MORLEY, L., GAUNT, H. J., MARSZALEK, K., VISWAMBHARAN, H., CUTHBERTSON, K., BAXTER, P. D., FOSTER, R., SUKUMAR, P., WEIGHTMAN, A., CALAGHAN, S. C., WHEATCROFT, S. B., KEARNEY, M. T. & BEECH, D. J. 2017. Piezo1 channels sense whole body physical activity to reset cardiovascular homeostasis and enhance performance. *Nature Communications,* 8**,** 350.

RODRÍGUEZ-HERNÁNDEZ, H., SIMENTAL-MENDÍA, L. E., RODRÍGUEZ-RAMÍREZ, G. & REYES-ROMERO, M. A. 2013. Obesity and inflammation: epidemiology, risk factors, and markers of inflammation. *International journal of endocrinology,* 2013**,** 678159-678159.

ROMAC, J. M. J., SHAHID, R. A., SWAIN, S. M., VIGNA, S. R. & LIDDLE, R. A. 2018. Piezo1 is a mechanically activated ion channel and mediates pressure induced pancreatitis. *Nature Communications,* 9**,** 1715.

ROMERO, L. O., MASSEY, A. E., MATA-DABOIN, A. D., SIERRA-VALDEZ, F. J., CHAUHAN, S. C., CORDERO-MORALES, J. F. & VÁSQUEZ, V. 2019. Dietary fatty acids fine-tune Piezo1 mechanical response. *Nature Communications,* 10**,** 1200.

ROTORDAM, M. G., FERMO, E., BECKER, N., BARCELLINI, W., BRÜGGEMANN, A., FERTIG, N., EGÉE, S., RAPEDIUS, M., BIANCHI, P. & KAESTNER, L. 2018. A Yoda1-Based Approach to Investigate Piezo1 Channels in Red Blood Cells Using Automated Patch Clamp Technology. *Blood,* 132**,** 1031.

SACKMANN-SALA, L., BERRYMAN, D. E., MUNN, R. D., LUBBERS, E. R. & KOPCHICK, J. J. 2012. Heterogeneity among white adipose tissue depots in male C57BL/6J mice. *Obesity (Silver Spring, Md.),* 20**,** 101-111.

SANDBERG, M. B., NYBO, M., BIRGENS, H. & FREDERIKSEN, H. 2014. Hereditary xerocytosis and familial haemolysis due to mutation in the

PIEZO1 gene: a simple diagnostic approach. *International Journal of Laboratory Hematology,* 36**,** e62-e65.

SANZ, M.-N., GRIMBERT, L., MOULIN, M., GRESSETTE, M., RUCKER-MARTIN, C., LEMAIRE, C., MERICSKAY, M., VEKSLER, V., VENTURA-CLAPIER, R., GARNIER, A. & PIQUEREAU, J. 2019. Inducible Cardiac-Specific Deletion of Sirt1 in Male Mice Reveals Progressive Cardiac Dysfunction and Sensitization of the Heart to Pressure Overload. *International Journal of Molecular Sciences,* 20**,** 5005.

SAOTOME, K., MURTHY, S. E., KEFAUVER, J. M., WHITWAM, T., PATAPOUTIAN, A. & WARD, A. B. 2017. Structure of the mechanically activated ion channel Piezo1. *Nature,* 554**,** 481-486.

SHARMA, A. M. & STAELS, B. 2007. Peroxisome Proliferator-Activated Receptor γ and Adipose Tissue—Understanding Obesity-Related Changes in Regulation of Lipid and Glucose Metabolism. *The Journal of Clinical Endocrinology & Metabolism,* 92**,** 386-395.

SHMUKLER, B. E., HUSTON, N. C., THON, J. N., NI, C.-W., KOURKOULIS, G., LAWSON, N. D., PAW, B. H. & ALPER, S. L. 2015. Homozygous knockout of the piezo1 gene in the zebrafish is not associated with anemia. *Haematologica,* 100**,** e483-e485.

SHMUKLER, B. E., VANDORPE, D. H., RIVERA, A., AUERBACH, M., BRUGNARA, C. & ALPER, S. L. 2014. Dehydrated stomatocytic anemia due to the heterozygous mutation R2456H in the mechanosensitive cation channel PIEZO1: a case report. *Blood Cells, Molecules, and Diseases,* 52**,** 53-54.

SHULMAN, G. I. 2014. Ectopic Fat in Insulin Resistance, Dyslipidemia, and Cardiometabolic Disease. *New England Journal of Medicine,* 371**,** 1131-1141.

SOLIS, A. G., BIELECKI, P., STEACH, H. R., SHARMA, L., HARMAN, C. C. D., YUN, S., DE ZOETE, M. R., WARNOCK, J. N., TO, S. D. F., YORK, A. G., MACK, M., SCHWARTZ, M. A., DELA CRUZ, C. S., PALM, N. W., JACKSON, R. & FLAVELL, R. A. 2019. Mechanosensation of cyclical force by PIEZO1 is essential for innate immunity. *Nature,* 573**,** 69-74.

SONG, Y., LI, D., FARRELLY, O., MILES, L., LI, F., KIM, S. E., LO, T. Y., WANG, F., LI, T., THOMPSON-PEER, K. L., GONG, J., MURTHY, S. E., COSTE, B., YAKUBOVICH, N., PATAPOUTIAN, A., XIANG, Y., ROMPOLAS, P., JAN, L. Y. & JAN, Y. N. 2019. The Mechanosensitive Ion Channel Piezo Inhibits Axon Regeneration. *Neuron,* 102**,** 373-389.e6.

SPIER, I., KERICK, M., DRICHEL, D., HORPAOPAN, S., ALTMÜLLER, J., LANER, A., HOLZAPFEL, S., PETERS, S., ADAM, R., ZHAO, B., BECKER, T., LIFTON, R. P., HOLINSKI-FEDER, E., PERNER, S., THIELE, H., NÖTHEN, M. M., HOFFMANN, P., TIMMERMANN, B., SCHWEIGER, M. R. & ARETZ, S. 2016. Exome sequencing identifies potential novel candidate genes in patients with unexplained colorectal adenomatous polyposis. *Familial Cancer,* 15**,** 281-288.

STARTEK, J. B., BOONEN, B., TALAVERA, K. & MESEGUER, V. 2019. TRP Channels as Sensors of Chemically-Induced Changes in Cell Membrane Mechanical Properties. *International journal of molecular sciences,* 20**,** 371.

STRABLE, M. S. & NTAMBI, J. M. 2010. Genetic control of de novo lipogenesis: role in diet-induced obesity. *Critical Reviews in Biochemistry and Molecular Biology,* 45**,** 199-214.

SUCHYNA, T. M., TAPE, S. E., KOEPPE II, R. E., ANDERSEN, O. S., SACHS, F. & GOTTLIEB, P. A. 2004. Bilayer-dependent inhibition of mechanosensitive channels by neuroactive peptide enantiomers. *Nature,* 430**,** 235.

SUN, W., CHI, S., LI, Y., LING, S., TAN, Y., XU, Y., JIANG, F., LI, J., LIU, C., ZHONG, G., CAO, D., JIN, X., ZHAO, D., GAO, X., LIU, Z., XIAO, B. & LI, Y. 2019. The mechanosensitive Piezo1 channel is required for bone formation. *eLife,* 8**,** e47454.

SUN, Z., GUO, S. S. & FÄSSLER, R. 2016. Integrin-mediated mechanotransduction. *The Journal of cell biology,* 215**,** 445-456.

SYEDA, R., FLORENDO, M. N., COX, C. D., KEFAUVER, J. M., SANTOS, J. S., MARTINAC, B. & PATAPOUTIAN, A. 2016. Piezo1 Channels Are Inherently Mechanosensitive. *Cell Rep,* 17**,** 1739-1746.

SYEDA, R., XU, J., DUBIN, A. E., COSTE, B., MATHUR, J., HUYNH, T., MATZEN, J., LAO, J., TULLY, D. C., ENGELS, I. H., PETRASSI, H. M., SCHUMACHER, A. M., MONTAL, M., BANDELL, M. & PATAPOUTIAN, A. 2015. Chemical activation of the mechanotransduction channel Piezo1. *Elife,* 4**,** e07369.

SZCZOT, M., LILJENCRANTZ, J., GHITANI, N., BARIK, A., LAM, R., THOMPSON, J. H., BHARUCHA-GOEBEL, D., SAADE, D., NECAISE, A., DONKERVOORT, S., FOLEY, A. R., GORDON, T., CASE, L., BUSHNELL, M. C., BÖNNEMANN, C. G. & CHESLER, A. T. 2018. PIEZO2 mediates injury-induced tactile pain in mice and humans. *Science Translational Medicine,* 10**,** eaat9892.

SZEKELY, Y. & ARBEL, Y. 2018. A Review of Interleukin-1 in Heart Disease: Where Do We Stand Today? *Cardiology and Therapy,* 7**,** 25-44.

TAYLOR, C. W. 2002. Controlling Calcium Entry. *Cell,* 111**,** 767-769.

THAKORE, P., BRAIN, S. D. & BEECH, D. J. 2018. Correspondence: Challenging a proposed role for TRPC5 in aortic baroreceptor pressure-sensing. *Nature Communications,* 9**,** 1245.

THE EUROPEAN POLYCYSTIC KIDNEY DISEASE, C. 1994. The polycystic kidney disease 1 gene encodes a 14 kb transcript and lies within a duplicated region on chromosome 16. *Cell,* 77**,** 881-894.

THORENS, B. 2015. GLUT2, glucose sensing and glucose homeostasis. *Diabetologia,* 58**,** 221-232.

TRAPANI, L., SEGATTO, M. & PALLOTTINI, V. 2012. Regulation and deregulation of cholesterol homeostasis: The liver as a metabolic "power station". *World journal of hepatology,* 4**,** 184-190.

TSUCHIYA, M., HARA, Y., OKUDA, M., ITOH, K., NISHIOKA, R., SHIOMI, A., NAGAO, K., MORI, M., MORI, Y., IKENOUCHI, J., SUZUKI, R., TANAKA, M., OHWADA, T., AOKI, J., KANAGAWA, M., TODA, T., NAGATA, Y., MATSUDA, R., TAKAYAMA, Y., TOMINAGA, M. & UMEDA, M. 2018. Cell surface flip-flop of phosphatidylserine is critical for PIEZO1-mediated myotube formation. *Nature Communications,* 9**,** 2049.

VAN PETEGEM, F. 2012. Ryanodine Receptors: Structure and Function. *Journal of Biological Chemistry,* 287**,** 31624-31632.

VENKATACHALAM, K. & MONTELL, C. 2007. TRP channels. *Annual review of biochemistry,* 76**,** 387-417.

WAJCHENBERG, B. L., GIANNELLA-NETO, D., DA SILVA, M. E. R. & SANTOS, R. F. 2002. Depot-Specific Hormonal Characteristics of Subcutaneous and Visceral Adipose Tissue and their Relation to the Metabolic Syndrome. *Horm Metab Res,* 34**,** 616-621.

WAN, J., RISTENPART, W. D. & STONE, H. A. 2008. Dynamics of shear-induced ATP release from red blood cells. *Proceedings of the National Academy of Sciences,* 105**,** 16432-16437.

WANG, L., ZHOU, H., ZHANG, M., LIU, W., DENG, T., ZHAO, Q., LI, Y., LEI, J., LI, X. & XIAO, B. 2019a. Structure and mechanogating of the mammalian tactile channel PIEZO2. *Nature,* 573**,** 225-229.

WANG, S., BINDER, P., FANG, Q., WANG, Z., XIAO, W., LIU, W. & WANG, X. 2018a. Endoplasmic reticulum stress in the heart: insights into mechanisms and drug targets. 175**,** 1293-1304.

WANG, S., CHENNUPATI, R., KAUR, H., IRING, A., WETTSCHURECK, N. & OFFERMANNS, S. 2016. Endothelial cation channel PIEZO1 controls blood pressure by mediating flow-induced ATP release. *J Clin Invest,* 126**,** 4527-4536.

WANG, W.-A., LIU, W.-X., DURNAOGLU, S., LEE, S.-K., LIAN, J., LEHNER, R., AHNN, J., AGELLON, L. B. & MICHALAK, M. 2017. Loss of Calreticulin Uncovers a Critical Role for Calcium in Regulating Cellular Lipid Homeostasis. *Scientific Reports,* 7**,** 5941.

WANG, Y., CHI, S., GUO, H., LI, G., WANG, L., ZHAO, Q., RAO, Y., ZU, L., HE, W. & XIAO, B. 2018b. A lever-like transduction pathway for long-distance chemical- and mechano-gating of the mechanosensitive Piezo1 channel. *Nature Communications,* 9**,** 1300.

WANG, Z., BABICHEVA, A., WU, L., YUAN, J. X. J. & WANG, J. 2019b. Endothelial Upregulation of Mechanosensitive Channel Piezo1 in Pulmonary Hypertension. *The FASEB Journal,* 33**,** 827.12-827.12.

WEHRWEIN, E. A. & JOYNER, M. J. 2013. Chapter 8 - Regulation of blood pressure by the arterial baroreflex and autonomic nervous system. *In:* BUIJS, R. M. & SWAAB, D. F. (eds.) *Handbook of Clinical Neurology.* Elsevier.

WEI-LAPIERRE, L., CARRELL, E. M., BONCOMPAGNI, S., PROTASI, F. & DIRKSEN, R. T. 2013. Orai1-dependent calcium entry promotes skeletal muscle growth and limits fatigue. *Nature Communications,* 4**,** 2805.

WELLEN, K. E. & HOTAMISLIGIL, G. S. 2005. Inflammation, stress, and diabetes. *The Journal of Clinical Investigation,* 115**,** 1111-1119.

WENG, Y., YAN, F., CHEN, R., QIAN, M., OU, Y., XIE, S., ZHENG, H. & LI, J. 2018. PIEZO channel protein naturally expressed in human breast cancer cell MDA-MB-231 as probed by atomic force microscopy. *AIP Advances,* 8**,** 055101.

WONG, T.-Y., JUANG, W.-C., TSAI, C.-T., TSENG, C.-J., LEE, W.-H., CHANG, S.-N. & CHENG, P.-W. 2018. Mechanical Stretching Simulates Cardiac Physiology and Pathology through Mechanosensor Piezo1. *Journal of clinical medicine,* 7**,** 410.

WOO, S.-H., RANADE, S., WEYER, A. D., DUBIN, A. E., BABA, Y., QIU, Z., PETRUS, M., MIYAMOTO, T., REDDY, K., LUMPKIN, E. A., STUCKY, C. L. & PATAPOUTIAN, A. 2014. Piezo2 is required for Merkel-cell mechanotransduction. *Nature,* 509**,** 622-626.

WU, J., YOUNG, M., LEWIS, A. H., MARTFELD, A. N., KALMETA, B. & GRANDL, J. 2017. Inactivation of Mechanically Activated Piezo1 Ion Channels Is Determined by the C-Terminal Extracellular Domain and the Inner Pore Helix. *Cell Reports,* 21**,** 2357-2366.

YANG, X.-N., LU, Y.-P., LIU, J.-J., HUANG, J.-K., LIU, Y.-P., XIAO, C.-X., JAZAG, A., REN, J.-L. & GULENG, B. 2014. Piezo1 Is as a Novel Trefoil

Factor Family 1 Binding Protein that Promotes Gastric Cancer Cell Mobility In Vitro. *Digestive Diseases and Sciences,* 59**,** 1428-1435.

ZARYCHANSKI, R., SCHULZ, V. P., HOUSTON, B. L., MAKSIMOVA, Y., HOUSTON, D. S., SMITH, B., RINEHART, J. & GALLAGHER, P. G. 2012. Mutations in the mechanotransduction protein PIEZO1 are associated with hereditary xerocytosis. *Blood,* 120**,** 1908-15.

ZENG, W.-Z., MARSHALL, K. L., MIN, S., DAOU, I., CHAPLEAU, M. W., ABBOUD, F. M., LIBERLES, S. D. & PATAPOUTIAN, A. 2018. PIEZOs mediate neuronal sensing of blood pressure and the baroreceptor reflex. *Science,* 362**,** 464-467.

ZHAO, C., SUN, Q., TANG, L., CAO, Y., NOURSE, J. L., PATHAK, M. M., LU, X. & YANG, Q. 2019. Mechanosensitive Ion Channel Piezo1 Regulates Diet-Induced Adipose Inflammation and Systemic Insulin Resistance. *Frontiers in Endocrinology,* 10**,** 373.

ZHAO, Q., ZHOU, H., CHI, S., WANG, Y., WANG, J., GENG, J., WU, K., LIU, W., ZHANG, T., DONG, M.-Q., WANG, J., LI, X. & XIAO, B. 2018. Structure and mechanogating mechanism of the Piezo1 channel. *Nature,* 554**,** 487-492.

ZHENG, W., GRACHEVA, E. O. & BAGRIANTSEV, S. N. 2019. A hydrophobic gate in the inner pore helix is the major determinant of inactivation in mechanosensitive Piezo channels. *eLife,* 8**,** e44003.

ZHU, J., MOTEJLEK, K., WANG, D., ZANG, K., SCHMIDT, A. & REICHARDT, L. F. 2002. beta8 integrins are required for vascular morphogenesis in mouse embryos. *Development (Cambridge, England),* 129**,** 2891-2903.